

Neutronics Calculations Relevant to the Conversion of Research Reactors to Low-Enriched Fuel

Vom Fachbereich Physik
der Technischen Universität Darmstadt

zur Erlangung des Grades
eines Doktors der Naturwissenschaften
(Dr. rer. nat.)

genehmigte Dissertation von
Dipl.-Phys. Alexander Glaser
aus Groß-Umstadt

Referent: Prof. Dr. Franz Fujara
1. Korreferent: Prof. Dr. Markus Roth
2. Korreferent: Dr. Armando Travelli
Argonne National Laboratory, USA

Tag der Einreichung: 9. Februar 2005
Tag der Prüfung: 27. April 2005

Darmstadt 2005
D17

Pages 43, 69, 81, 83, 87, 88, 91, 126, 147, 152,
155, and 210 are best viewed in color

Dedicated to those who actively support the international efforts to end the use of highly enriched uranium in the civilian nuclear fuel cycle and, in particular, to those users and operators of research reactors who willingly accept the implications that come along with this commitment to nonproliferation and global security.

ZUSAMMENFASSUNG

Im Rahmen der neu entfachten Diskussion zu Strategien der Nichtverbreitung von Kernwaffen und der Verhinderung von Nuklearterrorismus hat hochangereichertes Uran (*Highly Enriched Uranium*, HEU) besondere Aufmerksamkeit auf sich gezogen. Im Gegensatz zu Plutonium ist hochangereichertes Uran relativ leicht als spaltbares Material in Kernwaffen verwendbar. Der mögliche Zugriff auf HEU durch Diebstahl oder Abzweigung stellt daher ein besonderes Proliferationsrisiko dar. Im zivilen Sektor kommt HEU heute praktisch nur noch als Brennstoff in Forschungsreaktoren zum Einsatz — und es stellt sich die Frage, wie rasch dessen Nutzung endgültig beendet werden kann.

Internationale Bemühungen zur Umstellung von Forschungsreaktoren auf nicht-kernwaffentaugliches, niedrig angereichertes Uran wurden und werden entscheidend durch die Entwicklung und Verfügbarkeit hochdichter Brennstoffe unterstützt. Effektive Urandichten im Brennstoff wurden so von ehemals $1,5 \text{ g/cm}^3$ auf heute $4,8 \text{ g/cm}^3$ gesteigert. Völlig unerwartet konnten im Jahr 2002 hervorragende Bestrahlungseigenschaften für Uran-Molybdän-Legierungen mit Urandichten von bis zu 16 g/cm^3 bestätigt werden. Die Entwicklung solcher Brennstoffe würde völlig neue Perspektiven für die Nutzung von niedrig angereichertem Uran eröffnen. Dabei erweist sich jedoch die Umstellung von sogenannten Ein-Brennelement-Reaktoren als besondere Herausforderung, was vor allem durch deren Kompaktkernbauweise und ‘starre’ Kerngeometrie bedingt ist.

Die Bestimmung des Potentials von solchen sogenannten monolithischen Brennstoffen zur Umstellung von Hochfluss-Reaktoren auf niedrig angereichertes Uran, unter besonderer Berücksichtigung der wissenschaftlichen Nutzbarkeit der Anlagen, stellen den wesentlichen Kern dieser Arbeit dar. Hierzu werden umfangreiche neutronenphysikalische Berechnungen für Ein-Brennelement-Reaktoren durchgeführt sowie Verfahren zur Reoptimierung von Kerngeometrien, die aufgrund der veränderten Eigenschaften der Brennstoffe mit reduzierter Anreicherung notwendig wird, entwickelt.

Um diese Berechnungen zu ermöglichen, wird im Rahmen dieser Arbeit insbesondere ein Programmsystem (M^3O) zur Durchführung von neutronenphysikalischen Berechnungen entwickelt. Dieses System baut auf existierende Computerprogramme auf (MCNP und ORIGEN2) und ist speziell für die Behandlung von Forschungsreaktorgeometrien optimiert. Zu den wesentlichen Charakteristika von M^3O gehört die Möglichkeit, komplexe dreidimensionale Reaktormodelle detailgetreu mittels *Mathematica* zu erzeugen. Diese Modelle können dann von dem Monte Carlo Neutronentransportcode MCNP verarbeitet werden. Zur Durchführung von Reaktorabbrandrechnungen wird von M^3O ferner eine optimierte Struktur von Abbrandzonen in der Brennstoffplatte von beliebigen Ein-Brennelement-Reaktoren ermittelt. Dieses hier entwickelte Verfahren (*Adaptive Cell Structure*, ACS) ermöglicht besonders detaillierte Berechnungen in den wichtigsten Bereichen der Brennstoffzone. Die Abbrandrechnungen werden durch MCODE an MCNP und ORIGEN2 gekoppelt, wobei insbesondere die Neutronenflussverteilung in der Brennstoffplatte sowie lokale, abbrand-abhängige und spektrum-gemittelte Wirkungsquerschnitte mit Monte Carlo Methoden bestimmt werden.

Die Reoptimierung von Reaktorgeometrien zur Nutzung von Brennstoffen mit reduzierter Anreicherung geschieht über die Methode der Linearen Programmierung. Hierzu wird über Störungsrechnungen mit MCNP die Sensitivität des Reaktorkerns gegenüber Variation grundlegender Reaktorparameter ermittelt, so dass eine beliebige Zielfunktion (bspw. der thermische Neutronenfluss) unter Berücksichtigung von wesentlichen Nebenbedingungen maximiert werden kann. Um die wissenschaftliche Nutzbarkeit einer Anlage für eine gegebene Umstellungsoptionen beurteilen zu können, wird schließlich ein einfacher Performance-Index herangezogen, der insbesondere auch den Schwierigkeitsgrad eines am Reaktor durchgeführten wissenschaftlichen Experiments über das Signal-zu-Untergrund Verhältnis berücksichtigt.

Zum Studium der grundlegenden neutronenphysikalischen Charakteristika von Ein-Brennelement-Reaktoren wird zunächst ein sogenannter ‘generischer’ Reaktor (*Generic Single Element Reactor*, GSER) definiert und untersucht. Hierbei wird insbesondere die Sensitivität der Berechnungen gegenüber Variation wesentlicher Simulationsparameter von Abbrandrechnungen (Struktur der Abbrandzonen sowie Anzahl der Zeitschritte) ermittelt. Als zweites wesentliches Beispiel wird schließlich der Forschungsreaktor München II (FRM-II) zur Untersuchung herangezogen. Zum einen kann dadurch die Genauigkeit der $M^{3}O$ -Rechnungen für einen konkreten Anwendungsfall verifiziert werden. Zum anderen wird an diesem Fallbeispiel nun das Potential monolithischer Brennstoffe ermittelt und das Reoptimierungsverfahren angewandt.

Im konkreten Fall des FRM-II kann gezeigt werden, dass bei Einsatz von monolithischem Brennstoff eine Anreicherung von 28–32% ausreichend wäre, um den Reaktor ohne größere Modifikationen bei stark reduzierter Anreicherung zu betreiben. Die Anwendung des Performance-Index für eine ausgewählte Umstellungsoption zeigt dabei, dass die wissenschaftliche Nutzbarkeit der Anlage gegenüber dem HEU-Design nahezu unverändert bleiben würde ($\pm 1\%$).

Das Potential von monolithischen Brennstoffen zur Umstellung von Forschungsreaktoren wäre demnach enorm. Allerdings werden im Rahmen dieser Arbeit verschiedene neutronenphysikalische Effekte identifiziert, die auf den veränderten Brennstoffeigenschaften beruhen und deutlich machen, dass die Umstellung von Hochfluss-Reaktoren im allgemeinen eine Reoptimierung der Kernausslegung erforderlich macht. Darüberhinaus zeigen die Überlegungen in dieser Arbeit, dass moderne Computersysteme (wie z. B. *Mathematica*), die mit ‘traditionellen’ Berechnungscodes gekoppelt werden, äußerst effektive Methoden zur Untersuchung von Forschungsreaktoren darstellen können. Die Verfügbarkeit von solchen Programmsystemen, wie das im Rahmen dieser Arbeit entwickelte und vorgestellte System $M^{3}O$, kann somit einen wichtigen Beitrag zu den internationalen Umstellungsbemühungen leisten.

Contents

1	Introduction	17
2	Highly Enriched Uranium and Proliferation Potential	25
2.1	Low-Enriched versus Highly Enriched Uranium	26
2.2	Proliferation Potential of Research Reactor Fuel	30
2.2.1	Nuclear material associated with reactor operation	30
2.2.2	Net strategic value of nuclear material	33
2.3	Global HEU Inventories and its Present Use in the Nuclear Fuel Cycle .	39
3	Neutron Scattering Experiments and Reactor Performance	45
3.1	Applications of Research Reactors	46
3.2	Neutron Instruments on Research Reactors	47
3.3	Beam Requirements	50
3.3.1	Preparation of the beam	50
3.3.2	Instrument-specific requirements	51
3.4	Assessment of Research Reactor Performance	52
3.5	Precision of Neutron Experiments	54
4	Characteristics of Advanced Nuclear Fuels	59
4.1	Classes of Nuclear Fuels	60
4.1.1	Ceramic fuels	60
4.1.2	Dispersion-type fuels	61

4.1.3	Monolithic fuels	63
4.2	Data for Selected Materials	64
4.2.1	Uranium isotopics	64
4.2.2	Fuel compositions	65
4.3	Development of High-Density Fuels: Status and Perspectives	67
5	Mathematica and Research Reactor Geometries	75
5.1	Generation of a Base MCNP Input Deck	76
5.2	Elements of a High-Accuracy Computational System for Research Re- actor Burnup Calculations	82
5.2.1	Generation of an adaptive cell structure	82
5.2.2	Adaptive cell structures for burnup calculations	86
6	Components of the Computational System M3O	89
6.1	General Burnup Equations and Functionality of the System	89
6.1.1	Practical strategy of solution	93
6.2	Monte Carlo Method and MCNP	96
6.2.1	Basic principles of the Monte Carlo method	97
6.2.2	Variance reduction techniques	98
6.2.3	Development and release history of MCNP	99
6.2.4	Specific concepts and features of MCNP	100
6.2.5	Cross-section libraries and $S(\alpha, \beta)$ -tables	104
6.2.6	Monte Carlo precision	106
6.3	ORIGEN2	108
6.3.1	Development and release history	108
6.3.2	Input and output data	109
6.3.3	Method of solution	110
6.4	MCODE	112

7	Definition and Analysis of a Generic Single Element Reactor	121
7.1	Reactor Design and Core Model	123
7.1.1	Adaptive cell structure for GSER analysis	124
7.2	Analysis of the Reference Design	128
7.2.1	Neutron flux in moderator tank	128
7.2.2	Burnup calculations	129
7.3	Assessment of Results	136
8	Versatility and Accuracy of M3O and FRM-II Analysis	139
8.1	Reactor Design and Core Models	140
8.1.1	Design considerations of the original core	143
8.1.2	Base MCNP Models of FRM-II	144
8.1.3	Impact of boron ring	148
8.1.4	Adaptive cell structure for FRM-II burnup analysis	151
8.1.5	Installations in moderator tank	153
8.2	Analysis of the Original HEU Design	156
8.2.1	Neutron flux in moderator tank	156
8.2.2	Neutron spectrum in fuel plate	159
8.2.3	Cycle length	160
8.2.4	Power density distribution in fuel plate	161
8.2.5	Burnup and residual enrichment of fuel	165
8.2.6	Local fission rate and density	166
8.2.7	Actinide and fission product inventory at EOL	170
8.2.8	Neutron importance of actinides and fission products	173
8.2.9	Comparison of results with available FRM-II data	177
8.3	The 1999 Pre-Criticality Conversion Options	180
8.3.1	Characteristics of the 1999 options	180
8.3.2	Summary of results and comparison with ANL data	184

9	Reactor Optimization and Linear Programming	191
9.1	General Aspects of Research Reactor Design	193
9.1.1	Design principles of the original MTR	193
9.1.2	Reactors for neutron beam research	195
9.2	Basic Theory of Linear Programming	199
9.3	Implementation	201
9.3.1	Design variables	201
9.3.2	Objective function	202
9.3.3	Constraints	202
10	Optimization and FRM-II	207
10.1	Monolithic LEU Fuel in Original Geometry	208
10.2	Modifications to the Original Core Design	209
10.3	Preliminary Conversion Option Candidates	211
10.3.1	Option A1: Monolithic reference case	212
10.3.2	Options A2 and A3: Elongated fuel element	212
10.3.3	Option A4: Increased meat thickness	213
10.3.4	Option A5: Increased width of cooling channel	214
10.4	Comparison and Selection of Type A Options	215
10.5	Optimized Options with Reduced Enrichment	220
11	The Net-Impact of Conversion on Reactor Performance	229
12	Conclusion and Outlook	235
A	Enriched Uranium and Weapon-Usability	239
A.1	Critical Mass	239
A.2	Neutron Emission Rate	243
A.3	HEU in Nuclear Weapons	246
A.4	Plutonium versus Highly Enriched Uranium	248

B Plutonium Production in Research Reactors	253
C Relevant Research Reactors	261
D MCNP Sample Input Deck	269
E MCODE Sample Input Deck	285

Acknowledgments

This project was inspired and initiated by the *Interdisciplinary Research Group in Science, Technology, and Security* (IANUS) of Darmstadt University of Technology (TUD). Working with the members of the IANUS group has provided great stimulation and its support has been genuine and indispensable over the years. A very special thanks goes to my advisors Prof. Franz Fujara and Dr. Wolfgang Liebert, who had pointed towards the relevance of the subject and encouraged me to pursue this research project. Also, I want especially to thank Prof. Emeritus Egbert Kankeleit for having brought technical security analysis to TUD.

My interest in and knowledge of the field have both benefitted enormously from invitations to the *International Summer School on Science and World Affairs*. On behalf of many others, I would like to thank the organizers of these meetings, Dr. David Wright and Dr. Lisbeth Gronlund (UCS/MIT), for the terrific and irreplaceable work they are doing.

I have been fortunate to spend the period between September 2001 and August 2003 at the *Massachusetts Institute of Technology* with the Technical Group of the MIT *Security Studies Program*. This has been a fascinating experience for me and I am particularly thankful to my colleagues Dr. Allison MacFarlane, Dr. Marvin Miller, Dr. George Lewis, and Prof. Ted Postol for their outstanding support and innumerable valuable discussions.

During my stay at MIT, I also had the opportunity to cooperate with MIT's Nuclear Engineering Department and became a 'temporary member' of the Physics & Core Group. I am deeply grateful to Prof. Mujid Kazimi for letting me join and interact with his distinguished team. I want to especially thank Dr. Eugene Shwageraus and Dr. Pavel Hejzlar for valuable discussions. A very special thanks goes also to Dr. Zhiwen Xu, who develops the MCODE computer system which became a part of M³O presented in this thesis. I am extremely grateful to Zhiwen and Prof. Kazimi for permission to use the code, even though I have left MIT in the meantime.

The focus of this thesis is on the conversion of research reactors to low-enriched fuel for nonproliferation reasons. The principal international scientific community and audience for this field of research is represented by the RERTR (Reduced Enrichment for

Research and Test Reactor) program and the respective international meetings held annually. I have been fortunate to participate and present my work at these conferences since 1999. The feedback I received and the contacts I made were essential to guarantee the quality of my work. I have benefitted enormously from discussions with Dr. James Matos, Dr. Jim Snelgrove, and Dr. Gerard Hofman. In addition, a most special thanks goes to Dr. Nelson Hanan, who always had time to discuss tedious technical details of neutronics calculations related to my progressing work.

A research project of this scope would have been very difficult to perform without continuous discussions with and feedback from my colleagues at TUD who shared the office with me: Matthias Englert and Christoph Pistner read and re-read chapters of this work in its final stages and their comments were extremely valuable. Christoph and I cooperated for many years on our respective projects. I am deeply grateful for that opportunity and think that we were a perfect team indeed.

I am extremely grateful to the sponsors and foundations that supported this research project over the years. I want to especially thank the IANUS group again for providing financial and administrative support; the Social Science Research Council (SSRC) that made possible my stay at MIT with a generous 2-year fellowship, and the Berghof Foundation for Peace and Conflict Research that supported this research project with a research grant awarded to the IANUS group. I owe these sponsors a lot for their support of this project and the confidence in its academic value and relevance to global security.

For his remarkable help, I would like to thank Bruce Harper, my friend from Wisconsin in Valencia, who proof-read the English language of this text. It must have been exhausting. No doubt, however, mistakes remain and I alone am responsible for them. I am also deeply grateful to Brigitte Schulda, the assistant of the IANUS group, for her professional assistance and company. Getting the work done would have been impossible without her.

Finally, I want to thank my parents who always supported my 'strange career' throughout the years. Above all though, I am grateful to my wife Paloma and I can't possibly express my gratitude adequately. *¡Que suerte he tenido de encontrarte!*

Abbreviations and Acronyms

ACS	Adaptive cell structure
BOL	Beginning-of-life
EOL	End-of-life
FRM-II	Forschungsreaktor München II
GSER	Generic single element reactor
IAEA	International Atomic Energy Agency
INFCE	International Nuclear Fuel Cycle Evaluation (1978–1980)
LEU	Low-enriched uranium
HEU	Highly enriched uranium
M ³ O	<i>Mathematica</i> -MCODE-MCNP-ORIGEN
MCODE	MCNP-ORIGEN Depletion
MCNP	Monte Carlo N-Particle, formerly known as Monte Carlo Neutron Photon
MT	Metric tonne, 1000 kg
MTR	Material Testing Reactor, 1952–1970, Oak Ridge National Laboratory
MWd(th)	Megawatt-days-thermal, 8.64×10^{10} J
ORIGEN	Oak Ridge (National Laboratory) Isotope Generation and Depletion Code
RERTR	Reduced Enrichment for Research and Test Reactors
SWU	Separative work unit, also kgSWU and tSWU
WGU	Weapon-grade uranium, HEU enriched to 90–93% in U-235

Chapter 1

Introduction

The end of the Cold War has created a new climate for international action to eliminate nuclear weapons, a new opportunity. It must be exploited quickly or it will be lost.

[Canberra Commission, 1996]

Less than a decade ago, the vision of complete and irreversible nuclear disarmament appeared as a consequent ultimate outcome of the unprecedented progress that was being made in disarmament and the radical steps that were being taken to support this process. Since then, the international climate has fundamentally changed and, as the Canberra Commission had warned, a historic opportunity has indeed been lost. The events of September 2001, and the response to them, certainly mark an important turning point in this transformation.

In particular, but not only, the nuclear-weapon states currently consider progress in nuclear disarmament of secondary relevance, arguing that the possibility of nuclear terrorism and the (further) proliferation of nuclear weapons pose the most serious threat to global security. Nevertheless, it is widely recognized that a revitalization of the nuclear disarmament process is essential to reduce the ‘demand’ for these weapons and a precondition to prevent the proliferation of nuclear weapons in the long term. Most recently, this requirement has been re-emphasized in the final report of the U.N. *High-level Panel on Threats, Challenges and Change* [United Nations, 2004] — and it’s also, of course, the fundamental bargain underlying the Nonproliferation Treaty.

In spite of the current standstill in nuclear disarmament, there are fortunately important related areas where the objectives and interests of the international community clearly coincide. In particular, there is now a broad international consensus about the importance and urgency of consolidating and reducing the stockpiles of nuclear-weapon materials located around the world. These measures are important because they lower

proliferation risks due to the potential diversion or theft of nuclear material. At the same time, reducing and eliminating excess stocks of these materials strengthens the nonproliferation regime in general and, ultimately, also supports irreversible nuclear disarmament.

In this context, highly enriched uranium (HEU) has attracted particular public and political attention. Several characteristics of HEU make it the material of choice for low-tech proliferators. In contrast to plutonium, it is relatively easy to handle and conceal due to its low level of radioactivity and, more importantly, only HEU can be used in the most basic weapon-design based on the so-called gun-type method. There is now a broad international consensus that this material has to be removed from the nuclear fuel cycle as soon as possible.

The current civilian HEU stockpile has been estimated to about 50 metric tonnes, which is much less than the inventory reserved for military purposes, but still enough for several thousand nuclear weapons or explosive devices. Virtually all of the civilian weapon-grade uranium is associated with the present or former use in HEU-fueled research reactors. During the 1960s, a large number of research reactors started to use HEU and, as a result, almost 50 countries received highly enriched uranium to fuel these facilities (Figure 1.1). Many HEU-fueled reactors have been shut down or converted to low-enriched fuel since then, but more than 100 reactors worldwide still use HEU in their cores.

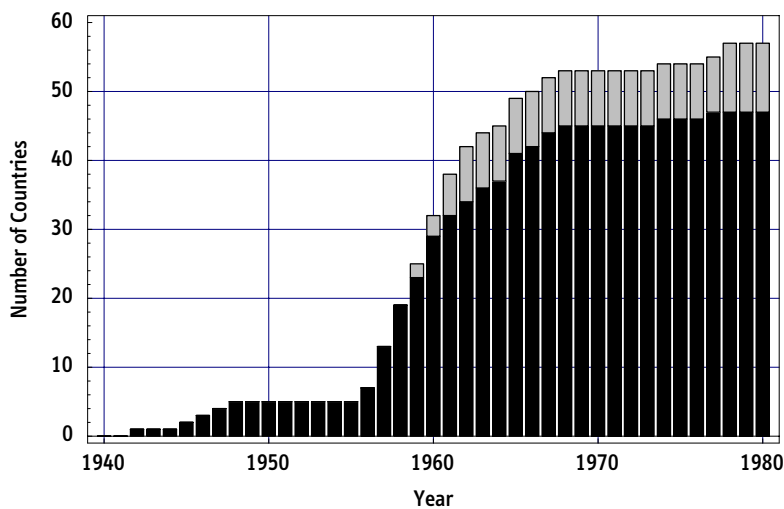


Figure 1.1: Number of countries operating research reactors and year when first facility went critical: total number (gray) and HEU (black).

Note that some reactors supplied within the *Atoms For Peace* Program between 1956–58 were fueled with low-enriched uranium at first and started to use HEU only after the export of this material had been authorized in the U.S. in 1958. Nevertheless, in this figure, these reactors are marked as HEU-reactors from their respective dates of first criticality. Data based on IAEA research reactor database handbooks.

Eliminating HEU from the civilian nuclear fuel cycle therefore requires a two-pronged approach. First, legacy materials stemming from the former use in research reactors, which are usually still being stored at the respective reactor sites worldwide, have to be consolidated and, ultimately, down-blended to low enrichment. Second, the remaining operational HEU-fueled research reactors in the world have to be converted to low-enriched uranium to eliminate the demand for fresh HEU. The latter has significantly dropped since the creation of the *Reduced Enrichment for Research and Test Reactors* (RERTR) Program in 1978, but still amounts to about one metric tonne per year.

Both areas have gathered considerable new momentum since 2002. Major national and international programs have been launched recently to carry out a complete global ‘cleanout’ of highly enriched uranium and other high-risk materials. Similarly, for the first time, the conversion of *all* research reactors worldwide has been defined as an explicit objective with a target date for completion within a decade. However, while the global ‘cleanout’ of HEU is an uncontroversial undertaking, the conversion of research reactors is a more complex technical and administrative process, because the interests of reactor operators and users are involved. Potential criteria to guide a conversion process include minimum reactor core modification, minimum changes in operational characteristics and neutron flux values, minimum licensing problems, minimum fuel cycle costs, etc. [IAEA, 1980b, p. 13].

From a purely technical perspective, highly enriched fuel is always superior to low-enriched fuel due to the higher concentration of fissile U-235 and the lower parasitic absorption in U-238 — both characteristics that however also explain the weapon-usability of HEU. To overcome this disadvantage of low-enriched fuels, the development of advanced high-density fuels for research reactors began within the framework of the RERTR program, raising effective uranium densities in the fuel several-fold compared to the initial 1.0–1.5 g/cm³ that were achievable until the 1980s (Figure 1.2). The availability of these fuels is a prerequisite for meeting most of the technical and economic criteria relevant in a conversion process. In 2002, a new potential fuel-type with an extraordinary uranium density of 16 g/cm³ (monolithic fuel) was discovered, which is now becoming the subject of an important international R&D-effort.

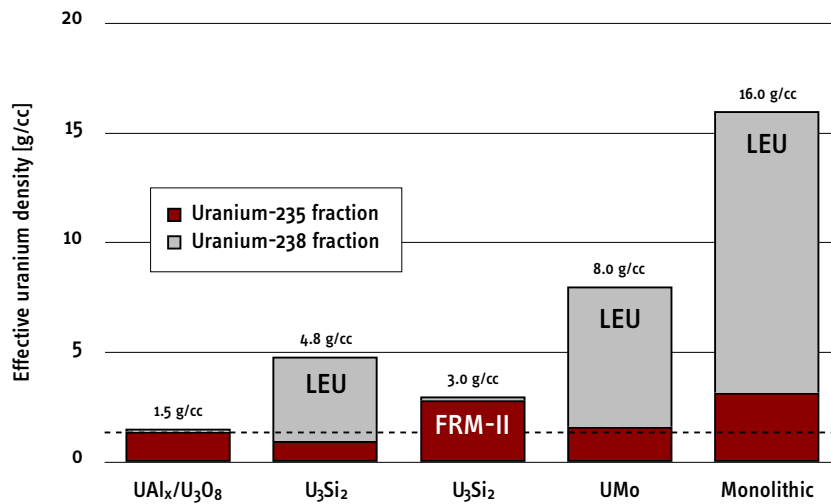


Figure 1.2: Effective uranium densities in research reactor fuels.

FRM-II is the only reactor worldwide that uses a uranium-silicide high-density fuel in conjunction with high enrichment. Reactor conversion is therefore particularly challenging and comparable U-235 densities can only be achieved with monolithic LEU-fuel, which is currently being developed.

The new spirit and urgency of converting the remaining HEU-fueled reactors to low-enriched fuel, combined with the prospects of new ultra-high-density fuels, provides the main impetus and defines the basic scientific objectives for this thesis.

- It is predictable that activities to convert existing research reactors will intensify in the near-term future, which in turn would simultaneously increase the need for corresponding neutronics calculations. Here, especially the analysis of the remaining high-flux reactors, which are most difficult to convert due to compact core geometries, may benefit from high-precision simulation tools to adequately set-up and study reactor parameters using complete three-dimensional core models.¹

The scope of the present thesis is to support this process in providing a new computational tool for neutronics calculations (M^3O), which is based on standard physics codes, while using the technical computing environment *Mathematica* as the primary user-interface. The use of such modern environments can be very convenient for a variety of reasons: their analytical capabilities allow for a broad range of calculations and data manipulation, while their interactive graphical

¹Most of the existing analytical work is focused on specific facilities and pursued by the reactor operators themselves or by other commissioned institutions. Little work is done from a more general perspective. In this context, the most prominent work has been performed by Argonne National Laboratory (ANL), which managed the RERTR program during the last 25 years. Similarly, the IAEA published a series of guidebooks to assist reactor operators in the conversion process [IAEA, 1980b, 1992].

user-interface facilitates intensive control of input parameters and interpretation of achieved results. At the same time, Monte Carlo methods play an increasing role in neutron transport and burnup analyses. In M^3O , the Monte Carlo code MCNP is employed, which offers the potential for high-precision modeling and analysis. Both major components, *Mathematica* and MCNP, are also used in an optimization tool developed below and based on the linear programming technique to optimize reactor performance by variation of the fundamental core parameters.

- The potential (and limits) of monolithic fuels, which can be roughly anticipated from Figure 1.2, is largely unknown today. Even though the conversion of a large number of medium-flux reactors would be relatively straightforward, the performance of monolithic fuel with low-enrichment in high-flux reactors is less obvious.

A second main objective of this thesis is therefore to study the neutronics performance of monolithic fuel for a specific type of high-flux reactors, namely the class of so-called single element reactors. These reactors can be considered to be the most difficult to convert to low-enriched fuel because they are characterized by very compact and inflexible core designs. Every existing reactor of this design still uses highly enriched uranium. In addition to a generic single element reactor, which is introduced for more fundamental purposes, the German research reactor FRM-II will be the primary test-case for the evaluation of monolithic fuel performance because it would be an obvious candidate to use this fuel in the future. As illustrated in Figure 1.2, conversion of FRM-II is also particularly challenging from a technical perspective.

In Chapter 2, the use of highly enriched uranium in the nuclear fuel cycle and its proliferation potential are reviewed from a technical perspective. The most important differences between low-enriched and highly enriched uranium are discussed, particularly with respect to weapon-usability, and the proliferation potential of research reactor fuel quantified. This analysis reconfirms that, from a nonproliferation perspective, an enrichment of (just less than) 20% indeed represents the optimum enrichment level for research reactors. Global HEU inventories and its present use in the nuclear fuel cycle conclude this introductory chapter.

Several appendices provide supplementary information on proliferation risks associated with the use of nuclear-weapon materials in the nuclear fuel cycle, i.e. aspects that are only briefly addressed in Chapter 2. To appreciate and correctly assess these risks, some technical data and considerations on the weapon-usability of enriched uranium are discussed in Appendix A. Fundamental properties of HEU are compared to those of plutonium, which illustrates their respective proliferation-relevant characteristics and the need to address these two nuclear-weapon materials with specially designed

nonproliferation strategies. Appendix B provides additional data on the plutonium production potential of certain reactor-types. Tables listing research reactors that are relevant in the conversion context are made available in Appendix C.

The primary focus of this thesis is on modern high-flux reactors used for neutron beam research and the possibility of fueling these facilities with low-enriched uranium. Chapter 3 summarizes the basic requirements on reactors and instruments from a user's perspective. A relatively simple performance index is suggested using maximum thermal and fast neutron fluxes to characterize reactor performance for neutron beam research in more detail. This index will be used later to assess corresponding results of neutronics calculations.

Chapter 4 introduces the primary classes of nuclear fuels that are (or have been) used in research reactors. Particular emphasis is placed on those fuels that are potentially relevant to the conversion of research reactors to low-enriched fuel, i.e. on high-density fuels developed specifically for that purpose. Data for selected materials and fuels that are used for the simulations in the main parts of the thesis are defined for reference purposes. Chapter 4 closes with a short overview of the status and the perspectives of high-density fuel development, summarizing current problems and perspectives as well as the R&D schedule for the next few years.

Chapters 5, 6, and 7 are mainly dedicated to a presentation of the conceptual approaches and the methodology used for subsequent analysis. Virtually all calculations performed are based, at least partially, on results generated with the Monte Carlo neutron transport code MCNP, developed at Los Alamos National Laboratory, which is generally considered the reference code for neutronics calculations. Designing detailed and faithful three-dimensional reactor models for MCNP is therefore a prerequisite for reliable and accurate results. *Mathematica* is used as the primary tool to generate MCNP input decks for single element reactors, and Chapter 5 introduces the conceptual approach to guarantee the most faithful models.

The basic MCNP input decks generated with this approach can be used for neutronics calculations aimed at determining 'static' properties of the reactor under consideration. This includes, in particular, the maximum neutron flux, which is generally among the most important characteristics of a research reactor used for neutron beam research. The second fundamental use of *Mathematica* is in the preparation of highly-accurate burnup calculations for single element reactors and Section 5.2 presents the essential elements of this system. In using a power density profile generated with MCNP for the fuel plate at BOL, a search-algorithm programmed in *Mathematica* identifies an optimum structure of burnup zones (adaptive cell structure, ACS) and generates the corresponding MCNP input deck. Due to the associated complexity of the required cell- and surface-cards, this approach would be practically infeasible without using a modern technical computing environment, such as *Mathematica*.

The functional elements provided by *Mathematica* are the basis for the computational system developed in the framework of this thesis. This system, which is designated M³O (*Mathematica*-M³CODE-MCNP-ORIGEN2), is specifically designed for neutronics calculations for single element reactors. Prediction of the irradiation behavior of nuclear fuels is one central category of results produced with M³O. The fundamental burnup equations are therefore presented in Chapter 6, where practical strategies of solution of these equations are introduced and justified.

In addition, Chapter 6 presents the individual components of this system and introduces their respective principles and functions. Particular emphasis is on the Monte Carlo Method, being the central technique for all calculations performed in the framework of this thesis. As indicated, and in addition to the overarching role of *Mathematica*, M³O contains separate control- and physics-codes, which are M³CODE, MCNP, and ORIGEN2. Here, M³CODE is a linkage-code developed at MIT that automates sophisticated burnup calculations in combining the neutron transport code MCNP and the point-depletion code ORIGEN2 (Oak Ridge National Laboratory).

With the computational system M³O available, and equipped with the ACS formalism for optimum burnup-zones, comprehensive neutronics calculations for arbitrary single element reactors can be performed. Chapter 7 is included to address and study some fundamental aspects of neutronics calculations of this type. To this end, the previously mentioned generic single element reactor (GSER) is introduced, which is used subsequently to perform a series of comparative calculations targeted at a general performance assessment of the system. Particularly, a sensitivity analysis for important parameters of ACS burnup calculations is performed, and precautions that may have to be taken to guarantee reliable results are identified. Some aspects relevant to all neutronics calculations (such as neutron flux normalization) are discussed.

Sample MCNP and M³CODE input decks for the generic single element reactor discussed in Chapter 7 are reproduced in Appendices D and E for reference purposes.

Chapter 8 leads over to the last major part of this thesis, which is dedicated to an assessment of the potential of high-density fuels for conversion of research reactors to low-enriched fuel. The case of FRM-II is used as the primary test-case for this analysis because its conversion will gauge the limits of any LEU fuel. Specifically, Chapter 8 focusses upon a detailed discussion and analysis of the current HEU design, which *en passant* demonstrates the versatility and accuracy of M³O for complex neutronics calculations.

A brief discussion of results obtained for some earlier conversion options for the reactor, which have been defined by Argonne National Laboratory in 1999, closes Chapter 8. M³O results are compared to the data published by ANL.

Before turning to the identification of specific conversion options based on monolithic fuels, a method to optimize single element reactor performance is proposed in Chap-

ter 9. Based on the linear programming technique and using MCNP-based perturbation calculations, this approach can be used to identify a set of reactor design variables that optimizes an objective function (usually, the thermal neutron flux), while simultaneously satisfying a pre-defined set of constraint conditions. Prior to presenting the details of this optimization tool, some general aspects of research reactor design are re-introduced to motivate the specific approach. The discussion focusses upon the original design principles of MTR-type reactors as well as on specific requirements of reactors for neutron beam research.

Chapter 10 applies the optimization tool to the case of FRM-II, using ultra high-density monolithic fuel, while reducing the uranium enrichment as far as possible. The optimization process proceeds in two steps. First, preliminary conversion option candidates are identified (type A options). These options satisfy some minimum design criteria, particularly the cycle length requirement, but they are not optimized for best overall performance. The most promising candidate options are then used as a ‘zeroth-order’ design and subject to the optimization process based on the linear programming technique introduced in Chapter 9. As a result, the final monolithic fuel conversion options for FRM-II are identified (type B options).

To conclude and complement the analysis, in Chapter 11, the simple performance index proposed in Chapter 3 is applied to the optimized conversion options identified for FRM-II. With these last results, conclusions and potential further work are formulated in Chapter 12.

Chapter 2

The Use of Highly Enriched Uranium in Research Reactors and Its Proliferation Potential

The main focus of this thesis is on one particular nuclear-weapon material, highly enriched uranium (HEU), and its present use in the nuclear fuel cycle.

The use of HEU in research reactors is of particular proliferation concern for a variety of reasons. It is the last remaining civilian application of a direct-use material, which is particularly easy to use in a nuclear weapon or explosive device. The fact that HEU-fueled reactors have been and still are operated in about 50 countries in the world, has led to broad geographical distribution of the material in fresh and irradiated form, while fuel fabrication, transports, and long-term interim storage create additional proliferation risks.

Originally, all HEU was exclusively produced for military purposes and, indeed, those stocks that have been available for civilian applications stem from excess military production capacities. Huge quantities of HEU are in existence today, while the possibility of renewed production of this material for military purposes, in particular by the gas centrifuge, received considerable attention in the years 2003 and 2004.¹ Both, existing stocks and renewed production of HEU, are potential proliferation concerns and may pose serious threats to global security.

The following sections review the main facts relevant in this context. First, the basic characteristics of enriched uranium in relation to its usability in reactors and nuclear weapons are discussed. The definitions of low enriched uranium (LEU) and highly enriched uranium (HEU) are introduced and the rationale for this choice clarified. To substantiate the argument, the effective proliferation potential of research reactor fuel

¹For a discussion, see for instance [Glaser, 2004a].

is assessed based on cell burnup calculations for an MTR-type reactor. Specifically, this analysis demonstrates the usefulness of setting an enrichment limit of 20% as the conversion goal for research reactors minimizing the overall proliferation potential. Finally, a summary of the global HEU production history, the present stocks in the military and civilian sectors, and the geographical distribution of the material is compiled. In addition, the number and distribution of remaining HEU-fueled reactors are listed and their annual fuel consumption rates estimated.

2.1 Low-Enriched versus Highly Enriched Uranium

Two major uranium isotopes naturally occur in appreciable concentrations. These are uranium-238 and uranium-235, with current isotopic fractions of 99.29% and 0.71%, respectively.² The relative concentration of these two isotopes, i.e. the enrichment or U-235 weight fraction of a given material stock, can be changed with a variety of isotope separation techniques exploiting physical effects to separate the species. As a matter of fact, the enrichment level determines the main characteristics of any uranium composition both for reactor-use as well as for weapon-use. These macroscopic effects are a consequence of the fundamental nuclear data of the various isotopes.

Microscopic capture (n, γ) and fission (n, f) cross-sections of U-235 and U-238 are shown in Figure 2.2. Uranium-235 displays a high probability of fission after neutron absorption throughout the entire energy range, i.e. from thermal to fast neutron energies. On the other hand, the even-numbered uranium-238 is fissionable only above a threshold energy of about 1 MeV, below this threshold neutron capture dominates the total absorption cross-section of this isotope.

To achieve a self-sustaining chain-reaction based on a fuel containing a mixture of both isotopes, i.e. based on a fuel of a given enrichment, only U-235 is immediately useful in a thermal spectrum present in light-water cooled and moderated reactors. However, due to the low total capture probabilities in U-235 and U-238, relatively low enrichments (< 5 wt%) are sufficient to achieve critical configurations.

The situation is fundamentally different in a fast neutron spectrum, which is typical for fast reactors, but also relevant for nuclear weapons or explosive devices. As can be concluded from the cross-section ratios inferred from Figure 2.2, a fast chain reaction is readily achievable for very high U-235 fractions. The situation becomes more complex once U-238 is present in significant amounts. In the unresolved resonance region above

²Other uranium isotopes have decayed since their creation having half-lives of less than 10^8 years. Only trace amounts of U-234 (0.0055%) remain today, while U-236 is artificially produced during irradiation of uranium fuel in nuclear reactors. In the following discussion, the trace constituents U-234 and U-236 are ignored. See Table 4.2 for their typical relative abundances in enriched uranium compositions.

10 keV, the added capture cross-sections of U-235 and U-238 begin to compete with fission in U-235. As a result, the average number of neutrons released per absorption can be expected to decrease notably. Raising the U-238 fraction in a material, simultaneously promotes the relevance of inelastic scattering in the configuration, which reduces the mean energy of the neutrons in a fast spectrum. Once a significant fraction of the neutron population reaches the resonance region of U-238, neutron capture starts to dominate all other processes. For natural uranium, which contains only 0.71 wt% of the isotope U-235, no unmoderated critical mass exists.

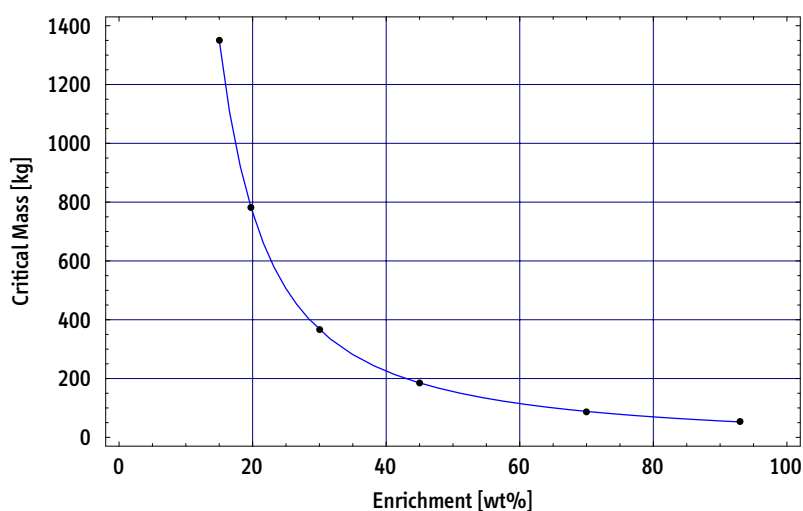


Figure 2.1: Critical mass of an unreflected (bare) uranium sphere as a function of the uranium-235 enrichment. MCNP 4B/C simulations at 300 K with ENDF/B-VI cross-section libraries. Assumed value of uranium density is 19 g/cm^3 . Enrichment is given in weight percent (wt%) for a binary mixture of U-235 and U-238.

As a consequence of these phenomena, the critical mass of uranium increases sharply as the enrichment of the material decreases. Figure 2.1 displays this behavior for an unreflected sphere of metallic uranium. The bare critical mass of uranium drops sharply from about 780 kg at 19.75% enrichment down to 53.3 kg at 93% enrichment.³

For a variety of reasons, the enrichment level is the crucial characteristic in determining the weapon-usability of uranium.⁴ Below a certain limit, weapon designers attest

³Only the general behavior is of importance here. Note however that absolute critical mass values can be reduced substantially by using neutron reflectors surrounding the fissile material. Even without explosive compression of the fissile material, the critical mass can be reduced by a factor of four with a beryllium reflector. For a discussion of weapon-relevant characteristics of HEU, see Appendix A.

⁴In addition to the higher critical mass, there are other factors that make the use of low-enriched uranium for the construction of a fission weapon more difficult or impractical. See Appendix A for a brief discussion of these aspects and additional critical mass data.

that the construction of a nuclear weapon or explosive device becomes impractical, even though not necessarily impossible. For this reason, low-enriched uranium (LEU) and highly enriched uranium (HEU) have been introduced: by definition, low-enriched uranium is characterized by a uranium-235 fraction of less than 20 wt%.⁵

The definition of LEU was first used by the U.S. Atomic Energy Commission in or prior to 1955.⁶ The same convention was later also adopted by the International Atomic Energy Agency (IAEA), which defines low-enriched uranium as “enriched uranium containing less than 20% of the isotope ^{235}U ” [IAEA, 2002, §4.12]. The IAEA classifies LEU as a so-called *indirect use material*, which in turn is defined as a nuclear material that cannot be used for “the manufacture of nuclear explosive devices without transmutation or further enrichment” [IAEA, 2002, §4.25 and §4.26].

From a technical perspective, the choice of the LEU limit is to some extent arbitrary. Likewise, the adequacy of the conversion goal for research reactors just below that limit (usually 19.75 wt%) is by no means obvious. Two factors are central in the process of defining the optimum enrichment level for research reactor fuel from a nonproliferation perspective: the weapon-usability of the fresh or irradiated fuel *and* the concurrent and inevitable plutonium production in the fuel during irradiation. Both aspects are explored in some detail below.⁷

⁵In the case of uranium-233, the LEU limit is set at 12 wt% due to the lower critical mass of this isotope. One can define a generalized definition of LEU by introducing corresponding weight factors for each fissile isotope. However, since U-233-containing uranium compositions are not used to fuel research reactors, the original LEU definition for U-235 is adequate and sufficient in the present context.

⁶Unfortunately, no official U.S. document could be identified that originally defined LEU and HEU. At the first Atoms for Peace conference held in Geneva in 1955 however, Alvin Weinberg reported that he had “just received information from my country that sample UO_2 -aluminum 20 per cent enriched fuel elements of the type which will be available to foreign countries have now been tested both in the LITR and in the MTR” (Session 9A, Vol. II, August 12, 1955, p. 430). Although, Weinberg does not use the term LEU in his paper nor in the discussion explicitly, his statements suggest that a policy was already in place distinguishing LEU and HEU. All domestic U.S. research reactors were HEU-fueled at that time. The export of HEU was authorized by the U.S. only in 1958.

⁷Armando Travelli, manager of the U.S. RERTR program, acknowledges this compromise in the proceedings of the first conference: “*The proliferation resistance of nuclear fuels used in research and test reactors can be considerably improved by reducing their uranium enrichment to a value less than 20%, but significantly higher than natural to avoid excessive plutonium production.*” [Travelli, 1978]. Similar arguments are used in the INFCE documents [IAEA, 1980a, Vol. 8, Section 4.2].

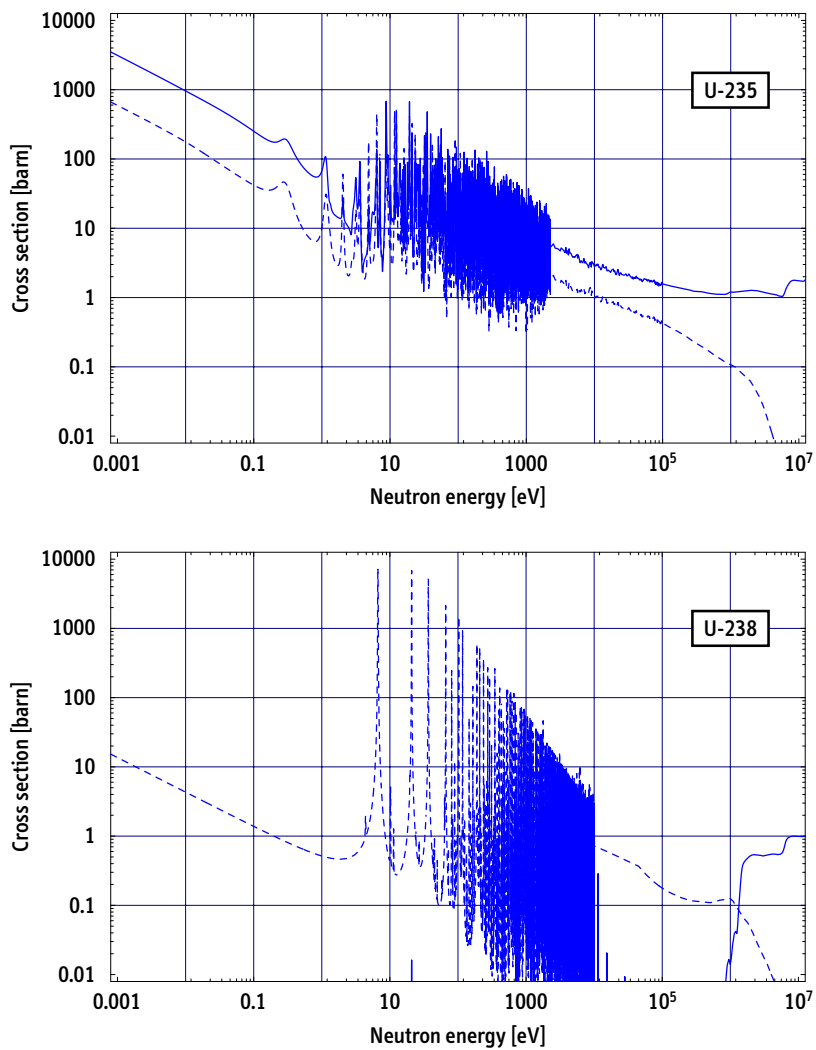


Figure 2.2: Fission (—) and capture (- -) cross-sections of U-235 and U-238.

Data from ENDF/B-VI.8 evaluation

2.2 Proliferation Potential of Research Reactor Fuel and Optimum Enrichment Level

The preceding section discussed the characteristics of enriched uranium in general and the weapon-usability of HEU in particular. Using HEU to fuel research reactors directly leads to a set of inevitable proliferation risks. However, in a complete technical analysis of the effective proliferation potential of research reactor fuel, at least two complementary aspects are relevant:

Weapon-usability of uranium. Any uranium composition with a U-235 content of at least 20% is classified as direct-use material, while uranium used in nuclear weapons is typically enriched to more than 90% (WGU, weapon-grade uranium). In spite of these facts and based upon data published in the open literature, it's nevertheless difficult to assess the net strategic value of a given uranium stock of intermediate enrichment, i.e. between 20% and 90%.

Plutonium production. The lower the enrichment level of any uranium-based nuclear fuel, the higher the plutonium buildup via neutron capture in uranium-238. In fact, plutonium production becomes the leading proliferation concern for reactors fueled with natural or slightly enriched uranium, while the uranium itself becomes rather unattractive.⁸

It is intuitively clear that it should be possible to identify an optimum uranium composition that suppresses plutonium buildup as far as possible while maintaining the initial uranium fuel equally unattractive for use in a nuclear weapon or explosive device. Detailed, albeit still idealized, scenarios for the operation of a generic MTR-type research reactor are defined and evaluated below.

2.2.1 Nuclear material associated with reactor operation

In order to get representative and reasonably accurate estimates of the spent fuel compositions required for the proliferation assessment below, cell burnup calculations are performed for a typical MTR-type reactor geometry using various initial uranium enrichments. These calculations are based on a computational system introduced later in this thesis (Chapter 6). Additional details and results of the calculations are presented in Appendix B.

The main results of these calculations used to assess the proliferation potential are summarized in Table 2.1. A variety of different fuel enrichments are studied, ranging

⁸See Appendix B for a brief discussion of dedicated plutonium production, in which natural or depleted uranium is irradiated to maximize plutonium buildup.

from 93% down to 5%. Below that limit, operation of a standard MTR-type geometry can be considered unrealistic, especially because of the low burnup that is achievable for such fuels. The effective U-235 density in all fuels is maintained constant by increasing the total uranium density for lower enrichments. The listed results are scaled to a 30 MW reactor and three different U-235-burnup levels are studied.⁹ Note that the irradiation time is not directly proportional to the burnup of the fuel due to the plutonium buildup and subsequent fission, an effect particularly pronounced for lower enrichment levels. Equivalently, the U-235 consumption per MWd(th) decreases for lower enrichment and higher average burnup of the fuel.

As expected, high enrichment minimizes the total mass of uranium required to fuel the hypothetical reactor. At the same time, plutonium production is minimal and amounts to less than 100 g per year of operation even for low burnup. Conversely, total fuel demand as well as plutonium production increase substantially for low-enriched or slightly enriched fuel.¹⁰

⁹U-235 burnup corresponds to the total fractional consumption of U-235 including fission, capture, and other processes.

¹⁰Even for lower enrichment levels, the total number of fuel elements to be handled essentially remains constant due to the increasing effective uranium density.

Enrichment	5%			10%		
Effective uranium density	18.96 g/cc			9.48 g/cc		
U-235 target burnup	20%	40%	60%	20%	40%	60%
Total in-core time of fuel	227.1 d	496.5 d	N/A	214.6 d	451.8 d	720.4 d
Annual uranium demand	1013.3 kg	463.4 kg		536.0 kg	254.6 kg	159.7 kg
U-235 consumption per MWd(th)	1.126 g	1.030 g		1.191 g	1.132 g	1.065 g
Average enrichment of spent fuel	4.1%	3.1%		8.2%	6.3%	4.3%
Total annual Pu production	3.464 kg	3.023 kg		2.046 kg	1.797 kg	1.534 kg
Average Pu-239 content	89.8%	79.5%		89.8%	79.2%	68.5%

Enrichment	19.75%			30%		
Effective uranium density	4.80 g/cc			3.16 g/cc		
U-235 target burnup	20%	40%	60%	20%	40%	60%
Total in-core time of fuel	208.3 d	429.5 d	668.1 d	205.9 d	421.0 d	648.8 d
Annual uranium demand	279.7 kg	135.6 kg	87.2 kg	186.2 kg	91.1 kg	59.1 kg
U-235 consumption per MWd(th)	1.227 g	1.190 g	1.148 g	1.242 g	1.214 g	1.183 g
Average enrichment of spent fuel	16.4%	12.8%	9.0%	25.4%	20.3%	14.5%
Total annual Pu production	1.228 kg	1.073 kg	0.910 kg	0.877 kg	0.765 kg	0.648 kg
Average Pu-239 content	89.7%	78.9%	67.8%	89.6%	78.7%	67.3%

Enrichment	45%			93%		
Effective uranium density	2.11 g/cc			1.02 g/cc		
U-235 target burnup	20%	40%	60%	20%	40%	60%
Total in-core time of fuel	204.2 d	415.0 d	634.2 d	201.4 d	404.7 d	610.5 d
Annual uranium demand	125.2 kg	61.6 kg	40.3 kg	61.4 kg	30.6 kg	20.3 kg
U-235 consumption per MWd(th)	1.252 g	1.232 g	1.209 g	1.270 g	1.263 g	1.265 g
Average enrichment of spent fuel	39.1%	32.2%	23.8%	87.9%	81.2%	70.1%
Total annual Pu production	0.604 kg	0.524 kg	0.442 kg	0.085 kg	0.076 kg	0.070 kg
Average Pu-239 content	89.6%	78.4%	66.5%	88.5%	73.5%	56.7%

Table 2.1: Nuclear material involved in the operation of a generic 30 MW MTR-type reactor operated for 300 days per year. Power density in the core and effective uranium-235 density in the fuel are maintained constant in all cases: 125 kW/l and 0.948 g/cc. All results based on cell burnup calculations performed with the code system presented in Chapter 6. Additional details in Appendix B.

2.2.2 Net strategic value of nuclear material

The main difficulty in assessing the strategic value of the fissile inventory associated with reactor operation is to compare the corresponding uranium and plutonium inventories and to make an estimate of their total strategic value, given the fact that either the uranium has to be separated from the fresh fuel and possibly further enriched or the plutonium has to be separated from the irradiated fuel. The feasibility of these two approaches depends upon the availability of the required nuclear infrastructure. The following analysis is therefore highly simplified in making inevitable *ad-hoc* assumptions in that respect. A case-by-case analysis would be required for a more detailed study, which is far beyond the scope of the discussion below.

Two assessment options are suggested in the following. Both are based on the fundamental assumption that a one-year's supply of fresh (unirradiated) fuel required to operate the reference reactor *and* a one-year's amount of spent fuel are available. The latter would be used for plutonium extraction, while assuming that the residual uranium contained in the spent fuel is discarded.¹¹

- Assessment A is based on the assumption that a limited amount of separative work, say from a laboratory or pilot-scale enrichment facility, is available to process diverted fuel. The objective would be to produce material enriched to weapon-grade (WGU, HEU at 93%) using the entire stock of pre-enriched uranium. The crucial assumption of this scenario is the choice of a fixed amount of separative work available for enrichment. In the analysis below, values between 10 kgSWU and 80 kgSWU are being considered.¹²
- Assessment B is based on the assumption that an enrichment below weapon-grade (93%), but above 20%, is indeed usable for a nuclear weapon or explosive device and that the additional technical obstacles can be overcome by the proliferator. No further enrichment is performed or needed. Obviously, for enrichment levels close to 20%, this approach is barely valid. To estimate the value of a given amount of uranium at a specified enrichment level, critical mass values for variable enrichment levels are used based on data listed in Table A.1 for a beryllium-reflected uranium sphere.

In both cases, the relative values of the uranium and the plutonium recovered are combined to produce an overall number for the strategic value of the material available.

¹¹The assumption that the uranium contained in the spent fuel would not be used in an actual proliferation scenario is somewhat unrealistic, especially for high initial enrichment levels, because its contribution to the total strategic value of the fissile material available may be significant.

¹²If much more enrichment capacity were available to the proliferator, there would be no need to divert the limited amount of safeguarded research reactor fuel. Instead, undeclared feed-stock of natural uranium could be used to produce HEU.

In the case of Assessment A, the equivalent amount of weapon-grade uranium (WGU) is determined with the standard expressions for uranium enrichment.¹³

$$\begin{aligned} SWU &= P V(N_P) + T V(N_T) - F V(N_F) \\ F &= P + T \\ N_F F &= N_P P + N_T T \end{aligned} \quad (2.1)$$

$$\text{with } V(N_i) = (2N_i - 1) \ln \left[\frac{N_i}{1 - N_i} \right]$$

The initial fuel inventory F with an isotopic fraction N_F of uranium-235 is processed with a given SWU capacity to produce the final product P with $N_P = 0.93$. The three unknown variables P , T , and N_T — the product mass, the tails (or waste) mass, and the tails enrichment — are determined one-to-one by the three above equations. Once the equivalent amount of the product WGU is known, the final estimate of the total strategic value is assigned via:

$$CM_A^* = \frac{m(\text{WGU})}{12 \text{ kg}} + \frac{m(\text{Pu})}{4 \text{ kg}} \quad (2.2)$$

The critical mass value CM_A^* introduced here combines the uranium and plutonium contributions with a weighting factor of 1:3 as can be obtained with reasonable accuracy from the data listed in Table A.1.

Even though the absolute value of CM^* will be of secondary relevance for the present discussion, note that the reference values used in (2.2) are lower than the values of the corresponding significant quantities (SQ) as defined by the IAEA. A significant quantity (SQ) of material is currently defined as 8 kg of plutonium of arbitrary isotopics, but with a content of less than 80% in the isotope Pu-238, and as 25 kg of highly enriched uranium, i.e. of any uranium composition with a U-235 fraction higher or equal to 20% [IAEA, 2002, §3.14]. Note that a significant quantity represents more material than is actually required to build a nuclear weapon in assuming that “losses due to conversion and manufacturing processes” are unavoidable.¹⁴ Yet, for instance, it has been confirmed that 4 kg of plutonium are sufficient to construct a nuclear weapon.¹⁵

¹³For a derivation and discussion, see for instance [Krass et al., 1983].

¹⁴Many scholars have argued that the current values of the significant quantities of plutonium and HEU are set too high and should be lowered considerably. For instance, Cochran and Paine [1995, p. 8] propose values of 1 kg and 3 kg for plutonium and HEU, respectively.

¹⁵“Hypothetically, a mass of 4 kilograms of plutonium or U-233 is sufficient for one nuclear explosive device” [RDD-7, 2001, Section V], declassified in 1994. Consistent with this fact, Willrich and Taylor

As indicated above, small separative work capacities between 10 kgSWU and 80 kgSWU are considered for Assessment A. If one assumes, for example, that centrifuge technology is available to process the feed material, a set of 50 machines could be used to produce 10 kgSWU in one month assuming that each centrifuge has an output of about 2.5 kgSWU/yr, a typical value for a first generation machine. Analogously, higher SWU production can be achieved with more machines, advanced technology, or an extended production period.

For Assessment B, expression (2.2) is modified to account for variable critical masses. Again, critical mass data for each respective enrichment level is used from Table A.1 in the Appendix.

$$CM_B^* = \frac{m(U)}{CM} + \frac{m(Pu)}{4 \text{ kg}} \quad (2.3)$$

Below an enrichment of 20%, the uranium contribution to CM_B^* is assumed to be zero based on the assumption that the use of the material for a nuclear explosive device is now impractical. No attempts have been made to characterize more accurately the weapon-usability of uranium at enrichment levels close to 20%. The strategic value therefore displays an artificial discontinuity at that point.¹⁶

Using the data generated with the burnup calculations discussed in the previous section and summarized in Table 2.1, expressions (2.1) through (2.3) are applied to determine strategic values for Assessments A and B. Numerical data are summarized in Tables 2.2 and 2.3 for a reference burnup of the fuel of 40% U-235. Figure 2.3 visualizes the strategic values CM_A^* and CM_B^* as a function of initial fuel enrichment.

The results of both assessments demonstrate that an enrichment level close to 20% does indeed minimize the strategic value of the fissile material involved in operation of a given MTR-type reactor. For enrichment levels of 15% and below, the plutonium component dominates proliferation concerns associated with research reactor fuel.¹⁷ For intermediate enrichments above 20%, the proliferation potential of the nuclear material strongly depends on the assessment type, i.e. on whether or not the uranium can or cannot be used without further enrichment. Nevertheless, the absolute values increase

[1974] define and use 4 kg of plutonium and 11 kg of weapon-grade uranium, i.e. the critical masses of the materials “inside a thick tamper of beryllium” (pp. 19–20), as strategically significant quantities in their analysis. One of the authors, T. B. Taylor, worked as a nuclear weapon designer at Los Alamos from 1949–1956. The designs of the smallest and the largest pure fission warheads in the U.S. nuclear arsenal are generally attributed to him.

¹⁶As previously indicated, the 20%-value does not represent a technical limit of a material’s weapon-usability. Ultimately, the usability depends upon the skills of the proliferator.

¹⁷Independently from the fact that plutonium production increases significantly for very low enrichment levels, such a fuel would be an inferior candidate for modern research reactors. For a specified U-235 inventory, very low-enriched fuel would require a larger core size, which reduces maximum neutron fluxes available for experiments.

in both cases above 20% and reach the maximum strategic value at 93% enrichment. The use of weapon-grade uranium to fuel a research reactor clearly maximizes the overall proliferation potential associated with research reactor operation.

The preceding discussion underlines the usefulness of the distinction between LEU and HEU. Uranium fuel below 20% virtually eliminates the possibility that the material could be directly used for the construction of a nuclear explosive device. Simultaneously and coincidentally, at an enrichment level close to 20%, plutonium production is sufficiently suppressed to minimize the total strategic value of the material — even if an attempt is made to enrich the available material. For both reasons, the 20%-limit represents a reasonable and arguably even optimum choice as a conversion goal for research reactors.

In addition, the availability of advanced nuclear technologies, for instance of a small capacity of gas centrifuges for uranium enrichment, does not change the research-reactor-related proliferation potential qualitatively. Both assessments (A and B) display a minimum at enrichment levels in the vicinity of the 20%-limit. That being said, it should be emphasized that it is still difficult and inherently ambiguous to estimate how rapidly the attractiveness or strategic value of enriched uranium increases between 20% and weapon-grade uranium (WGU) enriched to 93%. Ultimately, attractiveness and net strategic value are determined by the experience and the skills of the proliferator. However, as will be briefly discussed in Appendix A, there is strong evidence that material enriched to 40–50% and higher can be used in a simple gun-type device. In that case, technical challenges to build a viable nuclear explosive device are drastically reduced, which highlights a special and unique proliferation concern of highly enriched uranium.

Fuel Enrichment	5%	10%	19.75%	30%	45%	70%	93%
Uranium Demand	463.4 kg	254.6 kg	135.6 kg	91.1 kg	61.6 kg	40.2 kg	30.6 kg
Plutonium Production	3.0 kg	1.8 kg	1.1 kg	0.8 kg	0.5 kg	0.3 kg	0.1 kg
WGU equiv. @ 10 SWU	0.5 kg	0.9 kg	1.6 kg	2.3 kg	3.7 kg	8.3 kg	30.6 kg
@ 20 SWU	0.9 kg	1.7 kg	3.1 kg	4.5 kg	7.0 kg	14.7 kg	
@ 40 SWU	1.8 kg	3.3 kg	5.9 kg	8.6 kg	12.8 kg	23.3 kg	
@ 80 SWU	3.5 kg	6.3 kg	10.9 kg	15.2 kg	21.2 kg	29.7 kg	
CM _A [*] @ 10 SWU	0.794	0.521	0.399	0.386	0.438	0.761	2.569
@ 20 SWU	0.832	0.591	0.525	0.570	0.718	1.294	
@ 40 SWU	0.906	0.725	0.761	0.905	1.201	2.008	
@ 80 SWU	1.047	0.973	1.174	1.457	1.897	2.542	

Table 2.2: Assessment A. Strategic value of available uranium and plutonium associated with one-year's operation of the reactor assuming that a small enrichment capacity is available to process fresh fuel. Reference burnup of the fuel is 40% U-235.

Fuel Enrichment	5%	10%	19.75%	30%	45%	70%	93%
Critical Mass of Uranium	very large	very large	143.8 kg	68.7 kg	35.5 kg	18.2 kg	11.7 kg
Uranium Demand	463.4 kg	254.6 kg	135.6 kg	91.1 kg	61.6 kg	40.2 kg	30.6 kg
Critical Mass Ratio	uranium considered not weapon-usable			1.32	1.74	2.21	2.62
Plutonium Production	3.0 kg	1.8 kg	1.1 kg	0.8 kg	0.5 kg	0.3 kg	0.1 kg
Critical Mass Ratio	0.76	0.45	0.27	0.19	0.13	0.07	0.02
CM _B [*]	0.76	0.45	0.27	1.51	1.87	2.28	2.64

Table 2.3: Assessment B. Strategic value of available uranium and plutonium associated with one-year's operation of the reactor assuming that no enrichment capacity is available and the material is weapon-usable as is. Reference burnup of the fuel is 40% U-235.

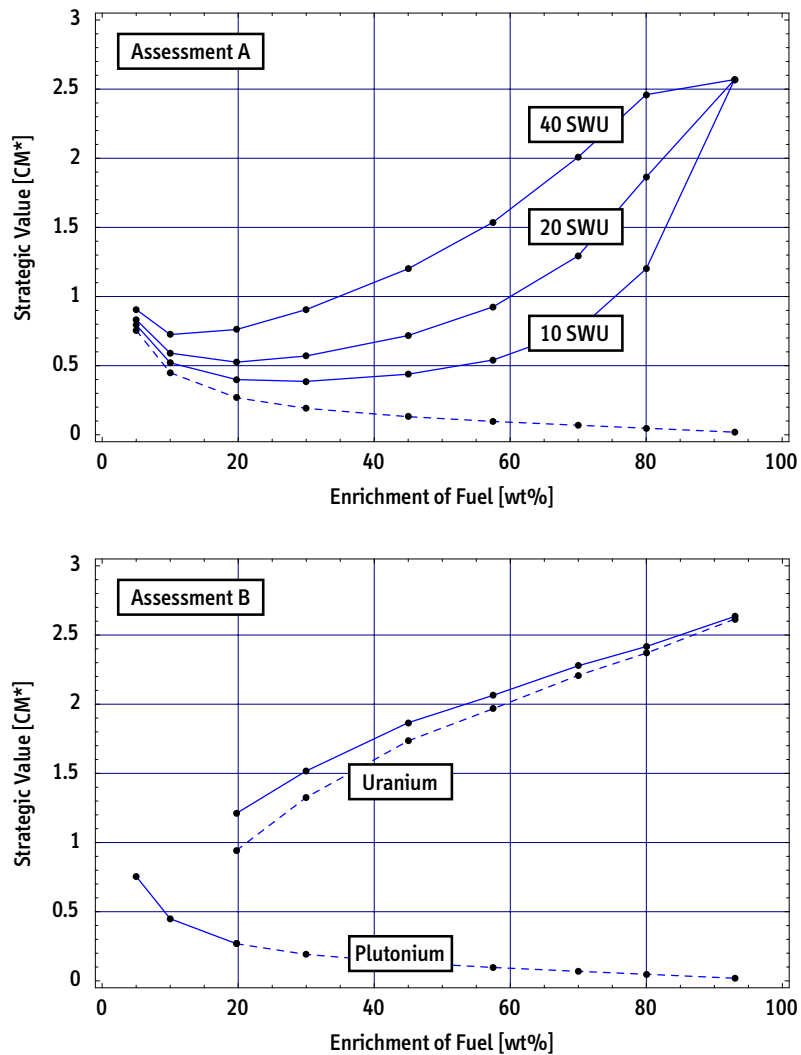


Figure 2.3: Assessment A: Strategic value of fissile materials associated with research reactor operation assuming that a given amount of separative work (SWU) is available to produce WGU. Dashed line indicates plutonium contribution to total value. Assessment B: Strategic value of fissile materials associated with research reactor operation assuming that uranium can be used directly. Dashed lines specify plutonium and uranium contributions.

2.3 Global HEU Inventories and its Present Use in the Nuclear Fuel Cycle

The production of enriched uranium began during World War II within the U.S. *Manhattan Project*. Although highly enriched uranium (HEU) was available at an early stage and employed in the nuclear weapon that destroyed Hiroshima on August 6, 1945, the production capacity was extremely low at that time. Only after the war, the large U.S. enrichment facilities under construction were completed.¹⁸ Similarly, the Soviet Union, the U.K., China, and France acquired enrichment capacities for their respective nuclear-weapon programs until the 1960s. In the case of the U.S., annual production rates of both materials peaked in the early 1960s at 80 MT and 6 MT for HEU and plutonium, respectively [Albright et al., 1997, Chapters 3 and 4].

Reportedly, the enrichment of uranium to HEU is currently halted in the U.S., Russia, the U.K., France, and China.¹⁹ Table 2.4 summarizes the estimated world inventory of HEU in the military and civilian sectors. In order to compensate for different enrichment levels, the concept of the HEU weapon-grade equivalent (wg-eq) or weapon-grade uranium (WGU) has been introduced.²⁰

Today, the determination of military HEU inventories, especially the task of reconstructing the existence of certain quantities from available historic production information, is extremely complicated because known stocks of enriched uranium may be repeatedly transformed in quantity and composition during their life-cycles. For instance, a known quantity of medium enriched uranium may be further enriched at a later time or irradiated HEU, after its use in a research or naval reactor and subsequent reprocessing, may be (and has been) re-used as fuel for other purposes without re-enrichment. These activities, which rarely occur in the case of plutonium, make HEU accountancy rather difficult. To a large extent, these circumstances explain the large uncertainties of the data listed in Table 2.4.

Information on existing HEU stocks is relevant in the context of research reactor conversion for a variety of reasons. For one part, the existence of excess stocks may encourage

¹⁸These facilities were based on the gaseous diffusion process, in contrast to the calutrons used during the war. See [Krass et al., 1983] for a discussion of military enrichment programs.

¹⁹China has no declared policy, but stopped producing HEU more than a decade ago. Pakistan and India are producing HEU for their nuclear weapon or other military programs. North Korea is apparently also pursuing uranium enrichment in addition to plutonium separation for military purposes.

²⁰Plutonium inventories are not discussed here. See [Albright et al., 1997] for a respective extensive discussion. Total global inventories of separated military and civilian plutonium amount to about 500 metric tonnes. Remarkably, all major nuclear-weapon states procured themselves with significant quantities of HEU that exceed in every case the corresponding weapons plutonium inventory. The mass ratio of the world inventory of military HEU compared to the inventory of weapons plutonium is currently higher than six.

Military HEU stocks		Military HEU consumption	
Russia	700–1,300 t	Russia	1.3 t/y
United States	650–750 t	United States	2.0 t/y
France	25–35 t	France	?
China	15–25 t	China	0.0 t/y
United Kingdom	20 t	United Kingdom	< 0.2 t/y
Pakistan	0.6–0.8 t		
South Africa	0.4 t		
India	< 0.4 t		
Subtotal	1,410–2,130 t	Subtotal	~ 3.5 t/y

Civilian HEU stocks		Civilian HEU consumption	
Subtotal	~ 50 t	Subtotal	< 1.5 t/y

Table 2.4: Estimated HEU world inventory and annual consumption in reactors. All values are rounded. Military reactor-use in nuclear-powered submarines and surface vessels, civilian use in research reactors and some Russian icebreakers. Estimates for HEU stocks and consumption from [Albright et al., 1997], [Albright and Kramer, 2004], and [Chunyan and von Hippel, 2001].

reactor operators to assume that HEU can be made available for an existing or planned facility. Conversely, as long as HEU-fueled reactors exist, there is a certain reluctance of HEU owners and potential suppliers to blend-down this material to low enrichment.

A significant fraction of the global HEU inventory is still allocated for or used in nuclear weapons. An inventory of about 200–300 metric tonnes can be assumed to be absorbed in deployed nuclear weapons worldwide.²¹ The remainder effectively is and partially has been declared excess or surplus to military needs. So far, only the U.S. and Russia have made corresponding declarations. In a groundbreaking bilateral agreement, Russia has declared excess 500 metric tonnes of HEU (assumed weapon-grade), which are now being blended-down to LEU and purchased by the U.S. for commercial use. In March 1995, the U.S. declared 174 metric tonnes of HEU surplus to its military needs.²²

One reason to maintain larger HEU reserves than those which are actually reserved for nuclear weapons is for the potential use of this HEU in military naval reactors that include surface vessels and submarines (Table 2.4, right). Indeed, most U.S. excess weapon-grade HEU is being placed in reserve for use in naval reactors.²³ This stockpile

²¹See [Glaser, 2003] for this estimate.

²²Only 33 metric tonnes of this quantity are enriched to at least 90% [Albright et al., 1997, p. 93]. As a consequence, the specified 174 tonnes correspond to a much lower amount of weapon-grade equivalent HEU.

²³DOE official cited in [Albright et al., 1997, pp. 93–94].

is large enough to fuel the entire U.S. nuclear-powered fleet for “many decades” [ONNP, 1995, p. 28] and could therefore be well above 100 MT. The total annual demand of HEU for naval reactors has dropped to less than 4 metric tonnes due to a sharp decline of the world’s operational nuclear fleet after the end of the Cold War. HEU fuel continues to be used in about 150 nuclear-powered submarines and military surface vessels [Chunyan and von Hippel, 2001]. In addition, on the civilian side, there are seven Russian nuclear icebreakers and cargo ships operated by the *Murmansk Shipping Company* that consume about 500 kg of HEU per year.²⁴

The primary consumption of HEU in the civilian sector is associated with the operation of the remaining HEU-fueled research reactors worldwide. Their annual fuel demand adds up to about one metric tonne of HEU, of which the 23 reactors with the highest HEU consumption listed in Table 2.5 already require 670–880 kg annually.²⁵ There are still nearly 50 operational HEU-fueled research reactors with a thermal power of at least 1 MW in the world [IAEA, 2000].²⁶ Tables C.1 and C.2 in the Appendix list the research reactors worldwide that are relevant in the conversion context.

As a result of the broad installation of HEU-fueled reactors in the 1960s, HEU has been supplied to about 50 countries worldwide. Figure 2.4 shows the original geographical distribution of the material that resulted from these activities. The U.S. exported a total of about 26 MT of HEU to at least 30 countries and Russia (HEU) to more than 10 other countries. The remaining HEU has been provided by secondary suppliers that include China, France, and the U.K.²⁷ By virtue of the international efforts to convert research reactors to low-enriched fuel and to ship-back the irradiated fuel to its country of origin, at least ten of these countries no longer have any HEU on their territories today.²⁸

²⁴Author’s estimate. Data on Russia’s nuclear icebreaker and cargo ship fleet compiled by Oleg Bukharin, private communication, November 2002. There is conflicting information upon the enrichment of the fuel used in the reactors (KLT-40) that power these vessels. While some sources assume the fuel to be weapon-grade, other sources suggest that the fuel may be enriched to 40% only. No independent verification of the KLT-40 design data is possible at this time.

²⁵As indicated in Table 2.5, in a few cases, no estimate of the annual HEU demand has been available. The total HEU consumption quoted above therefore underestimates the likely actual value.

²⁶Reactors with at least 1 MW of thermal power require regular refueling, while facilities operated at lower power levels usually have a life-time core or all the fuel stored on-site. See Appendix C for tables of those reactors listed in the IAEA database and relevant in the conversion context. Note that the IAEA database is known to be incomplete. Nonetheless, it is the only reference with official information provided by the IAEA member states. As of September 2000, the IAEA database listed a total of 142 HEU-fueled reactors worldwide.

²⁷In addition, as listed in Table 2.4, HEU has been produced by a few more countries. Among those, only South Africa has now dedicated its HEU inventory, which it had originally produced for its nuclear-weapon program, to operate the local 20 MW research reactor.

²⁸As of 2004, removal of fresh *and* irradiated HEU has been completed in the cases of Austria, Brazil, Colombia, Denmark, Iraq, the Philippines, Slovenia, South Korea, Spain, Sweden, and Thailand. In addition, between 2002 and 2004, fresh HEU fuel had been removed from Bulgaria, the Czech Republic, Libya, Romania, and Yugoslavia in widely reported operations.

Country	IAEA Code	Name	Criticality	Power	Enrichment	HEU Demand
USA	US-0070	ATR	1967/07	250 MW	93%	120–175 kg/yr
USA	US-0137	HFIR	1965/08	85–100 MW	93%	91–150 kg/yr
Russia	RU-0024	SM-2	1961/10	100 MW	90%	43–110 kg/yr
China	CN-0004	HFETR	1979/12	125 MW	90%	75 kg/yr
Russia	RU-0013	MIR-M1	1966/12	100 MW	90%	62.2 kg/yr
Kazakhstan	KZ-0003	EWG-1	1972/01	60 MW	90%	?
France	FR-0017	HFR	1971/07	58.3 MW	93%	54.8 kg/yr
Germany	DE-0051	FRM-II	2004/03	20 MW	93%	40.5 kg/yr
Netherlands	NL-0004	HFR	1961/11	45 MW	93%	38.3 kg/yr
Belgium	BE-0002	BR-2	1961/06	80–100 MW	74–93%	29 kg/yr
USA	US-0204	MURR	1966/10	10 MW	93%	23.5 kg/yr
Germany	DE-0006	FRJ-2	1962/11	23 MW	80–93%	19.2 kg/yr
Poland	PL-0004	MARIA	1974/12	17–30 MW	36–80%	?
France	FR-0022	ORPHEE	1980/12	14 MW	93%	15.8 kg/yr
Russia	RU-0008	WWR-M	1959/12	18 MW	90%	3.7–14.4 kg/yr
USA	US-0126	NBSR	1967/12	20 MW	93%	13 kg/yr
South Africa	ZA-0001	SAFARI	1965/03	20 MW	87–93%	12.6 kg/yr
USA	US-0120	MITR-2	1958/07	4.9–10 MW	93%	1.6–12 kg/yr
Romania	RO-0002	TRIGA-2	1979/11	14 MW	20–93%	11.8 kg/yr
Russia	RU-0010	IVV-2M	1966/04	15 MW	90%	3.5–9 kg/yr
Kazakhstan	KZ-0002	IGR	1961/01	10 MW	36–90%	?
Australia	AU-0001	HIFAR	1958/01	10 MW	60%	8.1 kg/yr
Russia	RU-0014	IRT-T	1967/07	6 MW	90%	5.6 kg/yr

Table 2.5: Research reactors with the highest annual HEU demand.

See Appendix C for references and further details.

The total amount of HEU still present in the civilian nuclear fuel cycle, which includes fresh and irradiated but not yet shipped-back fuel, has been estimated to be approximately 50 metric tonnes [Albright and Kramer, 2004]. This material is largely stored as fuel elements in wet or dry storage at reactor sites or interim storage facilities. The most recent survey on spent fuel from research reactors, performed under the auspices of the IAEA and based on 210 out of about 550 reactors, listed 22,686 HEU and 40,184 LEU fuel elements stored worldwide [Ritchie, 1998].²⁹

Some of the proliferation risks associated with existing HEU stocks are being addressed by national and international programs, such as the U.S. *Foreign Research Reactor Spent Nuclear Fuel* (FRRSNF) acceptance program. Many independent analysts, however, have argued more recently to extend these existing efforts both in scope and funding [Bunn et al., 2002, von Hippel, 2004]. They urge to increase the rate of upgrades in the security of military and civilian stocks, to accelerate the disposition of declared excess HEU stocks (‘Accelerated HEU Blend-Down’), to consolidate civilian ‘orphan’ stocks, and to provide incentives to facilities around the world to give up their HEU or plutonium (‘Global Cleanout & Secure’). Due to the heightened public and

²⁹In addition to these numbers, another 32,932 assemblies were located in reactor cores. Only the number of assemblies and not the mass inventories were published. It is unlikely that more up-to-date or more detailed data will be released publicly in the future.

political concern about nuclear terrorism,³⁰ these proposals have received considerable attention since 2002. Most importantly, the major U.S.-sponsored \$450 million *Global Threat Reduction Initiative* (GTRI) has been launched in May 2004. Its main objectives have been endorsed by the participants from more than 90 member states at an international partner conference organized by the IAEA in September 2004.

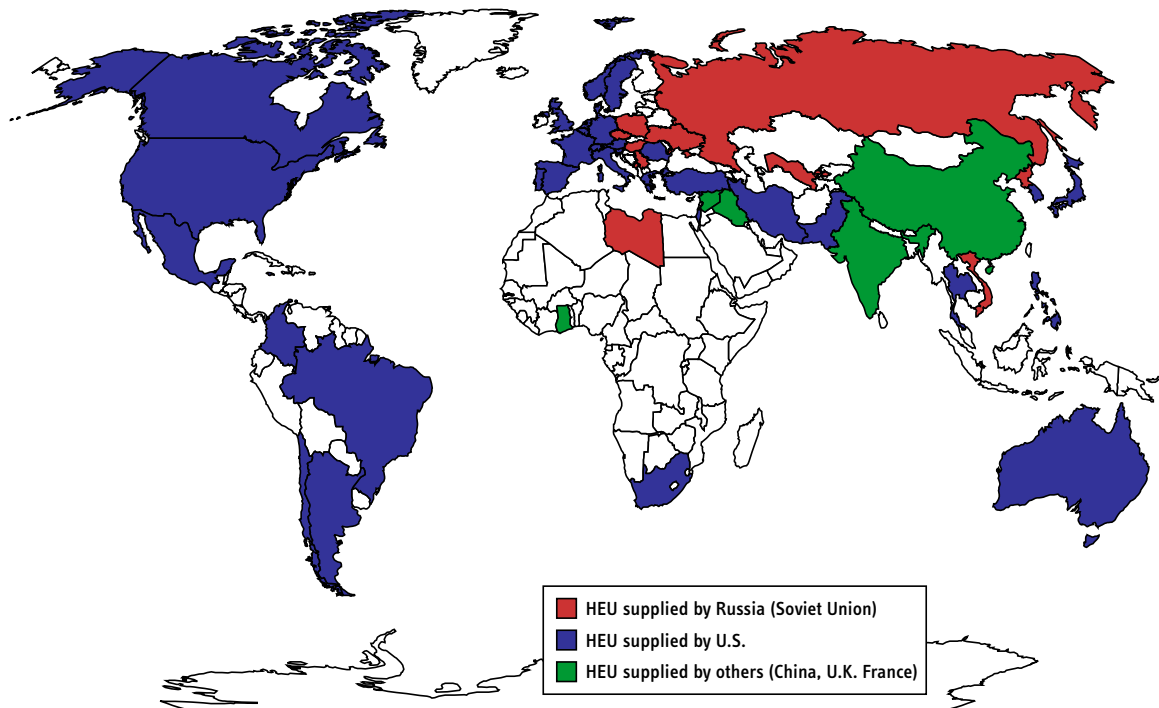


Figure 2.4: Geographical distribution of highly enriched uranium.

See Footnote 28 for the list of countries that do no longer have HEU on their territories (2004)

The GTRI almost exclusively addresses HEU-related proliferation risks and seeks to ‘repatriate’ fresh and irradiated HEU of U.S. and Russian origin within a decade and explicitly supports the conversion of the remaining HEU-fueled research reactors worldwide at the earliest possible date.

These initiatives are of utmost importance. It has to be emphasized, however, that they can be only partially successful as long as high-flux reactors are operated with HEU: as indicated in Table 2.5, these reactors require most of the fresh HEU today and the global annual demand of this material cannot be reduced substantially, if their conversion is not a top priority. While conversion of most of the remaining medium-flux reactors in the world is a relatively straightforward technical process, which is

³⁰In addition to the above-mentioned HEU-related issues, questions have been raised about the potential vulnerability of research reactors to sabotage [Bunn et al., 2003].

primarily determined by available funding and may therefore be strongly accelerated by the GTRI initiative, conversion of high-flux reactors — and of single element reactors, in particular — is not. High-flux reactor conversion depends upon the availability of very high-density fuels, and an internationally coordinated research and development effort may be needed to qualify these fuels within an adequately short time frame. In addition, the performance of these high-flux reactors is a critical criterion, and operators will be reluctant to support a conversion process if a more than marginal degradation in performance results.

The prerequisites for successful early conversion of high-flux reactors are therefore manifold. First, the general impact of conversion on the scientific usability of a given facility has to be estimated as accurate as possible. To this end, in the following chapter, the particular requirements of neutron-beam research are reviewed in order to develop a simple performance index for later use. Second, an assessment of the potential of the new high-density fuels for high-flux reactor conversion is needed. Chapter 4 summarizes the current status and perspectives of fuel development for research reactors. Ultimately, the neutronics calculations presented below (Chapters 7 and following) combine these diverse threads in using detailed three-dimensional reactor models to determine the performance of new high-density fuels with low-enrichment, which are currently being developed, in single element reactor geometries.

Chapter 3

Neutron Scattering Experiments and Research Reactor Performance

The purpose of this chapter is to give a brief overview on the main applications of research reactors with special emphasis placed on high-flux reactors, which are primarily used for neutron scattering experiments today. To this end, instruments used on research reactors are briefly introduced and the beam characteristics preferred by the various types of instruments discussed. In order to be able to assess the *relative* performance of various conversion options for research reactors later on, a simple performance index is suggested that can be used to assess neutron experiments of varying degree of difficulty (signal-to-noise ratio).

Research with neutrons contributes to many aspects of condensed matter research today. As the neutron does not carry electric charge, its primary interaction with nuclei is mediated via the short range strong nuclear force. The neutron-nucleus interaction can be well described theoretically (Born-approximation), which allows direct and unambiguous interpretation of experimental data. The neutron can therefore be used as a unique probe in a broad range of scattering experiments. The fundamental problem of neutron-based research, however, is the neutron's relative inaccessibility: free neutrons are difficult to produce, and even the strongest sources, based on the fission or the spallation process, provide extremely weak beam intensities compared to photon- or electron-beams. This circumstance explains the particular emphasis on both the maximum neutron flux level provided by the neutron source *and* on the most advanced instrumentation and measurement techniques employed in the analysis. These are, of course, important aspects that have to be taken into account when considering the conversion of a given research reactor to low-enriched fuel.

3.1 Applications of Research Reactors

Three broad categories can be distinguished for applications of neutron sources used today: these are basic research (scientific applications), medical applications, and commercial or industrial use. For completeness, in the case of research reactors, the additional categories of teaching and training may be added. Indeed, as shown in Table 3.1, the utilization of research reactors for these educational purposes, which is primarily targeted at students in nuclear engineering and reactor operators, still dominate the overall use of research reactors worldwide today.

Application	Reactors	Application	Reactors
1. Neutron activation analysis	71	6. Material structure studies	34
2. Teaching	68	7. Neutron radiography	32
3. Training	63	8. Transmutation	21
4. Materials or fuel tests	53	9. Geochronology	14
5. Isotope production	48	10. Neutron capture therapy	9
		Other uses	47

Table 3.1: Applications of research reactors today.

Table adapted from [Dodd et al., 2002, p. 52], data based upon a survey among operators

The requirements in terms of neutron flux, reactor facilities, equipment, personnel, etc. for these applications have been discussed in [IAEA, 2001]. Even though most of the applications listed in Table 3.1 benefit from a high average value of the thermal neutron flux,¹ medium-flux reactors are usually sufficient and adequate to meet typical requirements in all categories.

Due to its commercial relevance, radioisotope production belongs to the more challenging applications of research reactors. Radioisotopes play important roles in medical applications, commercial use, and basic research. The fundamentals of their production have been summarized in [Yeldon et al., 1986]. To a good approximation, the production rate directly increases with the neutron flux and with the total volume of irradiation positions, in which a given average neutron flux is surpassed. Even though there remain only a few major commercial suppliers of radioisotopes today, this activity provides the rationale for operation of a significant number high-power reactors, which are all classified as research reactors.

The primary use of neutrons in science is in neutron beam research to study the fundamental properties of nuclei and condensed matter, i.e. for material structure studies

¹Note however that some of the above-mentioned applications, namely teaching and training, do not even require a specific performance of the reactor at all.

using neutron scattering techniques.² It is widely recognized that this field of research places the highest demands on the neutron flux level and the spectral characteristics of the available neutrons. As will be illustrated below, the quality of a typical neutron scattering experiment mainly depends upon the counting statistics that can be achieved for a given beam or acquisition time, but also on the signal-to-noise ratio present at the probe or detector.

There are numerous discussions of the fundamentals of neutron scattering as well as of modern experimental techniques and detector technologies. Fender [1986] and Brückel et al. [2001] provide excellent overviews of the field,³ while Richter and Springer [1998] assess the future availability of neutron scattering facilities in the OECD countries and Russia. Applications in neutron scattering provide the main incentive to build and operate high-flux reactors today.⁴ The primary focus of this thesis is on these high-flux reactors, because those were and usually still are HEU-fueled. Due to the design concept of these reactors, they are also the most difficult to convert to low-enriched fuel.

3.2 Neutron Instruments on Research Reactors

Depending on the temperature of the moderator, thermalized neutrons are characterized by a wavelength that corresponds to typical interatomic distances or molecular dimensions (1–4 Å or 5–80 meV). At the same time, excitations in condensed matter, which are typically on the order of meV, can be easily resolved in the spectrum of the scattered neutrons. In other words, the neutron is simultaneously sensitive to the structure *and* the dynamics of matter.⁵ Two major classes of neutron instruments that

²Free neutrons can also be used to study the fundamental properties of the neutron itself. These include, for instance, the precise measurements of the half-life of the free neutron or of the upper limit of the charge of the neutron. Both quantities are relevant to theories in nuclear and particle physics [Wilson, 1986, Dubbers, 1997].

³Various contributions from [Brückel et al., 2001] are referenced in the following discussion. Note that these articles do not necessarily represent unique and original contributions to the field of neutron scattering theory or application — they do, however, give good and up-to-date overviews on their corresponding subjects.

⁴Irradiation and medical applications may also be performed at HFR's, but represent a category of subordinated relevance and are not further addressed in detail below. Particularly, the design of reactors for irradiation tests and radioisotope production is rather different from the design of reactors optimized for neutron beam research.

⁵Using special types of moderators and instruments, the spatial and temporal resolution of neutron scattering experiments can be extended to both lower and higher wavelengths (moderator temperatures) and momentum/energy transfers. Note also that the neutron couples to the electron-system in the probe via its spin and the associated magnetic dipole moment, which can be used to study the magnetic properties of materials. For practical applications, it is also of great importance that neutrons are weakly absorbed by most materials. For this reason, neutrons can be used with complex

are typically used on research reactors can therefore be distinguished: diffractometers and spectrometers. Table 3.2 summarizes some of the most important instrument-types in these categories and lists typical operational requirements for them.

Area of research	Instrument	Benefit of pulsed operation
Structural determination (Diffractometry)	Diffractometer	very high
	SANS	small
Dynamics (Spectroscopy)	Triple-axis spectrometer	none (disadvantageous)
	TOF (thermal)	small
	TOF (cold)	high
	Backscattering	none
	Spin-Echo	high

Table 3.2: Selected instruments on research reactors or spallation sources.

Diffractometers are sensitive to the momentum transfer that occurs in the scattering process and the static structure factor $S(\vec{Q})$, which is determined in a general diffraction experiment.

$$\frac{d\sigma}{d\Omega} \sim S(\vec{Q}) = \int_{\omega} S(\vec{Q}, \omega') d\omega'$$

With complete knowledge of $S(\vec{Q})$, one can directly determine the structure of the probe in real space, i.e. the parameters of the unit cell of the crystal (direct lattice). Important types of diffractometers used for ‘wide-angle’ scattering include the two-axis powder diffractometer and the single-crystal diffractometer. Depending on the particular type of probe or experiment, the requirements on these instruments can be quite different.⁶

In addition to the classic two-axis diffractometers, the technique of small-angle neutron scattering (SANS) has been developed more recently to study large structures of up to several thousand Ångstroms [Schwahn, 2001]. As the momentum transfer scales inversely with the length of scale of investigation, typical scattering angles are very small for this type of analysis. In order to obtain adequate resolution at the detector

sample environments as well as with scattering samples in bulk material.

⁶Neutron diffraction in fluids and glasses involves a broad range of relevant absolute momentum transfers, which has to be covered by the instrument, while the resolution may be of secondary relevance. In contrast, elastic scattering (Bragg-reflection) dominates diffraction in crystalline solids, which in turn puts a particular emphasis on very good resolution for this type of experiment [Heger, 2001].

position, the distance between probe and detector has to be as high as 10–40 m, where the scattered neutrons are typically counted in a two-dimensional area detector.

In spectroscopy, in addition to the momentum transfer, the energy transfer that occurs in an arbitrary (inelastic or quasi-elastic) scattering process is measured. Knowledge of the scattering function $S(\vec{Q}, \omega)$ can be used to reconstruct the dynamics in the probe.

$$\frac{d^2\sigma}{d\Omega dE} \sim S(\vec{Q}, \omega)$$

The phenomena that are studied with spectroscopic methods have evolved from excitation energies that are easily accessible (meV) to both smaller and larger energy transfers (from eV down to neV), which pose more challenging requirements on experiments and instruments. There is an extensive literature on methods and techniques used in neutron spectroscopy. For a general overview, see for instance [Monkenbusch, 2000]. The most widely used instrument in neutron spectroscopy is the triple-axis spectrometer. This ‘classical’ instrument is a direct extension of the two-axis diffractometer, with an additional analysator crystal added between probe and detector. As its name indicates, there are three relevant axes or angles, which are those between the neutron beam and the monochromator, the probe, and the analysator.

The second standard technique or instrument used in neutron spectroscopy is the time-of-flight (TOF) spectrometer [Monkenbusch, 2001]. Using short neutron pulses to define a time-origin, neutron energies are deduced from their time-of-flight between source and probe (monochromator side) and/or between probe and detector (analysator side). Various experimental setups using the time-of-flight technique are conceivable and widely employed.⁷ The requirement of neutron pulses to apply TOF-techniques suggests that research reactors and spallation sources will perform rather differently with this spectrometer-type. In particular, the use of choppers is required for reactors operated in the continuous-wave (CW) mode, which inevitably reduces the intensity of the beam by typically two orders of magnitude. With certain limitations, TOF-techniques are therefore preferably used with spallation sources. TOF-spectroscopy is particularly powerful for isotropic- or weakly anisotropic-scattering samples. In this case, large detector areas can be installed, which compensates for the low average intensity of a pulsed beam.⁸

⁷In addition to the classic TOF-technique, which uses monochromatic neutron pulses and determines the time-of-flight between probe and detector to measure the energy transfer, the so-called inverted TOF-spectrometer is of particular relevance for use in neutron scattering experiments: in this case, a neutron pulse characterized by a broader wavelength band (Maxwell spectrum) disperses between source and probe, while only one selected wavelength λ_0 is counted in the detector-bank. Depending upon the time-of-detection relative to the pulse, the original energy of the neutron can be inferred. In addition, the original neutron spectrum has to be measured by a monitor close to the probe.

⁸As indicated in Table 3.2, there are additional advanced types of instruments used in neutron spec-

3.3 Beam Requirements

Table 3.2 qualitatively specifies if a typical experiment carried out with a particular instrument-type benefits from pulsed operation of the neutron source, i.e. how research reactors generally compare against spallation sources. Most, but not all, instruments favor a pulsed mode and it is therefore important to differentiate correspondingly when assessing the relative performance of research reactors. It should be noted, however, that it is still inherently difficult to directly compare a continuous-wave neutron source with a pulsed source due to their characteristic advantages and disadvantages, which are partially counter-balanced with the respective preferred types of instruments used on them.

3.3.1 Preparation of the beam

A general dilemma of neutron sources is due to the fact that neutrons cannot be generated directly with exactly the characteristics (energy, direction, etc.) required for a given experiment. Instead, the neutrons are produced via the fission or the spallation process, which both display their respective process-inherent neutron-energy spectra. Typically, the neutrons are then exposed to a moderator (usually light-water, heavy-water, or graphite) to achieve thermal equilibrium with the medium. The neutron spectrum is now given by a Maxwellian energy distribution characterized by the temperature of the moderator.

In order to use these neutrons for a scattering experiment, a directed neutron beam has to be formed and adequately prepared. The preparation process can only be done by *selection*, i.e. by removing all ‘unsuited’ neutrons from the beam. Since higher energy- and spatial-resolution (monochromization and collimation) reduces the intensity of the beam, in general, a reasonable compromise has to be made between resolution and intensity of the neutron beam.

Most of the neutron scattering experiments require knowledge of the neutron’s energy with adequate precision prior to interaction with the probe. In the case of continuous-wave sources, the neutrons therefore have to be monochromized by either a velocity selector or by a monochromator crystal first. In this process, depending upon the

troscopy. A discussion of these measurement techniques is beyond the scope of this short overview, but the neutron spin-echo spectrometer [Monkenbusch and Zorn, 2001] and the backscattering spectrometer are of particular importance for modern neutron scattering experiments. Their energy resolutions range from several neV to μeV . In particular, the spin-echo instrument exploits the velocity change of the neutrons in the scattering process, i.e. emphasizes the neutron’s particle character, as the TOF-technique does. Pulsed sources are therefore preferable with this type of instrument. In contrast, the backscattering- or π -spectrometer is conceptually similar to the triple-axis spectrometer, which puts an emphasis on average neutron flux and CW-operation.

required energy resolution, a large fraction of the neutron flux is lost. In contrast, in pulsed sources that use neutrons from a spallation process, monochromization of the neutrons is often not required. Instead, neutron energies may be determined based on their time-of-arrival at the detector relative to the neutron pulse. This energy-dispersive (EDP) method permits broader exploitation of the wavelength-band and therefore reduces intensity losses. Even though this technique can be theoretically used with many types of instruments, both diffractometers and spectrometers, some are more suited than others, as will be briefly discussed below.

3.3.2 Instrument-specific requirements

For experiments on structural determination, the conventional (wide-angle) and the small-angle (SANS) diffractometers are the most common and most important types of instruments. Standard two-axis powder and single-crystal diffractometers are among the instruments that are able to fully exploit the peak neutron flux of pulsed sources, while SANS instruments cannot benefit from a pulsed neutron flux to the same extent. Inevitably, monochromization required for use with CW-sources drastically reduces the efficiency of the diffraction experiments because more than 95% of the neutrons in the beam are typically removed by the monochromator crystal to select the desired wavelength. Instead of employing this angular-dispersive (ADP) method, the energy-dispersive method can be used with diffractometers on pulsed sources. As discussed in [Heger, 2001], in this case, the sample is directly exposed to the polychromatic pulse of neutrons and the detector positioned at a fixed scattering angle. Neutron energies are then determined via a time-of-flight measurement.

This advantage of pulsed sources versus sources operated in a CW-mode is much less pronounced for SANS. Due to the large distance between probe and detector (10–40 m), neutron dispersion in the beam direction is significant. Under unfavorable experimental conditions, low energy neutrons from an earlier pulse would overlap with high energy neutrons from the following one. SANS experiments are therefore preferably carried out at research reactors, where pulse rate and neutron energy band can be adjusted specifically for each experiment.

In neutron spectroscopy, the triple-axis spectrometer is sensitive only to the average neutron flux (i.e. not the peak flux). As a result, this instrument is not well suited for pulsed sources, which are generally characterized by lower time-averaged neutron flux levels compared to high-flux reactors.

In contrast, TOF spectrometers *a priori* require pulsed operation, which favors their use with spallation neutron sources. Especially, if used with the inverted TOF-spectrometer, a (polychromatic) neutron pulse may be directly delivered to the probe without prior monochromization or velocity selection. Nevertheless, this inherent superiority of pulsed neutron sources for use with TOF-methods is less pronounced for

several types of experiments. Two fundamental problems emerge: repetition rate and wavelength resolution [Mezei, 2002, pp. 3.13–3.14].⁹ The neutron pulse length and the source to sample-detector distance determine the wavelength resolution on the instrument. Particularly, in the cases of SANS and TOF-spectroscopy with thermal neutrons, typical spallation source conditions are far from optimum, essentially because repetition rate and pulse length (or wavelength resolution) cannot be optimized independently for all types of instruments and experiments. High-flux reactors with flexible adjustment of pulse length and repetition rate are more efficient in these situations.

In conclusion, instruments that are most relevant for the use in research reactors, i.e. that preferably use the average and *not* the peak neutron flux, are primarily the triple-axis spectrometer, the backscattering spectrometer,¹⁰ and to a smaller extent SANS-instruments. Taking into account the various disadvantages and advantages of the two primary neutron sources (research reactors and spallation sources), it is nevertheless widely recognized that a pulsed source highly is superior to traditional CW-sources. Most importantly, it can be expected that some of the shortcomings of the pulsed and less flexible mode of operation of spallation sources can be overcome by the extended use of new neutron guide technologies (supermirrors), which allow the extraction of neutrons down to less than 1 Å. Furthermore, triple-axis spectrometers could be replaced by TOF spectrometers, if pulsed sources dominated the neutron source availability.

3.4 Assessment of Research Reactor Performance

The average thermal neutron flux is typically used as the main quantity to describe the generic performance of a research reactor — and the discussion in later chapters makes no exception in this regard. A more detailed analysis, however, and as the preceding discussion has shown, would have to be reactor- *and* experiment-specific to draw useful conclusions. Such a discussion is beyond the scope of this thesis, but as an example, main results of an assessment performed by Richter and Springer [1998] are summarized in Table 3.3 for some important high-flux and medium-flux reactors.¹¹

The main interest of the user is a maximum strength and quality of the neutron beam available at experimental positions. Instead of simply using the maximum thermal neu-

⁹A fixed repetition rate has to be chosen upon the design of the spallation source facility. In order to allow the full wavelength band to be accepted at the detector without frame overlap for a general scattering experiment, a conservative (low) repetition rate of about 20–100 Hz is typically preferred. This range of values is, however, in conflict with optimum repetition rates of high-power proton accelerators, which are on the order of 1 kHz.

¹⁰For the purposes of the present discussion, the backscattering spectrometer can be considered a special type of the triple-axis spectrometer.

¹¹The original analysis of Richter and Springer [1998] is focused on research reactors *and* spallation neutron sources used for neutron beam research.

Reactor	Thermal power	Institute	FOM	Availability
HFR	58 MW	ILL Grenoble	134.4	225 days/yr
FRM-II	20 MW	TU Munich	61.2	260 days/yr
HFIR	85 MW	ORNL	37.8	210 days/yr
Orphee	14 MW	ORS Saclay	70.0	240 days/yr
BER-II	10 MW	HMI Berlin	40.0	240 days/yr
FRJ-2	23 MW	FZ Jülich	40.0	200 days/yr
FRG-I	5 MW	GKSS Geesthacht	15.2	200 days/yr

Table 3.3: Performance characteristics of selected research reactors.

Figures-of-merit derived by and taken from [Richter and Springer, 1998], availability data are author's estimates

tron flux directly, a figure-of-merit (FOM) may be used to characterize the respective performance of a reactor for neutron scattering experiments. The specific definition of the figure-of-merit suggested in [Richter and Springer, 1998] incorporates the number of instruments n as well as a weight factor W for the thermal neutron flux.

$$\text{FOM} = n 2^{\log \phi^*} \quad \text{with} \quad \phi^* = \phi \cdot 10^{-13} \text{ (n/cm}^2\text{s)}^{-1} \quad (3.1)$$

Richter and Springer [1998] argue that a linear relationship between flux and weight factor “would heavily underestimate the importance of smaller sources” while a logarithmic scaling “would underestimate the great scientific value of high-flux sources” (p. 20). The suggested factor $W = 2^{\log \phi}$ has been identified as a compromise between both extremes and, according to the authors, been endorsed by a number of experts on neutron research. According to (3.1), typical weight factors are:

$$10^{13} \text{ n/cm}^2\text{s} \rightarrow W = 1 \quad 10^{14} \text{ n/cm}^2\text{s} \rightarrow W = 2 \quad 10^{15} \text{ n/cm}^2\text{s} \rightarrow W = 4$$

To obtain the figure-of-merit for a specific facility as listed in Table 3.3, the weight factors are multiplied by the total number of instruments available for neutron scattering experiments at the site [Richter and Springer, 1998, pp. 23 and 25]. In this process, all available instrument-types are treated equivalently.

In addition to the performance of the equipment as aggregated in the figure-of-merit, the availability of the reactor is an additional relevant aspect, which has not yet been accounted for and listed separately in Table 3.3. For obvious reasons, minimum reactor down-times are advantageous for the user.¹² Disregarding irregular shutdowns for

¹²Each experiment is executed within one cycle and only the figure-of-merit is relevant for it.

refurbishment, maintenance, etc., refueling operations dominate scheduled shutdowns of the facility. Specifically in the case of single element reactors, the achievable cycle length clearly determines their respective up- and down-times. 2–3 weeks are typically needed to discharge the fuel element, reload the core, and restart the reactor. The average number of fuel elements required annually largely explains the variations of the capacity factors of the facilities listed in Table 3.3.

In spite of the usefulness of such an approach that uses characteristic attributes of a given research facility (for instance the total number of instruments installed), a performance assessment based on aggregated numbers may also be misleading, in particular because each instrument is weighted equally. In the following, a simple performance index is developed that does not attempt to quantify the scientific usability of a neutron research facility in *absolute* terms, which is or would be required to compare distinct facilities among each other. Instead, only the *relative* performance of a given facility for different core geometry and fuel options is assessed. The following index estimates the relative variation of the beam time required to achieve the same relative error of the measurement depending upon the level of difficulty of a given experiment. Although, more limited in scope, this approach is sufficient and adequate in the present context.

3.5 Precision of Neutron Experiments

The precision of neutron scattering experiments is primarily determined by the count rates at the detector. In general, the maximum thermal neutron flux available in the moderator close to the core of the reactor directly scales the flux ultimately delivered to the instrument, even though the latter may be lower by several orders of magnitude.

For research reactors, the maximum neutron flux that is practically achievable is primarily determined by the requirements to divert and dissipate the energy released in the fission process. Assuming that one neutron per fission event is available for experiments, i.e. for other purposes than to maintain the chain reaction in the core, about 200 MeV per neutron have to be removed from the system. This value contrasts with the spallation process, where less than 50 MeV per neutron are released. For this reason, an inherent upper limit of the steady-state thermal neutron flux can be specified for research reactors:

$$\phi_{\text{th,max}} \approx 1\text{--}10 \times 10^{15} \text{ n/cm}^2\text{s}$$

At these flux levels and beyond, cooling requirements lead to severe mechanical and

Nonetheless, averaged over a large number of users and experiments, the availability factor of the facility determines its effective performance.

thermal-hydraulic problems that cannot be overcome with traditional designs of research reactors or any other neutron source based on the fission process.¹³

The considerations on relative measurement times presented below are mostly valid for scattering experiments on research reactors that are carried out relatively close to the neutron source, where the background is correlated more strongly to the fast neutron flux component penetrating the reactor shielding or escaping via the beam tubes. This is mainly the case for experiments carried out with thermal or hot neutrons, less so for cold neutrons, which are usually guided to remote experimental setups in the neutron guide hall. These instrument- and experiment-specific considerations have to be taken into account for a more differentiated assessment of the scientific usability of a modern high-flux reactor.

As discussed above, most — but not all — types of instruments benefit from high average neutron fluxes. These are the instruments primarily focused in the following. The total number of events N_{tot} recorded by a detector contains signal data N_{sig} and noise N_{noi} .

$$N_{\text{sig}} = N_{\text{tot}} - N_{\text{noi}} \quad (3.2)$$

The absolute error of the measurement decreases with \sqrt{N} . Furthermore, the count rates of the experiment N_{tot} and of a separate background measurement N_{noi} are assumed uncorrelated and random. In this case, the absolute error of N_{sig} can therefore be estimated to:

$$\Delta N_{\text{sig}} = \sqrt{(\Delta N_{\text{tot}})^2 + (\Delta N_{\text{noi}})^2} = \sqrt{N_{\text{tot}} + N_{\text{noi}}} = \sqrt{N_{\text{sig}} + 2 N_{\text{noi}}} \quad (3.3)$$

Introducing the signal-to-noise ratio f , the relative error of the signal can be written as follows.

$$\frac{\Delta N_{\text{sig}}}{N_{\text{sig}}} = \frac{\sqrt{N_{\text{sig}} + 2 N_{\text{noi}}}}{N_{\text{sig}}} = \frac{\sqrt{1 + (2/f)}}{\sqrt{N_{\text{sig}}}} \quad \text{with} \quad f = \frac{N_{\text{sig}}}{N_{\text{noi}}} \quad (3.4)$$

The ultimate objective of the analysis presented in later chapters is to compare two or more reactor configurations and to assess their relative performance. Measurements may be considered equivalent if their respective relative errors are identical.

¹³The highest thermal neutron flux available today is achieved in the Grenoble High-Flux-Reactor at the *Institute Laue-Langevin* (ILL) and reaches 1.5×10^{15} n/cm²s at 58 MW thermal power. The U.S. Advanced Neutron Source (ANS, 330 MW) was designed to for a flux of $5\text{--}7 \times 10^{15}$ n/cm²s, but was cancelled in 1995 in the planning stages of the project.

$$\frac{\Delta N_1}{N_1} \stackrel{!}{=} \frac{\Delta N_2}{N_2} \quad \text{or} \quad \frac{\sqrt{1 + (2/f_1)}}{\sqrt{N_1}} \stackrel{!}{=} \frac{\sqrt{1 + (2/f_2)}}{\sqrt{N_2}} \quad (3.5)$$

The (additional or reduced) acquisition time required for the same relative error of two results will be a crucial criterion in the following discussion. Assuming that the signal is proportional to the thermal neutron flux originating from the probe, the number of detected signal events is given by $N \sim \phi_{\text{th}} t$. Equation (3.5) can be reorganized correspondingly.

$$\frac{\phi_{\text{th},2} t_2}{\phi_{\text{th},1} t_1} \approx \frac{N_2}{N_1} = \frac{1 + (2/f_2)}{1 + (2/f_1)} \quad \text{and} \quad \frac{t_2}{t_1} \approx \frac{\phi_{\text{th},1}}{\phi_{\text{th},2}} \frac{1 + (2/f_2)}{1 + (2/f_1)} \quad (3.6)$$

For the limiting cases of very high and very low signal-to-noise ratios, equation (3.6) simplifies to:

$$f \gg 1 \rightarrow \frac{t_2}{t_1} \approx \frac{\phi_{\text{th},1}}{\phi_{\text{th},2}} \quad \text{and} \quad f \ll 1 \rightarrow \frac{t_2}{t_1} \approx \frac{\phi_{\text{th},1}}{\phi_{\text{th},2}} \frac{f_1}{f_2} \quad (3.7)$$

As expected, for high values of f , the signal-to-noise ratio is irrelevant for a comparison of two neutron sources. Only the relative strength of the signal is decisive in this situation. In the opposite extreme, i.e. under difficult experimental conditions, the relative acquisition time scales directly with f . In this case, the strength of the signal *and* the signal-to-noise ratio are both equally important for the overall performance of the experimental setup.

To proceed at this stage, the signal-to-noise ratio has to be characterized further. The discussion here follows the arguments outlined in an Appendix to [Axmann et al., 1999a] and [Axmann et al., 1999b]. The authors make two important assumptions about the origin and the magnitude of f :

- The noise measured at the detector is directly proportional to the fast flux ϕ_{fast} originating from the core of the reactor. This undesired flux component reaches the experimental setup, is slowed down in the shielding or other structural materials, and reaches the probe or the detector where it cannot be distinguished from the signal.
- The shielding of the reactor and the experimental positions in the neutron hall are designed such that the static (self) background C of the detector is approximately equal to the expected noise generated by the reference fast flux component. This is a plausible assumption, because there would be no benefit to improve or weaken the shielding substantially against ϕ_{fast} for a pre-defined (and inevitable) static background in the detector.

With these assumptions, f can be written as:

$$f = \frac{N_{\text{sig}}}{N_{\text{noi}}} \approx \frac{\phi_{\text{th}}}{C + \phi_{\text{fast}}} \quad \text{with} \quad C \approx \phi_{\text{fast}} \quad (3.8)$$

In the following, it is assumed that the shielding of the experimental setup was originally designed for the fast flux component of the reference core, i.e. $C = \phi_{\text{fast},1}$. The signal-to-noise ratios of the two experimental conditions are therefore given by:

$$f_1 \approx \frac{\phi_{\text{th},1}}{2 \phi_{\text{fast},1}} \quad \text{and} \quad f_2 \approx \frac{\phi_{\text{th},2}}{\phi_{\text{fast},1} + \phi_{\text{fast},2}} \quad (3.9)$$

To facilitate an ultimate comparison, the thermal and fast flux components of the situations are related via two performance factors α and β .

$$\phi_{\text{th},2} = \alpha \phi_{\text{th},1} \quad \text{and} \quad \phi_{\text{fast},2} = \beta \phi_{\text{fast},1} \quad (3.10)$$

The new signal-to-noise ratio f_2 can be expressed as a function of these factors and the original value f_1 as defined in (3.9).

$$f_2 = \frac{\alpha \phi_{\text{th},1}}{\phi_{\text{fast},1} + \beta \phi_{\text{fast},1}} = \frac{\alpha}{1 + \beta} \frac{\phi_{\text{th},1}}{\phi_{\text{fast},1}} = \frac{2 \alpha}{1 + \beta} f_1 \quad (3.11)$$

Combining (3.6) and (3.11) yields a general expression that will be valuable for a comparison of the relative performance of neutron sources. The expression for the relative acquisition times required for the same relative error of the results takes into account variations of the signal strength *and* is applicable for arbitrary difficulty levels of the experimental conditions characterized by the original signal-to-noise ratio.

$$\frac{t_2}{t_1} = \frac{1}{\alpha} \left[1 + \left(\frac{1 + \beta}{\alpha f} \right) \right] \cdot \left[1 + \left(\frac{2}{f} \right) \right]^{-1} \quad (3.12)$$

Figure 3.1 illustrates the general behavior of (3.12) for an arbitrarily chosen, predefined increase of the fast flux component ($\beta = 1.10$) correlated with three different values of the relative strength of the thermal neutron flux.

According to [Axmann et al., 1999a] and [Axmann et al., 1999b], the signal-to-noise ratio characterizes the difficulty level of neutron beam experiments as follows:

- Simple experiment with $f \approx 5$
- Typical experiment with $f \approx 1$
- Difficult experiment with $f \approx 0.15$

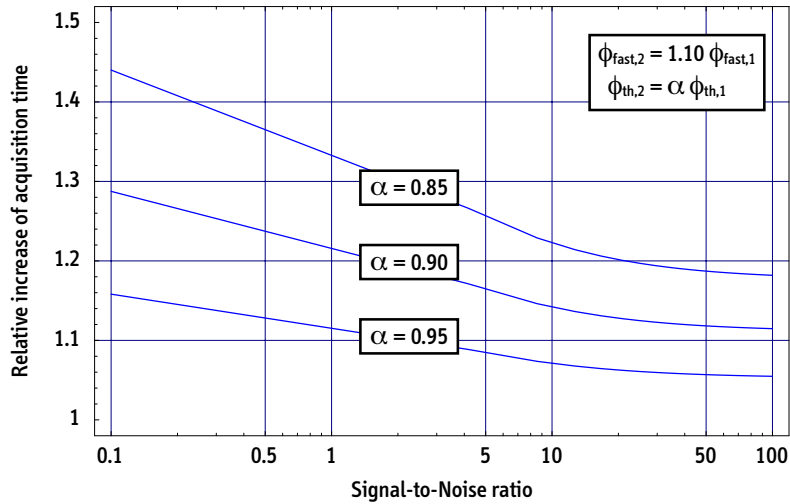


Figure 3.1: Relative increase of the acquisition time required for a constant relative error of the desired result as a function of the difficulty level of the experiment characterized by the signal-to-noise ratio. In the example shown, the fast neutron flux increase is fixed at $\beta = 1.10$. Three different loss-levels of the thermal neutron flux (signal) are plotted.

Consistent with this assessment, the exemplary data plotted in Figure 3.1 demonstrates that for large signal-to-noise ratios the relative increase of acquisition time is mainly due to the respective reduction of the signal. Conversely, the required acquisition time for a given relative signal strength increases under difficult experimental conditions. In the present example, a 10%-increase of the fast neutron flux, roughly leads to a two-fold increase of the additional beam time required when compared to a simple experiment.¹⁴ In a practical application, Equation (3.12) will be used in Chapter 10 to assess the relative performance of conversion options of FRM-II.

¹⁴Note however that the lower signal-to-noise ratio is a consequence of both the reduced signal *and* the increased noise. Even for constant fast flux, the acquisition time would increase in the present example.

Chapter 4

Characteristics of Advanced Nuclear Fuels Relevant to Uranium Enrichment Reduction Efforts

The use of highly enriched uranium (HEU) today as a nuclear fuel is limited to research reactors and naval propulsion reactors.¹ The rationale of maximizing the fissile density in the cores of these reactors is, mainly, to minimize the dimensions of the core while still accommodating an adequate total U-235 inventory in the fuel.² In the case of research reactors, compact cores allow for the highest neutron leakage rate, neutrons which are then available for experiments or for other purposes not-related to the maintenance of the chain reaction in the core.³

This chapter briefly introduces the classes of nuclear fuels that are relevant for potential use in research reactors of the MTR-type and define the basic terminology used in this context. A detailed discussion of nuclear fuel design, however, is far beyond the scope of this section and the reader is referred to the relevant literature [Olander, 1976, Frost, 1982]. Compositions of the reference fuels, which are used in the M³O computer simulations, are provided. Finally, the current status and perspectives of high-density fuel development are summarized. The potential qualification of so-called monolithic fuel is of particular relevance in the present context, because it would enable the conversion of the remaining HEU-fueled reactors worldwide.

¹Historically, HEU has also been used or tested in high-temperature reactors. However, all designs currently under consideration use low-enriched fuel, i.e. fuel enriched to less than 20%.

²See Section 9.1 for an overview of general design principles of research reactors.

³In the case of propulsion reactors, and in particular in the case of submarine reactors, a minimum core size may be preferable due to the constraints imposed by the surrounding structure of the vessel (minimum diameter of the hull), while the cycle length or life-time of the core is, again, of paramount importance to the operators.

4.1 Classes of Nuclear Fuels

MTR-type reactors in general, and high-flux reactors in particular, are operated at very high power densities and therefore require a high surface-to-volume ratio of the fuel.⁴ Plate-type or tube-type geometries are obvious candidates to satisfy this condition, although some Russian reactor designs also use ‘twisted’ cross-shaped fuel pins, which have comparable surface-to-volume ratios.

The design of a plate-type fuel compared to typical pin-type fuels is fundamentally different with respect to the retention of fission gases released during irradiation. In the case of pin-type fuels, fission gases are mainly accommodated in a gap between the fuel pellets and the cylindrical fuel cladding. In plate-type fuels, cladding and fuel zone (meat) are bonded, and a different mechanism has to be provided to accommodate the gaseous fission products and to support the swelling of the fuel. With the exception of the Caramel fuel, which is briefly discussed next, in plate-type fuels, fission gases are contained in the fuel zone itself, usually by a matrix material, in which the fuel particles are dispersed. The following discussion briefly introduces the main plate-type designs available today. Aluminum-based dispersion fuels are by far the most common type in use, but monolithic fuel may become an important alternative in the future.

4.1.1 Ceramic fuels

The most common ceramic fuel is uranium-dioxide (UO_2), which is primarily used in commercial power reactors. For this reason, extensive literature and experience exist for UO_2 -pin-type fuels. In research reactors, ceramic fuels are less common and less favorable due to the poor thermal conductivity of UO_2 and due to the difficulty of fabricating plates with this material. One exception to this rule is the so-called Caramel fuel, which was developed by the French CEA in the 1970s [Schwartz, 1978].

Caramel fuel consists of a large number of small uranium-dioxide pastilles (caramels), each about $2 \times 2 \text{ cm}^2$ and with a thickness of 1.5–4.0 mm. A layer of these pastilles is arranged on a rectangular surface, separated by a spacer grid. This fuel region is covered with two zircaloy plates to form the fuel plate itself. Such a design enables the fission gases released during irradiation of the fuel to be accommodated in the regions between the fuel pastilles. Caramel fuels were produced with low enrichment, usually below 10%, and used in some French research reactors. In particular, the irradiation reactor OSIRIS used Caramel fuel until 1995, when its fuel was replaced by uranium-silicide dispersion fuel. Caramel fuel was originally developed for use in propulsion reactors of French submarines [Schwartz, 1978, p. 3].

⁴See also discussion in Section 9.1.1 on the origins of the MTR-type design.

4.1.2 Dispersion-type fuels

Dispersion-type fuels, or simply dispersion fuels, consist of small fuel particles (\varnothing typically $< 100 \mu\text{m}$) embedded into a non-fissile and ideally inert matrix material, which guarantees adequate irradiation behavior of the fuel. The fundamental idea of dispersion fuels is to isolate the fuel particles such that the fission gases released during irradiation can be accommodated locally within the matrix. As a consequence, no additional gap or void between the fuel and the cladding is needed to contain fission products or to support swelling of the fuel. Dispersion fuels are therefore prime candidates for use in fuel plates. A discussion of common fabrication processes can be found in [Hofman and Snelgrove, 1994, pp. 52–54]. The effective thermal conductivity of dispersion fuels can be very high if the matrix material is properly chosen. As a result, centerline temperatures in the fuel are low in comparison to ceramic fuels. Dispersion-type fuels therefore permit extremely high power densities or average fission rates as well as exceptional maximum fission densities at end-of-life.

Within the class of dispersion fuels, four different fuel-matrix permutations are conceivable: these are metallic or ceramic fuel particles in a metallic or ceramic matrix. In practice, only fuels with metallic matrices have been used extensively in research and other reactors. These fuels are briefly discussed below with special attention on the predominant aluminum-based dispersion fuels. Table 4.1 summarizes the most important properties of common uranium compositions used as dispersants as well as common metallic matrix materials.

	Density	WF(U)	T_{melt}	η [W/(m K)]
Uranium-Aluminide UAl_x	6.4 g/cc	71.9 wt%	1590 °C	
Triuranium-Octaoxide U_3O_8	8.2 g/cc	84.6 wt%		18–23
Uranium-Dioxide UO_2	10.9 g/cc	88.2 wt%	2750 °C	6–10
Uranium-Silicide U_3Si_2	12.2 g/cc	92.6 wt%	1650 °C	15
Uranium-Molybdenum $\text{UMo}(8\text{wt}\%)$	17.4 g/cc	92.0 wt%	1135 °C	10–20
Uranium-Molybdenum $\text{UMo}(6\text{wt}\%)$	17.5 g/cc	94.0 wt%	1135 °C	10–20
Metallic uranium U	19.0 g/cc		1135 °C	28
Aluminum Al	2.7 g/cc		660 °C	224
Zirconium Zr	6.5 g/cc		1855 °C	20
Magnesium Mg	1.7 g/cc		650 °C	156

Table 4.1: Properties of uranium dispersants and matrix materials [Hofman, 1996].

Hofman and Snelgrove [1994] discuss dispersion fuels in great detail and particularly focus on the thermophysical, mechanical, and chemical properties of dispersion fuels as

well as processes related to irradiation-induced swelling of the fuel. An earlier, broader discussion of this fuel-type can be found in Frost [1982, Chapter 11]. Specific aspects of high-density dispersion-type fuels for research reactor conversion are addressed in [Bretscher and Matos, 1996, Bretscher et al., 1996]. Most generally, progress made in the field of dispersion fuel R&D, including theoretical modeling as well as experimental results and data, are discussed in the series of proceedings of the international RERTR conferences, held annually since 1978.

Aluminum-based dispersion fuels

For several reasons, aluminum-based dispersion fuels are the standard fuel for MTR-type research reactors. As indicated above, research reactors may be operated at relatively low temperatures and metallic components in the fuel are therefore acceptable. Aluminum is a favored matrix material because it is both widely available and characterized by a very high thermal conductivity.

As listed in Table 4.1, several dispersants are suited and have been used in aluminum-based dispersion fuels. As a maximum effective uranium density is the main design objective of the fuel, the theoretical density of the dispersant and the weight fraction of uranium $WF(U)$ in the compound are important characteristics. Note that the volume fraction of the dispersant in the matrix is typically limited to 30–50% in order to guarantee stable irradiation behavior of the fuel.

Early dispersion type fuels used with HEU since the 1960s were primarily based on UAl_x and U_3O_8 dispersants, which achieve effective uranium densities of up to 1.5 g/cm^3 . Efforts to make high-density fuels available that could be used with LEU lead to the development of fuels using U_3Si_2 and uranium-molybdenum alloys as dispersants. Uranium-silicide fuel at 4.8 g(U)/cm^3 has been the standard LEU fuel since the early 1990s. The current status and the perspectives of fuel development for research reactors are briefly discussed at the end of this chapter.

Non-aluminum-based dispersion fuels

In cermet fuels, the ceramic fuel particles are dispersed in a metallic matrix. The most common combination is UO_2 in a Zircaloy or stainless steel. The rationale of using cermets is to overcome some shortcomings of the pure ceramic (UO_2) fuels: Cermets provide highly reliable fuel element performance. Due to the dispersion-type structure (fission products are accommodated in the matrix), cermets can be used in plates fabricated with the standard picture-frame technology. The effective uranium density is significantly lower than in ceramic fuels, leading to a strong economic penalty. Cermets have been used with highly-enriched uranium in military propulsion reactors [Hofman

and Snelgrove, 1994, p. 49], where aluminum-based dispersion fuels cannot be used due to the high operating temperatures in these PWR-type reactors.⁵

4.1.3 Monolithic fuels

Using uranium metal directly as a fuel material would obviously maximize the density of fissile material in the fuel. Furthermore, and in contrast to oxides, metals are characterized by high thermal conductivities, leading to a flat temperature gradient and a low centerline temperature in the fuel. Unfortunately, metallic uranium displays poor irradiation behavior and is subject to phase changes between 300 K and its (low) melting temperature, which makes it unusable in power reactors. Nevertheless, some uranium-rich alloys are known to stabilize the γ -phase of uranium down to room temperature. The most promising candidate material is a uranium-molybdenum alloy with a molybdenum content of 5–15 wt%, with a performance optimum at approx. 10 wt%. Uranium-molybdenum fuels were used in some prototype fast reactors in the early 1960s,⁶ but they were never considered for MTR-type fuels because metallic fuels cannot be fabricated with the established picture-frame technology for plate-type fuel, which uses the roll-bonding process.

As will be discussed in Section 4.3, in the years 2000–2002, problems emerged with dispersion fuels using uranium-molybdenum alloy as a dispersant. During the analysis of these problems, micro-plates containing pure U-Mo(10) alloy were irradiated under research reactor conditions. Rather unexpectedly, the fuel behaved extremely well up to a very high burnup of 70–80% U-235 showing locally contained fission bubbles (Figure 4.1). These results were first reported in early 2002 and discussed in [Hofman and Meyer, 2002]. Today, monolithic fuels represent the most promising candidate for the next generation of high-density fuels for research reactors.

The main focus of R&D efforts for monolithic fuels is currently on adequate fabrication techniques, and a variety of promising processes have been identified to produce MTR-type fuel plates [Clark et al., 2003, 2004a,b]. Among these processes are friction-stir welding, transient liquid phase bonding, and hot-isostatic pressing. Test-plates of monolithic fuels fabricated with these techniques will be irradiated starting in 2005 (see Section 4.3).

⁵The technical challenges of converting submarine reactors to low-enriched fuel have been discussed in [Ippolito Jr., 1990]. Independent analysis of naval reactors is complicated by the fact that their core and fuel designs are classified in the U.S. and elsewhere.

⁶These are the U.K. Dounreay Fast Reactor and the U.S. Fermi reactor [Sesonske and Yevick, 1966, Sections 11.5 and 11.7].

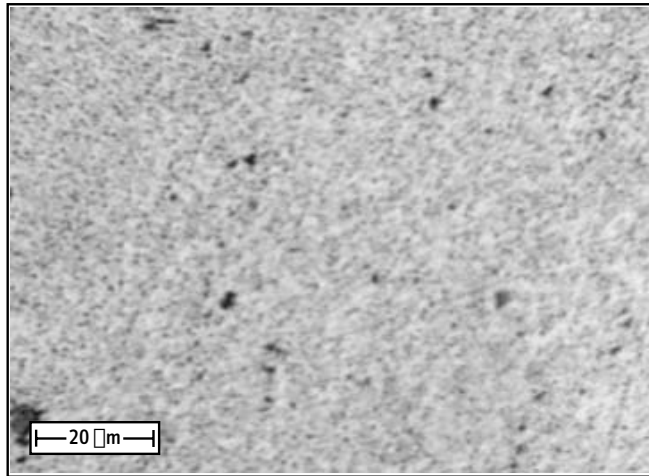


Figure 4.1: Bubble morphology of monolithic fuel at 70–80% burnup.

ET703623.1 A/G623F1 enlarged to about 1500 \times , picture courtesy of G. Hofman (ANL) and R. Finlay

4.2 Data for Selected Materials

The main results of this thesis will be produced in extensive neutronics calculations discussed in several chapters below. The details of these results depend upon the precise material compositions used to set-up the models for these simulations. Essential materials are defined and specified here: these include both the uranium isotopics at various enrichment levels, as well as the composition of actual fuel zones, which may or may not include matrix materials and porosity.

4.2.1 Uranium isotopics

For subsequent calculations (Chapters 7, 8, and 10), reference compositions for low-enriched and highly enriched uranium of various enrichment levels are required. Even though it is inevitable that the isotopics of these materials represent idealized compositions, they facilitate a consistent assessment of a set of neutronics calculations, both for different fuels in the same reactor geometry as well as for the same fuel in different reactors or reactor core geometries. Uncertainties in the isotopic composition of uranium at enrichment levels arise for various reasons. Most importantly, the composition of the source material depends upon the supplier and, in particular, on the type of uranium enrichment process used.

- Weapon-grade HEU of U.S. origin typically contains 93 wt% of the fissile isotope U-235, while the corresponding HEU of Russian origin is usually enriched to

90 wt%.⁷ The remaining weight fraction in HEU is mostly U-238, though U-234 and U-236 are also present in non-negligible concentrations

- In the case of LEU, additional uncertainties in the isotopics arise due to extra production options for the fuel. In particular, the LEU might contain reprocessed HEU fuel (60–80% enriched) which has been down-blended with depleted, natural, or low-enriched uranium. By definition, the uranium-235 content has to be less than 20 wt% and is typically adjusted at 19.75 wt%.
- Uranium of enrichment levels higher than 20 wt%, but lower than 90–93 wt%, are less common. In some Russian or Russian-supplied research reactors, a uranium enrichment of 36% or 63% is used. Earlier in the history of the international conversion efforts, an enrichment level of 45 wt% was sometimes considered as an intermediate step in the conversion process.

The standard WG-HEU composition for all calculations below is based on [Miller and Eberhard, 1982, p. C-1], representing typical material supplied by the U.S. Department of Energy. Table 4.2 lists the weight fractions and number densities for the uranium main isotopes U-234, -235, -236, and U-238.⁸

As indicated, a precise composition of low-enriched fuel is even more difficult to provide. In the following, a medium contamination of the fuel with the even-numbered isotopes is assumed: 0.20 wt% of U-234 and 0.05 wt% of U-236 (Table 4.2).⁹ It should be emphasized that the traces of U-234 and U-236 noticeably affect the overall fuel performance and therefore, in particular, the achievable cycle length of a reactor for a specified reactor geometry. Not considering these isotopes in the initial material compositions would yield somewhat unrealistic results.

4.2.2 Fuel compositions

Tables 4.4 through 4.7 at the end of this chapter list the reference number densities for the various fuel-types used in simulations below. Included are the most important dispersion-type fuels UAl_x -Al, U_3Si_2 -Al, and UMo -Al as well as monolithic fuels discovered only recently. Number densities of the fuel compositions are calculated with

⁷It is unclear if Russia also produced significant stocks of HEU enriched to 93% or beyond. Estimates of the HEU global stockpiles usually introduce the weapon-grade equivalent to circumvent these details (see Chapter 2).

⁸Matos and Snelgrove [1992, p. 19] quote a similar composition for HEU supplied by the U.S. Department of Energy: 1.00% U-234, 93.19% U-235, 0.44% U-236, and 5.37% U-238.

⁹Hanan et al. [2000] provide a similar LEU composition. The sensitivity of initial concentrations of U-234 and U-236 on the mass inventory of spent fuel from research reactors is discussed in Pond and Matos [1995, Appendix B].

	Highly Enriched Uranium (U.S. Origin)		Low-Enriched Uranium (medium U-236 content)	
U-234	0.90 wt%	0.02316 e21 at/g(U)	0.20 wt%	0.00515 e21 at/g(U)
U-235	93.00 wt%	2.38279 e21 at/g(U)	19.75 wt%	0.50602 e21 at/g(U)
U-236	0.10 wt%	0.00255 e21 at/g(U)	0.05 wt%	0.00128 e21 at/g(U)
U-238	6.00 wt%	0.15179 e21 at/g(U)	80.00 wt%	2.02382 e21 at/g(U)
	235.212 g/mol		237.444 g/mol	

Table 4.2: Uranium compositions of HEU and LEU used in this study. Additional uranium compositions exceeding the LEU limit (20–35%, used later in this study) are based on constant U-234 and U-236 weight fractions taken from the LEU composition.

atomic mass data taken from [Audi and Wapstra, 1995], using nominal densities from [Hofman, 1996], and isotopic uranium compositions from Table 4.2.

As discussed above, dispersion-type fuels contain a uranium-compound dispersed in an aluminum matrix. The volume balance in the fuel meat is given by the sum of the fractional volumes occupied by the fuel particles,¹⁰ the matrix material, and the residual void.

$$V_{\text{total}} = V_{\text{fuel}} + V_{\text{matrix}} + V_{\text{void}} = 1.0$$

Once the target uranium density in the fuel or, equivalently, the volume fraction of the dispersant in the meat is specified, the porosity of the fuel must be estimated. The porosity is defined as the fractional volume of void in the meat and, in general, increases with increasing volume fraction of the fuel particles in the aluminum matrix. Porosity originates from an imperfect flow of matrix aluminum around the fuel particles during production of the fuel plate. Porosity is technically inevitable, but also required to accommodate fission gas release during irradiation of the fuel. Note that the porosity strongly depends upon the fuel fabricator, since various fabrication technologies and processes are available and employed.

Even though the porosity is essentially irrelevant in the context of neutronics calculations, typical porosity values have been used to adjust the number densities, i.e. to reduce the volume of the matrix material, for the various fuel-types correspondingly.

$$V_{\text{void}} \approx 0.072 V_{\text{fuel}} - 0.275 V_{\text{fuel}}^2 + 1.320 V_{\text{fuel}}^3 \quad \text{for} \quad V_{\text{fuel}} \leq 0.5$$

¹⁰Fuel particles may also be designated *dispersed phase* or *dispersant*.

This cubic fit has been obtained based on experimental data obtained for uranium-silicide fuels [Matos and Snelgrove, 1992]. Nevertheless, this expression has also been used for other dispersion-type fuels and provides useful estimates for the porosity to be expected [Bretscher and Matos, 1996].

The reference compositions of monolithic fuel at various enrichment levels are summarized in Table 4.7. As discussed in the previous section, monolithic fuel is a pure uranium-molybdenum-alloy and no matrix material is present in the fuel zone. The weight fraction of molybdenum in the reference alloy has been adjusted to a hypothetical value of 8.05 wt% in order to obtain a material with an effective uranium density of exactly 16.0 g/cm³. It seems likely that the molybdenum content could be reduced further (possibly down to 5–6 wt%), which would entail a corresponding increase of the effective uranium density in the fuel.

4.3 Development of High-Density Fuels: Status and Perspectives

The early dispersion-type fuels for MTR-type research reactors were based on UAl_x fuel particles embedded in an aluminum matrix (UAl_x-Al). As discussed above, the effective uranium densities attainable with these fuels were in the order of 1.0–1.5 g/cm³. This value was considered adequate at the time when used in conjunction with highly enriched uranium. The objective of substituting HEU with LEU fuel in research reactors required the development of dispersion fuels with higher effective uranium densities in order to match or approach the original U-235 content (Figure 1.2). The qualification of uranium-silicide fuels with typical densities of 4.8 g/cm³ in the 1980s represented the first major milestone in this respect.

Fuel development efforts were restarted in the 1990s with the objective to demonstrate and qualify the next generation of high-density fuels. Until very recently, uranium-molybdenum dispersion fuels with effective uranium densities of up to 8 g/cm³ were considered the prime candidate to replace the uranium-silicide LEU fuels in use today. Rather unexpectedly, and first reported in 2002, serious problems with these fuels emerged during the series of irradiation tests performed in France and in the U.S.¹¹ Table 4.3 lists the key characteristics of irradiation tests for this fuel-type that have been carried out and examined to date.

The problem encountered during irradiation of UMo-dispersion fuels consists in an unfavorable swelling behavior (pillowing) of the fuel plates, which is due to porosity

¹¹The problems were first reported in 2002, but they had been identified prior to that. In the light of later results, two earlier U.S. irradiation tests (RERTR-4 and RERTR-5) were later reevaluated. Their overall results are ambiguous and listed as ‘unclear’ in Table 4.3.

Experiment Reactor	RERTR-1 ATR (USA)	RERTR-2 ATR (USA)	RERTR-3 ATR (USA)	RERTR-4 ATR (USA)	RERTR-5 ATR (USA)
Effective uranium density	4.0 g/cm ³	4.0 g/cm ³	8.5 g/cm ³	6–8 g/cm ³	6–8 g/cm ³
Average burnup	40%	70%	40%	80%	50%
Maximum heat flux	70 W/cm ²	50 W/cm ²	400 W/cm ²	210 W/cm ²	320 W/cm ²
Max. clad. temperature	70 °C	65 °C	150 °C	130 °C	175 °C
Status/Result	OK	OK	OK	unclear	unclear

Experiment Reactor	UMUS HFR (NL)	FUTURE BR2 (BE)		IRIS-1 OSIRIS (F)	IRIS-2 OSIRIS (F)
Effective uranium density	8.0 g/cm ³	8.0 g/cm ³		8.0 g/cm ³	8.0 g/cm ³
Average burnup	15%	25%		50%	30%
Maximal heat flux	250 W/cm ²	340 W/cm ²		140 W/cm ²	240 W/cm ²
Max. clad. temperature	110 °C	130 °C		75 °C	100 °C
Status/Result	failed	stopped		OK	stopped

Table 4.3: Data and results for the U.S. (top) and French (bottom) irradiation experiments. Data originally compiled in [Lemoine et al., 2004]. The U.S. experiments use micro- or miniplates, while the French experiments are based on full-sized fuel plates.

buildup in the interaction layer between the fuel particles and the aluminum matrix. Problems occur at high temperatures combined with high fission rates [Hofman et al., 2004]. Successful and failed tests are visualized in Figure 4.2. Various countermeasures have been suggested to suppress this effect. Among the most promising candidates is the addition of small amounts of silicon to the matrix material. A general overview of the current status of the international efforts to qualify uranium-molybdenum dispersion-type fuels is given in [Lemoine et al., 2004]. This review includes the French, the U.S., the Russian, and the Argentine fuel development programs. Further relevant details regarding past and future irradiation experiments are presented in [Hamy et al., 2004, Hofman et al., 2004, Leenaers et al., 2004].

The U.S. development team has essentially abandoned the option of qualifying uranium-molybdenum fuels for use in high-flux reactors with extreme life-averaged fission rates and fission densities at EOL. Similarly, development of UMo-dispersion fuels in France might also be halted if further tests of monolithic fuels yield favorable results.¹²

¹²“If the monolithic fuel appears to have behaved well in full-sized plates to high ($\sim 75\%$) burn-up, the decision may well be made to stop any further work on dispersion fuel in order to avoid the high cost of the element irradiations” [Lemoine et al., 2004, p. 39].

Several irradiation tests are now being designed and will be performed and analyzed in the years 2005–2007. The U.S. experiments RERTR-6 and RERTR-7 are both scheduled to begin in 2005 and both include UMo-dispersion *and* monolithic fuel test plates. Specifically, RERTR-6 includes a total of 32 mini-plates (14 dispersion-type + 18 monolithic) and explore a variety of matrix modifications for UMo-dispersion fuels and two distinct fabrication techniques for monolithic fuels. Additional detailed information on the design of RERTR-6 and RERTR-7 is provided in [Clark et al., 2004b].

On the French side, IRIS-3 and IRIS-4 are primarily focused on countermeasures to suppress the porosity problem of UMo-dispersion fuels. IRIS-3 will be conducted with a modified matrix material (UMo-Al + x%Si), while IRIS-4 envisions the use of coated particles to isolate the fuel from the matrix material. Only in IRIS-5, which is currently scheduled to begin in 2006, would monolithic fuels be tested.

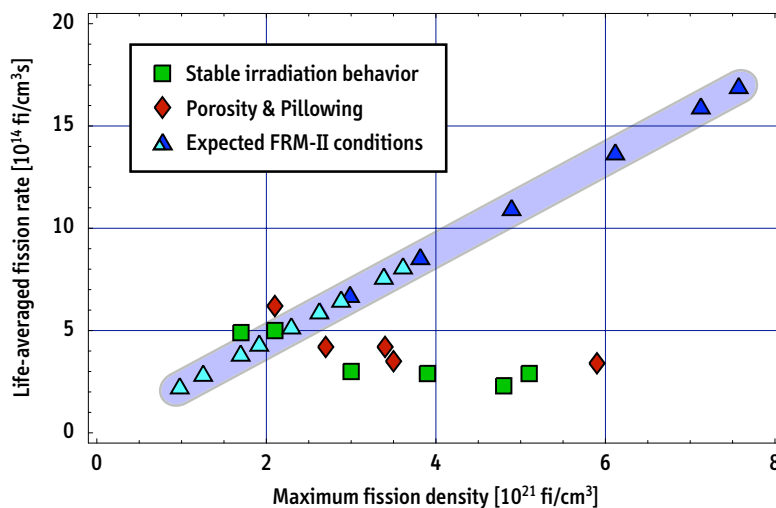


Figure 4.2: Local life-averaged fission rate and averaged local fission density at EOL in the fuel particles. Representation for a performance assessment of UMo-dispersion fuel (stable versus failure) suggested in [Hofman et al., 2004, Figure 4]. Indicated are previous irradiation tests (listed in Table 4.3) that performed well (\square) and tests that failed or were stopped prematurely to avoid failure (\diamond). FRM-II data was obtained in M^3O simulations for UMo-dispersion fuel at 50% enrichment (\triangle). Light-blue symbols represent central segments of the fuel plate with 8 g/cm^3 , dark-blue symbols segments in the periphery of the plate with 4 g/cm^3 effective uranium density.

Uranium-Aluminum (UAl_x) Dispersion-Type Fuel			
Density of compound: 6.4 g/cc			
Weight fraction of uranium in compound: 71.94%			
	HEU at 0.75 g(U)/cc	HEU at 1.15 g(U)/cc	HEU at 1.50 g(U)/cc
Dispersive Phase	16.29 vol%	24.98 vol%	32.58 vol%
Porosity	1.0 vol%	2.0 vol%	4.0 vol%
U-234	0.0000173685	0.0000266318	0.0000347371
U-235	0.0017870899	0.0027402046	0.0035741799
U-236	0.0000019134	0.0000029340	0.0000038269
U-238	0.0001138398	0.0001745543	0.0002276796
Aluminum	0.0505165874	0.0539985713	0.0512614616
Total	0.0524367991	0.0569428959	0.0551018850

Table 4.4: Properties and number densities of UAl_x -Al fuels.Theoretical number densities used for neutronics simulations, all values given in [10^{24} at/cm³]

Uranium Silicide (U_3Si_2) Dispersion-Type Fuel
Density of compound: 12.2 g/cc
Weight fraction of uranium in compound: 92.63%

	HEU at 1.5 g(U)/cc	HEU at 3.0 g(U)/cc	LEU at 4.8 g(U)/cc
Dispersant	13.27 vol%	26.54 vol%	42.44 vol%
Porosity	1.0 vol%	2.5 vol%	8.0 vol%

U-234	0.0000347371	0.0000694741	0.0000247019
U-235	0.0035741799	0.0071483597	0.0024289050
U-236	0.0000038269	0.0000076538	0.0000061230
U-238	0.0002276796	0.0004553591	0.00097143279
Silicon	0.0025602823	0.0051205645	0.0081160386
Aluminum	0.0516399114	0.0427404459	0.0298322744
Total	0.0580406170	0.0555418572	0.0501223709

Table 4.5: Properties and number densities of U_3Si_2 -Al fuels.

Theoretical number densities used for neutronics simulations, all values given in [10^{24} at/cm³]

Uranium-Molybdenum (UMo8) Dispersion-Type Fuel Density of compound: 17.4 g/cc Weight fraction of uranium in compound: 91.95%

	LEU at 8.0 g(U)/cc	HEU (35%) at 8.0 g(U)/cc	HEU (50%) at 4.0 g(U)/cc	HEU (50%) at 8.0 g(U)/cc
Dispersant	50.0 vol%	50.0 vol%	25.0 vol%	50.0 vol%
Porosity	3.0 vol%	3.0 vol%	3.0 vol%	3.0 vol%

U-234	0.0000411699	0.0000411699	0.0000205849	0.0000411699
U-235	0.0040481740	0.0071739793	0.0051242709	0.0102485419
U-236	0.0000102051	0.0000102051	0.0000051025	0.0000102051
U-238	0.0161905425	0.0131042204	0.0050342468	0.0100684936
Mo-092	0.0006806702	0.0006806702	0.0003403351	0.0006806702
Mo-093				
Mo-094	0.0004152437	0.0004152437	0.0002076218	0.0004152437
Mo-095	0.0007071325	0.0007071325	0.0003535662	0.0007071325
Mo-096	0.0007331733	0.0007331733	0.0003665866	0.0007331733
Mo-097	0.0004154351	0.0004154351	0.0002077175	0.0004154351
Mo-098	0.0010389655	0.0010389655	0.0005194828	0.0010389655
Mo-099				
Mo-100	0.0004063298	0.0004063298	0.0002031649	0.0004063298
Aluminum	0.0283119474	0.0283119474	0.0433714939	0.0283119474
Total	0.0529989888	0.0530384719	0.0557541741	0.0530773077

Table 4.6: Properties and number densities of UMo-Al fuels.

Theoretical number densities used for neutronics simulations, all values given in [10^{24} at/cm³]

Monolithic Uranium-Molybdenum Alloy Fuel			
Density of compound: 17.4 g/cc			
Weight fraction of uranium in compound: 91.95%			
	LEU at 16.0 g(U)/cc	HEU at 25% at 16.0 g(U)/cc	HEU at 30% at 16.0 g(U)/cc
U-234	0.0000823397	0.0000823397	0.0000823397
U-235	0.0080963481	0.0102485419	0.0122982502
U-236	0.0000204101	0.0000204101	0.0000204101
U-238	0.0323810850	0.0302560763	0.0282322585
Mo-092	0.0013613403	0.0013613403	0.0013613403
Mo-093	—	—	—
Mo-094	0.0008304873	0.0008304873	0.0008304873
Mo-095	0.0014142649	0.0014142649	0.0014142649
Mo-096	0.0014663465	0.0014663465	0.0014663465
Mo-097	0.0008308702	0.0008308702	0.0008308702
Mo-098	0.0020779311	0.0020779311	0.0020779311
Mo-099	—	—	—
Mo-100	0.0008126596	0.0008126596	0.0008126596
Total	0.0493740828	0.0494012679	0.0494271585

Table 4.7: Properties and number densities of monolithic fuels.

Theoretical number densities used for neutronics simulations, all values given in [10^{24} at/cm³]

This page intentionally blank

Chapter 5

Mathematica as a Tool to Generate and Analyze Complex Research Reactor Fuel Element Geometries

Modern technical computing environments, such as *Mathematica* or *Matlab*, provide powerful tools and techniques for research reactor analysis and are also equipped with advanced graphical user-interfaces. In addition, as will be discussed in Chapter 6, reactor calculations can now be efficiently supported by neutronics codes based on the Monte Carlo method due to the dramatic improvement of computer performance in recent years. In particular for the analysis of very compact reactor cores, where an accurate three-dimensional model of the core becomes almost indispensable, Monte Carlo techniques are a very valuable asset.

In combining these approaches, a system has been developed that emphasizes an interactive interface based on *Mathematica* to generate complex research reactor geometries, while using standard burnup and Monte Carlo neutronics codes in the background (ORIGEN2 and MCNP). The resulting computational system can be used to generate complete MCNP models of reactor cores, to optimize and prepare the input for burnup calculations, and finally to analyze the results of the calculations.

Specifically, there are two central and distinct operations performed with *Mathematica*. First, the software is used to set up complete three-dimensional MCNP models of arbitrary single element reactors. To this end, modules and functions are provided that facilitate flexible, accurate, and fast generation of MCNP input — a feature that is particularly useful when numerous alternative configurations of a reactor core are studied in an optimization process as will be the case below. Second, *Mathematica* is used to prepare special MCNP models for burnup calculations to be performed with M^3O , which is introduced in the next chapter. In both instances, the primary reason for using *Mathematica* is to address the challenges originating from the complexity of the

core geometry, benefitting greatly from the interactive user-interface of the software. *Mathematica* finally provides convenient means for the numerical and graphical evaluation of the neutronics calculations. Adequate modules can be used to read MCNP and MCODE output files for analysis. The functionality and implementation of such procedures are both fairly straightforward and therefore will not be further discussed below.

The entire set of simulations performed in the context of this thesis is set up and analyzed using *Mathematica*, Version 4.1.5 for Mac OS X, which was released in 2001 [Wolfram, 2001]. The most important *Mathematica* modules programmed and used below will be made available on the thesis' website indicated in the back matter section.

5.1 Generation of a Base MCNP Input Deck

The fundamental idea of using *Mathematica* for the purpose of research reactor analysis is to collect important operations in integrated modules and functions and, hence, to focus the analyst's attention on the process of identifying the optimum model itself. Traditional programming languages and environments, such as FORTRAN or C, generally lack a possibility of immediate visual and numerical feedback that would assure the user of the current quality of the model.

The main challenge in setting-up a detailed model for a general single element reactor is to define the large number of MCNP cells and surfaces required to represent the complex geometry of the core. Furthermore, involute-shaped fuel plates, which are typical for single element reactors, cannot be modeled in MCNP directly. Instead, the plates have to be represented by a composite of standard MCNP surfaces.¹

The primary objective of the automated *Mathematica* modules is to generate a working base MCNP input deck.² To this end, fundamental geometric design information of a given single element reactor is collected in a formatted list, which can then be passed to pre-defined functions made available in a package loaded at start-up of the *Mathematica* notebook. For example, the corresponding lists (`coredata`) for HFIR and FRM-II are:³

```
coredata = {{6.915, 12.815, 50.8},
           {{-0.0635, -0.0381, 0.0381, 0.0635}}, 171, 0.127, 1}
```

¹MCNP models of single element reactors used previously therefore replaced the involute-shaped plates with concentric rings [Mo et al., 1995] or homogenized the fuel-clad-coolant system completely [Redmond II, 1990].

²The objective is *not* to generate a complete MCNP model with every possible characteristic detail, which can usually be added conveniently by hand in a second step.

³See Chapter 7 for a table of existing single element reactors.

```
coredata = {{6.5, 11.45, 70},
            {{-0.068, -0.03, 0.03, 0.068}}, 113, 0.22, 1}
```

The first sublist of `coredata` specifies the inner and outer diameters of the core tubes as well as the active height of the fuel element (all units in cm, as requested by MCNP). The second sublist defines the geometry of the individual fuel plates themselves. Listed are the transverse coordinates of cladding and meat with the origin at the center of the plate.⁴ The remaining numerical values represent the number of fuel plates in the core, the width of the cooling channel, and the orientation of the plate.⁵ The following main functions are available to the user during the set-up process and verification of the model:

```
PlotCore[coredata]
GenerateInvolute[coredata, refpoints]
PlotInvolute[points, coredata, paraboladata, circledata, zoom]
```

Typical output of `PlotCore` and `PlotInvolute` is shown in Figures 5.1 through 5.3 for a set of sample design information. Additional data required for `PlotInvolute` are generated by `GenerateInvolute`, which approximates the involute defining the fuel plate by a combination of surfaces available in MCNP. The surface types used are parabolas (SQ) for the inner part and circles (C/Z) for the outer part of the involute.

The fit of the approximating functions to the original involute is based upon a pre-defined number of reference points on the involute. The key advantage of using *Mathematica* for these tasks is to have immediate visual and numerical feedback on the accuracy of the functions used to represent the involute-shaped fuel plate in the MCNP model. Figure 5.2 shows a typical situation for two sets of parameters used in the approximation process. In addition, two characteristic parameters are available to control the quality of the representation.

$$\alpha = \frac{1}{n} \sum_i^n \left[(x_i - x_i^*)^2 + (y_i - y_i^*)^2 \right] \quad \text{and} \quad \beta = y'_c(x_0) - y'_p(x_0) \quad (5.1)$$

The first parameter α describes the average square deviation of the approximating function from the involute with respect to all reference points. In the definition of α , (x_i^*, y_i^*) represents the closest point on the parabola or circle to the corresponding reference point (x_i, y_i) on the involute itself. The second parameter β in (5.1) measures

⁴Asymmetric fuel plates are also possible.

⁵The maximum number of fuel plates is determined by the inner radius of the core tube, the thickness of the fuel plate, and the width of the cooling channel. However, a lower number of plates may be chosen, which then leave the inner core tube with an angle of less than 90° . The orientation of the plate can be $+1$ or -1 . Unfortunately, due to a bug in MCNP related to the definition of parabolic surfaces, only positive orientations can be used at this time.

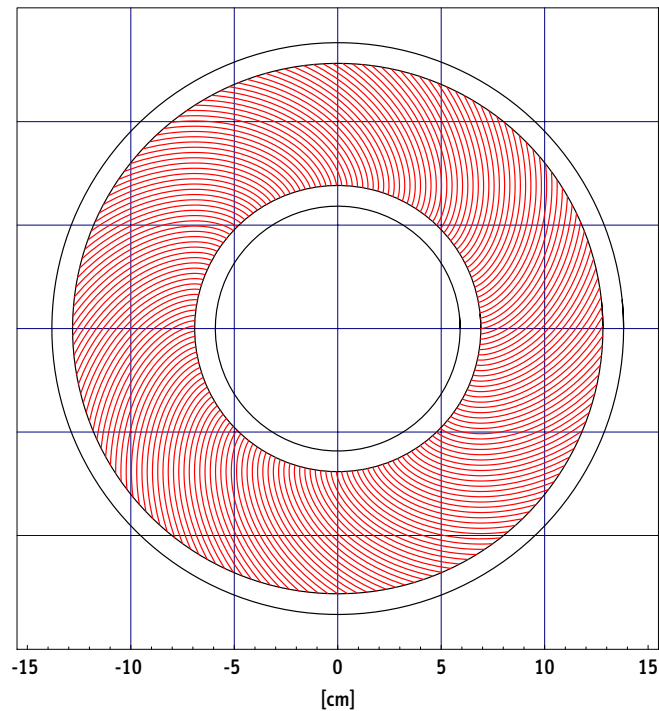


Figure 5.1: Results generated with *Mathematica* for an analysis of a single element reactor. Plot of fuel element generated with `PlotCore` function. Dimensions shown are for the inner fuel element of HFIR [Cheverson and Sims, 1971].

the discontinuity of the derivatives y'_p and y'_c of the approximating functions (parabola and circle) at the point of intersection x_0 . Obviously, both characteristic parameters should be as small as possible for a faithful representation of the fuel plate in MCNP.

Once the user is satisfied with the accuracy of the surfaces proposed by the system to approximate the fuel plate, he or she can directly generate the corresponding MCNP input, which is written (to disk) by the following functions:

```
WriteMCNPCells[dirpath, mcnpinfo]
WriteMCNPSurfaces[dirpath, surfacestrings, coredata]
```

A complete listing of an MCNP input deck is reproduced in Appendix D. With the files of the cell and surface sections combined, a first executable MCNP file can be prepared by adding the cells and surfaces defining the surroundings of the core as well as the obligatory data cards defining materials, source, etc. At this stage, a first general analysis of the reactor can be performed with MCNP by adding the desired tallies to the input file. In particular, neutron spectra and flux levels can be determined conveniently with the present model.

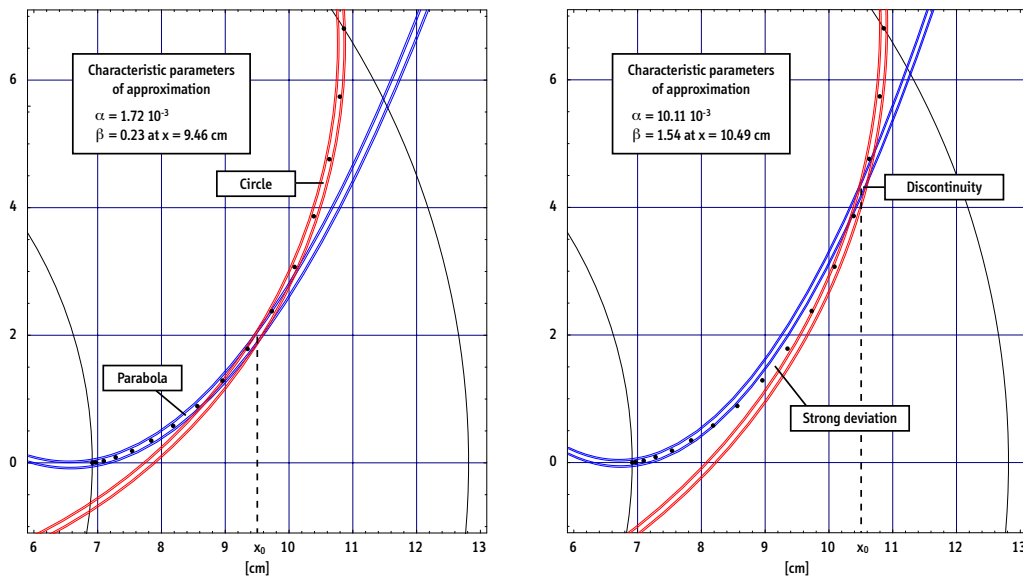


Figure 5.2: Good and bad approximations of an involute (sample data for HFIR). Dots indicate the precise coordinates of the original involute. The characteristic parameter α denotes the average square deviation from the involute of each reference point, β quantifies the discontinuity of the derivatives at the intersection x_0 of parabola and circle.

A crucial property of any complex three-dimensional MCNP reactor core model is its accuracy in the total volume of those cells containing fissile material. In the present case, this value cannot be computed directly by MCNP due to the complexity of the (asymmetric) surfaces used. To determine the fuel volume and, hence, the total fuel inventory in the core, the method of *stochastic volume calculation* can be employed. The voided model is flooded with neutrons from a homogeneous source. The value of a track-length (F4) tally in the cell of *unknown* volume is compared with the value scored in a cell of *known* volume located nearby.⁶ If small deviations from the expected volume are revealed, the corresponding correction factor can be used to generate the final version of the core model in a consecutive run of the *Mathematica* module. In general, the volume determined by the procedure described above is in excellent agreement with the expected value. In some cases, deviations on the order of 0.1% have been observed. The volume can be corrected by using a slightly biased value for the fueled length or the meat thickness during set-up of the model.

⁶See Section 6.2 for a brief discussion of MCNP tallies.

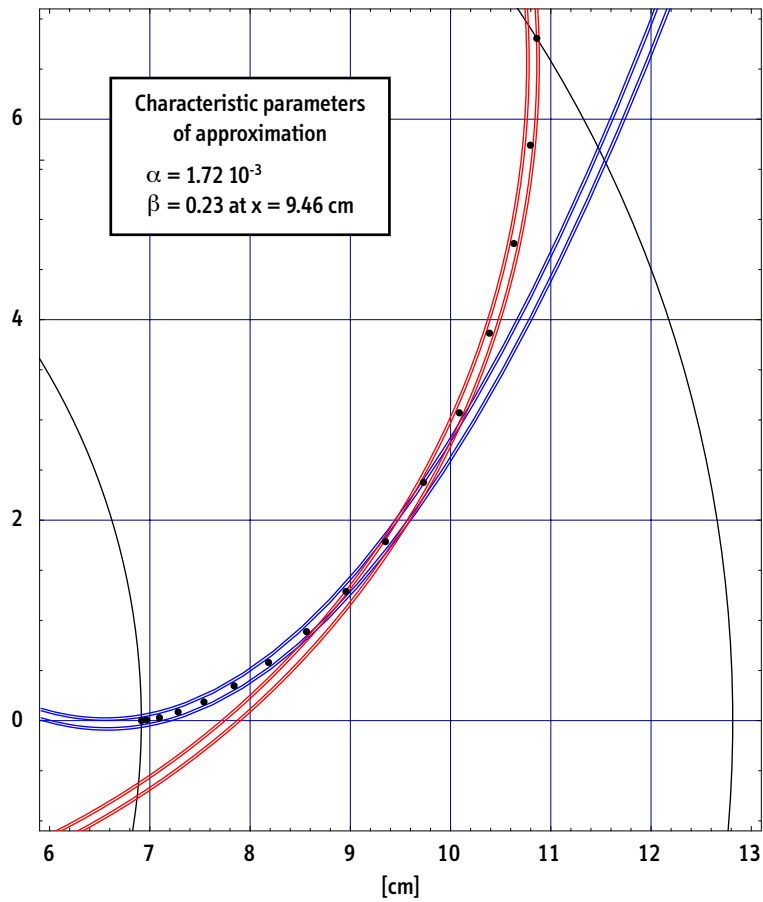


Figure 5.3: Results generated with *Mathematica* for an analysis of a single element reactor. Approximation of involute suggested by `GenerateInvolute` and plotted with `PlotInvolute`. Dots indicate the precise coordinates of the original involute. Shown dimensions are for the inner fuel element of HFIR [Cheverton and Sims, 1971].

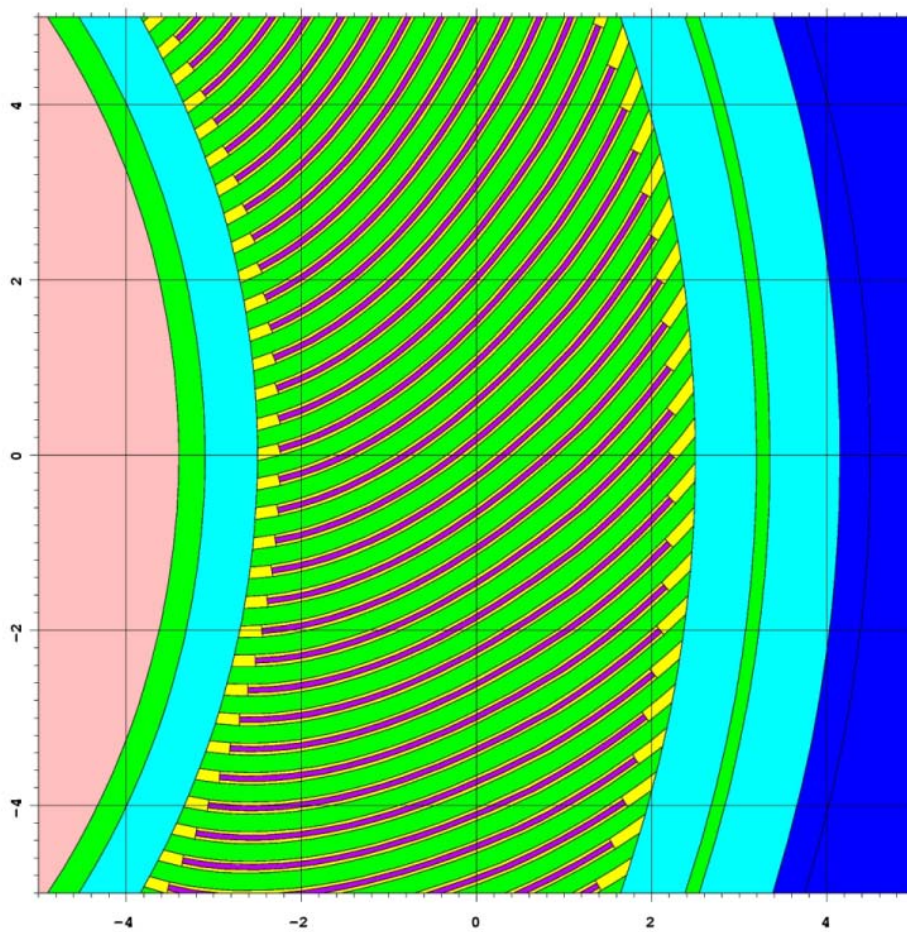


Figure 5.4: MCNP model of fuel element (top view).

5.2 Elements of a High-Accuracy Computational System for Research Reactor Burnup Calculations

The fundamental advantage and main reason to use Monte Carlo methods for burnup calculations is the possibility to generate extremely accurate burnup-dependent one-group cross-sections and neutron fluxes for arbitrary core and fuel geometries. Yet, a set of values determined for a material at a given position and time remains accurate only in a local region, in which neutron spectrum and flux vary weakly — and only for a limited period of time, during which changes of the local isotopic composition are minor. Since spatial effects (flux distribution, power density distribution, local burnup, etc.) are particularly pronounced for plate-type fuels used in compact reactor cores, a large number of burnup zones, i.e. of different material compositions to be tracked, is indicated. However, while a fine burnup mesh is easily handled by deterministic codes, a very large number of zones of small volume, each containing a distinct material composition, becomes impractical for analysis with Monte Carlo methods.

The approach pursued here tries to combine the best of both worlds: it uses Monte Carlo techniques to determine burnup-dependent cross-section and flux data for M^3O (Chapter 6), while reducing the number of burnable materials to be treated explicitly in MCNP to a number manageable by the code. More specifically, the objective is to restrict the number of burnable material compositions to less than 100 — possibly even down to the order of 10 materials only. Earlier versions of this specific approach to burnup calculations for research reactors have been presented in [Glaser et al., 2003].

Note that in the following, for the purpose of brevity, the term *material* is often used instead of *material composition* or *burnable material composition*. Each material typically consists of a large number of isotopes containing actinides, fission products, and fuel matrix.⁷

5.2.1 Generation of an adaptive cell structure

Instead of having a regular and strictly rectangular structure with burnup zones of equal size, a characteristic *adaptive cell structure* (ACS) is introduced here. The idea of such an adaptive cell structure is to join smaller areas within the plate with expected similar burnup behavior in one single burnup zone. The basic MCNP model generated with the procedure described above can then be updated and used for subsequent burnup calculations executed with a standard zero-dimensional burnup code.

⁷Table 6.4 lists the nuclides treated explicitly in M^3O by default.

As a first step, a *template* is required to serve as the basis of the adaptive cell structure to be generated. To this end, the fueled region of the plate in the base MCNP input deck is subdivided into very fine segments (typically several thousands) of equal volume. The corresponding additional input required for this procedure is again written by *Mathematica*. Based on this modified MCNP model, one time-intensive MCNP run is needed to generate the required tally-data. *Mathematica* extracts the data from the MCNP output-file to generate the final template, which can be used for all calculations for a specified core geometry.

In the following, the power density profile in the fuel plate is chosen as the standard template for all cell structures generated below. Figure 5.5 shows such a sample profile for the fuel plate of a generic single element reactor to be introduced in Chapter 7 of this thesis.

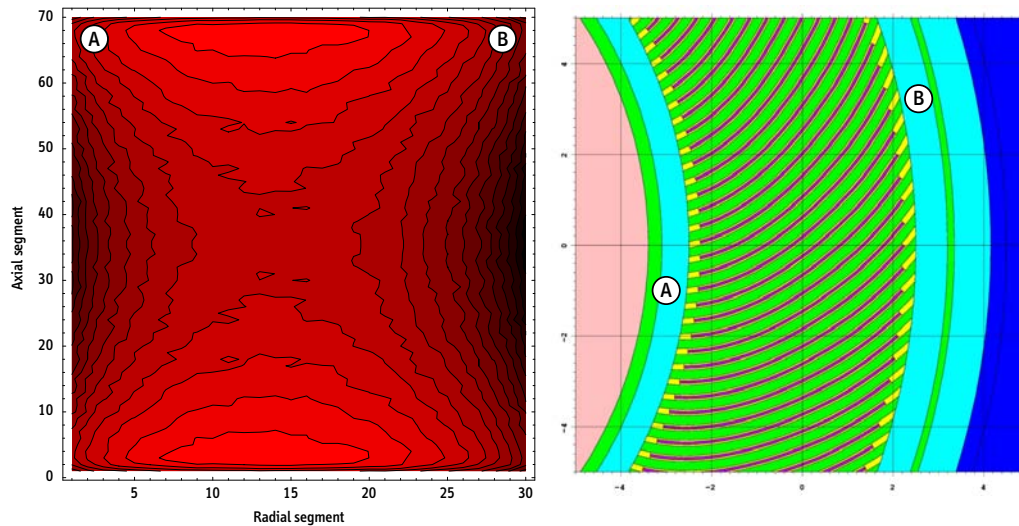


Figure 5.5: Example of a template for generation of an adaptive cell structure (ACS).

Axially symmetric power density profile obtained for the fresh core of the generic single element reactor introduced in Chapter 7

Once a template is available, an algorithm programmed in *Mathematica* is used to find a cell structure that approximates the given power density profile in the plate by rectangular segments, which can be handled by MCNP. The level of detail reproduced by the cells can be adjusted by a set of parameters and criteria of the search algorithm. The process of generating the cell structure can be subdivided into two fundamental steps: the choice of the number of materials or burnup zones and the parameters of the search algorithm that define further details of the cell structure.

As an example, Figure 5.6 illustrates the division of the template shown in Figure 5.5 into six domains. In this case, the classification is simply based on the minimum and maximum power densities in the plate. Each domain represents a constant range of

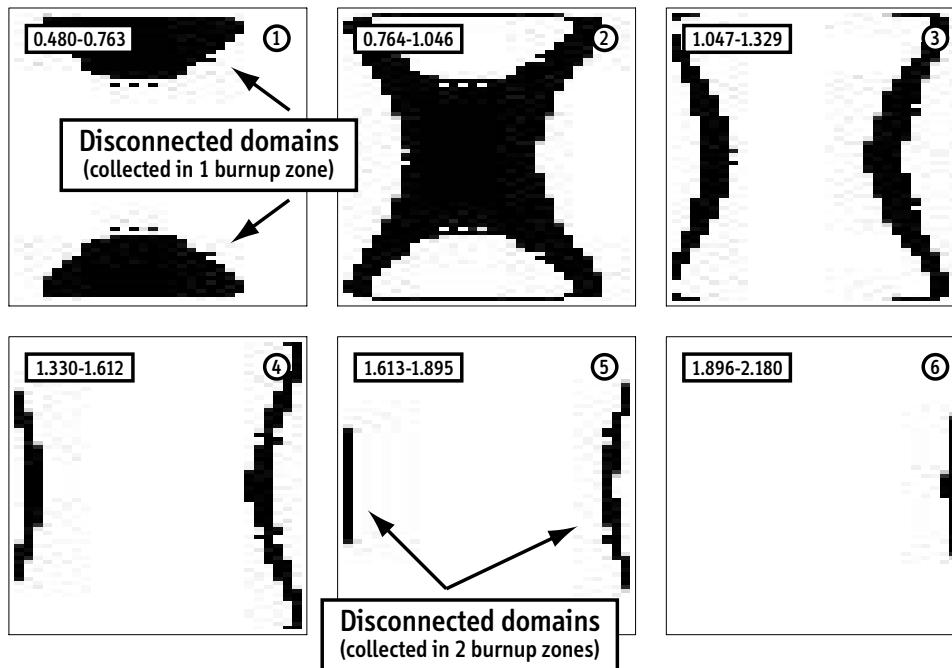


Figure 5.6: Domains used to generate adaptive cell structure.

Boxed intervals designate power density ranges normalized to average value in the core

power density values in the plate (intervals indicated in the figure).⁸ Generally, the individual domains obtained by this procedure may consist of a set of disconnected regions in the fuel plate. In an intermediate step, the code therefore isolates each of these subdomains and the user decides, which domains are collected in one or more burnup zones depending upon the expected irradiation conditions. For example, in Figure 5.6, domains ①, ②, and ⑥ would be collected in one burnup zone each, while ③, ④, and ⑤ would be split into two zones each due to the asymmetry of the problem in radial direction.

Once the number and the general structure of the burnup zones are specified, the search algorithm generates the final cell structure for ultimate use in MCNP. Two basic parameters of the algorithm determine the automated process:

Search order: The algorithm treats one domain at a time and the sequence of this procedure can be specified by the user. If greater domains are discretized first, the total number of MCNP cells required to describe the fuel plate will be lower

⁸Other rules for selecting the initial structure are conceivable. For instance, regions with the highest initial power densities may be divided into additional domains because spatial dependency of the fuel burnup will be particularly pronounced in those regions of the plate.

because large segments of the plate can be grouped together in very few rectangular cells. Conversely, if smaller domains are discretized first, the level of detail reproduced by the cell structure will be closer to the original template.

Fuzziness: More important than the search order, the fuzziness parameter determines, which fraction of each new ‘stripe’ added to an existing rectangular area may lie outside the valid domain as defined by the template. In addition, since templates are obtained in Monte Carlo simulations which are subject to statistical fluctuations, artifacts are inevitable (see Figure 5.7). Below a specified threshold, these artifacts have to be ignored. A low fuzziness is equivalent to a high sensitivity to variations in the local power density and leads to a higher number of MCNP cells generated.

Controlled by the search parameters, the search algorithm seeks to situate the largest possible rectangular area in the specified domain and records its coordinates for later use. The complement of this area defines one or more subdomains, which are addressed in the next step of the iteration process. Figure 5.7 shows a sample domain and its representation based on rectangular cells as suggested by the search algorithm.

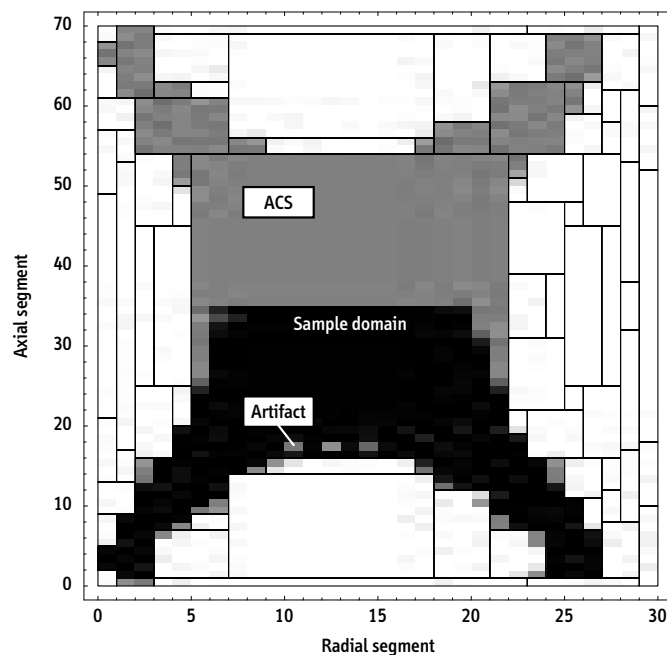


Figure 5.7: Lower section of a sample domain from template (black) and discretized cell structure as proposed by the search algorithm (grey) for a specified number of burnup zones and a particular set of search parameters.

Upon completion of the iterative search, the *Mathematica* module translates the cell data into MCNP syntax and writes the corresponding input to disk. Note that the number of surfaces required to describe the entire cell structure may be significant. In Appendix D, a complete MCNP input deck for a generic single element reactor is reproduced. The effectiveness of the adaptive cell structure technique is tested in Chapter 7 for the same generic reactor against alternative core models and techniques for Monte Carlo burnup calculations.

5.2.2 Adaptive cell structures for burnup calculations

Typical adaptive cell structures obtained for a generic single element reactor are shown in Figure 5.8. For illustrative purposes and based on the same template of a power density profile in the fuel plate, six different ACS's are generated by varying one variable at a time. Most importantly, the user has to choose the number of burnable materials to be tracked. Depending upon the required level of detail required, search order and fuzziness are selected. If the correct representation of small zones is prime, for instance to determine peak local fuel burnup, smaller domains should be discretized first. Finally, if a low number of total MCNP cells is preferred to limit the complexity of the model, a high value of the fuzziness parameter is recommended.

If the distribution of fuel in the plate is non-uniform, additional details have to be included in the model. In particular, the fuel density may display a discontinuity (graded fuel) or the meat thickness may be variable along the plate. These features are present in the cases of FRM-II and HFIR, respectively, and require separate treatment of different zones in the plate. A template and a sample ACS for a generic fuel plate with graded fuel is shown in Figure 5.9.

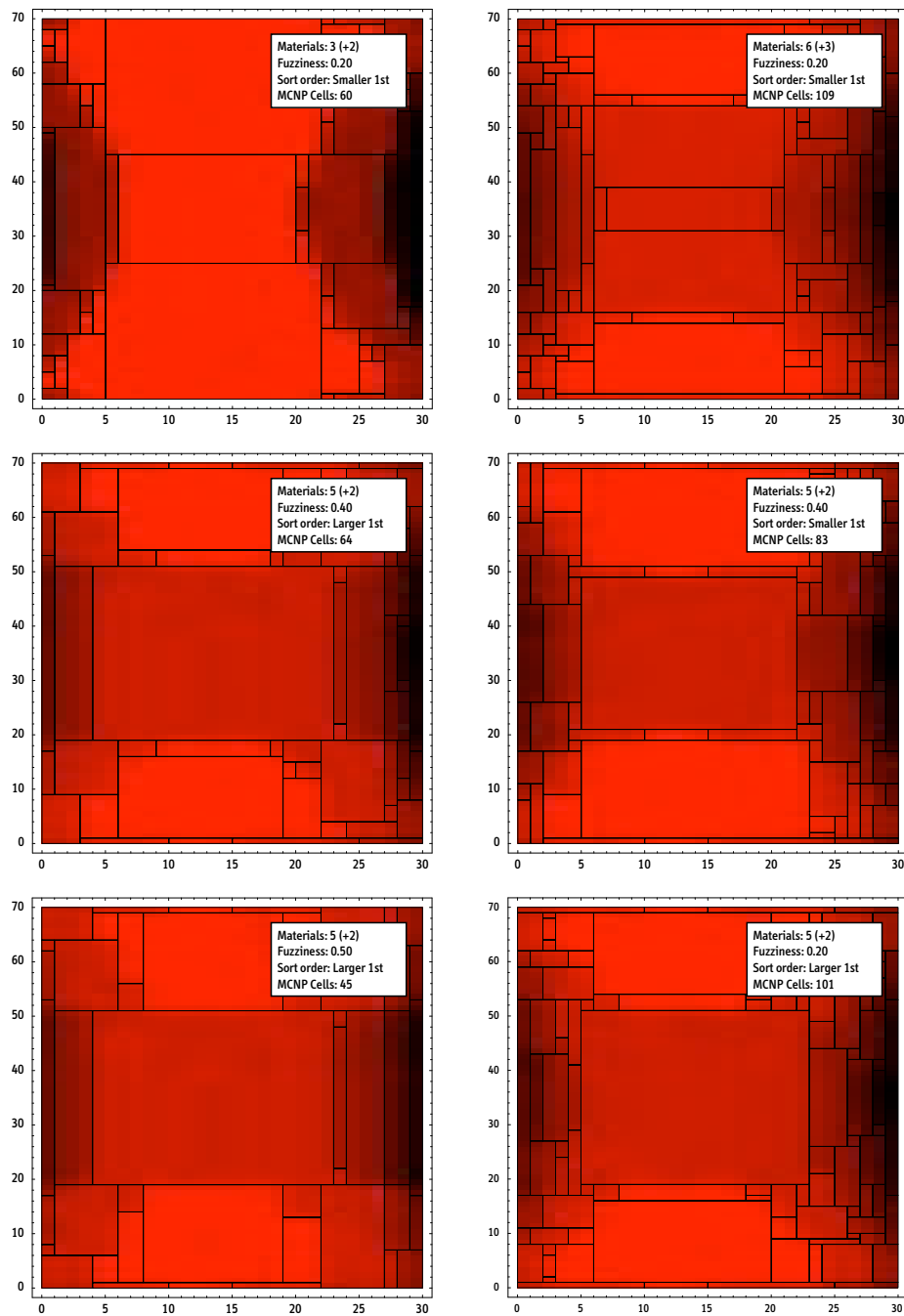


Figure 5.8: Discretized fuel plate of generic single element reactor. Sensitivity of adaptive cell structure (ACS) to variation of search algorithm parameters. All structures based on the same power density template. Top row: variation of number of domains (MCNP materials), middle row: change of search order, i.e. larger or smaller domains discretized first, and bottom row: variation of fuzziness. See text for further details.

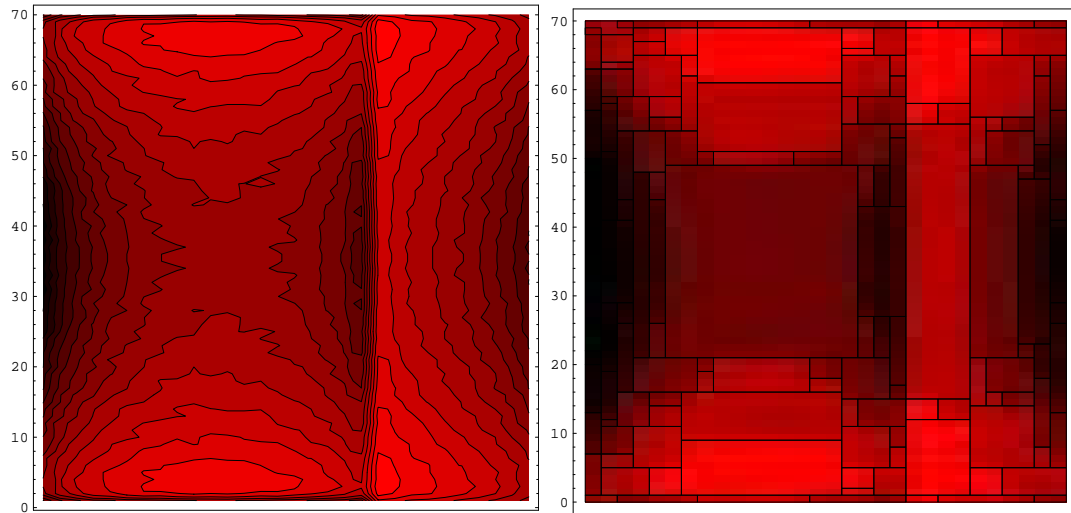


Figure 5.9: Example of a power density profile (left) and an adaptive cell structure (right) for a generic fuel plate with one discontinuity in the fuel density. Dimensions of length and height of plate are not to scale.

Chapter 6

Components of the Computational System M³O

The components of the computational system, which is the basis for all neutronics calculations below, are introduced in this section and their respective functions described. The elements of the system are the Monte Carlo neutron transport code MCNP, the burnup code ORIGEN2, and the linkage program MCODE. In addition, dedicated *Mathematica* modules control problem set-up and analysis of results. Abbreviated designation of the system will be M³O (*Mathematica*-MCODE-MCNP-ORIGEN2).

Before turning to the physics codes used in M³O, the nature of the problem to be solved is described, the required functionality of the computational system defined, and the structural arrangement of its components specified.

6.1 General Burnup Equations and Functionality of the Computational System

The general time-dependent evolution of an arbitrary nuclear material exposed to a neutron flux is expressed by the following set of differential equations.¹

¹Unless otherwise noted, here and in the following, all expressions are assumed to be for a given temperature. Particularly, the temperature dependency of the microscopic cross-sections is not explicitly indicated.

$$\begin{aligned} \frac{d}{dt} N_i(\vec{r}, t) = & - \left[\int_0^\infty dE \sigma_a^i(E) \phi(E, \vec{r}, t) + \lambda_i \right] N_i(\vec{r}, t) \\ & + \sum_{j \neq i} \left[\int_0^\infty dE f_{j \rightarrow i}(E) \sigma_a^j(E) \phi(E, \vec{r}, t) + l_{j \rightarrow i} \lambda_j \right] N_j(\vec{r}, t) \end{aligned} \quad (6.1)$$

In these equations, the so-called *burnup equations* for the number densities of the nuclides N_i ,² $\sigma_a^i(E)$ is the total absorption cross-section for neutrons and λ_i the decay constant of a given nuclide. The fraction of neutron absorption in nuclide j leading to formation of nuclide i is described by the transition probability $f_{j \rightarrow i}$ and includes, in particular, radiative capture (n, γ), induced fission (n, f), direct reactions (n, xn), etc. Note that for a given j , $\sum_i f_{j \rightarrow i}$ is not necessarily normalized to unity because the nuclide number is generally not conserved in an absorption process, in particular if j is a fissionable isotope and fission products are created. The fraction of radioactive disintegration of nuclide j leading to formation of nuclide i is described by $l_{j \rightarrow i}$ and includes α -, β^- -, and β^+ -decays, but also de-excitation of metastable states.

The equations as formulated in (6.1) do not distinguish between different types of nuclides, although a few general categories can be defined for typical nuclear fuels: these are the actinides ($Z > 90$), the fission products (typically: $35 < Z < 65$), as well as the structural materials, the matrix materials, and a few low- Z activation products. Figure 6.1 shows the section of the chart of the nuclides with those actinides that are most important for neutronics calculations.³

In addition to the availability of a comprehensive database of microscopic cross-sections for all relevant nuclei, the neutron flux distribution in the system has to be known in order to solve the above set of burnup equations. To describe ϕ most generally, the angular neutron flux $\phi(\vec{r}, E, \vec{\Omega}, t)$ is introduced to account for anisotropic phenomena.

$$\phi(\vec{r}, E, \vec{\Omega}, t) = v(E) n(\vec{r}, E, \vec{\Omega}, t) \quad \text{with} \quad v(E) = \sqrt{2E/m_n} \quad (6.2)$$

The correlation between nuclide composition and neutron flux is characterized by the Boltzmann transport equation, which describes the dynamics of the neutron population for arbitrary geometries and material compositions in its most complete mathematical form.

²Number densities and concentrations are both measured in [at/cm³] and used as synonyms below.

³Compare with Table 6.4 for a list of those actinides that are explicitly included in the MCNP simulations.

							Cm-243 29.1 a	Cm-244 18.10 a	Cm-245 8500 a	
						Am-240 50.8 h	Am-241 432.2 a	Am-242 141 a 16 h	Am-243 7370 a	Am-244 10.1 h
				Pu-237 45.2 d	Pu-238 8774 a	Pu-239 2.411 10 ⁴ a	Pu-240 6563 a	Pu-241 14.35 a	Pu-242 3.750 10 ⁵ a	Pu-243 4.956 h
				Np-236 1.54 10 ⁵ a	Np-237 2.140 10 ⁶ a	Np-238 2.117 d	Np-239 2.355 d	Np-240 65 m		
U-232 68.9 a	U-233 1.592 10 ⁵ a	U-234 0.0055 2.455 10 ⁵ a	U-235 0.7200 7038 10 ⁸ a	U-236 2.342 10 ⁷ a	U-237 6.75 d	U-238 99.2745 4.468 10 ⁹ a	U-239 23.5 m			
Pa-231 3.276 10 ⁴ a	Pa-232 1.31 d	Pa-233 270 d	Pa-234 6.70 h							

Figure 6.1: Section of the chart of the nuclides showing the actinides relevant for burnup calculations based on uranium fuels. Simplified data and color convention, indicating half-lives and main decay modes, from Karlsruhe chart of the nuclides [Pfennig et al., 1998].

$$\begin{aligned}
\frac{1}{v(E)} \frac{d\phi(\vec{r}, E, \vec{\Omega}, t)}{dt} &= -\vec{\Omega} \cdot \nabla \phi(\vec{r}, E, \vec{\Omega}, t) - \Sigma_t(\vec{r}, E, \vec{\Omega}, t) \phi(\vec{r}, E, \vec{\Omega}, t) \quad (6.3) \\
&+ \chi(E) \int_{E'} dE' \int_{\vec{\Omega}'} d\vec{\Omega}' \nu \Sigma_f(\vec{r}, E', \vec{\Omega}', t) \phi(\vec{r}, E', \vec{\Omega}', t) \\
&+ \int_{E'} dE' \int_{\vec{\Omega}'} d\vec{\Omega}' \Sigma_s(\vec{r}, E' \rightarrow E, \vec{\Omega}' \rightarrow \vec{\Omega}, t) \phi(\vec{r}, E', \vec{\Omega}', t)
\end{aligned}$$

Here, the macroscopic cross-sections Σ_t , Σ_f , and Σ_s specify the total interaction, the fission, and the double-differential scattering cross-sections, respectively. In all cases, if more than one nuclide is present in the material at position \vec{r} and time t , individual contributions are summed to obtain respective total values.

$$\Sigma(\vec{r}, E, \vec{\Omega}, t) = \sum_i N_i(\vec{r}, t) \sigma_i(E, \vec{\Omega}) \quad (6.4)$$

In the Boltzmann equation, the neutron accumulation rate is reduced by the leakage term $\vec{\Omega} \cdot \nabla \phi(\vec{r}, E, \vec{\Omega}, t)$ as well as by absorption or scattering processes that scale with the total macroscopic cross-section $\Sigma_t(\vec{r}, E, \vec{\Omega}, t)$. Positive contributions occur through

fission processes, which are quantified by the total fission rate and weighted with the fission neutron spectrum $\chi(E)$, as well as by neutron scattering events leading from $(E', \vec{\Omega}')$ to $(E, \vec{\Omega})$.

The coupling of equations (6.1) and (6.3) illuminates the inherent difficulty of solving the burnup equations in their most general form, as the neutron flux is itself a function of the isotopic composition and distribution of the material in the configuration. Irradiation of the fuel therefore leads to the indicated time-dependency of ϕ and would require simultaneous solution of burnup and Boltzmann equations.

Nonetheless, even if the Boltzmann equation is considered for time-invariant material compositions, its solution is impossible for all practical purposes due to the complex structure of the microscopic cross-sections, which has been illustrated for the major uranium isotopes in Figure 2.2. Their structure translates into a similarly complex structure of the local neutron flux in the system. Most importantly, in the vicinity of an absorption resonance at E_R , the neutron flux ϕ collapses because the neutron population reaching E_R per unit-time is finite for a specified strength of the source in the system.⁴ As a result of this effect, local reaction rates, which could have been dominated by one or more pronounced resonances of a single nuclide, may be reduced by orders of magnitude if the concentration of the nuclide itself is non-negligible. The determination of products of the type $\sigma(E) \cdot \phi(E)$ is therefore a most difficult task.

In practice, analytical expressions for the neutron flux distribution cannot be found even for moderately complex configurations of nuclear materials. A major part of the literature on reactor theory and physics is therefore devoted to appropriate approximation methods that yield useful results for neutron flux distributions and averaged cross-sections. Traditional strategies to solve the Boltzmann equation are based on neutron diffusion theory and use multigroup-approaches, in which a spatial and an energy mesh is used to discretize the problem and to determine group-averaged quantities. More sophisticated techniques add explicit consideration of directional properties (discrete ordinate method). For weakly absorbing media and away from the system's boundary or interfaces between dissimilar materials, results based on diffusion theory are adequate for most applications [Knief, 1992, Chapter 5], [Glasstone and Sesonske, 1994, Chapters 3 and 4].

The most powerful and accurate, though non-analytical approach, which is also used in this thesis and introduced further below, is to use the Monte Carlo method to determine neutron flux distributions and actual reaction rates. This technique bypasses the problem of self-shielding because individual particles are tracked and continuous-

⁴In the related case of spatial self-shielding, a nucleus at position \vec{r} may not even be exposed to neutrons of energy E_R because these neutrons are absorbed beforehand by nuclei of the same species closer to the source of neutrons. For instance, the central zone of an absorber pin may be impenetrable to (and therefore irrelevant for) incident neutrons because virtually all neutrons are consumed in the periphery of the pin.

energy cross-section data used. Furthermore, contrary to standard diffusion theory, the Monte Carlo method is a truly three-dimensional method that can easily handle compact and complex geometries characteristic for research reactors. In order to apply the Monte Carlo method to execute reactor burnup calculations, a series of further assumptions are made. In essence, the fundamental equations are simplified as usual by spatially discretizing nuclide composition, neutron flux, and one-group cross-sections and by using averaged data for pre-defined time steps. A discussion of the Monte Carlo method and the particle transport code MCNP follows in Section 6.2

6.1.1 Practical strategy of solution

The general burnup equations (6.1) can be written in more compact, but equivalent, form by introducing the total neutron flux $\phi_{\text{tot}}(\vec{r}, t)$ and spectrum-averaged one-group cross-sections $\sigma(\vec{r}, t)$, which are also simply termed effective cross-sections.

$$\phi_{\text{tot}}(\vec{r}, t) = \int_0^\infty dE \phi(E, \vec{r}, t) \quad \text{and} \quad \sigma(\vec{r}, t) = \frac{\int_0^\infty dE \sigma(E) \phi(E, \vec{r}, t)}{\int_0^\infty dE \phi(E, \vec{r}, t)} \quad (6.5)$$

The effective cross-sections, which no longer represent intrinsic physical properties of the nuclei, formally acquire spatial and time dependencies.⁵ Combining (6.1) and (6.5) yields the following expression.

$$\begin{aligned} \frac{d}{dt} N_i(\vec{r}, t) = & - [\sigma_a^i(\vec{r}, t) \phi_{\text{tot}}(\vec{r}, t) + \lambda_i] N_i(\vec{r}, t) \\ & + \sum_{j \neq i} [f_{j \rightarrow i}(\vec{r}, t) \sigma_a^j(\vec{r}, t) \phi_{\text{tot}}(\vec{r}, t) + l_{j \rightarrow i} \lambda_j] N_j(\vec{r}, t) \end{aligned} \quad (6.6)$$

The spatial dependency of the burnup equations can be removed from the burnup equations by spatially discretizing the equations, i.e. by defining sufficiently small zones or cells, in which variations of all relevant physical properties are ignored. In other words, spatially averaged values for the total neutron flux *and* for the one-group cross-sections are the basis to calculate spatially averaged nuclide compositions in these cells. The burnup equations can be rewritten as indicated below and are then solved for each cell separately, while the user has to verify that the discretized problem faithfully reproduces the actual neutronics.

⁵Similarly, the transition probabilities $f_{j \rightarrow i}$ are now functions of space and time because their values vary as the relative importance of the various neutron-induced processes varies once the nuclide composition and the neutron spectrum evolve during irradiation of the fuel. Note that the $f_{j \rightarrow i}$ from (6.1) and (6.6) are not equivalent.

$$\begin{aligned} \text{For each cell: } \frac{d}{dt} N_i(t) = & - [\sigma_a^i(t) \phi_{\text{tot}}(t) + \lambda_i] N_i(t) \\ & + \sum_{j \neq i} [f_{j \rightarrow i}(t) \sigma_a^j(t) \phi_{\text{tot}}(t) + l_{j \rightarrow i} \lambda_j] N_j(t) \end{aligned} \quad (6.7)$$

Calculations based on discrete burnup-zones as defined by (6.7) are called *cell-burnup* or *point-depletion calculations*. In the simplest case, a single cell may be sufficient to describe the entire problem, the most common one being a fuel pin of infinite length in an infinite lattice — a model that can be used to approximate the average burnup and composition of light-water reactor fuel under typical conditions [Pistner, 1998]. The situation is more complex for research reactors, where the desired high leakage factor for neutrons favors a compact design of the core, which in turn leads to strong spatial dependencies of neutron flux, spectrum-averaged cross-sections, and ultimately fuel burnup. In this case, an adequate spatial discretization of the burnup equations may be a significant part of the problem. A system designed to identify an optimum structure of the burnup zones for the fuel plates of single element reactors is devised in the framework of this thesis and has been presented in Chapter 5.2.

As indicated, the determination of the spectrum-averaged one-group cross-sections $\sigma(t)$ that appear in (6.7) is still a highly complex task due to the effects of spectral and spatial resonance self-shielding, which may occur in one burnup zone or across a series of zones. These cross-sections are determined in M³O with the Monte Carlo method via MCNP. To solve the burnup equations, the average neutron flux and the one-group cross-sections are usually assumed constant for a pre-defined time interval. This final approximation reduces (6.7) to a set of first-order differential equations with constant coefficients, which can be collected in a transition matrix \mathcal{A} .⁶

$$a_{ij} = \begin{cases} -\sigma_a^i \phi_{\text{tot}} - \lambda_i & \text{for } i = j \\ f_{j \rightarrow i} \sigma_a^j \phi_{\text{tot}} + l_{j \rightarrow i} \lambda_j & \text{for } i \neq j \end{cases} \quad (6.8)$$

$$\text{For each cell and burnup step: } \frac{d}{dt} \vec{N}(t) = \mathcal{A}|_{t=t_i} \cdot \vec{N}(t) \quad (6.9)$$

Once all cells have been depleted for a given time step, a new set of cell neutron fluxes and cross-sections is determined. Section 6.3.3 outlines the corresponding solution procedure as implemented in ORIGEN2/M³O in some detail.

Figure 6.2 illustrates the functional relationship of the individual codes that constitute the computational system M³O, and which are described in the remainder of this

⁶For convenience, the coefficients in the burnup equations are collected in the transition matrix \mathcal{A} and the nuclide densities merged to a vector \vec{N} . For obvious reasons, these objects do not represent mathematical entities with the respective fundamental properties.

chapter. At the lowest level of the system, the Monte Carlo particle transport code MCNP and the general point-depletion code ORIGEN2 perform the actual neutronics calculations. Communication between both programs is coordinated by the linkage program MCODE. In particular and as will be detailed further below, MCODE regularly updates a base MCNP input deck of the reactor to enable determination of required flux and cross-section data. These data are then passed to ORIGEN2 for the next burnup step. Most importantly, this computational approach enables ORIGEN2 to use spectrum-averaged cross-sections that are adequate for the given reactor geometry and current fuel burnup. The initial set-up of the problem, and in particular the set-up of the base MCNP input deck, is prepared by using numerous modules programmed in *Mathematica*. The specific tasks of *Mathematica*, which forms a central part of M³O, are laid out in Chapters 5 and 9 of this thesis. Furthermore, *Mathematica* is also used to evaluate and visualize the results returned by MCNP and MCODE.

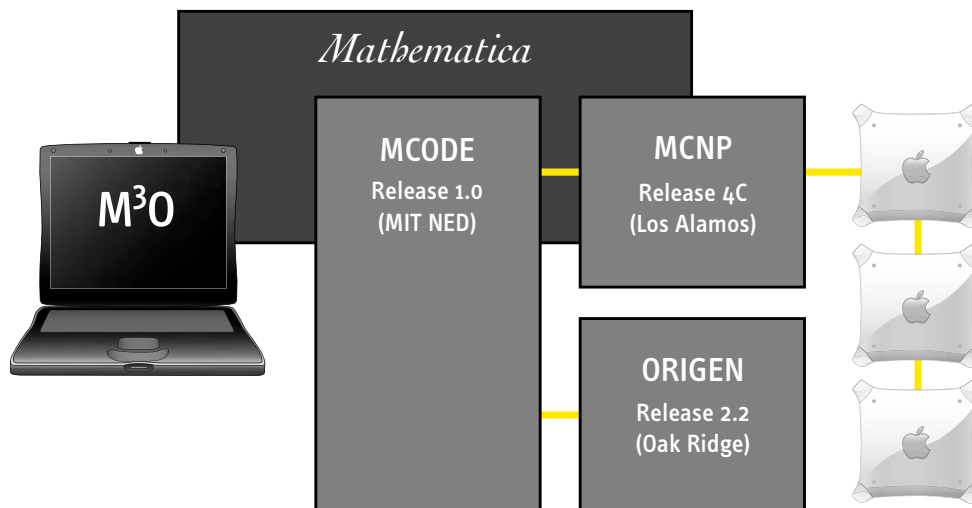


Figure 6.2: Computational system M³O for research reactor analysis.

6.2 Monte Carlo Method and MCNP

“The greatest usefulness of the Monte Carlo method is in those calculations that cannot be performed reasonably in any other way, that is, the Monte Carlo method should be considered a method of last resort and should never be used as a substitute for thought.”

[Sangren, 1960, p. 163]

“MCNP (and any general Monte Carlo Code) is little more than a collection of random decision points with some simple arithmetic in between.”

MCNP Manual, [Briesmeister, ed., 1993, p. 2-1]

The origins of the Monte Carlo method date back to the 1940s, when J. von Neumann, N. Metropolis, S. Ulam, E. Fermi, and others first considered the application of statistical sampling techniques for the solution of neutron diffusion problems.⁷ As its name suggests and as will be discussed below, the Monte Carlo method consists in carrying out a ‘theoretical experiment’ by tracking a large number of individual particles to determine characteristic data for the modeled configuration based on the average behavior of these particles. The basic Monte Carlo method, in which all essential features of random walk are applied to the problem of neutron transport in bulk matter are already developed, is laid out in [Cashwell and Everett, 1959]. For obvious reasons, interest in and the usefulness of the Monte Carlo method increased with the development of electronic computers since the 1970s. Some basic principles of the method, general variance reduction techniques, as well as MCNP-specific concepts and features are briefly discussed in the following. Particular attention is also devoted to cross-section libraries, which largely determine the *accuracy* of any result obtained with Monte Carlo particle transport (systematic error), and to the *precision* of results, which in turn is determined by the statistics of the simulation and common to all methods based on statistical sampling techniques (uncertainty).

⁷These research and development efforts were carried out within the *Manhattan Project*. First Monte Carlo simulations were designed for and performed with the ENIAC machine in 1945/46. Reportedly, E. Fermi used a ‘manual’ Monte Carlo method already in the 1930s and later developed a mechanical Monte Carlo device, the FERMIAC, to simulate neutron transport in fissile material at Los Alamos. For a personal account of the origins of the Monte Carlo method, see for instance [Metropolis, 1987].

6.2.1 Basic principles of the Monte Carlo method

Conceptually, the Monte Carlo method is the simplest of all conceivable mathematical approaches to solve any problem related to particle transport in bulk matter.⁸ Instead of deriving approximated analytical solutions from the fundamental transport equations, individual particles are simply followed from the source to a terminal event using appropriately distributed random or pseudo-random numbers to choose among allowed processes and events along the trajectory. Ultimately, by virtue of the central limit theorem (CLT) and the strong law of large numbers, the average behavior of the particles of the physical system is then inferred from the average behavior of the simulated particles. The precision of the results, i.e. the estimated standard deviation of a mean value, is closely related to the total number of particles tracked.

Even though no transport equation is ever written down, the Monte Carlo method is nevertheless equivalent to a solution of the Boltzmann equation, as it corresponds to the evaluation of the source integrals in (6.3) by a random-sampling method. The fundamental basis of the applicability of the Monte Carlo method is the principle that individual physical events and particle interactions in the modeled geometry are uncorrelated and can therefore be simulated sequentially, i.e. one particle at a time.

As it tracks particles explicitly, the Monte Carlo method does not require the use of energy groups nor of a spatial and angular mesh. As a result, Monte Carlo codes are able to use point-wise (continuous energy) cross-section data, which eliminates the need for multigroup-averaging and automatically guarantees correct treatment of cross-section resonances. Furthermore, as events are sampled directly from first-principle physical laws, there is no need to approximate the angular distribution of scattered particles by Legendre polynomials either, as is the case with codes based on diffusion theory.

Due to the very nature of the approach, there is no necessity to simplify any element of the geometry. In reactor calculations, the Monte Carlo method therefore allows for accurate and detailed representation of fueled regions, coolant channels, structural materials, etc. Codes based on the Monte Carlo method are particularly useful and far superior to deterministic codes for systems characterized by high leakage factors with strong local variations of the neutronics and boundary conditions that are difficult to treat satisfactorily with deterministic methods. In fact, computer codes based on analytical methods, such as two- and three-dimensional diffusion codes, are verified and validated against Monte Carlo calculations.

Powerful Monte Carlo codes for neutron transport became internationally available in the 1980s, but its use was usually limited to dedicated workstations and supercomput-

⁸The Monte Carlo method can be applied to much broader problems in modern engineering, mathematics, and physics and is by no means restricted to particle transport analysis. In this more general context, Monte Carlo techniques are particularly relevant in integration and optimization methods [Liu, 2001].

ers at that time. Only the development of the personal computer, and its performance increase of the last ten years, has allowed the use of the Monte Carlo method for scientific applications on a broad base in universities and elsewhere. Most of the simulations performed in the context of this thesis, and in particular the full-scale reactor calculations presented in Chapters 7, 8, and 10, would have been impossible to perform with a realistic amount of computing time even five years ago.⁹

6.2.2 Variance reduction techniques

The most straightforward approach to Monte Carlo would be to faithfully simulate each particle track as well as each event and interaction as expected to occur in nature, i.e. based upon the actual mean free path, the cross-sections for all processes, etc. However, this approach, sometimes called *Analog Monte Carlo Method*, is highly inefficient in most instances; and a variety of strategies can be devised — reaching ‘from the obvious to the esoteric’ — to optimize a Monte Carlo simulation in order to get the best results for a given number of tracked particles or assigned computer time.¹⁰ These strategies can be categorized as variance reduction techniques and, to varying degrees, all serious Monte Carlo codes make use of them.

The basic idea of variance reduction is to dedicate the maximum amount of computer-time to those particles in phase space (position, direction, energy) that are most likely to make a meaningful contribution to the desired results — and to avoid using computer time for particles that are unlikely to do so. Some standard variance reduction techniques are briefly summarized in the following.

The fundamental concept for most variance reduction techniques is to assign a weight factor W to each particle, which may or may not be equal to unity at the source. The particle weight W is then modified in the course of the particle’s life.

Implicit capture and forced collision. Losing a tracked particle to an absorption (capture) process, is an undesired event in any Monte Carlo simulation — particularly, if a particle is considered valuable because it is traveling in an important region of the geometry, possibly far from the source, and significant computer time had already been used to transport the particle to its present location. Instead, in standard Monte Carlo particle transport codes, the concept of implicit capture or survival biasing is used to avoid losing particles. Here, the weight of a tracked particle is always reduced by the capture probability at each collision event and radiative capture being subsequently excluded from the list of allowed processes. The particle therefore is never killed by

⁹Some results in this thesis are based on up to 40 million neutron histories and required generation of 8.5×10^{10} random numbers per simulation.

¹⁰Indeed, it has been emphasized that “for many problems, variance reduction is not just a way to speed up the problem but is absolutely necessary to get any answer at all” [Briesmeister, ed., 1993, p. 1-11].

capture. Conceptually similar to implicit capture, forced collision guarantees that a particle does always interact in a zone of high interest if such an event is advantageous for the tally statistics. If forced collision is used, the particle weight is adjusted correspondingly in each event.

Particle splitting and Russian roulette. Both concepts, particle splitting and Russian roulette, belong to the important category of *population control methods*. In the first case, if the weight of a given particle surpasses a defined threshold, for example because the particle is entering an important region of the geometry, the statistics of the Monte Carlo results can be improved by splitting this particle into two or more sub-particles and to reduce the weight of each one by the corresponding factor, conserving the overall total weight value. In the second case, for particles whose weight has decayed significantly, the particle is discarded or ‘killed’ with a pre-defined high probability (Russian roulette). If the particle survives this process, its weight is increased correspondingly, which guarantees weight conservation on average. Russian roulette is an effective tool to avoid using computer time on unimportant particles by tracking fewer ones with increased weight in unimportant regions of the geometry.

6.2.3 Development and release history of MCNP

Monte Carlo N-Particle (MCNP) is a general-purpose Monte Carlo code, originally developed by the Monte Carlo Group (Group X-6) in the Applied Theoretical Physics Division (X-Division) at Los Alamos National Laboratory [Briesmeister, ed., 2000].¹¹ The code used to be limited to particle energies of up to 20 MeV, which is sufficient for problems involving neutron-induced fission in critical configurations. However, the code has recently been extended to energies of up to 5 GeV for neutrons and protons by merging MCNP with previously independent high-energy physics codes [Waters, 2002]. The new code, developed independently from MCNP, is now designated MCNPX, the most current release of which is the version 2.5.E from February 2004. The physics relevant to this thesis can be adequately treated with the standard MCNP code.¹²

¹¹The first Monte Carlo code released by LANL was MCS in 1963. Subsequent improved and generalized codes included MCN (1965), MCNG (1973, photon transport added), and MCNP (1977, improved coupled neutron-photon transport). With the release of MCNP3 in 1983, the code was first made available internationally. The most recent releases of MCNP are 3A (1986), 3B (1988), 4 (1990), 4A (1993), 4B (1997), 4C (2000), and 5 (2004). Information on the release history from [Briesmeister, ed., 1993, pp. 2-1–2-4] and more recent versions of the code manual.

¹²Nonetheless, since MCNP itself is a functional part of the extended high-energy version, MCNPX is used in some instances, as its development seems to proceed faster than the development of the standard MCNP code.

6.2.4 Specific concepts and features of MCNP

A detailed discussion of MCNP-specific concepts and features is beyond the scope of this discussion and the reader is referred to code manuals of the most recent releases of MCNP [Briesmeister, ed., 1993, 1997, 2000] as well as to the extensive literature on specific applications of MCNP published by Los Alamos and others.

With regard to the implementation of the Monte Carlo method itself, it should be noted that all variance reduction techniques discussed above are implemented in MCNP and used by default. In addition, more advanced and more specialized techniques and features — weight windows, deterministic transport, etc. — have also been implemented in more recent versions of the code. As it is common to most codes used for Monte Carlo particle transport, the material composition of any system modeled in MCNP is assumed invariable in time. In general, the latter is only approximately true since transmutation occurs in particular in the case of neutron transport problems in fissile material and the Monte Carlo simulation creates a ‘snapshot’ of the configuration.¹³

The general structure of MCNP input, the concept of tallies to generate results, and some particularities of criticality calculations are briefly summarized below.

General structure of MCNP input

Each MCNP input file is subdivided into three main sections: the cell card section, the surface card section, and the data card section. The cell card section defines all cells or volumes by logically combining the surfaces provided in the surface card section and specifies the materials (composition and density) filling the corresponding cells. With these two sections of the input deck, the geometrical and physical set-up of the problem is complete. The data card section specifies all material compositions used in the problem, defines the particle source and the tallies to be collected in the simulation, and specifies further details required to run the simulation, including the mode of operation: particle types to be tracked, criticality calculation, etc.

As an example, a sample MCNP input deck, which generates a detailed model of the core of a generic single element reactor, is reproduced in Appendix D. A detailed description of MCNP input and syntax is provided in [Briesmeister, ed., 1993, Chapter 3] as well as in more recent releases of the code manual.

¹³Even though the number of tracked particles may be large, i.e. in the order of several millions, this number is still negligible on a macroscopic scale. New codes are now under development that integrate simulation of the neutronics and burnup of the material on a microscopic scale. For instance, the *Monte Carlo Continuous Energy Burnup* (MCB) code follows this approach and performs an ‘in flight transmutation trajectory analysis’ [Cetnar et al., 2002].

Monte Carlo results and tallies

Due to the nature of the Monte Carlo method, MCNP does not solve specific equations and consequently does not return analytical results. In practice, prior to running the simulation, the analyst has to decide what types of information he or she wants to extract. Results are generated by collecting relevant data along individual particle paths and include track lengths in cells, particle directions, etc. Any quantity of the indicated form can be tallied.

$$C \int_V \int_E \int_t R(E) \phi(\vec{r}, E, t) dt dE dV$$

There are a total of seven tally types for neutrons, but only a few of them are relevant for the neutronics calculations to be performed here: these are the track length estimate of cell flux (F_4) as well as, for a few specific analyses, the surface flux (F_2) and the surface current (F_1). Tally data are normalized to be per starting particle and have to be scaled to absolute values by the analyst using additional information on the modeled system.¹⁴ Most importantly and as an example, the track length estimate of the neutron flux in a cell is given by the following expression.

$$F_4 = \frac{1}{V} \int_V \int_E \int_t \phi(\vec{r}, E, t) dt dE dV = \frac{1}{V} \left(\frac{1}{n} \sum_{i=1}^n W_i L_i \right) \quad (6.10)$$

The neutron flux ϕ is defined as the total track length traveled by all neutrons per unit time and volume.¹⁵ As indicated, tallies can be modified by operators or so-called *tally multipliers* of additive and/or multiplicative response functions taken from the available MCNP cross-section libraries. In the case of tally-type F_4 , these multipliers can be used to determine reaction rates for arbitrary nuclides and processes. In conjunction with the total neutron flux from a standard F_4 tally to normalize all tally values, spectrum-averaged cross-sections for arbitrary nuclides and processes can be determined. Those cross-sections are the basis for the burnup calculations performed in the following chapters.

$$F_4^* = \frac{1}{V} \int_V \int_E \int_t \sigma(T, E) \phi(\vec{r}, E, t) dt dE dV \quad (6.11)$$

¹⁴In general, the user knows the strength of the particle source, i.e. its emission rate or the total power released in the system, and may use this information to scale tally data to obtain final results. Once a normalization factor has been specified for one tally, this value can be used for all other tallies calculated in a given MCNP run.

¹⁵Note that, even though the unit of the neutron flux [n/cm²s] may suggest the opposite, it is not useful and generally not possible to refer to a specific area or surface that is crossed by the particles characterized by ϕ , unless a mono-directional neutron beam is observed.

By including additional material cards in the MCNP input deck for *each* nuclide that one is interested in, the corresponding cross-section data $\sigma(T, E)$ is loaded upon initialization and spectrum-averaged one-group cross-sections can be calculated during the simulation. Note that a material does *not* have to be present in the corresponding MCNP cell, for which cross-section data are calculated. So-called infinite-dilution cross-sections are determined under these circumstances.¹⁶ As indicated, the microscopic cross-sections are generally temperature-dependent, mainly due to the Doppler broadening of the absorption resonances. This dependency is not made explicit in the following because only steady-state situations at constant temperatures are considered in this thesis. Cross-section libraries are used at the respective temperatures.

Criticality calculations

Criticality calculations are an important specific feature of MCNP and require a separate discussion, because the Monte Carlo simulation itself is organized differently. Specifically, in standard simulations, a fixed particle source is defined for the problem prior to execution of MCNP and each tally is normalized per started neutron from that source. In contrast, in criticality calculations, no fixed source is specified, but the positions of the fission events themselves are used to define the source dynamically during the simulation. Since a criticality calculation is organized in so-called generations (see below), the source changes from cycle to cycle. Starting with an initial source provided by the user or available from an earlier MCNP run, the normalized neutron density distribution ideally approaches an equilibrium distribution early in the simulation.

As in many other Monte Carlo codes, MCNP uses the concept of *neutron generation* to structure and perform criticality calculations. A generation is defined as a selected number of neutrons followed from their source or ‘birth’ to their termination or ‘death’. A particle is terminated once it escapes from the system, i.e. the particle enters a region of zero importance, or once a terminal event is selected. While direct reactions of the type (n, xn) are considered internal to a cycle, compound nucleus reactions, such as neutron capture or induced fission, terminate the fate of tracked particles.¹⁷ Eventually, the stored positions of all fission events that occurred during a cycle are used to set-up the source for the next generation of neutrons.

The central result of a criticality calculation is the determination of the effective multiplication factor k_{eff} of the system, which is simply defined as follows.

$$k_{\text{eff}} = \frac{\text{Number of neutrons in the } N\text{th generation}}{\text{Number of neutrons in the } (N - 1)\text{th generation}} \quad (6.12)$$

¹⁶Infinite-dilution cross-sections are equivalent to the highest cross-section-values for a specified neutron spectrum because the effect of resonance self-shielding is absent.

¹⁷The time-scale of a direct reaction is in the order of 10^{-22} s, whereas a compound nucleus formed after neutron absorption survives for about 10^{-16} s.

Effective multiplication factors of exactly one, less than one, or greater than one corresponds to critical, sub-critical, and supercritical configurations, respectively. By introducing the infinite multiplication factor k_∞ for the equivalent system with infinite extension, and therefore without neutron leakage, one can also express the k -values in terms of the effective macroscopic cross-sections of the system.

$$k_\infty = \frac{\text{Production}}{\text{Absorption}} = \frac{\bar{\nu} \langle \Sigma_f \rangle}{\langle \Sigma_a \rangle} \quad \text{and} \quad k_{\text{eff}} = \frac{\text{Production}}{\text{Absorption} + \text{Leakage}} = P_{\text{nl}} k_\infty \quad (6.13)$$

These expressions for k_∞ and k_{eff} appear deceptively simple as the fundamental quantities, i.e. the effective macroscopic cross-sections of the entire system and the non-leakage probability P_{nl} , are of course unknown; and their determination would be equivalent to the solution of the fundamental transport equations. Again, diffusion theory can be used to derive formulae for k_∞ and k_{eff} that are valid under certain conditions and for specified simple geometries. Most generally, k_{eff} can be written in an integral form.

$$k_{\text{eff}} = \int_V \int_0^\infty \int_E \int_\Omega \nu \Sigma_{\text{fis}} \phi \, d\Omega \, dE \, dt \, dV \quad (6.14)$$

$$\cdot \left[\int_V \int_0^\infty \int_E \int_\Omega \Sigma_{\text{abs}} \phi + (\nabla \cdot \vec{J}) \, d\Omega \, dE \, dt \, dV \right]^{-1}$$

MCNP uses three different methods to estimate the k_{eff} : a collision estimator, an absorption estimator, and a track length estimator. As their names indicate, these estimators tally different characteristics once a neutron enters a cell containing fissionable materials. MCNP produces a final combined estimate for k_{eff} and confidence intervals based on these individual estimators using a maximum likelihood estimate.¹⁸

The fundamental theoretical problem of calculating the k_{eff} of any nuclear system, which is *not* exactly critical, is population control. Specifically, in a supercritical system, an exponential growth of the neutron population has to be prevented cycle-by-cycle by selecting an adequate set of neutrons for the next generation without distortion of the neutron population, i.e. without biasing the real k_{eff} of the system. There is an ongoing debate among developers and users of Monte Carlo codes, about which mathematical techniques are best suited to control the neutron population under these circumstances. Cullen et al. [2003] discuss the similarities and differences of so-called

¹⁸Usually, the individual estimators are positively correlated. Due to the diversity of allowed variance reduction techniques, which may bias collision, absorption, and track length values differently, the combination of k_{eff} -estimates is a non-trivial procedure.

static and dynamic methods used for population control in criticality calculations in great detail.¹⁹

6.2.5 Cross-section libraries and $S(\alpha, \beta)$ -tables

The basis for the simulation of all fundamental processes in MCNP, or any other Monte Carlo transport code, are the cross-sections and other nuclear data for neutrons and correlated secondary particles, which are organized in comprehensive data libraries. Cross-sections primarily depend upon the nucleus the neutron is interacting with, as well as upon the energy of the incident neutron and the temperature of the medium. The cross-section values $\sigma(T, E)$ are derived from both experimental data as well as from theoretical models, if direct experimental measurement is impossible. Ultimately, cross-sections are summarized and organized in so-called *Evaluated Nuclear Data Files* or libraries [CSEWG, 2001]. To use these evaluated data libraries with specific neutronics codes, such as MCNP, the data has to be adequately formatted to suit the requirements of the code and of the specific problem to be solved. In the case of MCNP, this task is done with the processing code NJOY for data in ENDF format [MacFarlane and Muir, 1994]. Numerous validated and comprehensive cross-section libraries for MCNP exist and many of them are distributed with the code itself [ORNL, 2001]. In Europe, additional libraries are maintained and distributed by the Nuclear Energy Agency (NEA) of the OECD.

MCNP primarily uses continuous-energy nuclear and atomic data libraries. Nuclear data tables exist for various classes of interactions and include neutron interactions, neutron-induced photons, photon interactions, etc. In the case of neutron interactions, continuous-energy and discrete reaction data are available, the latter based on multigroup-averaged cross-sections. In addition to cross-section data, the MCNP libraries also include angular distributions for scattering, fission yields, Q-values, etc. [Briesmeister, ed., 1993, Chapter 2, III].

The calculations performed in this thesis are largely based on data from [Gil, 2001], a comprehensive collection of cross-section data derived from the ENDF/B-VI (Release 5) collection. Since research reactors are operated at relatively low pressures and temperatures, nuclear data evaluated for a temperature of 300 K are used in virtu-

¹⁹The subtleties of this computational problem are beyond the scope of this discussion. Nonetheless, it should be emphasized that MCNP uses a population control method, the so-called k -static method, that is unreliable for highly sub- or supercritical systems under *very specific* circumstances. Corresponding situations are not encountered in the reactor calculations performed below. The systems studied in this thesis require a thermal neutron spectrum to achieve criticality and, even at BOL, are not very supercritical. For these reasons, MCNP can be expected to provide extremely reliable and accurate results.

ally all simulations.²⁰ Cross-sections are required for all materials used in the model of the reactor: these include structural materials, the coolant and moderator, as well as the nuclides built-up in the fuel and treated explicitly in MCNP, which are listed in Table 6.4.

Thermal scattering matrix $S(\alpha, \beta)$

For low energies, the scattering behavior of neutrons depends upon binding effects in the material and the possibility to excite vibrational modes, if the target nucleus is a low- A material embedded in a molecule or lattice. In this case, incoherent inelastic scattering, which can be described by the following expression [MacFarlane and Muir, 1994, Chapter VII], strongly contributes to the thermal scattering cross-sections of neutrons.

$$\sigma(E, E', \mu) = \frac{\sigma}{2kT} \sqrt{\frac{E'}{E}} \exp\left(-\frac{\beta}{2}\right) S(\alpha, \beta) \quad (6.15)$$

E and E' are the energies of the incident and the scattered neutron, μ is the cosine of the scattering angle in the laboratory system, and σ the integral scattering cross-section of the bound nucleus for the limit of low neutron energies at $T = 0$. The scattering matrix $S(\alpha, \beta)$ itself is a function of the momentum transfer α and the energy transfer β , which are both defined as dimensionless quantities.

$$\alpha = \frac{E' + E - 2\mu\sqrt{E'E}}{AkT} \quad \text{and} \quad \beta = \frac{E' - E}{kT} \quad (6.16)$$

For gaseous and unbound nuclei, MCNP explicitly calculates the scattering matrix $S(\alpha, \beta)$ with the corresponding analytic expression.

$$S(\alpha, \beta) = \frac{1}{\sqrt{4\pi\alpha}} \exp\left(-\frac{\alpha^2 + \beta^2}{4\alpha}\right) \quad (6.17)$$

In all other occasions, i.e. for specified material compositions, the values of $S(\alpha, \beta)$ are tabulated in additional libraries and can be requested by the code. Since incoherent inelastic scattering is most relevant for materials containing low- A nuclei, MCNP provides tabulated data for hydrogen in light water, deuterium in heavy water, beryllium, or graphite, but also for more complex compositions such as methane, polyethylene, etc. [Briesmeister, ed., 1993, Appendix G].

²⁰Maximum coolant temperatures are usually below 50–60 °C. Only for the liquid deuterium employed in cold neutron sources at 20 K, cross-section data evaluated for 0 K was used and corrected for the specified value.

6.2.6 Monte Carlo precision

The Monte Carlo method determines arbitrary physical quantities by tracking and simulating a large number of individual particles and events. The values obtained in those simulations are statistical values and their precision depends in particular upon the quality of the statistics, which in turn is strongly determined by the total number of particles simulated.

More generally, one has to distinguish between *accuracy* and *precision* of Monte Carlo results. Only the precision, which is associated with the residual statistical error, will be discussed in the following. In addition, there may still exist a discrepancy between a result obtained in a simulation and a direct observation or measurement, i.e. the physical world. This systematic error or bias may be due to errors in the cross-section libraries, material compositions, physical description of the geometry (model), etc. For obvious reasons, this type of error cannot be identified or even reduced via better statistics. However, systematic errors can be expected to be minimal compared to other computational techniques because the Monte Carlo method facilitates the most accurate representation of the geometry of the physical system *and* uses point-wise cross-section data.

Be $f(x)$ the probability density function of a random variable x having a sufficiently strong central tendency. In this case, it is useful to characterize this variable (observable) by a variety of characteristic numbers, the *moments* of the distribution, some of which are introduced below. The true mean or expected value of a random variable x with probability density function $f(x)$ is given by:

$$E(x) = \int x f(x) dx \quad (6.18)$$

In general, the probability density function $f(x)$ is *a priori* unknown. Nonetheless, an estimated mean $\langle x \rangle$ can be calculated from the finite set of data (x_1, \dots, x_N) obtained in the Monte Carlo simulation. As indicated below, by virtue of the *Strong Law of Large Numbers*, the sample mean $\langle x \rangle$ tends to $E(x)$ as N approaches infinity.

$$\langle x \rangle = \frac{1}{N} \sum_{i=1}^N x_i \quad \text{and} \quad \langle x \rangle \approx E(x) \quad \text{for large } N \quad (6.19)$$

The second moment of a random variable x is known as the variance, which characterizes the dispersion width of x around the expected value $E(x)$. The integral in (6.20) defining the variance can be rewritten to obtain an expression, which is often more convenient in practical situations.

$$\text{Var}(x) = \sigma^2 = \int (x - E(x))^2 f(x) dx = E(x^2) - (E(x))^2 \quad (6.20)$$

As indicated, the square root of the variance is defined as the standard deviation σ , which is further discussed below. Again, the variance σ^2 will generally be an unknown property of the sampled variable and, in analogy to the sample mean, an estimated value S^2 of the variance $\text{Var}(x)$ is defined.

$$S^2 = \frac{1}{N-1} \sum_{i=1}^N (x_i - \langle x \rangle)^2 = \frac{N}{N-1} (\langle x^2 \rangle - \langle x \rangle^2) \approx \langle x^2 \rangle - \langle x \rangle^2 \quad (6.21)$$

Note that S^2 is essentially independent of the total number N of particles tracked.²¹ In analogy to equation (6.19), $\langle x^2 \rangle$ is defined as:

$$\langle x^2 \rangle = \frac{1}{N} \sum_{i=1}^N x_i^2$$

In random-walk problems executed with the Monte Carlo method, the user is typically not interested in the variance of individual events around a mean value, but rather in the uncertainty $S_{\langle x \rangle}$ of the sample mean, which is related to S as defined in (6.21) via the following expression [Taylor, 1982, Chapter 5].

$$S_{\langle x \rangle} = \frac{S}{\sqrt{N}} \quad \text{or} \quad S_{\langle x \rangle} \sim \frac{S}{\sqrt{T_{\text{sim}}}} \quad (6.22)$$

The fact that the precision of a result only increases with \sqrt{N} is an inherent disadvantage of the Monte Carlo method. In particular, in making the plausible assumption that the total number of simulated particles is directly proportional to the duration T_{sim} of a given simulation, a four-fold increase of computer time is for instance required to reduce the uncertainty of a Monte Carlo result by a factor of two. This circumstance emphasizes the importance of using variance reduction techniques as a primary method to improve statistics of a Monte Carlo simulation.

Ultimately, the central limit theorem can be used to provide confidence intervals for Monte Carlo results. The theorem states that for large N , the distribution of the sample mean $\langle x \rangle$ of a random variable x with probability density function $f(x)$ is characterized by a Normal or Gaussian distribution.²² In those cases, confidence intervals for the true

²¹Note also that, in the definition of S , the denominator to normalize the sample data is $(N-1)$ and not N . Consult any good statistics textbook for an explanation of this subtlety. In this regard, Press et al. [1995] comment that “if the difference between N and $N-1$ ever matters to you, then you are probably up to no good anyway” (p. 611).

²²In addition, the moments of the distribution have to exist.

mean $E(x)$ can be specified [Bronstein and Semendjajew, 1989].

$$\begin{aligned} 68\% \text{ confidence interval: } & \langle x \rangle - S_{\langle x \rangle} < E(x) < \langle x \rangle + S_{\langle x \rangle} \\ 95\% \text{ confidence interval: } & \langle x \rangle - 2 S_{\langle x \rangle} < E(x) < \langle x \rangle + 2 S_{\langle x \rangle} \end{aligned} \quad (6.23)$$

By default, and in addition to the sample mean $\langle x \rangle$, MCNP prints the relative error R , which is defined as the ratio of the estimated standard deviation $S_{\langle x \rangle}$ and the estimated mean, for all tallies requested by the user.

$$R = \frac{S_{\langle x \rangle}}{\langle x \rangle} \quad (6.24)$$

MCNP also performs a series of statistical checks of the tally data, which are summarized in the output file and which have to be reviewed by the user to verify that the simulation is statistically stable.

6.3 ORIGEN2

The *Oak Ridge (National Laboratory) Isotope Generation and Depletion Code* (ORIGEN2) is a general zero-dimensional point-depletion and radioactive decay code used to calculate time-dependent characteristics of nuclear materials, in particular during irradiation in a reactor of a specified type. Besides MCNP, ORIGEN2 is the second central component of M³O performing neutronics calculations for all simulations. Its basic features are briefly summarized in this section; for an in-depth discussion of the code however, see [Croff, 1980, 1983, Ludwig, 2002].

6.3.1 Development and release history

Oak Ridge National Laboratory (ORNL) released the first version of ORIGEN in the early 1970s. At that time, its principal purpose was to generate spent fuel and waste characteristics — including isotope composition, radiation levels, etc. — to study and design reprocessing plants or other facilities of the nuclear fuel cycle. Based on simple tabulated data of half-lives, thermal cross-sections, resonance integrals, etc., ORIGEN produced representative estimates, which were considered satisfactory for the designated purpose.

Development of ORIGEN2 began in 1975 and a revised and significantly extended version of ORIGEN was released in 1980. With ORIGEN2 the concept of commands

was introduced and more flexible and transparent ways to use and exchange data bases were included. For more than 20 years, no changes to the source code were made and subsequent releases in 1986 and 1991 (version 2.1) focused upon additional/updated data libraries and portability of the code to other platforms. The ORIGEN2 release used in M³O is version 2.2 from May 2002.²³

6.3.2 Input and output data

ORIGEN2 distinguishes three classes of nuclides that consist of 130 actinides, 850 fission products, and 720 activation products, which may include structural materials and low-Z impurities. Out of the total of 1700 nuclides known by ORIGEN2, only 1300 are unique (including 300 stable ones), because some elements occur in more than one category.

In addition to the specific problem description, ORIGEN2 requires three different types of input data bases to perform burnup calculations and to generate additional properties of the irradiated nuclear material. These are radioactive decay data, photon production data, and cross-section libraries.²⁴ Based on this data, ORIGEN2 generates a diverse set of output tables, which are summarized in Table 6.1. The standard output specifically includes mass, isotopic composition, radioactivity, toxicity, neutron absorption rate, neutron and photon emission, as well as heat generation. As indicated, most data is given both in absolute and fractional units. Radiotoxicity is quantified by the volume of water or air required to dilute the toxicity of the material to acceptable levels.

In general, a single radioactive decay library and a single photon production library will be sufficient and adequate for all practical problems encountered. The situation for cross-section data is entirely different. Spectrum-averaged one-group cross-sections are reactor- or spectrum-specific *and* evolve during irradiation of the fuel.

ORIGEN2 provides a set of cross-section libraries for most common reactor and fuel-types.²⁵ In addition, the code permits the substitution of cross-section data with external data provided by the user. This important feature is the basis for the M³O/MCODE code system, which generates its own cross-section data for most nuclides by means of the MCNP Monte Carlo methods outlined above. The remaining nuclides, not explicitly treated in MCNP, will be mainly fission products with negligible macroscopic

²³Release 2.2 eliminates a bug, which caused an underreporting of the mass of fission products if a significant fraction of fission events occurred in so-called unconnected actinides [Ludwig, 2002], [Xu, 2003, p. 89].

²⁴Fission yield data are listed with the cross-section libraries.

²⁵Among the 50 or so libraries that come with ORIGEN2 are cross-sections for pressurized-water, boiling-water, CANDU, and fast reactors. The libraries also distinguish between different LEU and MOX fuel compositions.

Table	Data type listed	Units
01–02	Isotopic composition	at%, wt%
03–06	Composition	at%, wt%, grams absolute and fractional
07–08	Radioactivity (total)	Ci absolute and fractional
09–10	Thermal power	W absolute and fractional
11–12	Radioactivity (total)	Bq absolute and fractional
13–14	Radioactive inhalation hazard	cubic meter air absolute and fractional
15–16	Radioactive ingestion hazard	cubic meter water absolute and fractional
17–18	Chemical ingestion hazard	cubic meter water absolute and fractional
19–20	Neutron absorption rate	neutrons per sec
21–22	Neutron induced fission rate	fissions per sec
23–24	Radioactivity (α)	Ci absolute and fractional
25	(α, n) neutron production	neutrons per sec
26	Spont. fission neutron production	neutrons per sec
27	Photon emission rate	photons per sec
28	—	—

Table 6.1: Standard ORIGEN2 output tables. See main text for details.

cross-sections, i.e. low concentrations or low microscopic cross-sections. These isotopes therefore have an insignificant impact on the neutronics and the error introduced by using a pre-defined ORIGEN2 cross-section is virtually nil.

6.3.3 Method of solution

As might be expected from the nature of the problem to be solved, “most of the calculations carried out by ORIGEN2 are essentially trivial” [Croff, 1983, p. 338]. Standard mathematical methods can be applied to solve the burnup equations if adequate precautions are taken.

If continuous external feed streams are excluded, the burnup equations are described by a set of homogeneous first-order ordinary differential equations. Written in matrix-form, this system is characterized by an extremely sparse transition matrix, typically with about 99.8% zero elements, i.e. no physical process leading to a transition between the corresponding nuclides, and widely spaced eigenvalues as can be expected for the range of half-lives that occur in nature.

As outlined in Section 6.1.1, the fundamental approximation to solve the burnup equations is to consider small time steps, during which the neutron flux $\phi_{\text{tot}}(t)$ and the one-group cross-sections $\sigma(t)$ are assumed constant. As a result, the original set of differential equations reduces to a simplified set with constant coefficients.

$$\frac{d}{dt}N_i(t) = -[\sigma_a^i \phi_{\text{tot}} + \lambda_i] N_i(t) + \sum_{j \neq i} [\sigma_{j \rightarrow i} \phi_{\text{tot}} + \lambda_{j \rightarrow i}] N_j(t) \quad (6.25)$$

Equivalently, this set of equations can be written in matrix form, in which the transition matrix \mathcal{A} for the current time step is now time-invariant, see (6.8) and (6.9).

$$\frac{d}{dt}\vec{N}(t) = \mathcal{A} \cdot \vec{N}(t) \quad \text{and} \quad \vec{N}(t) = \exp(\mathcal{A}t) \cdot \vec{N}(t = t_0) \quad (6.26)$$

Various reaction-types are determined by cross-sections and fission yields, and scale with the local (total) neutron flux. With the total power level released in the modeled fuel volume fixed (power level normalization), the neutron flux has to be calculated in order to finalize generation of the transition matrix \mathcal{A} .²⁶ The recoverable energy R_i per fission of the nuclide (Z_i, A_i) is obtained from an empirical formula, which has been found to be accurate within 1% for all relevant fissionable isotopes.

$$\phi_{\text{tot}} = \frac{6.242 \times 10^{18} P(\text{MW})}{\sum_i (N_i \sigma_i R_i)} \quad \text{and} \quad R_i(\text{MeV}) \approx 0.0013 (Z_i^2 \sqrt{A_i}) + 33.12 \quad (6.27)$$

The expression for the neutron flux is valid for the known initial composition of the fissile isotopes, i.e. at the beginning of the time step. To produce the most accurate results possible, ORIGEN2 expands expression (6.27, left) in a second-order Taylor series with the isotope concentrations N_i as independent variables. With this procedure, a value of the averaged neutron flux is determined and a corresponding correction factor used for all flux-dependent elements in the transition matrix \mathcal{A} . To solve the system of differential equations, a composite solution is constructed sequentially.

Asymptotic solution, Part 1. Short-lived nuclides that do *not* have long-lived precursors are treated in the first phase of the solution process.²⁷ These isotopes reach or maintain equilibrium within the current time step because their production rate is virtually constant and their removal life much shorter than the time interval. Most fission products belong to this category and their concentration at the end of the time step is given by the asymptotic solution.

Matrix exponential method. The main part of the solution is based upon the matrix exponential method for a reduced transition matrix \mathcal{A}_R with *all* short-lived nuclides

²⁶Alternatively, ORIGEN2 allows the user to specify the neutron flux directly (flux normalization), which is however barely useful for typical burnup calculations.

²⁷ORIGEN2 distinguishes short-lived and long-lived isotopes relative to the length of the current time step.

excluded. In the homogeneous case, which is the only case relevant in the present context, the system of differential equations and its solution can be written as:

$$\frac{d}{dt}\vec{N}(t) = \mathcal{A}_R \cdot \vec{N}(t) \quad \text{and} \quad \vec{N}(t) = \exp(\mathcal{A}_R t) \cdot \vec{N}(t = t_0) \quad (6.28)$$

ORIGEN2 expands the exponential function in a series to generate the solution $\vec{N}(t)$ for the current time step, and includes a sufficient number of higher-order terms to achieve a specified accuracy of the results.

Asymptotic solution, Part 2. A small number of short-lived isotopes does have long-lived precursors. The production rate of these nuclides varies as the concentration of the corresponding parent evolves in the given time interval. Using the previously determined solution for the long-lived parents, nuclides in this category are treated by ORIGEN2 in the final phase of the solution process using a Gauss-Seidel successive substitution algorithm.

In M³O, the analyst does not directly process ORIGEN2 input and output. Instead, the linkage code MCODE, which is briefly described next, prepares all input files required during reactor burnup calculations and also reads and evaluates the results returned by ORIGEN2.

6.4 MCODE

Two central elements of a computational system for reactor analysis have been introduced so far. First, a Monte Carlo code is employed to determine extremely accurate effective cross-sections of nuclear materials of fixed composition arranged in an arbitrary geometrical configuration, and to determine the corresponding flux and power distribution in the core. Second, a depletion code is used to calculate the time-dependency of the composition of nuclear materials during irradiation, i.e. during exposure to a neutron flux, at a given and fixed location (point-depletion). In other words, one code (MCNP) covers space, but not time, while the second code (ORIGEN2) covers time, but not space. What is missing is a third component combining the specific capabilities of MCNP and ORIGEN2 in order to construct a computational system, which can be used to perform full-core reactor burnup calculations extending in both time *and* space.

The idea and the concept of linking a Monte Carlo code with a point-depletion code is not new. Indeed, every laboratory or institute engaged in nuclear reactor calculations can be assumed to use one or another linkage code for the described purpose. Some of these codes are publicly available, the most common ones being *MCNP-ORIGEN Coupling Utility Program* (MOCUP) developed at Idaho National Engineering and Environmental Laboratory [Moore et al., 1995] and MONTEBURNS developed at Los

Alamos National Laboratory [Poston and Trelue, 1999], both first released in the 1990s. Pistner [1998, 2005] designed a code system for burnup calculations (MCMATH), which is equally linked to MCNP, but uses *Mathematica* instead of ORIGEN2 to solve cell burnup equations.²⁸

The system developed in the framework of this thesis is based on a third, more recent linkage code, which tries to eliminate a few deficiencies of previous programs: *MCNP-ORIGEN Depletion* (MCODE) is developed and maintained at the Nuclear Engineering Department of the *Massachusetts Institute of Technology* (MIT) and has been benchmarked against existing validated burnup codes [Xu et al., 2002, Xu, 2003]. Among the unique features of MCODE are its usability and functionality.

Usability. MCODE simplifies the input required to be provided by the user to its logical minimum, avoiding any redundancy of the data. In addition to the base MCNP input deck, which defines the physical set-up and initial material compositions, a single short MCODE input or control file is needed to specify a complete reactor burnup calculation.²⁹ As a large number of burnup zones are allowed, the MCODE input defines all active MCNP cells, average power density, time steps, and additional data required to initialize ORIGEN2. A sample MCODE input deck is reproduced in Appendix E.

MCODE automatically generates all MCNP and ORIGEN input files required during a complete reactor burnup calculation and evaluates the corresponding output files written in the process. In addition, MCODE logs all intermediary I/O, and also writes a detailed output file summarizing relevant results in a set of tables upon termination of the calculation (see Table 6.2).

Functionality. The physics of the simulation is entirely contained in MCNP and ORIGEN2, i.e. no additional neutronics calculations are performed by MCODE. The main function of the linkage program is to manage the data required and generated by the physics codes and to distribute and fuse this data in a coherent way. In fact, the performance of any linkage code is determined by the strategy, in which the neutronics codes are coupled. As will be briefly discussed below, MCODE uses a sophisticated predictor-corrector method for that purpose, which proves to minimize inevitable errors resulting from the discreteness of the selected time steps.

²⁸MCMATH is currently restricted to single-cell burnup calculations targeted at LWR fuel performance analysis, which is why it was not selected for the multi-zone approach required for research reactors.

²⁹The code determines the entire set of required input data, which can be derived from information already available to the code at this stage. No manual intervention during the simulation is necessary since MCODE regenerates all intermediary input files for MCNP and ORIGEN2.

Table	Data type listed
1	Reactivity versus time/burnup
2	Region averaged flux and conversion ratio table
3	Burnup/power map
4	Actinide number density and one-group cross-section table
5	Fission product number density and one-group cross-section table
6	Composition table (grams)
7	Neutron absorption rate table (neutrons/sec)
8	Neutron importance ordering at EOL

Table 6.2: MCODE output tables, generated for all active cells and time steps (if applicable).

In the following the functionality of MCODE is briefly summarized and its performance juxtaposed to other linkage codes. As discussed in Section 6.3.3, the challenge in solving the burnup equations stems from the time-dependency of the transition matrix. Its elements change because the spectrum-averaged one-group cross-sections evolve during irradiation and, while the total power release in the reactor is maintained constant, the total neutron flux varies as the nuclear fuel is burned. In order to solve the set of differential equations, the transition matrix has to be assumed constant for a given period of time, which reduces the burnup equations to a set of ordinary differential equations with constant coefficients.

$$\frac{d}{dt}\vec{N}(t) = \mathcal{A}|_{t=t_i} \cdot \vec{N}(t) \quad (6.29)$$

The simplest method to perform burnup calculations (with regularly updated transition matrices) is to use the matrix \mathcal{A} generated at time t_i during the entire time interval $\Delta t = (t_{i+1} - t_i)$. At time t_{i+1} , the next Monte Carlo simulation is executed to provide the data for a new transition matrix.

$$\vec{N}(t_{i+1}) = \exp[\mathcal{A}|_{t=t_i} \Delta t] \cdot \vec{N}(t_i) \quad (6.30)$$

Using beginning-of-time-step data inevitably introduces obvious systematic errors in the nuclide vectors calculated with this method. Nonetheless, these errors may be acceptable if sufficiently small time steps are chosen. Linkage codes based on this approach exist and may produce satisfactory results, MOCUP being the most prominent example in this category [Moore et al., 1995].

In order to balance this inherent bias, various approaches are conceivable. One strategy is to use transition matrices generated in-between the pre-defined time steps — and

not at the limits of the intervals themselves, where the nuclide vectors are requested by the user. In particular, a matrix filled with data generated for the middle of the time step can be assumed to contain values close to the true average values of the time-dependent matrix elements.

$$\vec{N}(t_{i+1}) = \exp \left[\mathcal{A} \Big|_{t=t^*} \Delta t \right] \cdot \vec{N}(t_i) \quad \text{with} \quad t^* = \frac{t_i + t_{i+1}}{2} \quad (6.31)$$

The previously mentioned linkage code MONTEBURNS uses the middle-of-time-step approach and produces reliable and accurate results [Poston and Trelue, 1999]. In a generic comparison of various coupling schemes, Xu [2003] finds that numerical errors can be reduced by an order of magnitude, if averaging techniques are used (pp. 70–73).

A second averaging technique is implemented in MCODE and is based on the *predictor-corrector method*. For a given initial nuclide composition at time $t = t_i$, a first transition matrix \mathcal{A}^P is generated and used by ORIGEN2 to calculate an estimated nuclide composition \vec{N}^P at $t = t_{i+1}$ (predictor run). Based on a second MCNP run for this composition, a new transition matrix \mathcal{A}^C is generated and used in a consecutive ORIGEN2 calculation, starting with the original nuclide composition, to obtain a second composition \vec{N}^C at $t = t_{i+1}$ (corrector run).

$$\begin{aligned} \vec{N}^P(t_{i+1}) &= \exp [\mathcal{A}^P \Delta t] \cdot \vec{N}(t_i) \quad \text{with} \quad \mathcal{A}^P = \mathcal{A} \Big|_{t=t_i} \quad \text{for} \quad \vec{N} = \vec{N}(t_i) \\ \vec{N}^C(t_{i+1}) &= \exp [\mathcal{A}^C \Delta t] \cdot \vec{N}(t_i) \quad \text{with} \quad \mathcal{A}^C = \mathcal{A} \Big|_{t=t_{i+1}} \quad \text{for} \quad \vec{N} = \vec{N}^P(t_{i+1}) \end{aligned} \quad (6.32)$$

The final nuclide composition, i.e. the composition to be used as the initial composition for the next burnup step, is obtained in taking the average number densities of both runs.³⁰

$$\vec{N}(t_{i+1}) = \frac{\vec{N}^P(t_{i+1}) + \vec{N}^C(t_{i+1})}{2} \quad (6.33)$$

Xu [2003] discusses advantages and disadvantages of the averaging techniques used in MONTEBURNS and MCODE. The major disadvantage of the predictor-corrector method as implemented here is the requirement to run two time-intensive MCNP simulations for each time step. With the duration of an ORIGEN2 burnup step being essentially negligible, the total running time of a calculation is almost doubled. However, the predictor-corrector method is preferred for MCODE because it is conceptually

³⁰Press et al. [1995] discourage the use of the corrector as the predictor for a third iteration.

simpler than, but also numerically superior to, the middle-of-time-step approach. Furthermore, with sharply increasing computing power, the drawback of additional MCNP runs is becoming less and less relevant.³¹

The general flow diagram of MCODE is illustrated in Figure 6.3. During each MCNP run, a new set of cross-sections as well as new flux and power maps are determined. These data are then used for the next burnup step performed with ORIGEN2. As specified in 6.3, MCODE requests (n, γ) cross-sections for all nuclides treated explicitly in MCNP and, in addition to that, $(n, 2n)$, $(n, 3n)$, and (n, f) cross-sections for the actinides. As indicated in Figure 6.3, the predictor-corrector method can be switched off if speed is preferred to additional accuracy.

	Reaction type	ENDF designation
Actinides	(n, γ)	102
	(n, f)	-6
	$(n, 2n)$	16
	$(n, 3n)$	17
Fission products	(n, γ)	102

Table 6.3: MCNP-tallied one-group cross-sections that substitute ORIGEN2 data.

After completion of the last task, MCODE cleanly collects all relevant data produced in each phase of the simulation in a single output file.³² As specified in Table 6.2, the output includes reactivity versus time and burnup, region averaged flux and conversion ratios, burnup and power maps, number densities, and also one-group cross-sections of actinides and fission products for each previously defined domain containing fissile material. MCODE also prints a sorted list of the neutron importance of all isotopes available in ORIGEN2 at EOL. The table can be used to verify that the most important nuclides are indeed considered explicitly in MCNP to account for neutron absorption — and not only in ORIGEN2, which tracks the corresponding number densities for a much larger set of nuclides.

Table 6.4 lists the actinides and fission products that will be tallied explicitly in MCNP in all reactor burnup calculations performed in the chapters below. The total of 65 nuclides includes 17 actinides and 48 fission products, which typically account for

³¹For a more balanced comparison of both techniques, one could impose the total number of MCNP runs required for a complete burnup calculation to be the same, with the assumption that the precision of the results should scale with the total computer time available. As MCODE needs two MCNP runs per time step, this condition would allow MONTEBURNS to use additional time steps in-between. Pistner [2005] shows that the predictor-corrector concept is still slightly superior to the middle-of-time-step approach under these circumstances.

³²In MCODE 1.0, a second binary, MCODEOUT, performs this task.

99.9% of all neutron absorptions at EOL.³³ The selected set of nuclides is optimized for burnup calculations that focus on reactor performance and, in particular, the achievable cycle length of a given fuel and core geometry. The set listed in Table 6.4 is not designed and not adequate for accident or spent fuel analyses, where a larger number of fission products has to be treated explicitly in MCNP to accurately estimate the radiological consequences of a release.³⁴ Note that the number of materials tracked in MCNP significantly influences total running time of the code, which requires the user to identify a reasonably sized set of nuclides. In some instances, cross-section data for specific isotopes may be unavailable in MCNP libraries.

³³The choice is relatively straightforward for the actinides, but more difficult for the large number of fission products. The ultimate choice of nuclides is based on preliminary simulations and MCODE runs, in which the absorption-ranking of the nuclides can be determined. In typical situations, the five most important nuclides (U-235, Xe-135, U-238, Sm-149, and U-236) already account for more than 95% of all neutron absorptions.

³⁴ORIGEN2 tracks a huge number of fission products (Section 6.3.2) and their time-dependent concentrations are available to the user. However, the accuracy of these data may be uncertain if generic cross-section libraries are used.

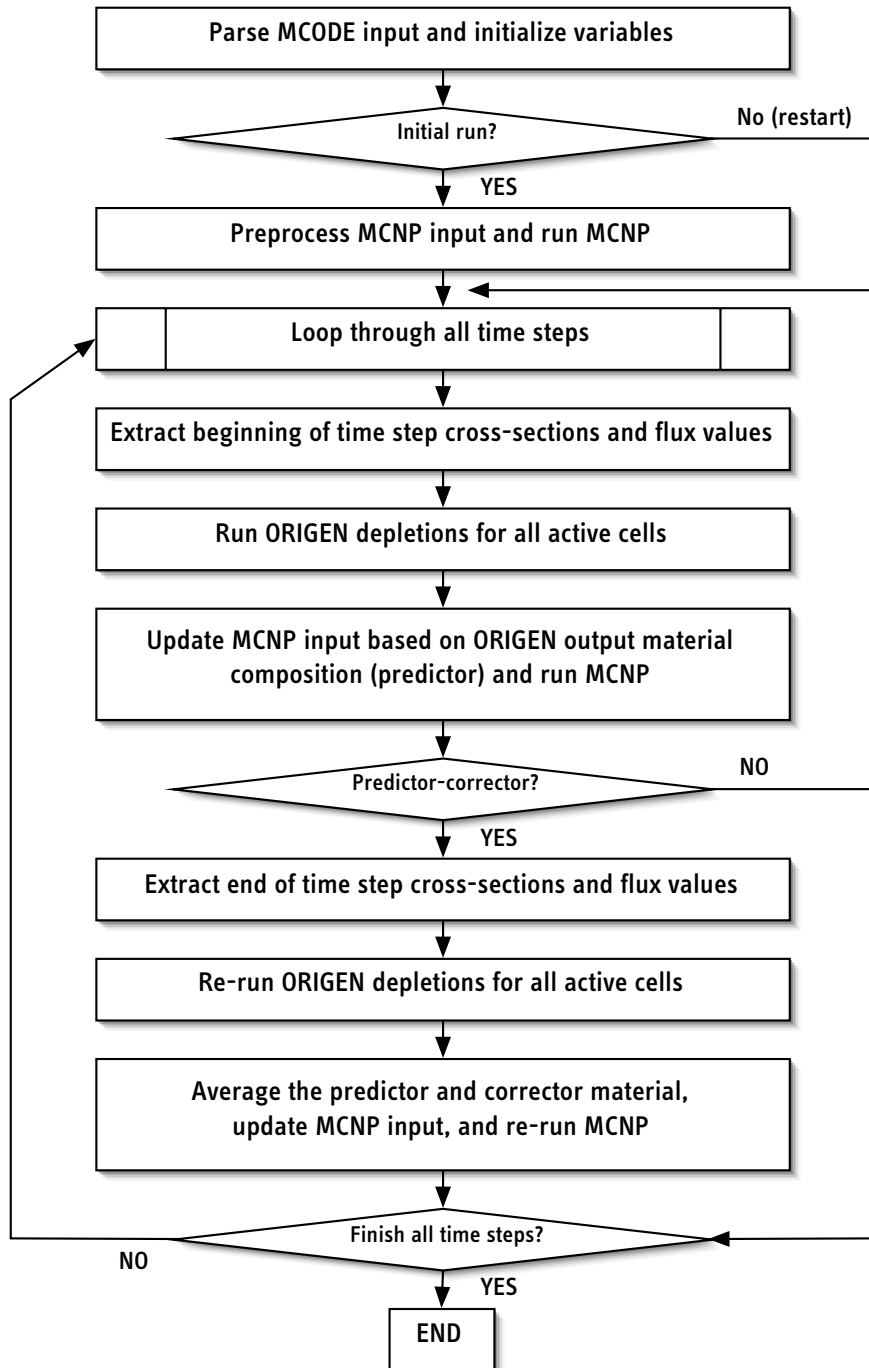


Figure 6.3: Flow diagram of MCODE [Xu, 2003, p. 63].

#	Element	Z	Nuclide
1	Krypton	36	Kr-083
2	Zirconium	40	Zr-093
3	Technetium	43	Tc-099
4	Molybdenum	42	Mo-092
5	Molybdenum	42	Mo-094
6	Molybdenum	42	Mo-095
7	Molybdenum	42	Mo-096
8	Molybdenum	42	Mo-097
9	Molybdenum	42	Mo-098
10	Molybdenum	42	Mo-099
12	Molybdenum	42	Mo-100
12	Ruthenium	44	Ru-101
13	Ruthenium	44	Ru-103
14	Rhodium	45	Rh-103
15	Rhodium	45	Rh-105
16	Palladium	46	Pd-105
17	Silver	47	Ag-109
18	Cadmium	48	Cd-113
19	Iodine	53	I-129
20	Xenon	54	Xe-131
21	Xenon	54	Xe-133
22	Xenon	54	Xe-135
23	Cesium	55	Cs-133
24	Cesium	55	Cs-134

#	Element	Z	Nuclide
25	Cesium	55	Cs-135
26	Lanthanum	57	La-139
27	Cerium	58	Ce-141
28	Praseodymium	59	Pr-141
29	Praseodymium	59	Pr-143
30	Neodymium	60	Nd-143
31	Neodymium	60	Nd-145
32	Neodymium	60	Nd-147
33	Neodymium	60	Nd-148
34	Promethium	61	Pm-147
35	Promethium	61	Pm-148
36	Promethium	61	Pm-148m
37	Promethium	61	Pm-149
38	Promethium	61	Pm-151
39	Samarium	62	Sm-149
40	Samarium	62	Sm-150
41	Samarium	62	Sm-151
42	Samarium	62	Sm-152
43	Samarium	62	Sm-153
44	Samarium	63	Sm-153
45	Europium	63	Eu-154
46	Europium	63	Eu-155
47	Europium	63	Eu-156
48	Gadolinium	64	Gd-157

#	Element	Z	Nuclide
1	Uranium	92	U-234
2	Uranium	92	U-235
3	Uranium	92	U-236
4	Uranium	92	U-237
5	Uranium	92	U-238
6	Neptunium	93	Np-237
7	Neptunium	93	Np-239
8	Plutonium	94	Pu-238
9	Plutonium	94	Pu-239

#	Element	Z	Nuclide
10	Plutonium	94	Pu-240
11	Plutonium	94	Pu-241
12	Plutonium	94	Pu-242
13	Americium	95	Am-241
14	Americium	95	Am-242m
15	Americium	95	Am-243
16	Curium	96	Cm-244
17	Curium	96	Cm-245

Table 6.4: Standard set of fission products and actinides treated explicitly in MCNP.

Note: as indicated, a much larger number of nuclides is tracked in M3O/ORIGEN2 without explicit re-calculation of effective cross-sections

This page intentionally blank

Chapter 7

Definition and Analysis of a Generic Single Element Reactor

Research reactors that use one compact fuel element (with involute-shaped MTR-type fuel plates) are particularly difficult to convert to LEU fuel. They were originally designed for rather high HEU densities and their core geometry is ‘inflexible’ when compared to standard MTR-type reactors where core re-configuration and optimization is usually possible. In order to study the characteristics of these facilities from a more general perspective, a *generic single element reactor* (GSER) is discussed below. The reactor model, which has been introduced elsewhere [Glaser and von Hippel, 2002], shows some typical characteristics of existing reactors in this category. Table 7.1 summarizes the main design and performance data of existing single element reactors as well as of the generic reactor discussed below.

The purposes of analyzing a generic single element reactor are manifold. First, the tools that have been developed in Chapters 5 and 6 are applied to a practical situation: *Mathematica* is used to generate MCNP reactor models and M³O is used for a subsequent analysis including burnup calculations. This basic analysis permits a general performance assessment of the computational system and a discussion of precautions that may have to be taken to guarantee reliable results. Second, the sensitivity of the results to the level of detail of the reactor model and of other computational details is explored. In particular, the impact of varying the number of burnup zones in the fuel plate, the choice of a specific adaptive cell structure (ACS), and the number of burnup steps are analyzed.

A detailed discussion of specific conversion options for research reactors is deferred to later chapters, where an actual conversion case study is performed. Note also that the discussion in this chapter is not intended to be a *validation* of the computational system. M³O is based exclusively on codes (MCNP, ORIGEN2, and MCODE) that have been validated extensively elsewhere. Rather, the purpose is to determine the *accuracy* and the *level of detail* of the results generated with the system used in this study. A verification of M³O results is included in Chapter 8, where data are checked against theoretical data for FRM-II obtained by other institutions using different computational systems.

	RHF (ILL)	FRM-II	HFIR		Generic SER
Fuel-type	UAl _x in Al	U ₃ Si ₂ in Al	U ₃ O ₈ in Al		UAl _x in Al
Enrichment	93 wt%	93 wt%	93 wt%		93 wt%
Thermal power	57 MW	20 MW	85 MW		30 MW
Uranium density [g(U)/cc]	1.17	1.5 and 3.0	0.78	1.15	1.50
Inner diameter	274 mm	130 mm	128 mm	286 mm	200 mm
Outer diameter	398 mm	229 mm	269 mm	435 mm	300 mm
Number of fuel plates	280	113	171	369	185
Active height of fuel plate	903 mm	700 mm	508 mm		700 mm
Thickness of fuel meat	0.51 mm	0.60 mm	max. 0.77 mm		0.60 mm
Thickness of cladding	0.38 mm	0.38 mm	0.25 mm		0.38 mm
Thickness of cooling channel	1.80 mm	2.20 mm	1.27 mm		2.00 mm
Total uranium inventory	9,200 g	8,108 g	9,430 g		6,627 g
Average power density in core	1.17 kW/cc	1.04 kW/cc	1.67 kW/cc		1.09 kW/cc
Coolant	D ₂ O	H ₂ O	H ₂ O		*
Fuel element: center	*	*	H ₂ O Trap		*
Fuel element: surrounding	D ₂ O	D ₂ O	Be-Reflector		*

Table 7.1: Key characteristics of single element reactors.

Asterisks (*) represent variable reflector, absorber, or coolant materials

7.1 Reactor Design and Core Model

The characteristics of the generic single element reactor (GSER) are summarized in Table 7.1. All dimensions and operational characteristics of this fictitious facility are chosen to be typical for those realized in comparable existing facilities. A transverse section of the fuel element of the GSER is depicted in Figure 7.1 below.

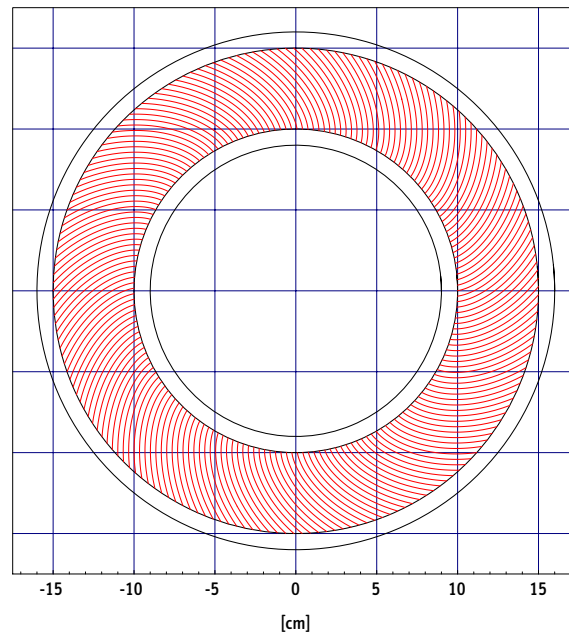


Figure 7.1: Fuel element of the generic single element reactor.

Figure 7.2 shows a drawing of the MCNP model indicating the main surfaces and cells required to set-up the model. The complete listing of the MCNP input deck is reproduced in Appendix D. Compared to an MCNP model of an actual reactor, not very many details have been included in the GSER model because the focus here is on fundamental aspects of the problem. Not included are, for instance, the support structures of the fuel element, safety rods, etc. Simplified compositions are used for the structural materials and the cladding. Specifically, pure aluminum replaces typical alloys (AG-3 or Al-6061), which contain trace amounts of other elements. Not considered either are beam tubes or experimental devices that would be located around the reactor, movements of control rods, etc. In all simulations, the full cylindrical and axial symmetry of the problem is therefore preserved.

The reference fuel of the GSER is HEU used in a UAl_x dispersion fuel at 1.5 g(U)/cm^3 . This fuel-type achieved the highest effective uranium densities in MTR-type fuel before development of high-density dispersion-type fuels began in the early 1980s as part of international RERTR-related activities. It is still used in some HEU-fueled research reactors today.

In principle, various moderator-coolant combinations are conceivable for single element reactors and some of them have indeed been realized (see bottom rows of Table 7.1). The GSER is studied in the inverse flux-trap mode, in which heavy water surrounds the core. The thermal neutron flux reaches its maximum outside the core and neutrons are extracted from this region via beam tubes. The High-Flux Reactor (HFR)¹ at ILL, Grenoble, as well as the FRM-II in Garching are operated in this mode.² Alternatively, a single element reactor can be designed for and used with the standard or central flux-trap mode. In this case, the reactor core is surrounded by a neutron reflector, for instance beryllium, while the central zone of the core is used for experiments or to irradiate materials. The light-water cooled High-Flux Isotope Reactor (HFIR) at Oak Ridge, USA, follows this design concept. Similarly, the model of the generic reactor introduced here could be reconfigured correspondingly to study the impact of conversion to low-enriched fuel for this specific reactor type.³

7.1.1 Adaptive cell structure for GSER analysis

The reference adaptive cell structure (ACS) selected for GSER analysis is shown in Figure 7.3. The reference structure accommodates 12 burnup zones in 93 cells and is based upon the power density profile in the plate as determined with MCNP at BOL.

In addition to using the ACS technique developed in Section 5.2, simple domain structures in the fuel plate are used for comparative calculations and sensitivity analyses. Three additional standard structures are studied: 1 burnup zone (entire plate), 6 burnup zones distributed in 9 MCNP cells, and 48 burnup zones distributed in 90 MCNP cells. The burnup zones in these standard models are distributed axially and radially symmetric, based on a ‘stiff’ set of MCNP cells. Figure 7.4 illustrates the situation.

¹Also abbreviated RHF (*Réacteur à Haut Flux*).

²Note that the Grenoble reactor is heavy-water cooled *and* moderated, while FRM-II is light-water cooled, but heavy-water moderated. The GSER discussed here follows the FRM-II design.

³This option is not discussed in this thesis.

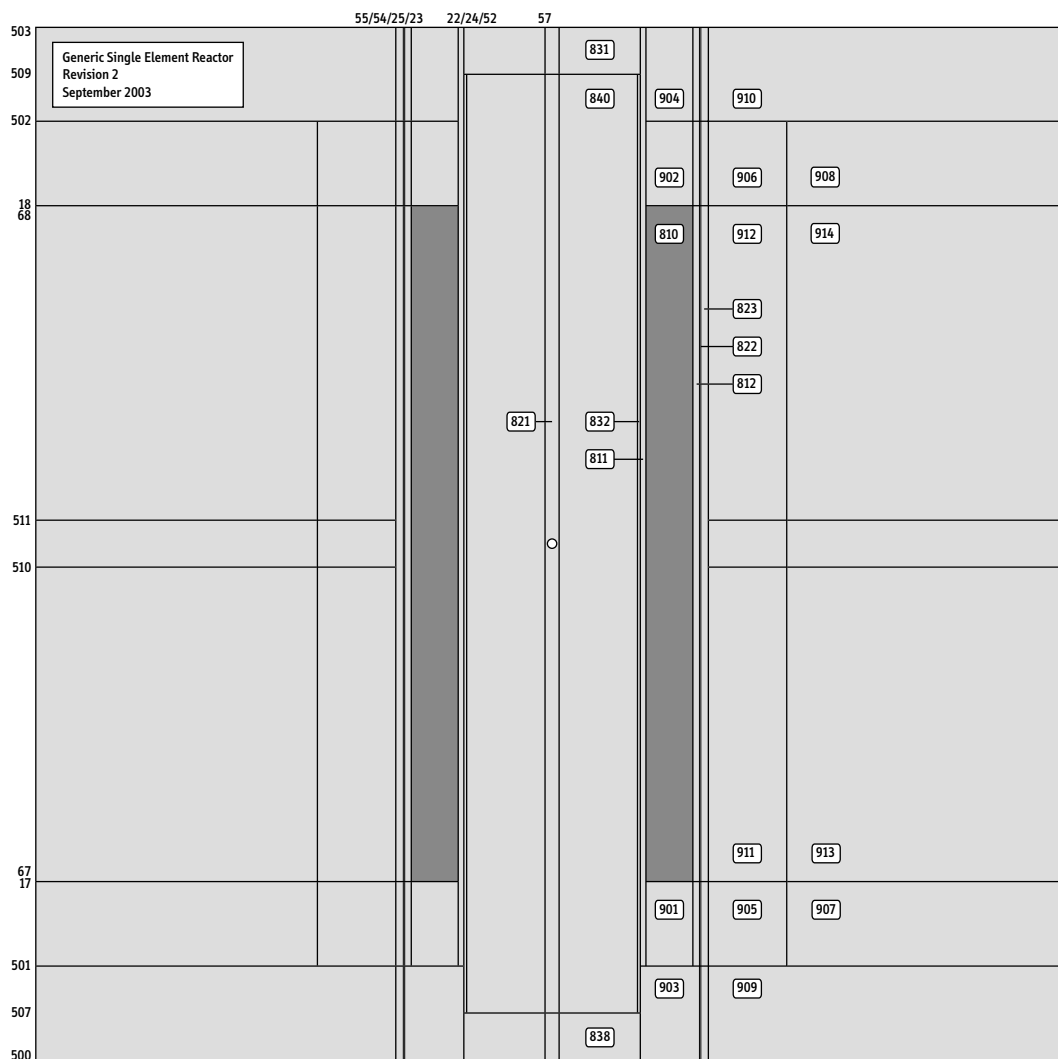


Figure 7.2: Side view of the MCNP model.

Numbers along the axes designate MCNP surfaces
 Boxed numbers are MCNP cells defined by these surfaces
 See Appendix D for listing of base input deck

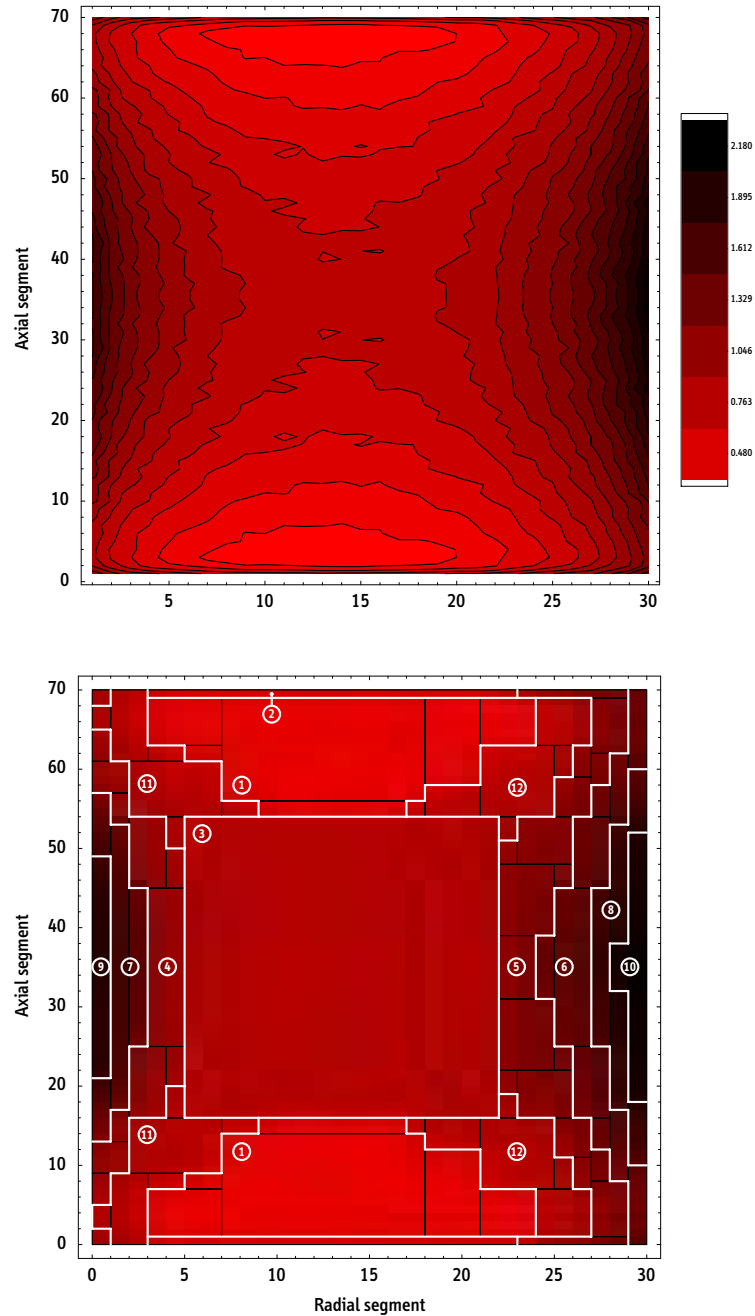


Figure 7.3: Reference adaptive cell structure for the GSER. Axial symmetric profile with central beryllium-follower fully inserted. 12 burnup zones (domains containing one material composition) in 93 cells.

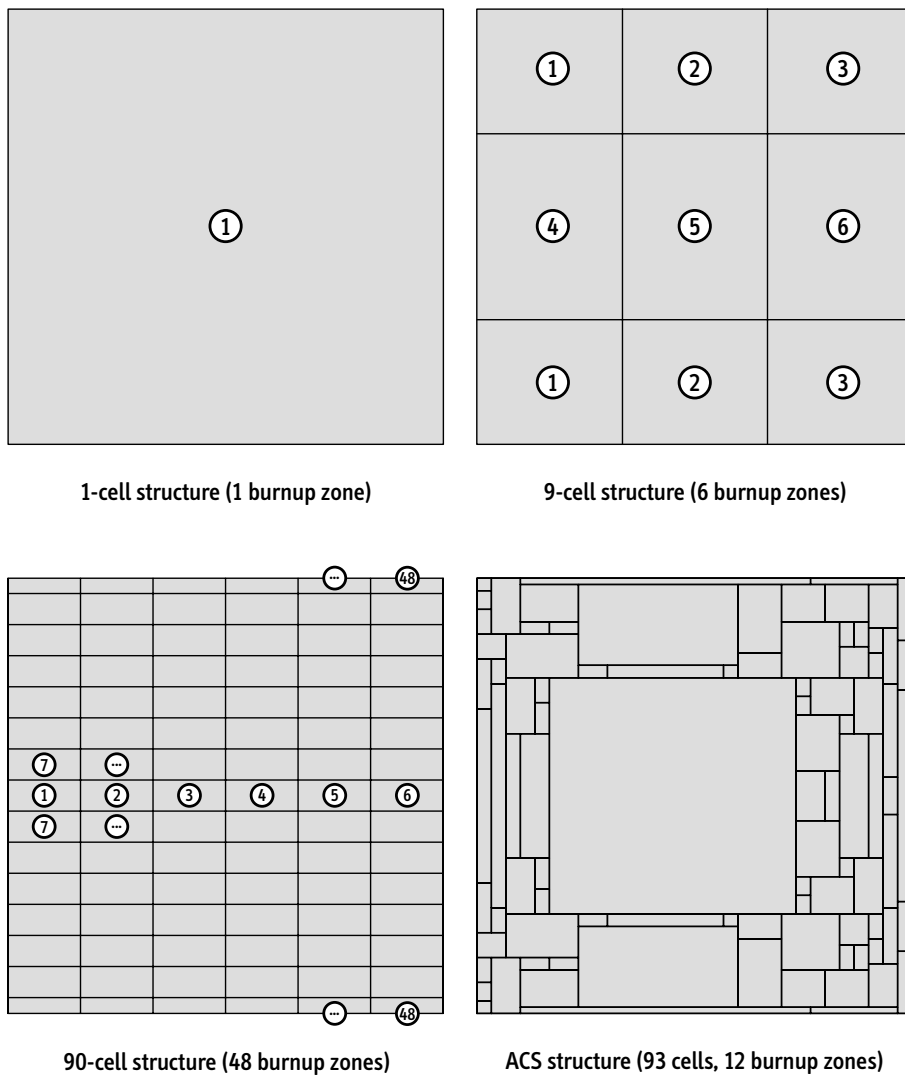


Figure 7.4: Simple plates and ACS for comparative calculations.

7.2 Analysis of the Reference Design

The main focus of this section is to discuss general strategies and procedures required for a correct interpretation of the data generated in MCNP calculations. Particularly for burnup calculations, results obtained with different zone structures of the plate are compared and their accuracies discussed.

7.2.1 Neutron flux in moderator tank

One of the principal results of any analysis focussing upon the performance of research reactors is the maximum thermal neutron flux achieved for a given design as well as the radial distribution of the flux in the zones accessible for experiments.

Tally data obtained in MCNP calculations are usually normalized per started neutron and have to be scaled to the energy release in the core to obtain absolute values. Essentially all the results discussed later are obtained for a completely inserted beryllium-follower. In such simulations, the core reactivity is significantly greater than $k_{\text{eff}} = 1$, which requires adequate correction of the thermal neutron flux data.

For a supercritical configuration, the neutron population in the core increases exponentially with a growth rate per generation characterized by k_{eff} . However, since all present results are understood to be valid for a steady state situation and normalized to a constant fission rate (constant thermal power), these excess neutrons cause an overestimation of the energy release in the core. As an immediate consequence, the neutron flux that is required for the specified total power is systematically underestimated by $1/k_{\text{eff}}$. As will be verified below, all neutron flux results obtained in Monte Carlo calculations therefore have to be corrected by k_{eff} .

$$\phi(\vec{r}) \approx k_{\text{eff}} \phi'(\vec{r}) \quad (7.1)$$

Figure 7.5 compares results obtained for a supercritical system, both uncorrected and corrected, with those of a critical system. To reduce initial reactivity of the configuration, a neutron poison (hafnium) has been added homogeneously to the material of the central control rod at a ratio of Be:Hf = 40:1.⁴

The maximum thermal neutron flux obtained for the nearly critical system is 9.68×10^{14} n/cm²s and is reached at a distance of 26.25 cm from the core center-line. As the initial reactivity of the GSER with a fully inserted beryllium-follower is $k_{\text{eff}} = 1.241 \pm 0.001$, the supercritical values scale correspondingly. The uncorrected neutron flux is 20% below the actual value (7.73 vs. 9.59×10^{14} n/cm²s). Off by less than

⁴The axial symmetry of the problem is therefore still preserved.

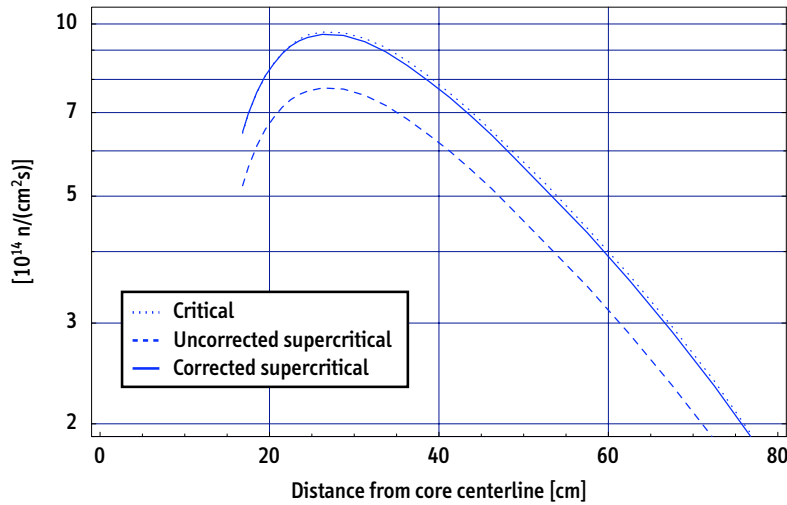


Figure 7.5: Correction of neutron flux values for systems with $k_{\text{eff}} \neq 1$.

MCNP input decks: GSER2.1 and GSER2.1y, 2.25 million neutron histories each
 $k(\text{eff}) = 1.241 \pm 0.001$ and $k(\text{eff}) = 0.998 \pm 0.001$, respectively

1%, the corrected flux is reasonably close to the best estimate. The thermal neutron flux as defined in (7.1) provides a very good approximation that is nearly independent of the position of the control rod, i.e. of the criticality status of the system. Neutronics calculations are simplified enormously if criticality of a given system need not be guaranteed at any point. However, some care should be taken when results of supercritical models are compared that are characterized by strongly divergent initial values of k_{eff} . Minor systematic errors do occur, as the discussion above demonstrates.

7.2.2 Burnup calculations

A second central category of results obtained in this study are based on burnup calculations performed with M³O. These are used to determine the cycle length of specified core designs as well as the general irradiation behavior of the fuel in the reactor. Before detailed results are derived and discussed in the case studies to follow (Chapters 8 and 10), the sensitivity of burnup calculations to variations in the parameters of the simulations are addressed. Specifically, the relevance of the number of burnup zones and relevance of the number of time steps is evaluated and their impact on the accuracy of results assessed. More general aspects of the calculations, such as total computer time requirements and recommended neutron histories per MCNP run, are discussed at the end of this section.

Reference simulation

A reference calculation is used to assess additional results obtained in calculations based on simplified models (less burnup zones) or accelerated execution (less time steps). Figure 7.6 shows reactivity versus cycle length for the reference calculation, which is based on the detailed ACS with 12 burnup zones illustrated in Figure 7.3 and on a narrow-spaced sequence of time steps (max. 5 days). Total running time of M³O/MCODE for this setup is about 100 hours, which corresponds to about 3.5 hours per MCNP run. As discussed in Section 6.4, MCODE typically runs in the predictor-corrector mode and requires two MCNP runs per time step.

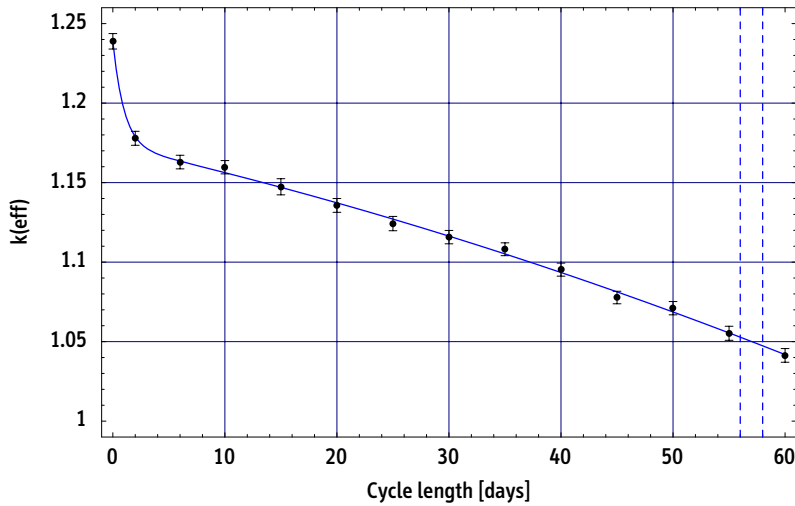


Figure 7.6: Cycle length of GSER as predicted by ACS reference simulation.

MCNP input deck: GSER2.4a.outp (14 burnup points)
 Total running time: about 100 hours on 1.5 GHz UNIX machine

The predicted cycle length is 56–58 days if a reactivity reserve at EOL of $k_{\text{eff}} = 1.05$ is assumed to account for losses due to the presence of installations and experimental devices not modeled in the present simulations. Additional data obtained in this reference calculation are discussed below when results are compared.

Sensitivity to number of time steps

The regular update of the neutron flux and cross-section data in MCODE is required to obtain accurate results for burnup calculations performed here and in later sections of this thesis. In particular, if more than one burnup zone is used, the adjustment of burnup-dependent data does affect the burnup and power maps, which in turn alters

the relative importance of different burnup zones. As can be read from Tables 7.2 and 7.3, this effect is however relatively small.

	1 zone		6 zones		48 zones		ACS	
	6 steps	14 steps	6 steps	14 steps	6 steps	14 steps	6 steps	14 steps
BOL	1.236	1.236	1.241	1.241	1.241	1.241	1.242	1.239
10 days	1.157	1.158	1.158	1.156	1.153	1.156	1.158	1.160
20 days	1.140	1.139	1.139	1.136	1.134	1.138	1.133	1.136
40 days	1.104	1.102	1.099	1.095	1.091	1.094	1.098	1.095
60 days	1.059	1.059	1.048	1.047	1.041	1.041	1.044	1.041

Table 7.2: Sensitivity analysis of simulation execution parameters. Impact of number of time steps on evolution of k_{eff} during irradiation. Absolute error for all values: $\Delta k_{\text{eff}} \approx \pm 0.004$ at a 95% confidentiality level.

MCNP input decks: 4a, 4s, 6, 6s, 7, 7s, 8, and 8s

Here, two sequences have been studied, one with 6 and one with 14 time steps.⁵ The predicted reactivity of the core as well as the nuclear inventory during irradiation both remain virtually unaffected in comparative calculations performed with more or less time steps and for all models under consideration, i.e. with 1, 6, and 48 burnup zones as well as with the ACS. The sensitivity of the calculations to the number of time steps increases as the level of detail (48 zones and ACS) increases, but remains of secondary relevance even there. In conclusion, finer time step sequences than those considered here are not required to obtain reliable results for single element reactors. This result is important, in particular because the total duration of an M³O calculation scales directly with the number of time steps chosen.

Note that in Table 7.2 there is one questionable data point, which is the k_{eff} at BOL for the core model with a single MCNP cell representing the fuel meat (one burnup zone). Even though the value of 1.236 (versus 1.241) is still within the statistical error margin, a systematic MCNP effect is likely to be the cause for this underestimation of core reactivity.⁶

⁵These are (0.2, 2, 10, 20, 40, 60) days and (0.2, 2, 6, 10, 15, 20, 25, 30, 35, 40, 45, 50, 55, 60) days.

⁶In criticality calculations for significantly supercritical systems, Monte Carlo codes have to regularly ‘comb’ the neutron population during the simulation to prevent divergence of the problem. The population control method implemented in MCNP (k-static criticality) is known to be inaccurate if and only if thermalized neutrons re-enter the system from an external reflector. This effect has been analyzed in detail and compared to other methods of solution in [Cullen et al., 2003].

Sensitivity to structure of burnup zones

As evidenced by Figure 7.7 and Table 7.3, the number and structure of burnup zones does indeed have a noticeable impact on the estimated achievable cycle length. First, note that this effect is *not* due to differing actinide inventories and compositions predicted by the simulations. Table 7.3 lists the corresponding data for uranium and plutonium at 60 days, or 1800 MWd(th), which are virtually identical for all models *and* sequences of time steps.⁷

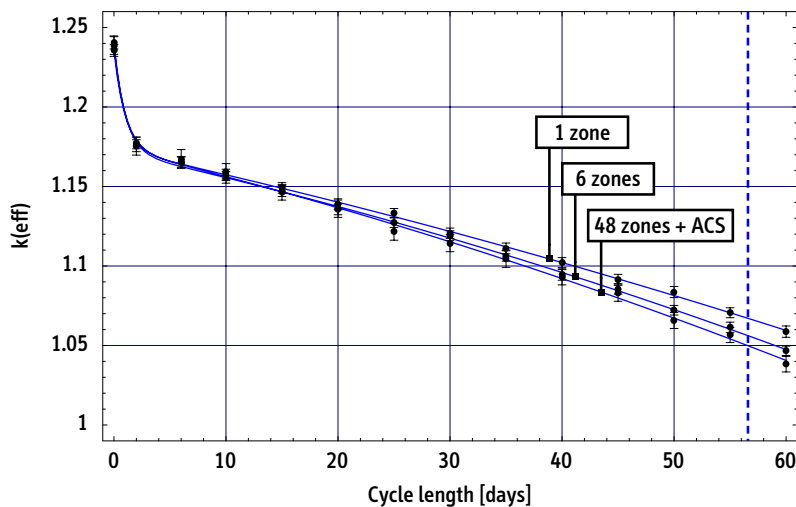


Figure 7.7: Sensitivity of burnup calculations (cycle length) to number of burnup zones.

MCNP input decks: GSER2.5a, and GSER2.6, and GSER2.7; 2.25 million neutron histories per run
Results for 48 zones and ACS are virtually identical, curves congruent, and only the ACS data shown.

Instead, due to the relatively low reactivity loss rate, minor differences in k_{eff} close to EOL lead to significant variations of the estimated cycle length. These changes are caused by the strongly inhomogeneous burnup of the fuel plate typical for single element reactors of the specified design, in which thermalized neutrons re-enter the core from the surrounding moderator tank and lead to accelerated burnup in the periphery of the plate. For obvious reasons, this ‘radially inward-directed’ burnup of the fuel cannot be detected with burnup models having only few burnup zones. Nonetheless, even the cycle length prediction obtained with the 6-zone model is already close the value predicted by the 48-zone and ACS models.

The effect of radially dependent neutronics can be observed qualitatively by comparing specific absorption rates of the most important nuclides in various segments of the

⁷Plutonium buildup is insignificant in this case because the reactor is HEU-fueled. Corresponding numbers are included in Table 7.3 only to demonstrate that there *are* minor differences in the results.

	6 time steps				14 time steps			
	1 zone	6 zones	48 zones	ACS	1 zone	6 zones	48 zones	ACS
k(eff) at 60 days	1.059	1.048	1.041	1.044	1.059	1.047	1.041	1.041
Estimated cycle length	> 60 d	59 d	56–57 d	57–58 d	> 60 d	59 d	56–57 d	57 d
Uranium inventory	4750 g	4750 g	4750 g	4750 g	4750 g	4750 g	4750 g	4750 g
U-235 burnup	36.5%	36.5%	36.5%	36.5%	36.5%	36.5%	36.5%	36.5%
Average enrichment	82.6%	82.6%	82.6%	82.6%	82.6%	82.6%	82.6%	82.6%
Plutonium inventory	11.3 g	11.2 g	11.2 g	11.3 g	11.2 g	11.2 g	11.2 g	11.3 g
Pu-239 fraction	78.7%	78.2%	77.8%	77.9%	77.9%	78.1%	77.8%	78.7%

Table 7.3: Sensitivity analysis of simulation execution parameters. Impact of number time steps and burnup zones on core reactivity, estimated cycle length, and nuclear inventory. All data at 60 days or 1800 MWd(th).

MCNP input decks: GSER2.4a, GSSER2.6, GSER2.7, and GSER2.8

plate.⁸ Table 7.4 lists selected data at end-of-life for the set of models under consideration. Even at EOL, burnup zones in the periphery of the plate are characterized by the absolute highest absorption rates in fissile U-235, while the U-235 to fission product (Xe-135 and Sm-149) absorption ratios are lowest in these regions. Pronounced U-235 depletion as well as increased importance of fission products in the peripheral segments of the plate do both contribute to a net-alteration of the core geometry and lead to an overestimation of the cycle length if simplistic burnup models are used.

The preceding discussion demonstrates the importance of using an adequately complex structure of the burnup zones to accurately predict the cycle length of the reactor. This contrasts with estimates of the actinide inventory and composition in the core, which are largely insensitive to this detail.

Level of detail of results

Linked to the previous discussion, the level of detail of results provided by the comparative set of burnup calculations is another important characteristic of the various core models. Figure 7.8 shows the uranium-235 burnup in each burnup zone for all models (6 zones, 48 zones, and ACS). The width of each bar corresponds to the volume of the corresponding zone, while the area of each bar is a measure for the total uranium-235 consumption in that zone. The total area covered by the bars is virtually identical for the various models all having the same average burnup of 36.5% and an EOL U-235 inventory of 4,750 g.

⁸Note that U-235 accounts for more than 85% of all absorptions in the fuel and that the relevance of the second most important nuclide (Xe-135) is already reduced by about a factor of 20.

Model	Zone	Volume	Specific absorption rate [10^{12} n/cm ³ s]				Ratio
			U-235	Xe-135	Sm-149	Sum	
1 zone	1	4417.86 cc	251.8	13.0	2.9	267.7	15.9
6 zones	6	631.12 cc	313.1	17.3	4.1	334.4	14.7
	5	631.12 cc	253.7	13.0	2.9	269.6	16.0
48 zones	6	52.59 cc	332.5	18.4	5.8	356.7	13.7
	5	52.59 cc	302.5	16.6	3.6	322.7	15.0
	4	52.59 cc	267.3	13.8	3.1	284.2	15.9
ACS	10	84.15 cc	331.4	18.4	7.1	356.9	13.0
	8	138.85 cc	328.1	18.2	5.7	352.0	13.7
	6	273.49 cc	315.4	17.4	4.3	337.2	14.5
	5	408.13 cc	293.9	16.2	3.4	313.5	15.0

Table 7.4: Specific absorption rates for the three most important nuclides: U-235, Xe-135, and Sm-149. Data at EOL (60 days) for different models and various segments of the fuel plates. See Figures 7.3 and 7.4 for model and zone designations.

MCNP input decks: GSER2.4a, GSSER2.6, GSER2.7, and GSER2.8

Most importantly, Figure 7.8 demonstrates that the models with stiff burnup structures (6 zones and 48 zones) cannot predict peak burnup values very accurately. While this is obvious for the coarse 6-zone model (maximum: 49.4%), even the cumbersome 48-zone model yields a peak value that is lower than the one predicted by the ACS model with only 12 burnup zones: 57.2% versus 62.3%. Conversely, the ACS model reproduces less detailed data in low-burnup segments of the plate, which are generally of less interest to the analyst. In summary, Figure 7.8 clearly illustrates the virtues of the ACS formalism as attention can be focussed specifically on important aspects of the calculation, while faithfully reproducing the performance of the reactor. At the same time, using larger MCNP cells in zones of little interest also reduces the statistical errors of MCNP data for a given number of neutrons tracked per simulation.

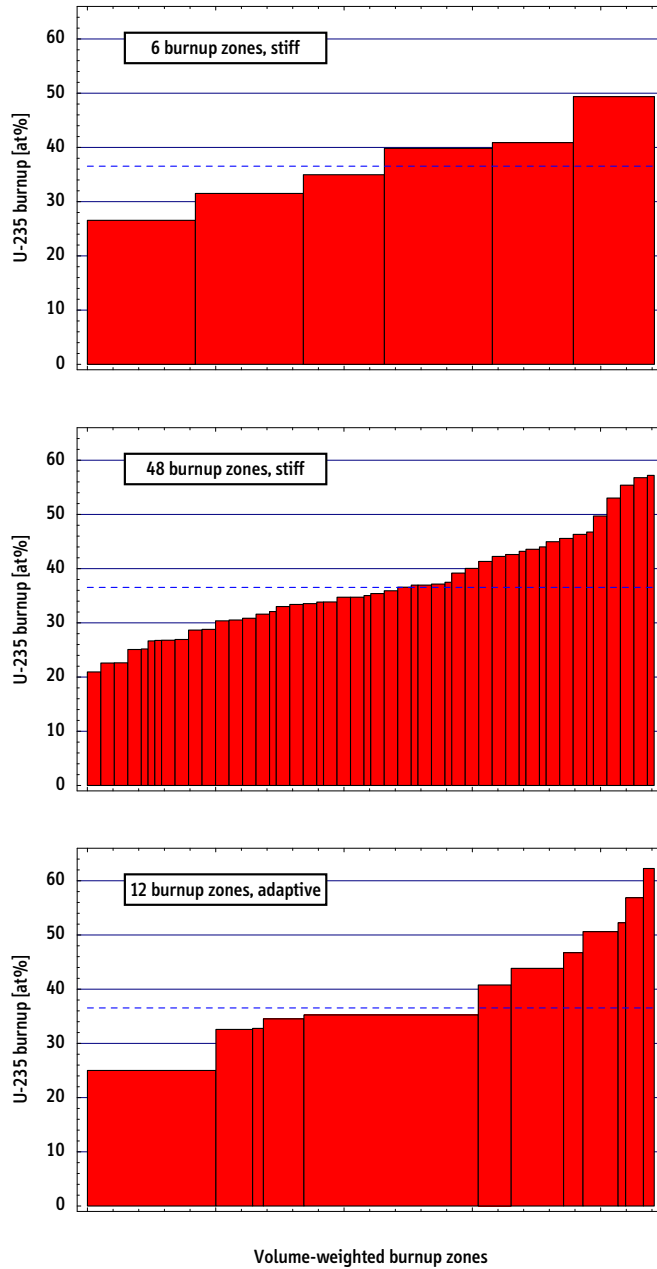


Figure 7.8: Uranium-235 burnup in segments of the fuel plate for the 6-zone model, the 48-zone model, and the ACS model in order of increasing burnup. The widths of the bars are proportional to the volumes of the respective zones. The dashed line indicates the average fuel burnup of 36.5%.

MCNP input decks: GSER2.4, and GSER2.6, and GSER2.8; 2.25 million neutron histories per run

7.3 Assessment of Results

The objective of the preceding analysis was to apply the adaptive cell structure (ACS) technique introduced in Section 5.2 to a practical problem and to compare the system to traditional approaches using a stiff set of burnup zones of equal size and equidistant distribution. To this end, a generic single element reactor has been introduced. Even though only one particular configuration of the reactor is analyzed here, the model could be modified to simulate various coolant-moderator combinations operated in the inverse or ordinary flux-trap mode.

With respect to burnup calculations using the Monte Carlo method to generate spectrum-dependent input data, the analysis of computational details leads to some important conclusions:

- End-of-life nuclide inventories and compositions are virtually identical for all models, being simple or complex. If only total averaged values are needed, calculations characterized by simple structures of the burnup zones *and* few time steps are sufficient and produce reliable results.
- Accurate prediction of the cycle length *does not* necessarily require a closely spaced sequence of time steps, i.e. a frequent update of cross-sections and flux distributions. This finding is important because the total computer time is essentially determined by the number of MCNP runs and, without introducing unacceptable errors, these can be reduced to some extent if execution time is critical.
- Accurate prediction of the cycle length however *does* require an adequate number and structure of the burnup zones in the fuel plate of single element reactors. In essence, the inhomogeneous fuel depletion in the plate is equivalent to an alteration of the core geometry and influences the neutronics in the core, which cannot be accounted for with simple models. For obvious reasons, and as has been confirmed above, a large number of zones or an adequately designed cell structure (ACS) is required to prevent overestimation of the achievable cycle length.
- Maximum values of burnup, power peaking values, etc. are best reproduced using the ACS formalism. For instance, using the initial power density profile in the fuel plate to set-up the cell structure guarantees adequate representation of high-power and high-burnup zones, which are critical for an accurate assessment of both reactor and fuel performance.

For these reasons, the ACS technique proves to be an effective and elegant approach to perform neutronics calculations for single element reactors. The ACS approach avoids

having to track a large number of materials in MCNP, which would ultimately differ little in their respective compositions and would therefore not contribute to the final results in any meaningful way. Instead, in the calculations performed with the ACS, the number of MCNP materials is typically reduced to 10–25, which is adequate to produce accurate data both for global as well as for local variables. As a consequence, this computational strategy also reduces statistical errors introduced by the Monte Carlo component of the system. In practice, for a regular burnup calculation based on about 10 updates of cross-section and flux data, about 70–80 hours of computer time are needed on a 1.5 GHz machine (20 MCNP runs tracking about 4 million neutrons each). The obvious downside of the ACS approach is the requirement to generate complex MCNP input representing the fueled regions of the plate. Without the *Mathematica* modules introduced in Section 5.2 this task could be considered infeasible. With these modules, however, an extremely powerful computational technique is available.

This page intentionally blank

Chapter 8

Versatility and Accuracy of the Computational System M³O and Analysis of the FRM-II

The primary objective of this chapter is to demonstrate the versatility of the computational system developed as part of this thesis and the accuracy of its results. The example of the German research reactor FRM-II has been chosen as the main facility for this purpose because extensive and detailed data exist and have been published by TUM and other institutes. The availability of this data facilitates a verification of M³O results significantly. The original HEU design of the reactor is studied in considerable detail to verify the computational system and the reactor models used in this thesis and to demonstrate the versatility and applicability of the system compared to other methods.

In addition, a set of conversion options, which has been developed and proposed for FRM-II during the 1999 discussions of a BMBF expert commission, is analyzed with M³O and results compared to data originally published by Argonne National Laboratory. These pre-criticality options were primarily based on currently licensed uranium-silicide fuels and required a fuel element of larger outer radius. Even though their implementation may be unlikely today,¹ a variety of valuable information of more general interest has been obtained for these options.

Once the accuracy and reliability of M³O has been demonstrated, the system is used to explore a variety of alternative fuel options for FRM-II in Chapter 10.

¹With start-up of the facility in 2004, the structural components of the reactor are now activated. Modification of these components would therefore be much more difficult and expensive to implement. In addition, as discussed below, with the discovery of new ultra-high-density fuels in 2002, new approaches to conversion became feasible making the 1999 options less attractive.

8.1 Reactor Design and Core Models

The new German research reactor FRM-II (Forschungsreaktor München II) is located in Garching near Munich and operated by Technical University of Munich (TUM). The facility has been under construction from 1996 to 2003, reached first criticality in March 2004, and nominal power in August 2004 using highly enriched fuel.²

Conceptually similar to the High Flux Reactor at ILL in Grenoble, France, the FRM-II operates in the so-called inverse flux-trap mode. A central rod with reflecting and absorbing sections is used to control criticality. An external reflector surrounding the core moderates and reflects neutrons leaking from the core. As a result, the thermal neutron flux in the external reflector is higher than in the core itself and the neutrons are extracted from that region via beam tubes. The inverse flux-trap mode has proven to be the most efficient design strategy to decouple neutron production and maximum neutron flux available for experiments outside the core, where sufficient space is available for beam tubes and other experimental devices.

FRM-II is designed for a thermal power of 20 MW and reaches a peak unperturbed thermal neutron flux of 8×10^{14} n/cm² s. The reactor uses one single fuel element containing a total uranium inventory of 8.1 kg, enriched to 93% in 113 involute-shaped fuel plates. A transverse section of the fuel element is illustrated in Figure 8.1. Base design data of the core and the main structural components are summarized in Table 8.1.

The estimated cycle length of FRM-II will be slightly higher than 50 days. The core is light water cooled and located in the center of a heavy water filled moderator tank where, in particular, a cold neutron source and the beam tubes are placed.

In the so-called unperturbed simulations, the fuel element enclosed by the central channel tube is located in the center of the moderator tank without additional experimental and reactor components in place. The tank has a height of 300 cm, a diameter of 250 cm, and contains heavy water with a density of 1.10 g/cc. A low content of hydrogen has been added in the simulations in order to account for light-water impurities (ratio hydrogen to deuterium: 0.2 at%). In a few additional simulations, the main beam tubes and the cold neutron source (CNS) have been modeled to estimate gamma and neutron heating in the CNS as well as the neutron flux and spectrum in the most important beam tube.³

²TUM press release from August 26, 2004. The fact that HEU would be used to fuel the reactor has caught early national and international attention and criticism. For a discussion, see for instance [Liebert, 1994, Ackermann et al., 1999, Glaser, 2002a].

³Corresponding input data are summarized in Section 8.1.5 and results discussed in Section 8.3.2.

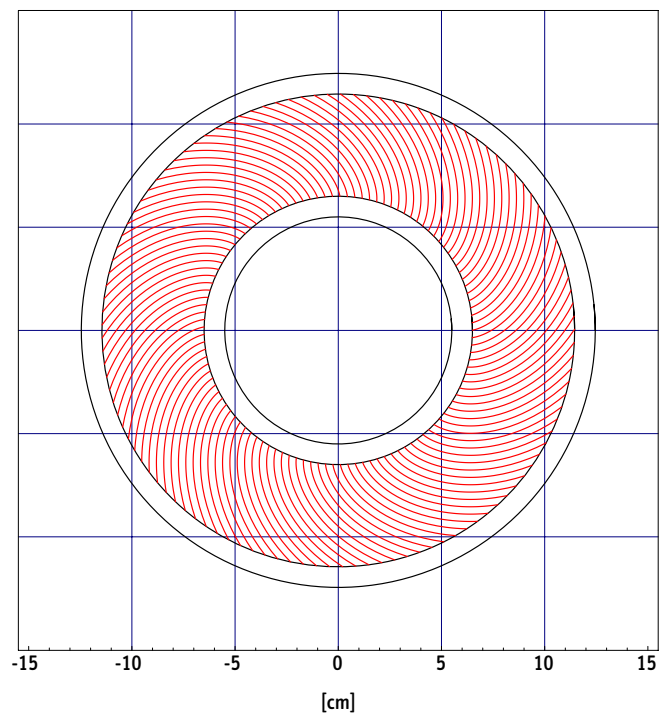


Figure 8.1: Transverse section of FRM-II core.

Dimensions of fuel element:		
Inner radius of hafnium-shell:	51.0 mm	(56.0 mm – 5.0 mm)
Inner radius of beryllium-canning:	54.0 mm	(56.0 mm – 2.0 mm)
Maximum radius of follower:	56.0 mm	(59.0 mm – 3.0 mm)
Minimum inner radius of FE:	59.0 mm	(118.0 mm / 2)
Outer radius of inner core-tube:	65.0 mm	(59.0 mm + 6.0 mm)
Minimum inner radius of active zone:	67.5 mm	(135.0 mm / 2)
Transition radius of uranium density:	105.6 mm	(from 3.0 g(U)/cc to 1.5 g(U)/cc)
Maximum outer radius of active zone:	112.0 mm	(224.0 mm / 2)
Inner radius of outer core-tube:	114.5 mm	(121.5 mm – 7.0 mm)
Maximum outer radius of FE:	121.5 mm	(243.0 mm / 2)
Inner radius of ZKR:	123.0 mm	(121.5 mm + 1.5 mm)
Outer radius of ZKR:	131.0 mm	(123.0 mm + 8.0 mm)
Dimensions of fuel plate:		
Thickness of fuel meat:	0.60 mm	
Thickness of cladding:	0.38 mm	
Thickness of cooling channel:	2.20 mm	
Arc-length of inner fuel zone:	51.50 mm	(with 3.0 g(U)/cc)
Arc-length of outer fuel zone:	10.90 mm	(with 1.5 g(U)/cc)
Arc-length of active zone of plate:	62.40 mm	
Arc-length of plate (inner to outer tube):	69.40 mm	
Total height of fuel plate:	720.0 mm	
Height of active zone:	700.0 mm	
Uranium inventory:		
Total mass of uranium in core:	8108.54 g	
Total mass of uranium per plate:	71.76 g	(in 113 plates)
Total mass of uranium-235 in core:	7540.94 g	
Total mass of uranium per plate:	66.73 g	(in 113 plates)

Table 8.1: FRM-II base design data.

8.1.1 Design considerations of the original core

The design and the geometry of the FRM-II core has been specified in numerous reports published by TUM beginning in the mid-1980s. Among the more prominent first publications are [Böning et al., 1983], [Böning et al., 1985], and [Zhang, 1986].⁴ Based upon these early analyses done at TUM, the final design of the FRM-II reactor core has been identified in [Röhrmoser, 1991]. The discussion below provides a brief summary of the operator's considerations that ultimately lead to the design of the FRM-II core.⁵

In particular, the main dimensions of the reactor core as well as the fuel plate characteristics were specified by Röhrmoser [1991] and are summarized in Table 8.1. The selection process was based on several important premisses, which include:

- Thermal power: 20 MW.
- Diameter of the fuel element: 20–25 cm.
- Desired cycle length of 48–50 days.

The maximum thermal neutron flux that accumulates in the surrounding moderator tank has been selected as the main objective function in guiding an optimization process of the core. Several operational constraints have to be considered in this process and include feasibility of heat removal (cooling requirements) and maximum fission density in the fuel at EOL.⁶

Variable parameters of the optimization process are the inner and outer diameter of the fuel element with the outer maximum of 25 cm, as well as the active height (typically 70–80 cm). With respect to the geometry of the fuel plate and the thickness of the coolant channel, only a variation of the fuel meat thickness is studied. The cladding thickness is fixed at 0.38 mm, which is a typical value used for plate-type dispersion fuels in Europe [Röhrmoser, 1991, pp. 115–116].⁷ An analysis of the coolant channel thickness revealed only a weak impact of this parameter on reactor performance, while cooling becomes increasingly difficult for narrower channels. A conservative and relatively large value of 2.20 mm is selected for the coolant channel thickness and kept

⁴Apparently, there are a number of internal reports written by TUM staff around 1980. These are not publicly available, but quoted in the above-mentioned publications.

⁵For an extensive discussion, the reader may consult [Röhrmoser, 1991].

⁶A complete list of assumptions and criteria that guided the design procedure is given in [Röhrmoser, 1991, p. 8 and p. 75]. See also Sections 9.1.1 and 9.1.2 for general aspects of research and high-flux reactor design.

⁷In the U.S., a smaller cladding thickness of 0.25 mm (10 milli-inch) is used in high-flux reactors, for instance in HFIR, in addition to the more common value of 0.38 mm (15 milli-inch). See Table 7.1 for a comparison of fuel plate data employed in existing single element reactors.

constant subsequently. As can be expected, the main design challenges arise from the desired compactness of core. Specific measures are required and investigated to limit power peaking in the fuel plate. Ultimately, a core design is adopted, in which the effective uranium density is reduced by 50% in the periphery of the plate.

Based on the restrictive premisses listed above, which include in particular the outer diameter of the core and the desired target length of 48–50 days, the author concludes that only HEU fuel can be used in FRM-II. Accordingly, HEU is required both to achieve initial reactivity *and* to accommodate sufficient fissile uranium-235 in the core. A short discussion of fuels with reduced enrichment (45% and 20%) confirms this fact [Röhrmoser, 1991, p. 127–130].⁸

In Chapter 10 of this thesis, an optimization process is proposed using the so-called *Linear Programming* technique, which is introduced in Chapter 9. Benefitting from the prospects of new uranium fuels with very high uranium densities (monolithic fuels), conversion options will be identified that nearly reproduce the performance of the current HEU design, while minimizing the enrichment levels required to achieve this objective. In contrast, the operator of FRM-II currently favors and primarily investigates the future use of UMo-dispersion fuels with an enrichment level of 50% in the reactor [Röhrmoser et al., 2004].

8.1.2 Base MCNP Models of FRM-II

The general structure of the FRM-II input decks generated for and used in the MCNP/M³O simulations below is similar to the generic single element reactor (GSER) introduced in Chapter 7. The input deck of GSER is reproduced in Appendix D. The most important difference between the input decks of GSER and FRM-II is the discontinuity of the effective uranium density in the plate used in FRM-II, which requires additional MCNP input and has to be handled separately when generating the adaptive cell structure used for burnup calculations (Section 8.1.4). Two base models of the FRM-II core are used for the simulations presented below:

Model A: The full model of the FRM-II core includes the entire set of design information available and faithfully reproduces every detail of the geometry. Particularly, Model A includes those components of the core that disturb the axial symmetry of the problem: these are the boron ring below the fuel element, whose characteristics are summarized in Table 8.2, as well as the reflecting and absorbing

⁸Along the same line of argument, even though based on an older version of the FRM-II core (KKE5 vs. KKE7), Zhang [1986] concludes that HEU obviously yields the best results and that an enrichment of 45% could be “just about acceptable” if a fuel with an effective uranium density of 6 g/cc could be developed (p. 105).

(beryllium and hafnium) sections of the central control rod. Few simulations have been performed with Model A.

Model B: The major part of the analysis discussed in this chapter is based on a core model preserving the axial symmetry of the problem. To this end, in Model B, the boron ring and the absorbing hafnium section of the control rod have been omitted. The beryllium-follower (control rod) is fully inserted in simulations based on Model B. Section 8.1.3 discusses the errors, which are introduced by these simplifications, and the conditions of their acceptability. Model B is used to determine the maximum unperturbed neutron flux in the moderator tank and in all burnup calculations for FRM-II.

Based on the base design data listed in Table 8.1 and using the *Mathematica* modules introduced in Chapter 5, the MCNP input for Models A and B is created. Specifically, the selected MCNP approximation of the involute-shaped fuel plate is shown in Figure 8.2. An MCNP plot of a transverse section of the FRM-II core is illustrated in Figure 8.3 showing, in particular, the discontinuity of the effective uranium density in the fuel plate represented by two different MCNP materials.

Height: 4.50 cm	z -Positions: -36.25 cm to -40.75 cm
Thickness: 0.35 cm	Radii: 11.45 cm to 11.80 cm
Number densities:	Boron-10: 0.0007842013 e24 at/cc
	Boron-11: 0.0028529170 e24 at/cc
	Aluminum-27: 0.0580307842 e24 at/cc

Table 8.2: Boron ring data as used in MCNP Model A.

Theoretical number densities used in MCNP models

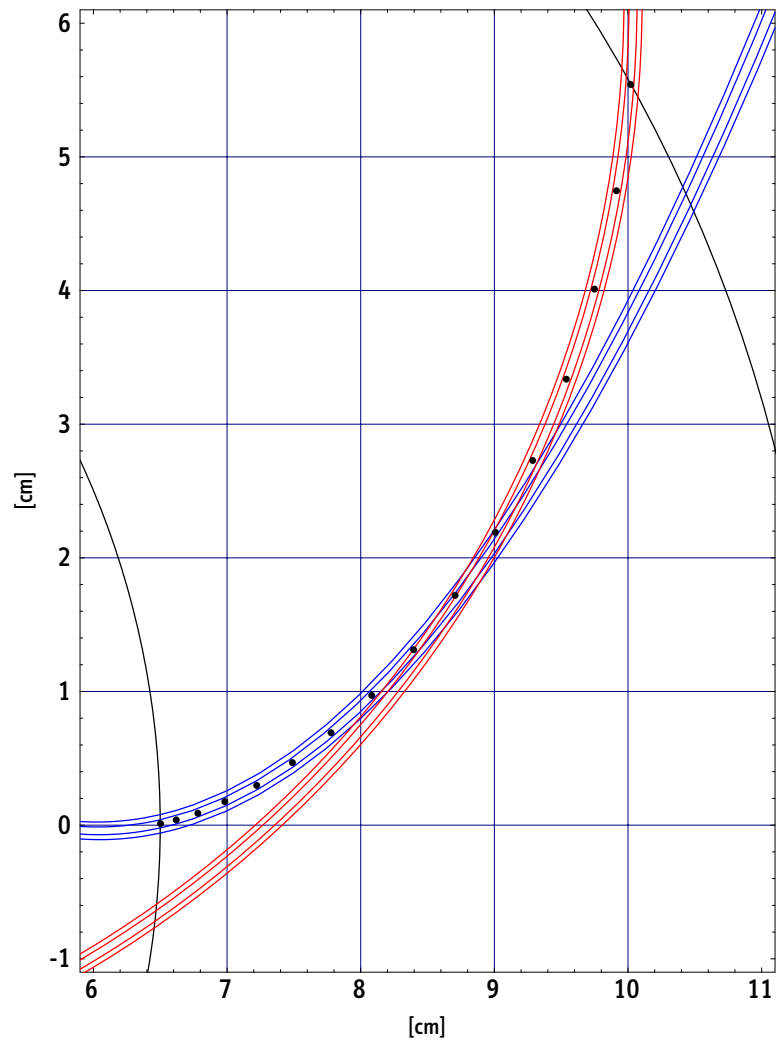


Figure 8.2: FRM-II involute as represented in MCNP.

See Figure 5.3 for explanation.

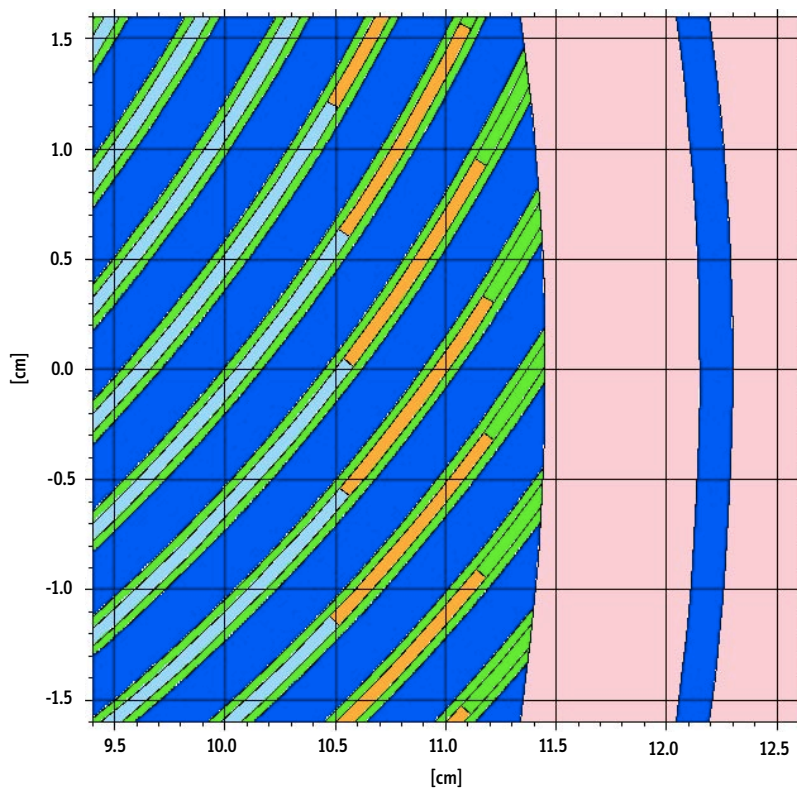


Figure 8.3: MCNP Model of FRM-II fuel element (MCNPLOT).

Light blue: fuel at 3.0 g(U)/cc, orange: fuel at 1.5 g(U)/cc, green: aluminum alloy (AlFeNi), pink: aluminum alloy (AG-3), dark blue: light water

8.1.3 Impact of boron ring

Two basic core models are used for the analysis of the FRM-II: one with and one without the boron ring included (Models A and B). Before proceeding any further, the impact of the ring on the reactivity of the fresh and irradiated core is determined.

The boron ring itself is located below the fuel element and represents the only difference between the two models used for the following comparison of the neutronics. The input data used to model the ring is listed in Table 8.2. Basic MCNP simulations for the fresh cores yield:

$$\text{Model A: } k_{\text{eff}} = 1.1920 \pm 0.0007$$

$$\text{Model B: } k_{\text{eff}} = 1.1990 \pm 0.0007$$

MCNP input decks: ModelA1.outp and ModelB1.outp, 4 million neutron histories each

The net-differences of the effective multiplication factor and the reactivity are:

$$\Delta k_{\text{BR}} \approx 0.007$$

$$\Delta \rho_{\text{BR}} = \rho_2 - \rho_1 = \frac{k_2 - 1}{k_2} - \frac{k_1 - 1}{k_1} = \frac{k_2 - k_1}{k_2 k_1} \approx 0.005$$

When using the core model without the boron ring included, the initial k_{eff} will be slightly overestimated by the amount calculated above, in particular during the early stages of burnup calculations. Nonetheless, the B-10 in the ring is rapidly burned out via (n, α) processes, which gradually reduces the poisoning effect of the ring. A rough estimate of the boron burnup follows.

The total boron inventory in the ring is 7.5 g of natural boron, containing 1.5 g of the isotope B-10. The burnout of the ring can be estimated using typical values for the spectrum-averaged (n, α) cross-section of B-10 and the spectrum-averaged neutron flux close to the periphery below the fuel element.⁹

$$\sigma_{\text{BOL}} = 1000 \text{ b}, \quad \sigma_{\infty} = 2150 \text{ b}, \quad \text{and} \quad \phi = 4 \times 10^{14} \text{ n/cm}^2\text{s}$$

MCNP input decks: ModelA1.outp and ModelA1.EOL.outp, 4 million neutron histories each

⁹ (n, α) processes dominate neutron absorption in B-10. In comparison, radiative neutron capture (n, γ) in B-10 is smaller by four orders of magnitude. All neutron cross-sections of the more abundant isotope B-11 (80 wt%) are small compared to the B-10-values.

These average values for σ and ϕ have been obtained in MCNP calculations performed for the fresh core based on two different set-ups. In a first simulation, the boron ring is correctly modeled to obtain values for BOL. In a second calculation, the boron inventory in the ring is removed to determine the infinite-dilution cross-section of B-10 for a completely burned ring, i.e. for $t \rightarrow \infty$. As expected, the cross-section increases with burnup due to the decrease of the spectral self-shielding of the boron in the ring. In the following, it is assumed that the value of σ scales linearly with the residual boron inventory. Since $N(t \rightarrow \infty) = 0$ is equivalent to $\sigma(t \rightarrow \infty) = \sigma_\infty$, a general expression for σ can be given.

$$\sigma(t) \approx -(\sigma_\infty - \sigma_{\text{BOL}}) \frac{N(t)}{N_0} + \sigma_\infty \quad (8.1)$$

The expression for σ can be used to formulate the basic equation describing the change of boron concentration in the ring.

$$dN = -\sigma(t) \phi N(t) dt = \left((\sigma_\infty - \sigma_{\text{BOL}}) \frac{N(t)}{N_0} - \sigma_\infty \right) \phi N(t) dt \quad (8.2)$$

A solution to this differential equation ($y' = ay^2 - by$ with $a, b > 0$) is given by:

$$N_{\text{B-10}}(t) = N_{\text{B-10}}(0) \left(\frac{\sigma_\infty}{\sigma_\infty + \sigma_{\text{BOL}}(\exp[\sigma_\infty \phi t] - 1)} \right) \quad (8.3)$$

In making the plausible assumption that $\Delta\rho_{\text{BR}}(t)$ and $\Delta k_{\text{BR}}(t)$ are proportional to $N_{\text{B-10}}(t)$, the time-dependent reactivity-worth of the boron ring can be estimated. As shown in Figure 8.4, the burnout of the ring is slightly suppressed in the early stages of the cycle due to the self-shielding of the boron.

Based on this simplified estimate, the B-10 inventory is reduced by 50% in the first 15 days of irradiation, while $T_{1/2}$ shortens in the later stages of the reactor cycle. At EOL, the B-10 in the ring has been burned out by more than 95% with an residual inventory of approximately 0.066 g.¹⁰ The estimated residual reactivity-worth of the boron ring at end-of-life (EOL) of the core is therefore given by:

$$\Delta\rho_{\text{BR}}(\text{EOL}) \approx 0.00022 \quad \text{or} \quad \Delta k_{\text{BR}}(\text{EOL}) \approx 0.00031$$

In conclusion, to a very good approximation, the boron ring can be reasonably omitted in most parts of the analysis below. The residual $k_{\text{BR}}(\text{EOL})$ is smaller than the uncertainties of typical MCNP results for the multiplication factor. The ring is irrelevant

¹⁰These results are consistent with data published previously by TUM. Röhmoser [1991, pp. 46–47] estimates a B-10 inventory of 0.065 g at EOL.

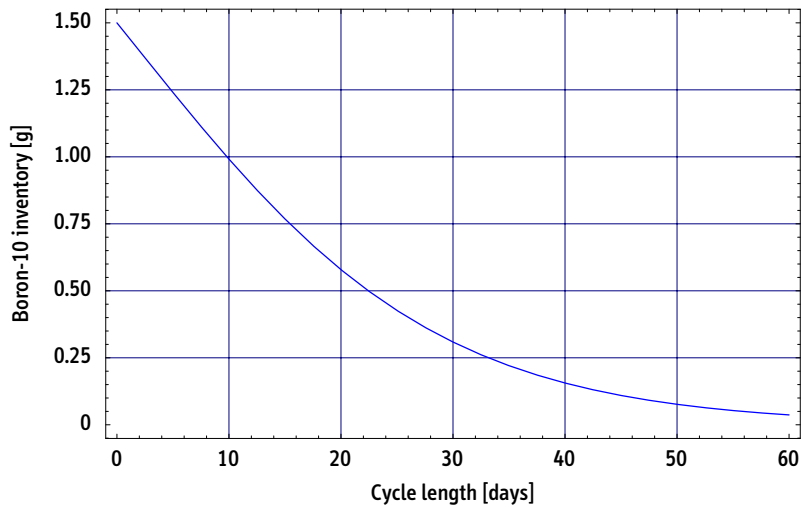


Figure 8.4: Estimated boron-10 inventory during irradiation.

for burnup calculations primarily aimed at determining the achievable cycle length of the core. Similarly, the maximum neutron flux at the mid-plane of the core is virtually unaffected by perturbations introduced by the ring.

Conversely, to include the boron ring in the model, whose prime function is to reduce the power peaking in the early stages of the irradiation cycle,¹¹ is consistent only if the control rod movement is equally simulated in the calculations. These operational details and procedures are beyond the scope of this analysis. Furthermore, in such a case, burnup calculations for the beryllium section of the control rod would be required, in addition to those for the boron ring [Röhrmoser, 1991, pp. 65–66]. In particular, for a comparison of various conversion options, where the relative performance of the models is the main result, simplified Model B will be the basis for the analysis.

In essence, using the axially symmetric model without the ring and without simulating the control rod movement, yields results averaged over the entire irradiation cycle. These include the neutron flux in moderator tank, the neutron spectrum in the plate, burnup and residual enrichment of the fuel, as well as total actinide and fission product inventory in the plate. Modeling the ring and the control rod movement would be most important to determine peak power densities in the early period of the irradiation cycle (BOL) and corresponding local fission rates and burnup in the fuel plate.

¹¹For the fresh core, the absorbing section of the central control rod (hafnium section) is inserted from the top. In this situation, the rod pushes the neutron flux to the lower part of the fuel element. Power peaking therefore occurs in the lower periphery of the plate.

8.1.4 Adaptive cell structure for FRM-II burnup analysis

All burnup calculations for FRM-II and its conversion options discussed in Chapter 10 are based on the axially symmetric Model B, i.e. without the boron ring included. This simplification is legitimate because, as will be shown below (Section 8.1.3), the residual impact of the boron ring on core reactivity at EOL is negligible. The ring is therefore irrelevant for an estimate of the achievable cycle length, which is the primary objective of the burnup calculations. Conversely, if the boron ring were included in the simulations of the core burnup, a couple of additional details, including the control rod movement as well as the burnup of boron ring and of the beryllium section of the rod, would need to be modeled simultaneously to produce consistent results. This level of operational detail is beyond the scope of this study.

Based on the analysis of Chapter 7, which showed that a limited number of adequately selected burnup zones faithfully reproduces the burnup behavior of a single element reactor core, the adaptive cell structure (ACS) for FRM-II is created. As previously mentioned, the ACS used for burnup calculations requires a specific approach due to the discontinuity of the effective uranium density in the fuel plate.

Figure 8.5 (top) shows the template of the power density as obtained for the axially symmetric problem at BOL. The selected cell structure used for FRM-II analysis is spanned by 130 MCNP cells and defines 21 burnup zones:¹² 15 zones represent the inner segment and 6 additional zones represent the outer segment of the fuel plate, in which the effective uranium densities are 3.0 g/cc and 1.5 g/cc, respectively. Note that the width of the unit segments in the radial direction are different in the two segments of the plate: the 51.5 mm in the inner section are subdivided into 32 segments (unit length: 1.61 mm), while the 10.9 mm of the outer section are subdivided into 8 segments (unit length: 1.36 mm). In order to get accurate local results for the zones in the fuel plate with the highest power densities and highest local burnup, micro-segments ⑳ and ㉑ are included.

¹²See Section 5.2.2 for details on ACS nomenclature and generation.

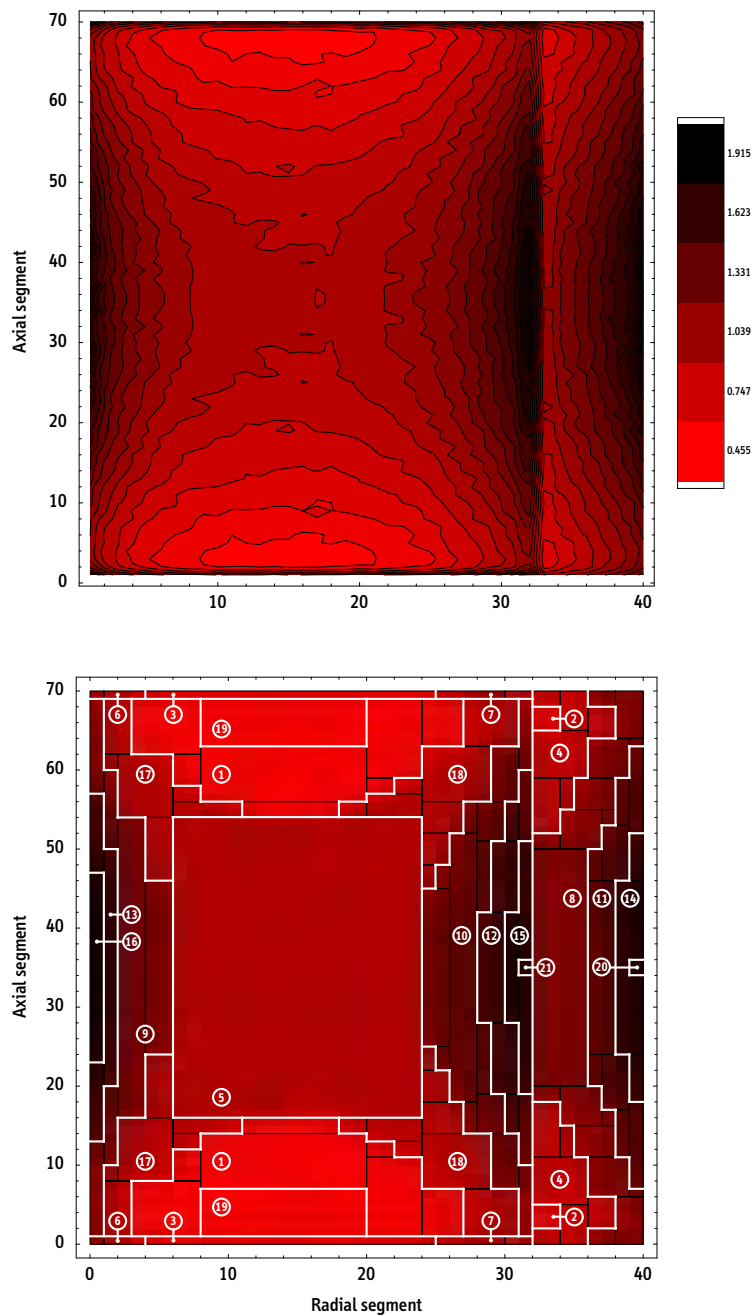


Figure 8.5: Adaptive cell structure for FRM-II analysis (130 cells, 21 zones).

Zone designations are selected by search algorithm (in no particular order)

8.1.5 Installations in moderator tank

In the most comprehensive calculations based on core Model A, simplified models of the cold neutron source and the horizontal beam tubes have been included in the final MCNP model.

With regard to the beam tubes, solely for the horizontal orientation and the z -position of the tubes, have numerical values been published [Axmann et al., 1999a, Appendix 1]. Positions of the noses and apertures of the tubes have been inferred from available technical drawings. Table 8.3 lists the estimated beam tube data as used with Model A and Figure 8.6 illustrates the situation.¹³ The beam tubes have been modeled as voided volumes in the heavy water moderator, which reproduces the main characteristics of the expected neutronics, while still more detailed simulations would also need to include the structural materials of the tubes.

The center of the cold neutron Source (CNS) is assumed to be located at $(x, y, z) = (-5, 40, 0)$ cm relative to the center of the reactor core. The simulations use a simplified model of the CNS, since complete and up-to-date design information of the device were not available. In the present case, the CNS is represented by a spherical zirconium shell of 31 cm diameter and a wall thickness of 0.5 mm [Gobrecht, 1998], [Gobrecht et al., 2002]. The CNS contains a liquid deuterium-hydrogen mixture (95 wt% D₂ and 5 wt% H₂) at an average density of 0.2 g/cc. Neutron scattering at low temperatures was corrected in MCNP with the DORTHO.O1T and the HORTHO.O1T cards for 20 K.

Further details of the device, such as the re-entrant hole, have not been modeled. As a result, *absolute* values obtained for the total gamma and neutron heating in the CNS can be expected to have some uncertainties. Nonetheless, the model is considered adequate for the present simulations, seeing that the main objective of the calculations is a *relative* comparison of the situation inside the CNS for the various core options considered below. Results for the perturbed calculations, in which the cylindrical symmetry is no longer conserved, are produced for the 1999 BMBF conversion options and are discussed in Section 8.3.

¹³As usual, the set-up of the corresponding MCNP model is executed with *Mathematica* modules.

BT #	x [cm]	y [cm]	z [cm]	Radius at P	Orientation in xy -plane	Aperture
1	-20	40	0	7 cm	0°	6°
2	-10	50	0	7 cm	48°	4°
3	25	25	30	5 cm	82°	4°
4	5	50	0	7 cm	128°	4°
5	38	-8	-1	5 cm	150°	4°
6	—	-53	30	7 cm	173°	0°
7	35	10	-20	7 cm	214°	4°
8	-20	-20	-20	5 cm	248°	4°
9	-40	-10	-20	5 cm	270°	4°
10	-35	-88	25	5 cm	320°	4°

Table 8.3: Data for horizontal beam tubes. (x, y, z) indicate the position of the beam tube nose (origin of the hemisphere, point P). The center of the core defines the origin of the coordinate system. Orientation in xy -plane relative to beam tube #1 (positive angles clockwise). Aperture in beam direction, orientation, dimensions, and positions taken or inferred from [Axmann et al., 1999b, Appendix 1].

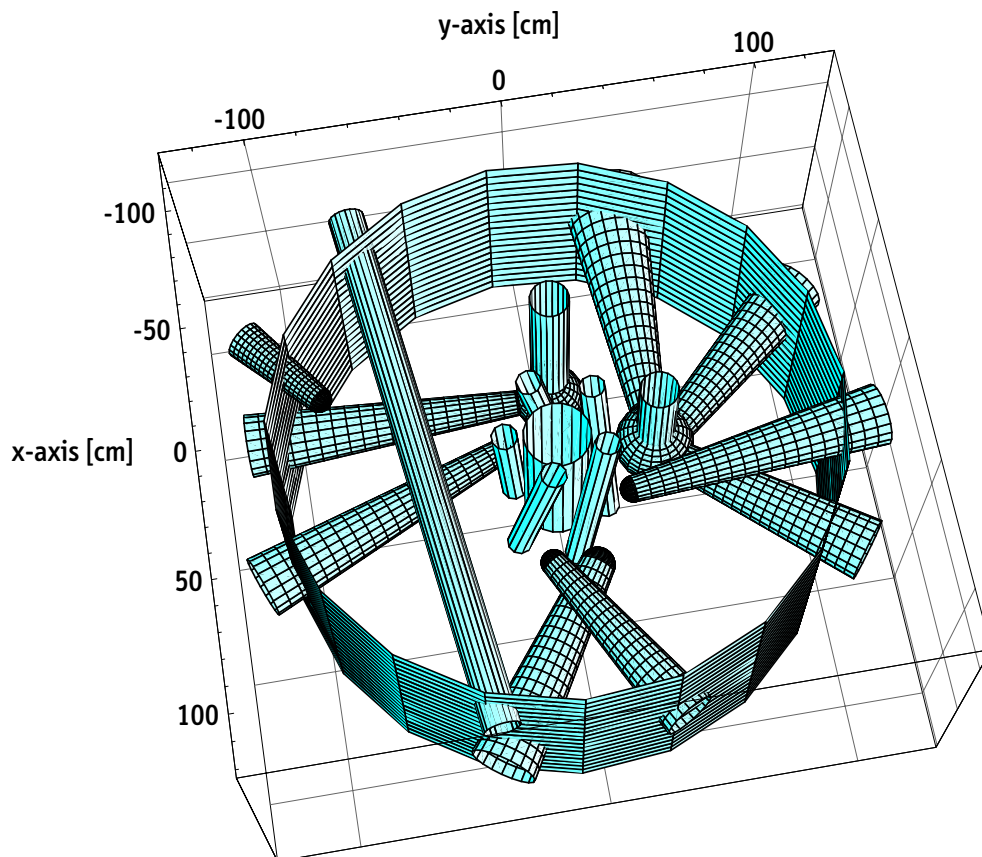


Figure 8.6: Illustration of the main components in the moderator tank of FRM-II: beam tubes 1 to 10, cold and hot neutron source and safety rods 1 to 5. The axes being defined as indicated, beam tube #1 runs parallel to the x -axis and is directed on the cold neutron source centered around $(x, y, z) = (-5, 40, 0)$ cm.

8.2 Analysis of the Original HEU Design

As indicated, the main purpose of studying the original HEU design is to demonstrate the versatility of the computational system and the reactor models used in this thesis and to confirm the accuracy of the results obtained. Without significant modifications to the base MCNP input deck, the model described in the previous section can be used directly to determine important operational characteristics of the reactor. Only for those parts of the analysis focused upon the time-dependent evolution of the fuel composition (burnup calculations), the MCNP model requires additional input for the adaptive cell structure (ACS) defined in Section 8.1.4 and related extensive modifications at regular time intervals during simulations. The following subsections (8.2.1 to 8.2.8) summarize the diverse results obtained in M³O simulations for the HEU reference design of FRM-II. The data is compared to results published by the Technical University of Munich (TUM), as far as they are available, at the end of this section.

8.2.1 Neutron flux in moderator tank

The base MCNP input deck can be used directly to determine the neutron flux and spectrum that are present in the moderator tank surrounding the reactor core. To this end, the corresponding MCNP cells are subdivided into suitable cylindrical shells. These subvolumes are tallied and the results correlated to reference values obtained in the center of the core for normalization. For a discussion of the normalization of results obtained in Monte Carlo calculations, see Section 7.2.

Figure 8.7 shows a contour plot of the thermal neutron flux that accumulates in the moderator tank for the axially symmetric Model B at BOL. In the following, only the flux levels available at the axial core center (mid-plane, $z = 0$ cm) are studied in more detail. Nonetheless, the actual torus-shaped volume in the moderator tank, in which the thermal neutron flux surpasses a defined threshold level, might be an equally useful characteristic to describe reactor performance, especially if the height of the fuel element is changed or the radial shape of the flux profile varies. To a good approximation, such a volume is generally proportional to the number of experimental devices that can be accommodated in a high-flux zone of the reactor and therefore is a useful measure to quantify the overall scientific usability of the facility.

The thermal neutron flux building up in the moderator tank is shown in Figure 8.8 as a function of distance from the core centerline. The profile exhibits a strong increase in the first 10 cm, which is due to the diffusion length of the leaking neutrons. The unperturbed flux reaches a maximum of 8.0×10^{14} n/cm² s at $r \approx 25$ cm (11 cm distance from the central channel tube), and collapses gradually for larger radii.

Note that for $r \approx 40$ cm, which corresponds to the central position of the cold neutron

source installed in the moderator tank,¹⁴ the unperturbed thermal neutron flux has dropped to 6.0×10^{14} n/cm²s. For a variety of geometric and engineering reasons, the cold neutron source — or any other experimental device — has not been located in the volume of the highest neutron flux generated by the reactor core.¹⁵

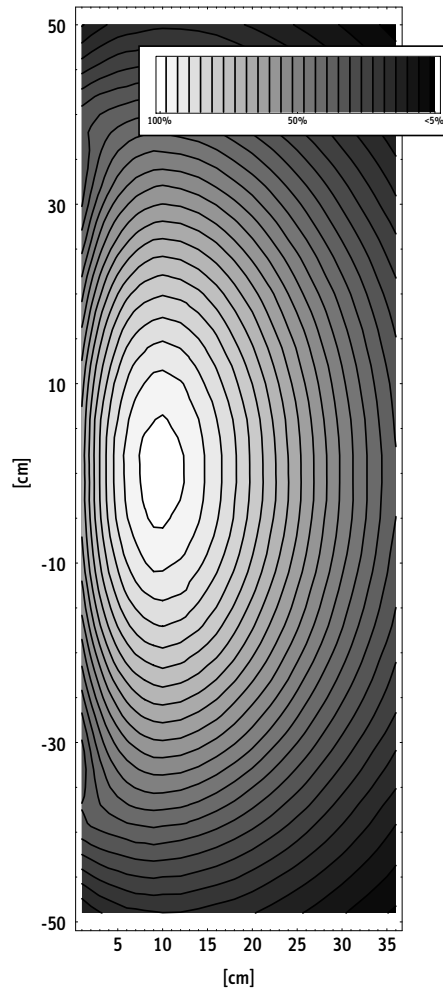


Figure 8.7: Contour plot of the thermal neutron flux in moderator tank.

¹⁴As discussed in Section 8.1.5, the CNS is centered around $(x, y, z) = (-5, 40, 0)$ cm, which corresponds to an axial distance from the core of about 40.3 cm.

¹⁵In particular, sufficient space has to be allocated for the five shut-down rods, which have a diameter of approx. 10 cm and run along the central channel tube. Locating the cold neutron source closer to the core does also increase the cooling requirements of the device due to higher neutron and gamma fluxes absorbed by the structural materials.

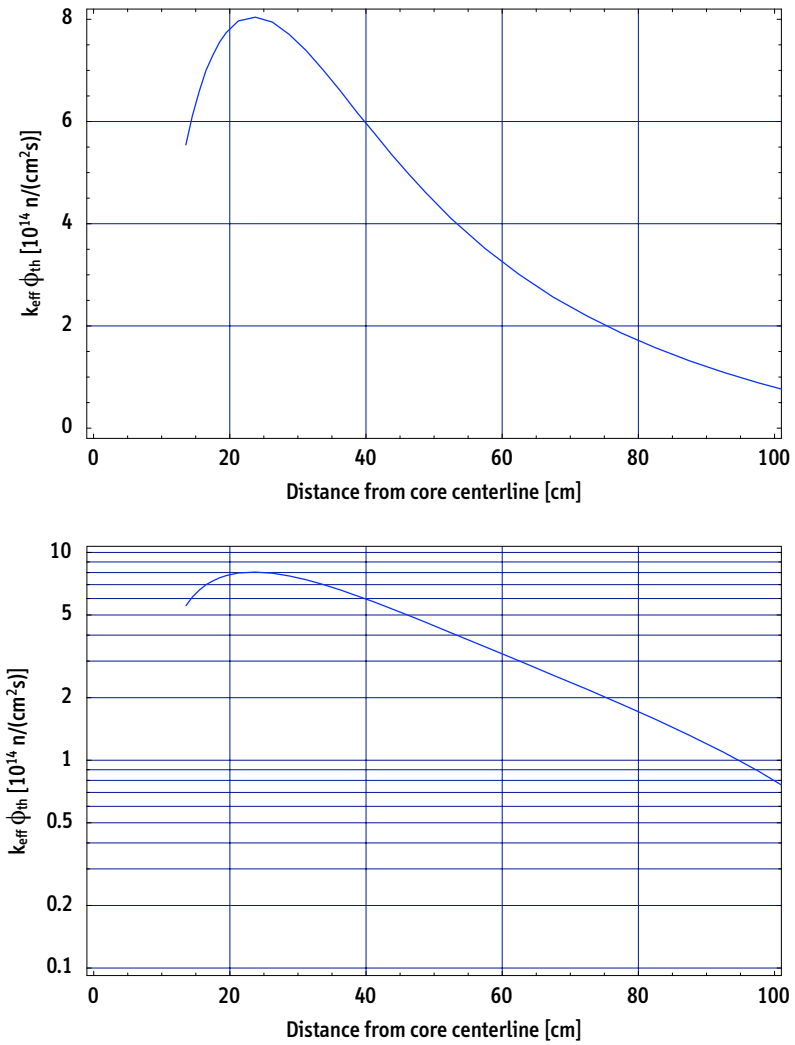


Figure 8.8: Radial distribution of thermal neutron flux in moderator tank.

MCNP input deck: FRMx2 (April 8, 2004), evaluated with: FRM.FluxAnalysis

8.2.2 Neutron spectrum in fuel plate

The neutron spectrum in the fuel is an important property to characterize the mode of operation and, ultimately, to optimize the performance of the reactor. In particular, for a given core geometry, power level and fissile inventory, it is mainly the neutron spectrum that determines the initial positive reactivity of the core and, hence, the achievable cycle length of the reactor.

Figure 8.9 shows the averaged neutron spectra in the inner and outer segments of the fuel plate at beginning of life of the core. For neutron energies between 1 eV and 10 keV, the flux level is nearly constant, indicating a typical thermalisation process, in which the average lethargy increase per scattering event is constant. Due to reflected neutrons re-entering the core from the moderator tank, the spectrum in the periphery of the plate is significantly more thermalized than the spectrum closer to the center of the core, showing a pronounced peak for thermal neutron energies. The strongly thermalized spectrum in the periphery results in unusually high spectrum-averaged fission cross-sections of the fissile isotopes, and would lead to unacceptable power densities in that segment of the plate if the uranium density were not reduced. As a countermeasure, the uranium density has been reduced to half its value in the outer section (10.9 mm) of the fuel plate.

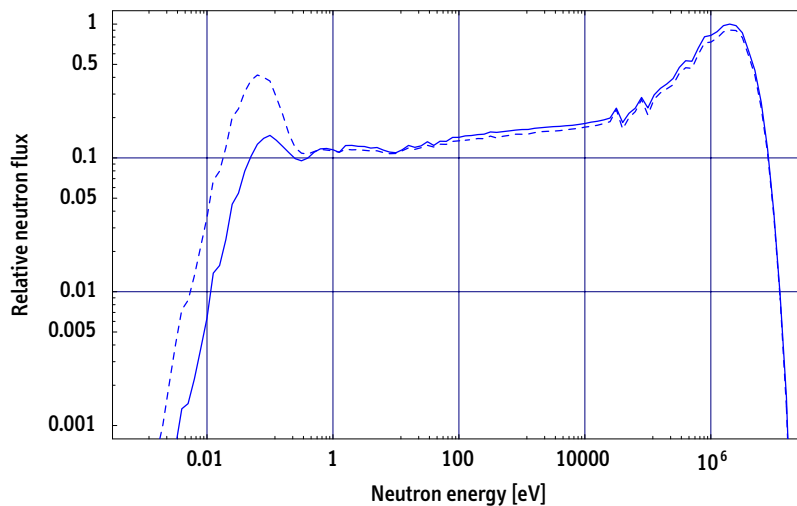


Figure 8.9: Normalized neutron spectrum in lethargy representation in FRM-II fuel plate at beginning of life averaged over inner (—) and (- -) outer segments of the plate.

MCNP input deck: FRMz2 (April 30, 2004), evaluated with: FRM_Spectrum

The fuel loading requirements for compact research reactor cores are strongly influenced

by the hardness of the neutron spectrum in the fissile region. In particular, if highly enriched fuel is replaced by fuel with lower enrichment, the uranium-235 has to be matched and, in practice, overcompensated even more as the H/HM-ratio or D/HM-ratio decreases. Single element reactors like the FRM-II are generally characterized by very hard neutron spectra compared to typical MTR-type reactors, which makes their conversion to LEU even more difficult.

8.2.3 Cycle length

Besides the maximum thermal neutron flux available for experiments, the achievable cycle length can be considered another important characteristic determining the overall performance of a neutron source used for scientific or industrial applications.¹⁶ In addition, the cycle length and the average burnup of the discharged fuel determine the total annual fuel demand of the reactor. Both have a strong impact on the economics and total operating costs of a given facility. For these reasons, the achievable cycle length will be an important criterion when evaluating conversion or design options of modern research reactors.

Figure 8.10 shows the evolution of k_{eff} versus time for the FRM-II Model B using the adaptive cell structure defined in Section 8.1.4. M³O calculations are based on a sequence of 17 time steps and use the predictor-corrector formalism to increase accuracy of results.

For a fully inserted beryllium-follower, an initial effective multiplication of $k_{\text{eff}} = 1.199$ is achieved. This is slightly higher than the value to be expected for simulations, in which the boron ring is included in the model. The boron's initial reactivity-worth has been estimated above to $k_{\text{BR}} = -0.007$,¹⁷ which corresponds to a corrected value of $k_{\text{eff}}^* = 1.192$. The latter value is in excellent agreement with results published by TUM for the fresh fuel element with the beryllium-follower fully inserted. As shown above, the boron ring has no impact on the total length of the irradiation cycle because it is burned out completely and loses its poisoning effect.

After the initial reactivity drop due to the xenon build up and attainment of equilibrium after about two full power days, the reactivity loss rate is nearly constant up to the full exposure of the fuel and equals $\Delta k/\Delta t \approx -1.35 \times 10^{-3}$ per day.

By definition, end of life (EOL) of the fuel element is reached when a pre-defined lower limit of k_{eff} is reached. In the present unperturbed calculations, no instruments or other

¹⁶Note that the absolute value of the cycle length is an extremely soft criterion. FRM-II achieves a cycle length of 52 days, but 14–17 days were considered acceptable for the unrealized U.S. Advanced Neutron Source [Redmond II, 1990, Bari et al., 1994], which was designed to compensate its short cycle with a much higher neutron flux level.

¹⁷See also [Mo et al., 1995, p. 2].

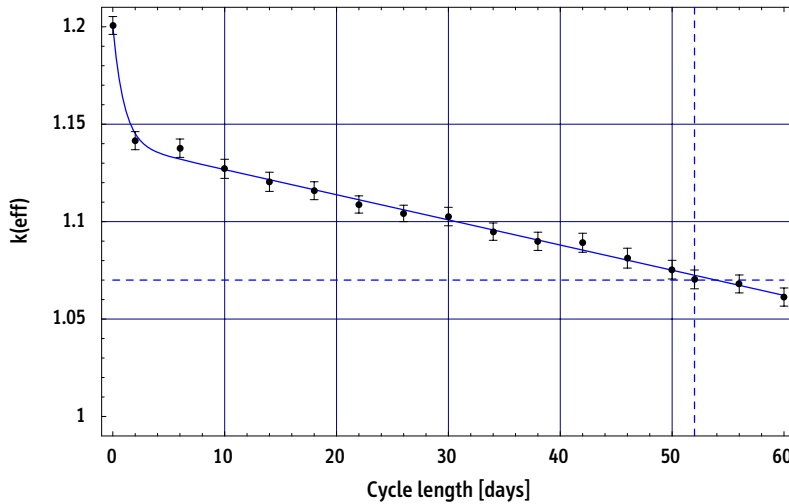


Figure 8.10: Cycle length of the original FRM-II HEU design.

M³O results, MCNP input deck: frmv3final, 17×2 MCNP runs, four million neutron histories each
Total running time: about 100 hours on 1.5 GHz UNIX machine

components are positioned in the moderator tank. The net reactivity loss due to the presence of these objects, which displace a significant volume of the D₂O moderator, has been estimated to $\Delta k = 0.05$. An extra safety margin of $\Delta k = 0.02$ can be added to guarantee a desired target cycle length,¹⁸ such that the maximum cycle length is reached when k_{eff} drops below 1.07.

With these assumptions, the M³O calculations yield a cycle length for the original HEU design of 52–54 days, i.e. precisely the value predicted by TUM in several, more recent publications (see discussion in Section 8.2.9).¹⁹ Equivalently, the value of 52 days also corresponds to the licensed maximum burnup of 1040 MWd(th) per fuel element, if the reactor is operated at 20 MW during the entire cycle.

8.2.4 Power density distribution in fuel plate

The average power density as well as the peak values observed at beginning of life or during irradiation (hot spot and hot channel factors) are key characteristics determining

¹⁸There are variety of reasons to include a margin for additional, unpredicted reactivity losses. These losses could be caused by impurities in the moderator, the reflector, or other structural materials being higher than originally assumed. Also, due to the aging of the reactor and neutron capture in permanent components of the reactor, the reactivity penalty can be expected to increase with time.

¹⁹In some earlier publications, slightly lower values were quoted by TUM. In particular, for an identical fuel element geometry, Röhrmoser [1991] quotes a more conservative value for the cycle length of 48 days only.

the feasibility of operating a nuclear reactor safely and reliably.

For the present design, an unacceptable power density would be obtained at the periphery of the plate due to neutrons re-entering the core from the moderator tank. These neutrons are extremely well moderated and the spectrum-averaged fission cross-section of U-235 is therefore extraordinarily high.²⁰ To suppress this effect and to flatten the radial power density profile, a reduced fuel density is employed in the periphery of the plate.

In the reactor burnup simulations performed here, two simplifications in the model have been made: first, the central control rod remains fixed with the beryllium reflector fully inserted and, second, the boron ring below the fuel element is not included. Both affect the power density distribution in the plate, although in opposite directions.²¹

As can be read from Table 8.4, the power density distribution evolves strongly during irradiation and generally leads to a flattening of the profile in the course of irradiation.

Figures 8.11 and 8.12 show the evolution of the local power densities for various important segments of the plate. In particular, in the periphery of the plate, where the fission rate is initially highest and the uranium density reduced to 1.5 g/cc, the power density decreases rapidly during irradiation due to the strong fractional burnup of uranium-235 (zones ⑭, ⑪, and ⑧). A similar effect is not observed in the sections of the plate, where the nominal uranium density of 3.0 g/cc is used. Even in the zones with high initial values adjacent to the discontinuity (zones ⑮, ⑫, and ⑩), the power densities remain high and virtually constant during the entire irradiation cycle.²² As indicated upon setup (Section 8.1.4), the micro-segments ⑳ and ㉑ are used to obtain values for maximum power densities and burnups. Due to their small size, strong variations of the power density in these segments can be expected. As the power density in some high-power zones decreases during irradiation of the fuel, the power density in the low-power zones gradually increase as shown in Figure 8.11 for zones ①, ⑤, and ⑲.

²⁰Note that the maximum power density is usually obtained in the center of a reactor core or of any other simple critical configuration, where the neutron flux is highest for geometrical reasons.

²¹Indeed, the sole function of the boron ring is to lower the power density below the fuel element during the first days of operation when the hafnium section of the control rod absorbs neutrons in the upper section of the plate, while the flux is pushed into the lower section of the fuel plate.

²²The zones adjacent to the central control rod are not discussed in detail here. The evolution of the power density in this area can be assumed to be unrealistic due to the omission of the control rod movement in the present calculations. The power density in the central zones of the plate is lower than in the periphery (Table 8.4) and therefore does not limit the performance of the reactor.

#	BOL	EOL	#	BOL	EOL	#	BOL	EOL
1	4.48 kW/cc	+8.2%	8	8.04 kW/cc	-13.3%	15	11.64 kW/cc	-0.5%
2	4.85 kW/cc	-0.2%	9	7.93 kW/cc	±0.0%	16	11.67 kW/cc	-8.4%
3	6.57 kW/cc	+3.6%	10	8.07 kW/cc	+6.6%	17	6.02 kW/cc	+4.1%
4	6.25 kW/cc	-6.3%	11	10.11 kW/cc	-22.7%	18	6.15 kW/cc	+9.0%
5	6.10 kW/cc	+5.2%	12	9.96 kW/cc	+3.5%	19	3.51 kW/cc	+9.7%
6	8.76 kW/cc	-4.6%	13	9.93 kW/cc	-4.7%	20	12.87 kW/cc	-34.1%
7	8.92 kW/cc	+1.3%	14	12.06 kW/cc	-31.0%	21	12.27 kW/cc	+0.5%
Volume weighted average							6.75 kW/cc	±0.0%

Table 8.4: Local power densities in FRM-II fuel plate at BOL and EOL (relative difference).

M3O results, file: frmv3.MCODE.11.out

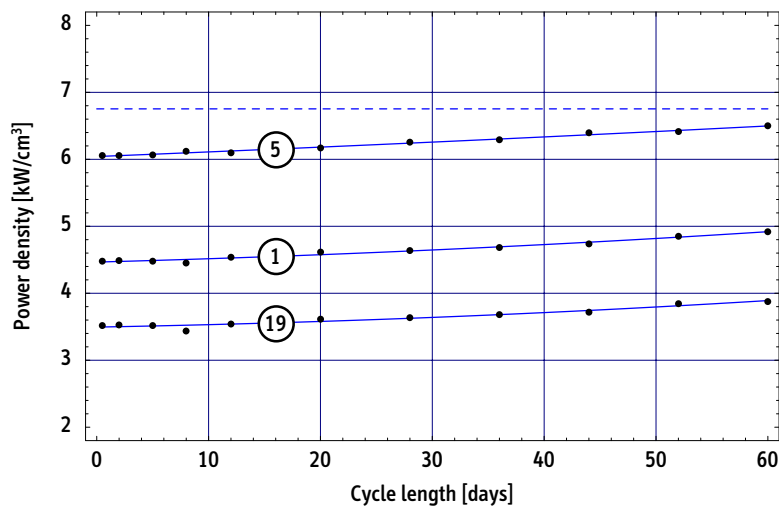


Figure 8.11: Evolution of power density in fuel: important low-power zones.

Dashed line indicates average power density in core (6.75 kW/cc)
 M3O results, MCNP input deck: frmv3final (11 burnup points) evaluated with: FRM_MCODEout.Table3

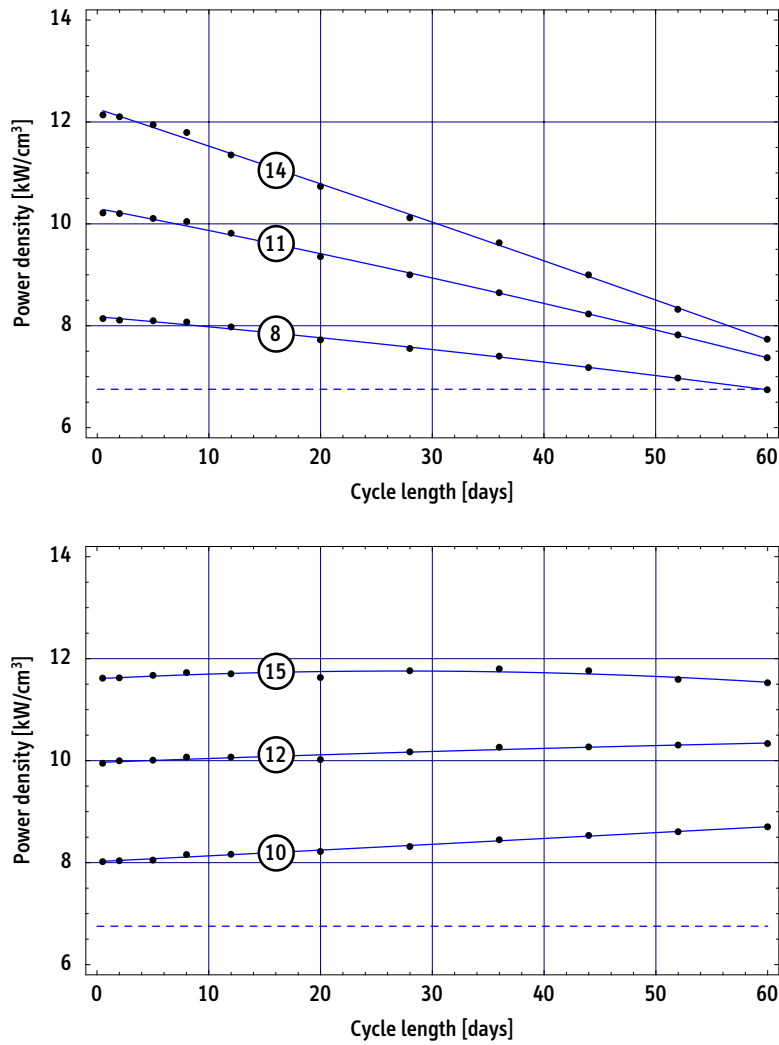


Figure 8.12: Evolution of power density in fuel: important high-power zones.

Dashed line indicates average power density in core (6.75 kW/cc)
 M3O results, MCNP input deck: frm3final (11 burnup points) evaluated with: FRM.MCODEout.Table3

8.2.5 Burnup and residual enrichment of fuel

The average uranium-235 burnup in the FRM-II fuel plate is unusually low due to the compactness of the core, the high leakage factor, and the resulting steep reactivity loss per burnup or time. Table 8.5 summarizes the uranium-235 burnup and residual enrichment, defined as the uranium-235 weight fraction of total remaining uranium, in the 21 zones of the selected adaptive cell structure at EOL, i.e. at the maximum total burnup of 1040 MWd(th) reached after 52 effective full power days.

#	Burnup	Residual Enrichment	#	Burnup	Residual Enrichment	#	Burnup	Residual Enrichment
1	11.2%	90.3%	8	35.3%	83.2%	15	27.5%	85.8%
2	22.8%	87.4%	9	19.0%	88.1%	16	26.5%	86.0%
3	15.4%	89.4%	10	19.7%	88.0%	17	14.8%	89.3%
4	28.2%	85.7%	11	42.1%	80.5%	18	15.2%	89.3%
5	15.1%	89.1%	12	23.9%	86.9%	19	8.8%	90.9%
6	20.1%	88.2%	13	23.1%	87.0%	20	50.2%	76.7%
7	20.4%	88.1%	14	47.7%	78.0%	21	28.9%	85.3%
Inventory weighted average							17.6%	88.6%

Table 8.5: Local U-235 burnup and residual enrichment in FRM-II fuel plate at EOL, 1040 MWd(th), 52 effective full power days. See Figure 8.5 for zone assignment.

Exemplary data are shown in Figures 8.13 and 8.14. Even though the average uranium-235 burnup after 52 days of operation is only 17.6%, the local burnup in several smaller sections of the plate is significantly higher. In the unperturbed simulations, the peak burnup is achieved at the outer periphery of the fuel plate and reaches 50.2% in a small volume of the plate.²³ This pronounced spatial dependency of burnup, of course, is characteristic for single element reactors. Note that the peak rather than the average burnup value is crucial for the overall fuel performance, and for the decision of whether or not a fuel can be used in a given reactor environment.

To a strong degree, burnup and residual enrichment are anti-correlated. Zones with low local burnup exhibit a high remaining uranium-235 fraction and vice versa. Figure 8.14 illustrates this situation. While the average enrichment at EOL is 88.6% (weight percent U-235 in total uranium), the value drops to less than 80% at the central periphery of

²³In reality, with the control rod movement taken into account, and in spite of the presence of the boron ring, the maximum burnup will be observed below the axial center of the fuel plate. It can be expected that the absolute value of the peak burnup will also differ slightly from the theoretical value calculated here.

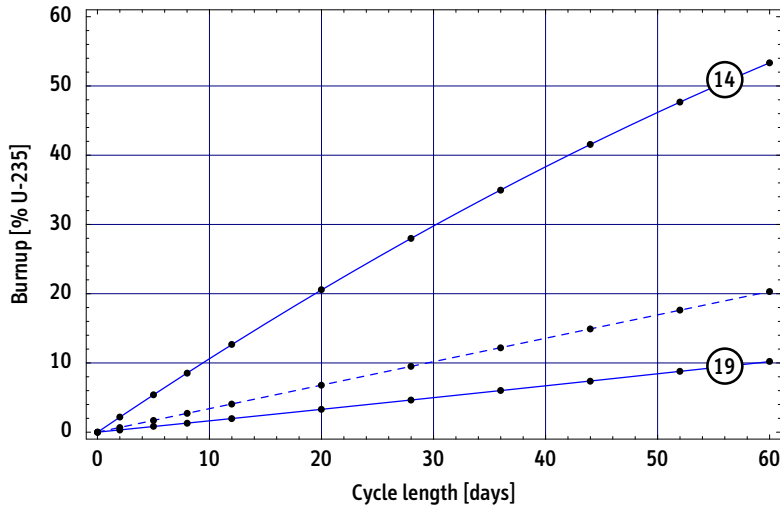


Figure 8.13: Local U-235 burnup in FRM-II fuel plate in selected zones and inventory-weighted average value (- -). See Figure 8.5 for zone assignment.

M3O results, MCNP input deck: frm3final (11 burnup points) evaluated with: FRM_MCODEout.Table4

the plate (zones ⑭ and ⑳). Conversely, enrichment remains above 90% in zones ① and ⑑, where burnup of the fuel is lowest.²⁴

8.2.6 Local fission rate and density

Overall fuel performance and the acceptability of a specific fuel-type for a given reactor design are primarily determined by the most unfavorable, i.e. in general not the average, conditions encountered locally in the fuel. In addition to maximum temperatures reached in the fuel under normal and accident conditions, the total damage as well as the average damage rate are both important characteristics in this context.

Typical variables to quantify the total damage suffered by the fuel due to fission events that occur during irradiation are (1) the maximum fractional U-235 consumption or burnup and (2) the maximum fission density at EOL. Similarly, the average local fission rate in the fuel is an adequate quantity to characterize the damage rate that has to be supported by the fuel. Ultimately, based on experimental test data, acceptable and unacceptable regions of operation can be specified to guarantee stable irradiation

²⁴For a discussion of the weapon-usability of the fuel, this strong inhomogeneity of burnup and enrichment is virtually irrelevant. If the uranium is extracted via reprocessing, the average composition of 88.6% is obtained. Selective extraction of the uranium from those segments of the fuel with high residual enrichment would be a highly inefficient procedure with little ‘benefit’ to the proliferator.

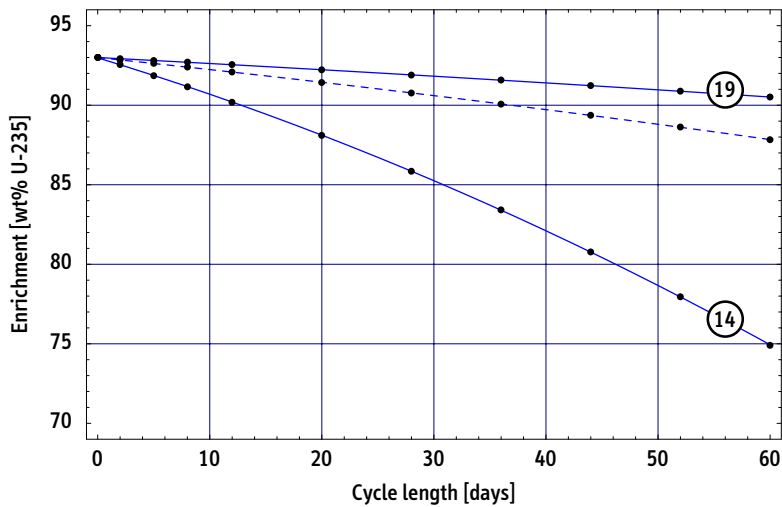


Figure 8.14: Average (---) and local enrichment in FRM-II fuel plate; minimum (zone 14) and maximum (zone 19). See Figure 8.5 for zone assignment.

M3O results, MCNP input deck: frm3final (11 burnup points), evaluated with: FRM_MCODEout_Table4

behavior of a given fuel-type.²⁵

Fission rate, fission density, and U-235 burnup are listed in Table 8.6 for important segments in the fuel plate of FRM-II. Figure 8.15 shows the evolution of the fission rate during irradiation in zones ⑭ and ⑮. As can be seen in the table and the figure, maximum fission rate, fission density, and burnup coincide in those segments of the plate where the effective uranium density is reduced to 1.5 g/cc. The peak fission rate exists at BOL in the small segment ⑳ at the periphery of the plate. Due to the reduced uranium density in that section of the plate, the U-235 is consumed rapidly and the fission rate drops substantially during irradiation. Fractional U-235 burnup is significantly lower in the main section of the plate with the nominal uranium density of 3.0 g/cc. As a result, the fission rate remains virtually constant during irradiation in these zones.

²⁵For instance, Hofman et al. [2004, p. 55] use experimental results to define corresponding regions for UMo-dispersion-type fuels. See Chapter 4 for details.

#	Fuel loading	FR at BOL [fi/(cm ³ s)]	FR at EOL [fi/(cm ³ s)]	Average [fi/(cm ³ s)]	FD at EOL [fi/(cm ³)	Burnup
14 20	13.3 vol%	29.1E14 31.0E14	20.1E14 20.4E14	24.9E14 26.2E14	11.2E21 11.8E21	47.7% 50.2%
15 21	26.6 vol%	14.0E14 14.8E14	14.0E14 14.9E14	14.1E14 14.8E14	6.3E21 6.7E21	27.5% 28.9%

Table 8.6: Local fission rates (FR) in fuel particles in selected zones at beginning-of-life and end-of-life, as well as averaged over the entire irradiation cycle of 52 days. The fission density (FD) achieved locally at the end of the cycle is juxtaposed to the corresponding burnup of the fuel in that segment. See Figure 8.5 for zone assignment.

MCNP input deck: frmv3, M3O results: frmv3.MCODE.11.out

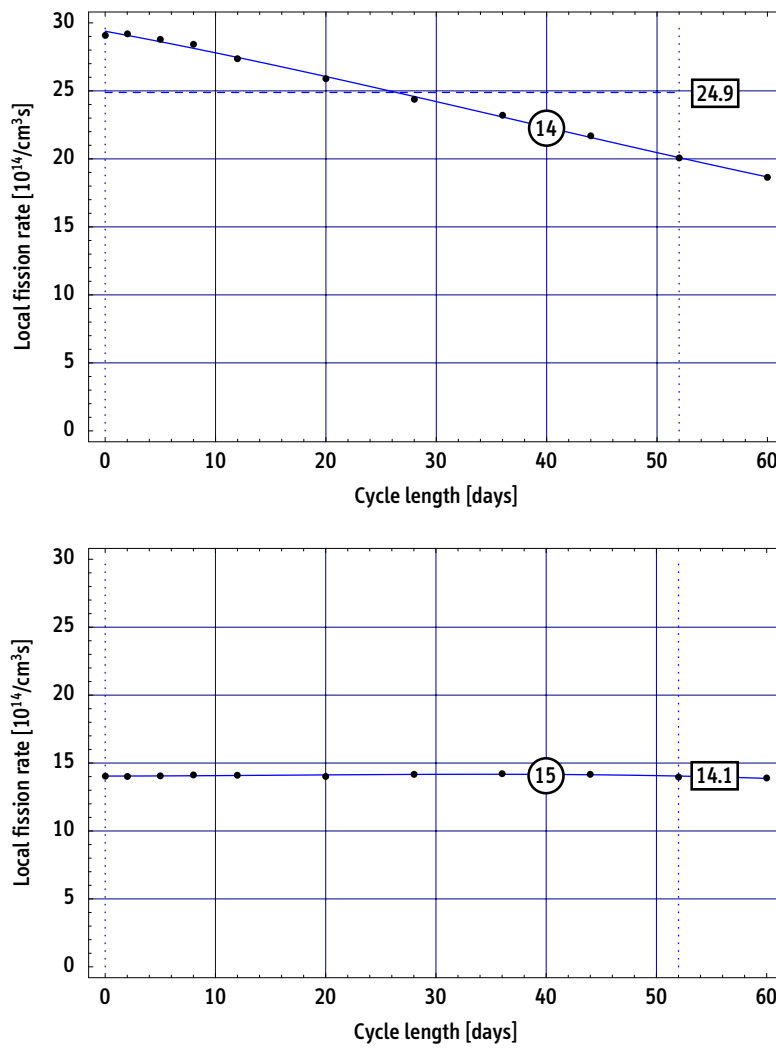


Figure 8.15: Local fission rates in fuel particles in zones 14 and 15.

Values of life-averaged local fission rates in respective zones are boxed
 MCNP input deck: frm3, M3O results: frm3.MCODE.11.out

8.2.7 Actinide and fission product inventory at EOL

ORIGEN2 tracks about 1300 unique nuclides in its point-depletion calculations carried out as a functional unit of M^3O (see Chapter 6). These nuclides include actinides and fission products as well as additional structural materials and low- Z activation products. Although not all of them are necessarily produced in non-vanishing amounts in every situation, in theory, the user has access to all relevant data (concentration, radioactivity, inhalation hazard, etc.) for this large set of nuclides built up in the fuel. Relatively few nuclides have non-negligible absorption rates in the fuel and are therefore relevant for neutronics calculations. The set of nuclides selected for explicit treatment in MCNP to generate accurate burnup-dependent one-group cross-sections is listed in Table 6.4 and contains 65 nuclides (17 actinides and 48 fission products).

Time-dependent inventories of selected uranium and plutonium isotopes are shown in Figures 8.16 and 8.17. As can be expected for the case of highly enriched uranium, in which neutron capture in U-238 is minimal, the total plutonium production is insignificant. At EOL (52 days), the total plutonium inventory in the entire core amounts to slightly less than 10 g with an Pu-239 fraction of 89.2 wt%. EOL inventory data of the isotopes explicitly treated in the MCNP simulations are summarized in Table 8.7 for an irradiation time of 52 days at 20 MW (1040 MWd(th)).

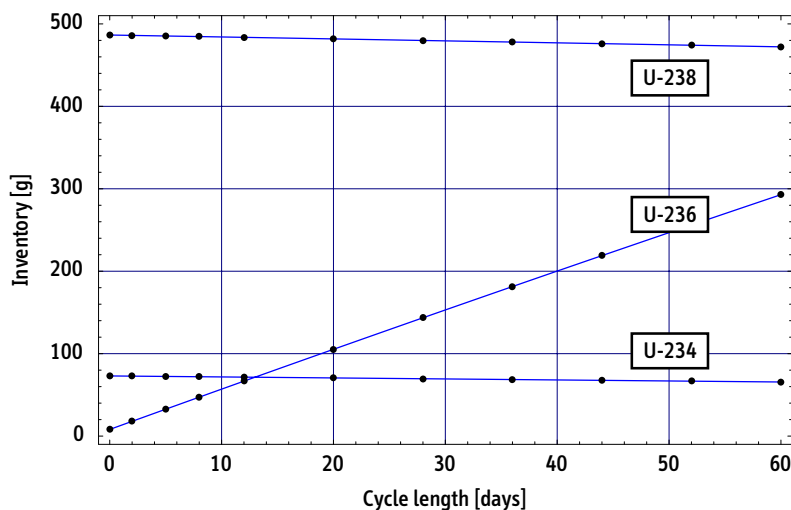


Figure 8.16: Inventory of minor uranium isotopes in HEU fuel of FRM-II.

MCNP input deck: frmv3, M3O results: frmv3.MCODE.11.out

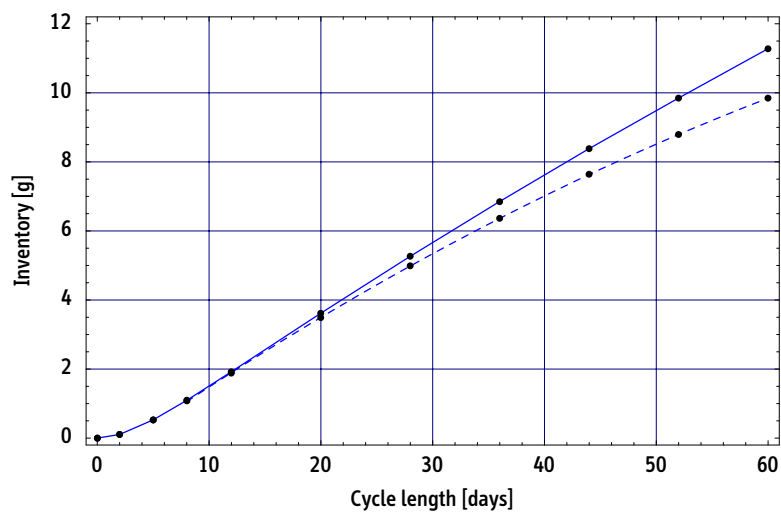


Figure 8.17: Total plutonium (—) and Pu-239 inventory (- -).

MCNP input deck: frmv3, M3O results: frmv3.MCODE.11.out

Nuclide	Inventory	Relative Absorption	Nuclide	Inventory	Relative Absorption
Kr-083	1.98 g	0.029%	Cs-135	5.05 g	0.009%
Zr-093	27.37 g	0.028%	La-139	41.58 g	0.019%
Tc-099 ◀	24.64 g	0.209%	Ce-141	23.20 g	0.026%
Mo-092	0.00 g	0.000%	Pr-141	15.07 g	0.011%
Mo-094	0.00 g	0.000%	Pr-143	13.34 g	0.070%
Mo-095	1.84 g	0.009%	Nd-143 ◀	22.73 g	0.247%
Mo-096	0.02 g	<0.001%	Nd-145 ◀	25.46 g	0.131%
Mo-097	25.80 g	0.016%	Nd-147	4.33 g	0.080%
Mo-098	26.47 g	0.006%	Nd-148	12.20 g	0.006%
Mo-099	2.09 g	0.002%	Pm-147 ◀	9.27 g	0.328%
Mo-100	29.08 g	0.004%	Pm-148	0.12 g	0.098%
Ru-101	23.52 g	0.077%	Pm-148m	0.08 g	0.087%
Ru-103	9.79 g	0.021%	Pm-149	0.53 g	0.023%
Rh-103 ◀	4.86 g	0.160%	Pm-151	0.10 g	0.004%
Rh-105 ◀	0.17 g	0.104%	Sm-149 ◀	0.40 g	0.926%
Pd-105	4.07 g	0.016%	Sm-150	6.94 g	0.056%
Ag-109	0.22 g	0.007%	Sm-151 ◀	0.99 g	0.325%
Cd-113	0.01 g	0.013%	Sm-152	3.38 g	0.164%
I-129	3.85 g	0.006%	Sm-153	0.14 g	0.006%
Xe-131 ◀	12.68 g	0.271%	Eu-153	1.49 g	0.048%
Xe-133	5.95 g	0.064%	Eu-154	0.14 g	0.013%
Xe-135 ◀	0.05 g	3.998%	Eu-155	0.08 g	0.036%
Cs-133 ◀	33.23 g	0.260%	Eu-156	0.14 g	0.004%
Cs-134	0.77 g	0.005%	Gd-157	<0.01 g	0.010%
U-234 ◀	66.62 g	0.528%	Pu-240	0.70 g	0.084%
U-235 ◀	6211.49 g	88.763%	Pu-241	0.23 g	0.015%
U-236 ◀	256.00 g	0.805%	Pu-242	0.01 g	<0.001%
U-237	1.32 g	0.017%	Am-241	0.00 g	0.000%
U-238 ◀	474.02 g	1.104%	Am-242m	<0.01 g	<0.001%
Np-237	3.12 g	0.054%	Am-243	0.00 g	0.000%
Np-239	0.81 g	0.006%	Cm-244	<0.01 g	<0.001%
Pu-238	0.12 g	0.002%	Cm-245	<0.01 g	<0.001%
Pu-239 ◀	8.79 g	0.488%			

Table 8.7: Total fission product and actinide inventory at EOL (52 days).

16 nuclides with relative absorption of at least 0.1% are highlighted
M3O results, file: frm3.MCODE.11.out, relative absorption data for cell 5 at 60 days

8.2.8 Neutron importance of actinides and fission products

Table 8.7 lists the 65 nuclides treated explicitly in MCNP and their relative neutron importance at end-of-life. This set of fission products and actinides account for 99.9% of all neutron absorptions in the core. The nuclides for the default set of MCNP nuclides are identified by means of the MCODE output (of a representative calculation), which lists absorption rates for all nuclides treated in ORGEN2 (about 1300 unique isotopes) and indicates whether their cross-sections have been determined via MCNP or have been taken from a specified ORIGEN2 library. Note that, even at end-of-life, a set of only 5 nuclides (U-235, Xe-135, U-238, Sm-149, and U-236) absorb more than 95%, and a set of 20 nuclides more than 99% of all neutrons.

The relative absorption rates for the five most important nuclides are listed in Table 8.8 for selected zones and time steps. Burnup zone ⑤ is a large segment in the center of the plate, while zones ⑭ and ⑮ are located along the periphery and along the uranium density discontinuity of the plate, respectively. Due to the strong variation of the neutron spectrum in the fuel plate (see for instance Figure 8.9), the spectrum-averaged one-group cross-sections vary in all burnup zones, both spatially and as a function of burnup. Exemplary cross-section data is shown in Figure 8.18 and Table 8.8.

Two effects are noteworthy: even though some cross-section values change strongly during irradiation, especially those of the dominant fission products xenon-135 and samarium-149, the corresponding relative absorption rates do not. The latter are balanced by an anti-correlated local concentration of the corresponding isotope — a typical compensatory effect encountered in all burnup situations.

In the case of HEU, the isotope dominating neutron absorption is uranium-235. As displayed in Table 8.8, the relative importance of U-235 varies very weakly across the plate. Nonetheless, as shown in Figure 8.19, the fission-to-capture ratio after neutron absorption clearly depends upon the local neutron spectrum in the plate. In the central and inner parts of the plate, where the spectrum is less thermalized, the ratio is 3.8–3.9 (zone ⑤), while it increases to 5.1–5.2 in the periphery of the plate (zone ⑭). The higher fission-to-capture ratio is the main reason for the strong power peaking in the periphery of the plate. The effect is partially suppressed and lowered to acceptable values by employing the reduced effective uranium density in that segment.

From a general perspective, the preceding analysis demonstrates the necessity to model burnup zones with sufficient detail in order to take local spectral conditions correctly into account. This is the primary design philosophy of the adaptive cell structure (ACS) system used for M³O.

		One-group cross-section			Relative absorption		
		Zone 5	Zone 14	Zone 15	Zone 5	Zone 14	Zone 15
U-235	2 days	29.32 b	104.44 b	52.21 b	94.74%	94.40%	94.52%
	28 days	31.04 b	113.84 b	58.32 b	93.47%	93.18%	93.44%
	52 days	33.94 b	127.52 b	67.32 b	92.92%	91.80%	92.49%
Xe-135	2 days	84232 b	449610 b	204420 b	3.97%	4.94%	4.63%
	28 days	92767 b	492570 b	233310 b	4.10%	5.10%	4.67%
	52 days	102420 b	537950 b	265290 b	4.18%	5.50%	5.08%
U-238	2 days	5.54 b	6.35 b	5.56 b	1.15%	0.37%	0.65%
	28 days	5.57 b	6.12 b	5.44 b	1.14%	0.44%	0.64%
	52 days	5.53 b	6.38 b	5.62 b	1.13%	0.60%	0.69%
Sm-149	2 days	2562 b	11147 b	5574 b	0.08%	0.24%	0.16%
	28 days	2787 b	12070 b	6251 b	0.84%	0.89%	0.87%
	52 days	3037 b	13090 b	7031 b	0.94%	1.17%	1.01%
U-236	2 days	9.12 b	9.27 b	8.62 b	0.07%	0.04%	0.05%
	28 days	7.73 b	7.70 b	7.36 b	0.44%	0.40%	0.38%
	52 days	6.96 b	7.08 b	6.54 b	0.84%	0.93%	0.73%

Table 8.8: Evolution of one-group cross-sections and relative absorption rates for the five most important nuclides. Data for selected zones and time steps. Absorption rates normalized for each zone and relative to the five specified nuclides (more than 95% of all absorptions). See Figure 8.5 for zone assignment.

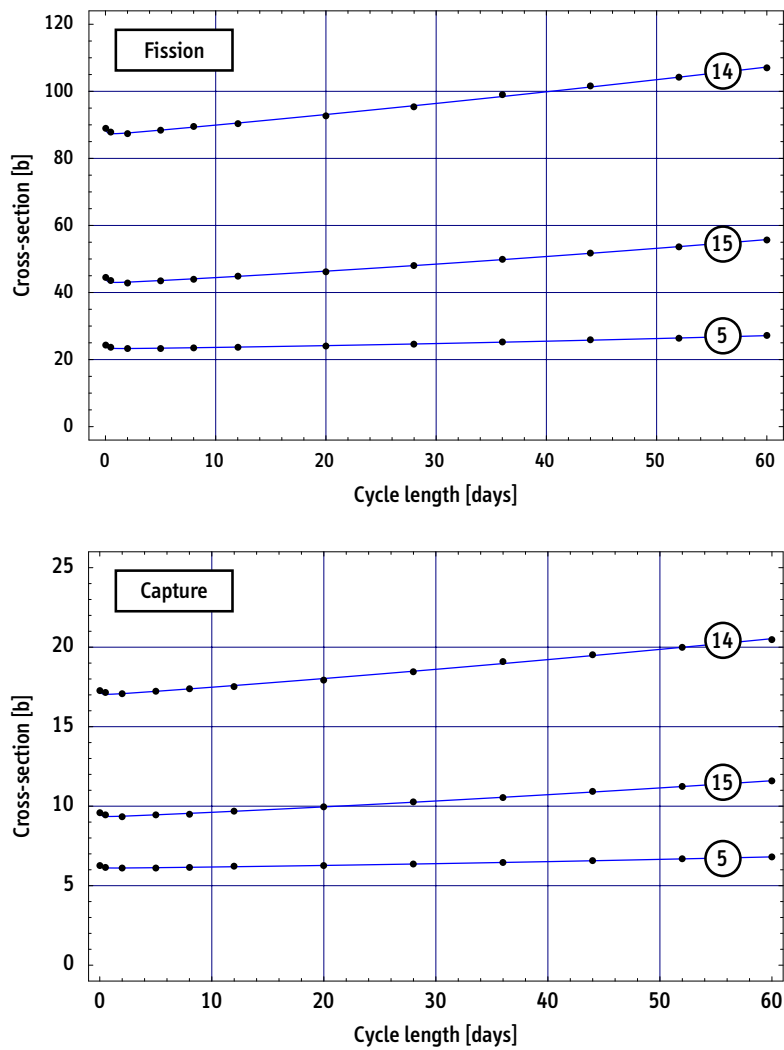


Figure 8.18: Spectrum-averaged fission and capture cross-sections of uranium-235 in selected zones. See Figure 8.5 for zone assignment.

MCNP input deck: frm3, M3O results: frm3.MCODE.11.out

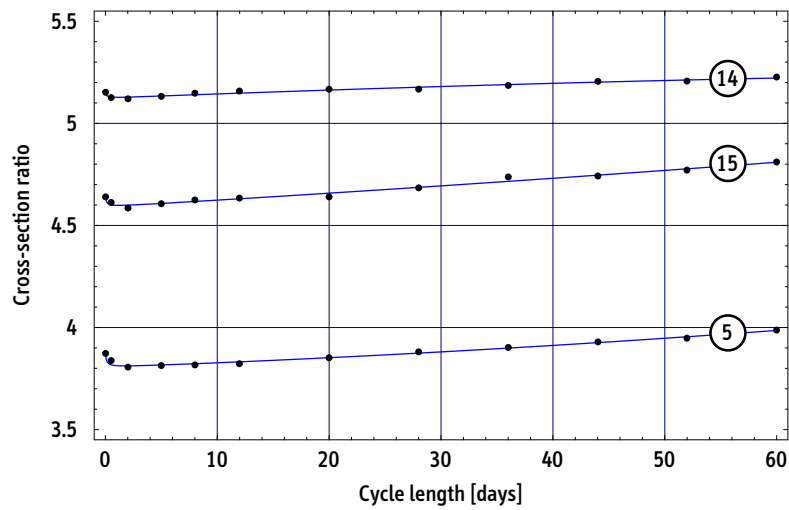


Figure 8.19: Uranium-235 cross-section ratio in selected zones: fission to capture.

MCNP input deck: frmv3, M3O results: frmv3.MCODE.11.out

8.2.9 Comparison of results with available FRM-II data

One of the main reasons to study the neutronics of FRM-II is to compare the results of the computational system M³O against theoretical data available from alternative sources, i.e. mainly data originally published by TUM. In the preceding sections (8.2.1 to 8.2.8), a diverse set of results has been generated using a detailed three-dimensional MCNP model of the FRM-II core. The most prominent M³O results are juxtaposed to results calculated by TUM in Table 8.9. For reference purposes, ANL results are also included, but these are based on early diffusion theory calculations using a preliminary model of the FRM-II core and can therefore be expected to be less accurate than TUM and M³O data.

Characteristic	ANL result	TUM result	M3O result
Max. thermal neutron flux	8.0E14 n/cm ² s	8.0E14 n/cm ² s	8.0E14 n/cm ² s
Cycle length	50 days	52 days	52–54 days
Initial k(eff), reflector inserted	1.194 ± 0.001	1.191 ± 0.001	1.192 ± 0.001
EOL inventory: U-234	unavailable	72.8 g	66.6 g
U-235		6221.0 g	6212.0 g
U-236		248.0 g	256.0 g
U-238		472.0 g	474.0 g
Np-237		3.7 g	3.1 g
Pu-239		8.6 g	8.8 g
Pu-240		0.7 g	0.7 g
Residual uranium enrichment	unavailable	88.7%	88.6%
Average burnup	17.3%	17.5%	17.6%
Peak burnup	unavailable	unavailable	50.2%
Maximum fission rate	35.4E14 fi/cc s	unavailable	31.0E14 fi/cc s
Maximum fission density	11.3E21 fi/cc	12.2E21 fi/cc	11.8E21 fi/cc

Table 8.9: Comparison of main results for FRM-II: TUM and M3O.

Beryllium-follower fully inserted, Argonne data from [Mo et al., 1995], TUM data from various references, including [Böning et al., 1999, Röhrmoser, 1991, Röhrmoser et al., 2004]; additional information provided upon request by BMU and quoted with permission

One of the most important characteristics of any modern research reactor used for neutron beam research is the maximum neutron flux level achieved in a volume accessible to experiments, i.e. in the moderator tank surrounding the core for a single element reactor operated in the inverse flux-trap mode. For the FRM-II reference design, TUM and M³O both predict a maximum value of 8.0×10^{14} n/cm²s at a distance of 25 cm from the core centerline. The precision of these results, which is due to the statistical uncertainty of the MCNP calculations, is very high and related errors are typically well below 1%. Note however that the accuracy of neutron flux estimates may be lower than

that. As discussed in Section 6.2.6, systematic errors for this type of simulation are very difficult to quantify and are mainly due to two sources: errors in the microscopic cross-section data-libraries and inadequate assumptions about material compositions used in the system.²⁶ It is reasonable to assume that the combined error of these inherent uncertainties may ultimately sum-up to a few percent, and can only be reduced by subsequent validation with experimental data obtained during operation of the facility. Similar arguments apply to most of the results generated in neutronics calculations, which include the initial core reactivities or cycle length estimates discussed below, even if these calculations are based on the Monte Carlo technique as they are here.

A second important result to characterize the reactor is the achievable cycle length, which is limited by the core reactivity dropping below a pre-defined limit. Again, the TUM and M³O numbers are in excellent agreement, with TUM quoting a 52-day cycle, while a cycle length of 52–54 days is predicted by M³O (Figure 8.10). Note however that the cycle length is highly sensitive to variations of the net reactivity ultimately bound by the components in the moderator tank and other effects not considered in unperturbed simulations. Therefore, the maximum cycle length achievable in practice may vary significantly from the values previously predicted in simulations. Based on the data shown in Figure 8.10, a Δk of ± 0.01 would add or subtract approximately 7 days, respectively.²⁷

Similarly, the achievable cycle length is also strongly dependent upon the initial core reactivity ρ_{ini} or k_{eff} of the core. The fact that both estimates (1.191 ± 0.001 versus 1.192 ± 0.001 with the boron ring included and the beryllium-follower fully inserted) virtually coincide is a prerequisite for an accurate prediction of the 52-day cycle, and an indication for the level of accuracy reproduced by the TUM and M³O core models.

Minor differences exist for the EOL inventories of the uranium isotopes. In the case of U-234, these can be explained with slightly different BOL compositions. As introduced in Section 4.2.1, an initial U-234 content of 0.9% and a U-236 content of 0.1% has been defined for HEU of U.S. origin. TUM assumes a slightly higher U-234 content of 1.0%, which corresponds to an initial theoretical inventory difference of about 8 grams. Since the BOL content of U-234 also determines its EOL inventory (see Figure 8.16),

²⁶For instance, assumptions have to be made about the (undesired) residual light water content in the heavy water (here: 0.2 at% hydrogen, 99.8 at% deuterium). Depending upon the supplier of the material, lower or higher contamination of the D₂O would directly affect parasitic neutron absorption in the tank and increase or decrease the neutron flux correspondingly. The precise composition of alloys used in structural components of the reactor, or even the specific uranium isotopes used in the fuel, have similar effects. In practice, attempts to quantify the combined impact of these uncertainties would not be very promising for the type of analysis performed here.

²⁷Due to the restrictions imposed by the license, the reactor is not allowed to operate beyond a burnup of 1040 MW(th) or more than 52 full power days at 20 MW — and would not be able to benefit from more favorable operating conditions. On the other hand, thanks to the rather conservative assumptions made by the operator regarding potential reactivity penalties, it is unlikely that the actual cycle length will be less than the predicted one of 52 days.

EOL values from TUM and M³O are both consistent with their respective initial fuel compositions. The relative inventory difference of U-235 of about 0.15% (+9 grams relative to the value quoted by TUM) indicates that M³O predicts a slightly lower fission-to-capture ratio and, therefore, a stronger buildup of U-236. Consistently, the U-236 content at EOL calculated by M³O is 8 grams higher. This effect also explains the higher average burnup value predicted by M³O (17.6% versus 17.5%) because more U-235 is consumed via neutron capture without releasing fission energy, as well as the lower residual enrichment of the fuel at EOL (88.6% versus 88.7%). Both values, i.e. average burnup and residual enrichment of the fuel, predicted by TUM and M³O can still be considered to be in very good agreement.

In addition to the uranium isotopes, inventory data for the next three most important actinides (Np-237, Pu-239, and Pu-240) are listed in Table 8.9. The number densities of all other actinides are such that their total inventory in the core at EOL amounts to less than one gram. Again, the absolute numbers obtained for these minor actinides are in good agreement.

A final category of data that can be compared to demonstrate the reliability of the computational system is given by the *local* values predicted for the maximum fission rate, maximum fission density, maximum burnup, and power peaking factor in the fuel plate. Here, M³O strongly benefits from the ACS formalism that automatically focusses attention on these regions in the plate. A consistent comparison of the data is, however, difficult since the movement of the control rod is not simulated in the present calculations. In addition, less TUM data has been accessible for this category of results.

The value of the maximum fission density reached locally in the fuel has been published for FRM-II. As it characterizes the total irradiation damage of the fuel, it is therefore an important quantity for an assessment of the performance of the fuel. The TUM and M³O maximum values are both predicted for the same segment of the plate, i.e. at the periphery of the core next to the D₂O moderator, and are in reasonable agreement given the fact that the control rod movement is not modeled in the M³O simulations.

In conclusion, the data calculated by TUM and M³O are in excellent agreement. This is particularly remarkable given the fact that completely different core models and calculational tools have been used in the respective simulations.

8.3 The 1999 Pre-Criticality Conversion Options

Prior to first criticality of the reactor in 2004, and even prior to the start of construction of the facility in 1996, a variety of conversion options for FRM-II had been proposed by several analysts and institutes. This section focuses upon the most important of those options, which were introduced in 1999, and envisioned both increased power levels of the reactor as well as geometrical changes of the FRM-II fuel element. Results obtained for core options are discussed to the extent to which they are still relevant to the ongoing analysis of FRM-II conversion. More importantly, results obtained with M^3O are compared to those published by Argonne National Laboratory as a second independent verification of the computational system and of the core models used in this thesis.

8.3.1 Characteristics of the 1999 options

Alternative LEU designs were first outlined by Argonne National Laboratory (ANL) as early as 1991 [Mo, 1991].²⁸ In 1995 and 1996, more specific and detailed calculations on the use of LEU in FRM-II were presented. These options maintained the cycle length and the maximum thermal neutron flux of the original design, while the reactor power would have been increased to 30–33 MW [Mo et al., 1995], [Hanan et al., 1996]. These earlier concepts, which were mainly developed before construction of FRM-II had started, are not discussed further in the remainder of this section.

Renewed interest in conversion of FRM-II emerged when a new German Federal Government was elected in 1998. Again, ANL provided the essential input for possible conversion strategies taking into account the advanced construction level at that time. Among proponents and critics of the HEU design however, there was strong disagreement on the scientific impact of FRM-II conversion at that time. Therefore, in order to support the decision-making process, independent computer simulations have been performed within the context of this thesis that provide additional detailed information on the scientific usability of the converted reactor.

The 1999 conversion options were first introduced during the negotiations of an expert commission that was established by the Federal Ministry of Education and Research (BMBF). These options constitute the technical basis of the final report issued by the commission [BMBF, 1999], in which three basic conversion strategies were considered.

²⁸As discussed in Chapter 9, the main scope of [Mo, 1991] is the application of the linear programming technique to optimize high-flux reactor performance in general. Design data of FRM-II is used to demonstrate the adequacy of the method and to identify an optimum LEU design of the reactor. Depending upon the imposed set of constraints, power levels between 35 MW and 53 MW were identified as maximizing the thermal neutron flux if LEU fuel at 4.8 g(U)/cc is used in the reactor.

- BMBF option 1: Increase of the thermal power of the reactor from 20 MW to 32 MW. Based on a larger fuel element and on standard uranium-silicide LEU fuel, this measure would have delivered the same thermal neutron flux and cycle length as the original HEU design. Option 1 was discarded by the commission at an early stage because it would have required major modifications of the facility and, as was argued, therefore entailed unacceptable costs and delays.²⁹
- BMBF option 2: Conversion of the reactor prior to completion. While maintaining the 20 MW power level and the original cycle length, option 2 would have implied the use of a fuel element with an increased outer radius and, hence, re-configuration and partial modification of the components in the moderator tank. Two different fuel options were considered (variants 2a and 2b, cf. Table 8.10 for details). In both cases, at a later date, the uranium-silicide fuel would have been replaced by an LEU uranium-molybdenum fuel without the need for further modifications of the reactor.
- BMBF option 3: Conversion of the reactor after completion. Option 3 envisioned start-up of the facility without modifications based on the original HEU design and delayed enrichment reduction of the fuel to a future date when new fuel-types with higher uranium densities are available. Again, two different strategies were discussed: conversion to LEU fuel using an enlarged fuel element, which would entail modification of the activated reactor (variant 3a, equivalent to the second step of variants 2a and 2b) or conversion to fuel enriched to 40–70%, which would not require any reactor modifications (variant 3b, cf. Table 8.10).³⁰

As indicated, all conversion options with the exception of variant 3b, which had been introduced by TUM, are based on fuel elements with an increased outer diameter to accommodate the uranium-235 inventory for an adequate cycle length. Figure 8.20 juxtaposes the TUM and ANL designs. Modifications of the moderator tank are inevitable and, in particular, the central channel tube has to be replaced for the 1999 ANL options. Nonetheless, re-orientation of the beam tubes and displacement of the cold neutron source were not foreseen. Additional data for the core proposed by ANL is summarized in Table 8.11 and can be compared with the design data of the original HEU design listed in Table 8.1.

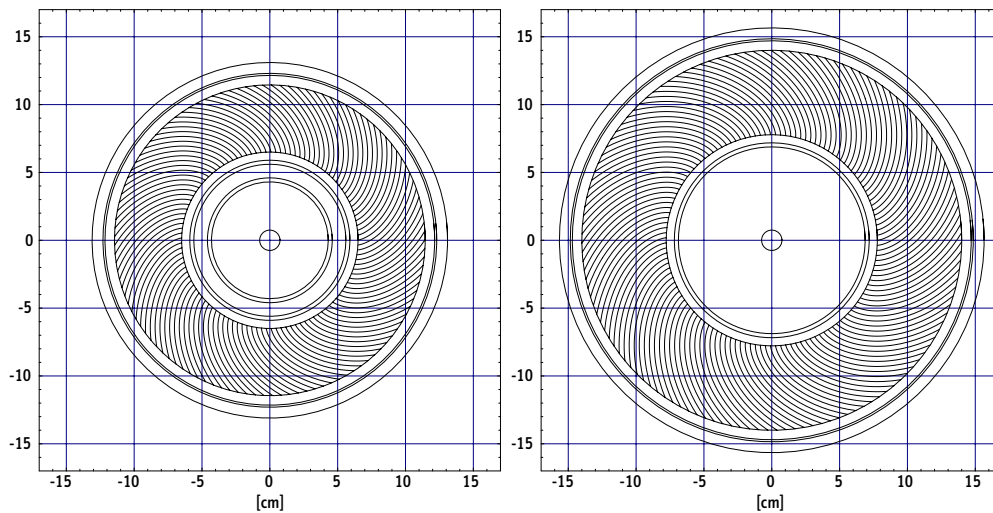
Extensive MCNP calculations have been performed for the 1999 ANL conversion options in the framework of this thesis. These calculations are based on detailed three-dimensional models of the alternative cores (TUM and ANL) using the standard *Mathematica* modules. The most important results of these calculations are presented and discussed below.

²⁹As mentioned above, this conversion strategy had already been published by ANL in 1995.

³⁰Variant 3b was eventually endorsed in the agreement between the German Federal Government and the State of Bavaria from October 2001 [BMBF, 2001].

		BMBF 2a	BMBF 2b	BMBF 3a	BMBF 3b
Start ($\geq 2002-04$)	Fuel-type Enrichment Uranium density	U_3Si_2 24-26 wt% 4.8 g/cm ³	U_3Si 19.75 wt% 6.2 g/cm ³	No action !	No action !
Goal ($\geq 2006-10$)	Fuel-type Enrichment Uranium density	UMo 19.75 wt% 7-9 g/cm ³			UMo 40-70 wt% max. 8.0 g/cm ³

Table 8.10: Data for FRM-II BMBF conversion strategies as introduced in 1999.

Figure 8.20: Geometry of the two alternative fuel elements for the FRM-II including the central control rod. HEU design (left) and LEU design as proposed by ANL in 1999 (right). Transverse section at $z = 0$. The active height is 70 cm for both designs.

Radii of cylindrical shells:		
Inner radius of hafnium-shell:	63,8 mm	(71,8 mm – 8,0 mm)
Inner radius of beryllium-canning:	66,8 mm	(71,8 mm – 5,0 mm)
Maximum radius of follower:	68,8 mm	(71,8 mm – 3,0 mm)
Minimum inner radius of FE:	71,8 mm	(80,3 mm – 8,5 mm)
Outer radius of inner core-tube:	77,8 mm	(80,3 mm – 2,5 mm)
Min. inner radius of active zone:	80,3 mm	(160,6 mm / 2)
Maximum outer radius of active zone:	137,5 mm	(275,0 mm / 2)
Inner radius of outer core-tube:	140,0 mm	(137,5 mm + 2,5 mm)
Maximum outer radius of FE:	147,0 mm	(140,0 mm + 7,0 mm)
Inner radius of ZKR:	148,5 mm	(147,0 mm + 1,5 mm)
Outer radius of ZKR:	156,5 mm	(148,5 mm + 8,0 mm)

Dimensions of fuel plate:		
Thickness of fuel meat:	0,76 mm	
Thickness of cladding:	0,38 mm	
Thickness of cooling channel:	2,20 mm	
Arc-length of active zone of plate:	80,93 mm	(@ 130 plates)
Arc-length of plate (inner to outer tube):	88,01 mm	(@ 130 plates)
Total height of fuel plate:	720,0 mm	
Height of active zone:	700,0 mm	

Table 8.11: FRM-II design data of 1999 ANL options.

8.3.2 Summary of results and comparison with ANL data

The most important results obtained for the different conversion variants have been previously published in [Glaser, 2002b] and are listed in Table 8.12 at the end of this section. All calculations performed for the 1999 ANL options are focused upon BOL characteristics of the core. ANL performed additional burnup calculations and thermal-hydraulic analyses confirming the overall feasibility of conversion based on these models.³¹

While the results for the different LEU options are very similar to each other, variant 2a is presumably the most attractive of the 1999 BMBF conversion options and is discussed below as an example.³²

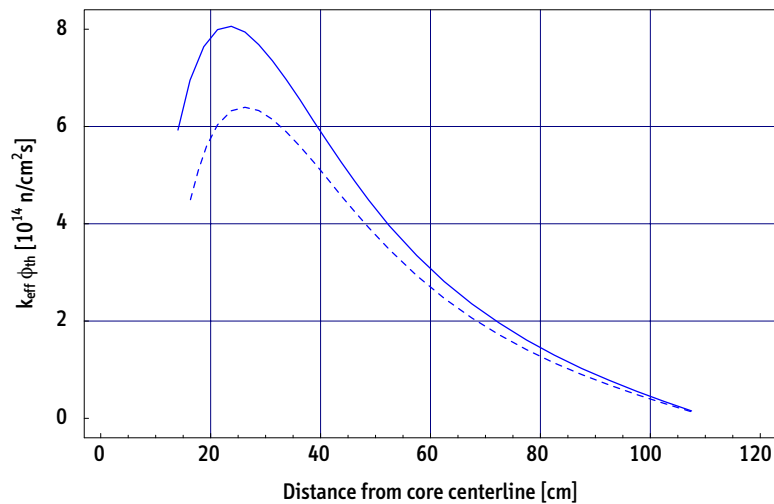


Figure 8.21: Radial distribution of thermal neutron flux for the HEU design (—) and for the conversion variant 2a (- -). The maximum value of the conversion variant reaches 79%, the thermal neutron flux at $r = 40$ cm reaches 87% of the HEU reference value.

The radial distribution of the thermal neutron flux for the unperturbed situation,

³¹See in particular [Hanan et al., 1999]. This reference also lists additional design information on the 1999 ANL options, some of which are discussed here.

³²The remaining strategies (2b, 3a, and 3b) each suffer from a serious disadvantage: variant 2b is based on U_3Si fuel which is characterized by an inferior irradiation behavior. Although this fuel is supposed to behave well under FRM-II conditions, additional licensing procedures to qualify the fuel would probably have been necessary. Therefore, the attractiveness of conversion option 2b is significantly reduced compared to option 2a, which uses standard U_3Si_2 fuel. Variant 3a requires modification of the activated reactor, and thus can be considered an extremely unrealistic option. Variant 3b relies on fuel clearly beyond the LEU limit and barely offers an advantage from the perspective of nonproliferation. Nonetheless, it is BMBF option 3b that is currently being pursued.

i.e. without additional experimental components in the moderator tank, is shown in Figure 8.21. The maximum value of conversion variant 2a reaches 79% of the HEU reference value. This peak value, however, appears close to the core where no neutrons are extracted for experiments and is therefore of little value when assessing the scientific usability of the reactor. A more relevant number is the neutron flux at the position of the cold neutron source at $r \approx 40$ cm. The reduction in the thermal neutron flux is less pronounced at this distance of the core: it reaches 87% of the HEU reference value.

As outlined in Section 8.1.5, the most important experimental components have also been modeled in more complex simulations (cf. Figure 8.6). In particular, the cold neutron source and the beam tubes are considered, in order to determine the gamma and neutron heating of the cold source as well as the neutron spectrum in the beam tubes at greater distances from the core. Note that, due to the limited availability of information on the design of the cold neutron source, precise estimates of the absolute values of the neutron and gamma heating may not represent actual values. However, a relative comparison of the heat deposited in the cold neutron source under equal simulation conditions provides a good assessment of the general situation.

During the discussions that took place in 1999, there was strong disagreement upon the question of whether the larger fuel element proposed by ANL would lead to increased heating of the cold source, which would in turn lead to unsurmountable cooling problems. This effect was not confirmed by the simulations which, in fact, support the results published by ANL. In the case of the variants 2a and 2b, the heat deposited in the cold neutron source increases by less than 1%, and in all other cases heat deposition decreases (see Table 8.12).³³

The neutron spectrum in beam tube #1, which by itself will be responsible for more than 40% of the scientific usability of the facility,³⁴ is shown in Figure 8.22. The maximum value of the cold neutron flux is reduced by slightly less than 10% compared to the original HEU design. The fast neutron flux, which is considered an undesired background signal, increases (between 1 eV and 10 MeV) by 17% on average. The relevance of this additional background is assessed in Sections 3 and 11.

The data obtained with M³O for the 1999 ANL options can be compared to the data published by ANL at the time. ANL studied a broad spectrum of possible strategies to convert FRM-II to low-enriched fuel, and published only the most important results on their respective performance. ANL's focus was to demonstrate the availability of options, not to single out and recommend one specific design.

³³A more recent publication by TUM suggests that the controversy regarding a possible increase in the heating of the cold neutron source may have been overemphasized. Apparently, it's possible to achieve significant additional cooling if required: "The refrigerator [...] can be upgraded [from 5 kW] to 8 kW refrigeration power by adding an extra compressor and further expansion turbines, in case of additional needs of refrigeration near the core (e.g. for a second CNS)" [Gutsmiedl and Gobrecht, 2001].

³⁴According to [Böning et al., 1999], the utilization factor of beam tube #1 will be 42.5%.

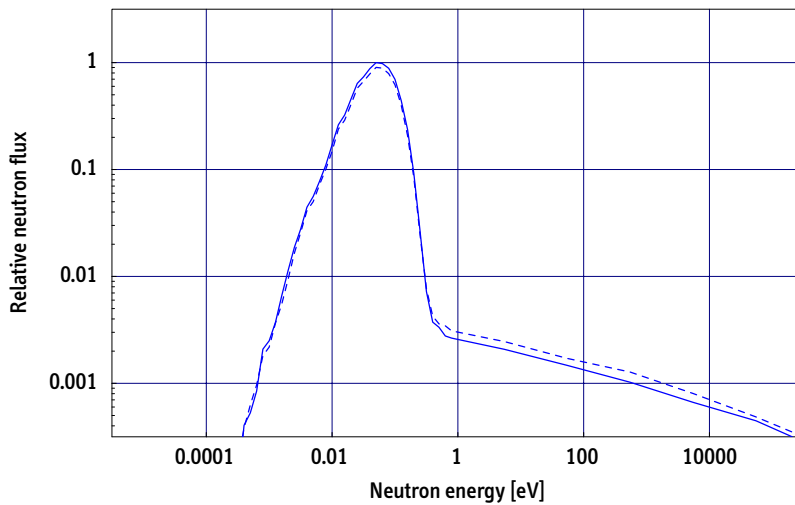


Figure 8.22: Neutron spectrum in beam tube #1 coupled to the simplified model of the cold neutron source. Position in the tube: $x = -70$ cm, axis as defined in Figure 8.6. Standard HEU design (—) and variant 2a (- -). Relative maximum value of LEU design: 90.7% of HEU value.

MCNP 4B/C calculations, 40 million neutron histories for each spectrum

Table 8.13 lists ANL and M³O results for the BMBF options 2A, 2B, and 3A with the ANL numbers taken from [Hanan et al., 1999, Table 2]. Note that the ANL models are very similar but not identical to the BMBF options, as some of them slightly differ in fuel enrichment and effective uranium density. Also, the respective models of the cold neutron source (CNS) differ because of the limited information that was available on the actual design of the device.³⁵ Only the numbers for the maximum neutron flux, the neutron flux at the position of the CNS, and the gamma and neutron heating of the CNS could be compared. All data are in good agreement, with some deviations in the heating data, which is however still negligible given the uncertainties in the models used for both the ANL and M³O simulations.

With start-up of FRM-II in March 2004, the 1999 conversion options based on a fuel element with larger outer dimensions became much less attractive — and their implementation much less likely. Nevertheless, the results presented above provide some insight that may still be relevant for future analyses required for FRM-II conversion.

- As the outer radius of the fuel element increases, the position of the peak thermal neutron flux simultaneously shifts towards larger radii. As the cold neutron source (CNS) is currently not centered around the peak value, but at a larger

³⁵See Section 8.1.5 for the simplified models of the CNS used here.

distance, increasing the outer diameter of the fuel element is beneficial to reactor performance if no other modifications are required.³⁶

- Even though the boundary of the LEU core is closer to the CNS, gamma and neutron heating of the device does not increase as might be initially expected. This is due to the substantially larger uranium inventory in the core, i.e. 30–50 kg versus 8.1 kg, which results in a more important spatial self-shielding of radiation stemming from the center of the core. In general, the higher relative importance of self-shielding in LEU fuel has to be taken into account for an overall assessment for each fuel option with reduced enrichment.
- The fast neutron flux or background in the main beam tube, as obtained in the MCNP calculations, increases if the outer radius of the fuel element moves closer to the CNS. This is due to both the proximity and the increased relative angle between the core boundary and the beam tube (line-of-sight).

The main drawback of the 1999 pre-criticality conversion options, independently from the reactor's operational status today and the prospects of their actual realization, are twofold. Most importantly, problems have surfaced since then regarding the irradiation performance for UMo-dispersion-type fuels, which are the basis for all BMBF options. Recent experiments revealed a poor irradiation behavior of these fuels at high burnup and operating temperature, which may preclude their use in FRM-II altogether (see discussion in Section 4.3). Furthermore, it is unclear to what extent the 1999 LEU options were re-optimized for LEU-use. Such an approach would be required to guarantee optimum performance of the converted reactor, as the neutron spectrum hardens significantly with the substantial increase of heavy metal inventory in the core.

The conversion options studied in the remainder of this thesis are therefore exclusively focussed upon an alternative fuel, which was discovered in 2002 and which achieves extraordinary effective uranium densities (monolithic fuel, 16 g(U)/cm³). In order to benefit from this new opportunity, an optimization tool is developed in the following chapter that can be used to re-optimize single element reactor cores that were originally designed for LEU.

³⁶Conversely, if the outer radius of the core should be reduced, which might be a theoretical option with monolithic fuels (Section 10.5), the maximum neutron flux moves further away from the CNS. This effect needs to be considered in a detailed analysis.

	HEU	BMBF 2a (Start)	BMBF 2b (Start)	BMBF 2 (Goal)	
Fuel-type Enrichment Uranium density	U ₃ Si ₂ ca. 93 3.0/1.5	U ₃ Si ₂ 26.00 4.8	U ₃ Si 19.75 6.2	UMo(6wt%) 19.75 7.1	[wt%] [g/cm ³]
<u>Unperturbed case</u>					
$\phi_{th,max}$ $\phi_{th,cns}$	8.06 5.69	6.40 (79.3%) 4.93 (86.6%)	6.44 (79.9%) 4.95 (87.0%)	6.27 (77.8%) 4.81 (84.6%)	[10 ¹⁴ n/(cm ² s)] [10 ¹⁴ n/(cm ² s)]
<u>Perturbed case</u>					
Relative heating of CNS	100.0%	100.8%	100.8%	98.7%	

	HEU (Start)	BMBF 3a (Goal)	BMBF 3b (Goal)		
Fuel-type Enrichment Uranium density	U ₃ Si ₂ ca. 93 3.0/1.5	UMo(6wt%) 19.75 7.1	UMo(6wt%) 50.00 8.0/4.0		[wt%] [g/cm ³]
<u>Unperturbed case</u>					
$\phi_{th,max}$ $\phi_{th,cns}$	8.06 5.69	6.27 (77.8%) 4.81 (84.6%)	7.63 (94.6%) 5.45 (95.9%)		[10 ¹⁴ n/(cm ² s)] [10 ¹⁴ n/(cm ² s)]
<u>Perturbed case</u>					
Relative heating of CNS	100.0%	98.7%	95.1%		

Table 8.12: Results of the calculations for the FRM-II conversion options BMBF2 and BMBF3. Quantities for the unperturbed case: maximum thermal neutron flux $\phi_{th,max}$ and thermal neutron flux at position of cold neutron source $\phi_{th,cns}$. Relative heating of the cold neutron source for the perturbed case with main experimental components in the moderator tank modeled. Values given in percent are relative to the standard HEU design (100%).

		Enrichment	Density	$\phi_{th,max}$	$\phi_{th,cns}$	CNS heating
BMBF 2A	ANL	24 wt%	4.8 g/cc	0.80	0.86	unavailable
	M3O	26 wt%	4.8 g/cc	0.79	0.87	1.01
BMBF 2B	ANL	19.75 wt%	6.2 g/cc	0.79	0.85	0.97
	M3O	19.75 wt%	6.2 g/cc	0.80	0.87	1.01
BMBF 3A	ANL	19.75 wt%	6.6 g/cc	0.77	0.84	0.95
	M3O	19.75 wt%	7.1 g/cc	0.78	0.85	0.99

Table 8.13: Comparison of main results obtained by ANL and M3O for thr 1999 pre-criticality options as defined by BMBF. ANL data from [Hanan et al., 1999, Table 2] for those models that are most similar, but not identical, to the BMBF options.

This page intentionally blank

Chapter 9

Optimization of Single Element Reactor Performance Using the Linear Programming Technique

The determination of adequate core parameters for a research reactor is a complex optimization process that depends upon a large number of design variables and conflicting constraints. As [Lake et al., 1986] underscore, “[t]here are innumerable trade-offs that arise, for example, between optimum neutronic and optimum thermal-hydraulic performance. The best design is one which arrives at the optimum reactor *system* performance” (p. 45, emphasis in the original). It should therefore be re-emphasized that neutronics calculations, which are the primary focus of this thesis, are only one (important) aspect among a few others that are relevant in the design of a research reactor and in the process of demonstrating its safe operation. For reference purposes, such an extended set of design constraints and trade-offs is listed in Table 9.1.¹

Nonetheless, the strong focus on reactor neutronics in the optimization process below is justified by a series of considerations. Most importantly, in the present context of reactor conversion, a base design using HEU fuel is already available. For this specific design, the thermal-hydraulics have been found to be satisfying and, more generally, the system performance can be assumed to be at or close to its optimum value. The methodology used for a re-optimization of the reactor for use with LEU employs the original base design as a starting point and evaluates the impact of perturbations on this model. In general, small modifications will be sufficient to re-identify the optimum performance of the core using fuel with reduced enrichment. Furthermore, allowed

¹Thermal-hydraulics of high-flux research reactors, and aspects that are related to them, are discussed in Gambill [1986] and include analyses of coolant, cladding, and fuel temperatures, fuel plate deflection, vibration, and erosion, critical flow velocities, cladding corrosion and oxide formation, as well as nucleate incipient boiling and critical heat flux issues.

modifications to the original design can be conservatively constrained such that their impact on thermal-hydraulics are expected to be small or even favorable.²

A methodology to optimize the neutronics performance of single element reactor performance based on the so-called *Linear Programming* technique is devised in Sections 9.2 and 9.3 and applied to the FRM-II in Chapter 10. To re-iterate the significance of the main optimization criterion represented by the maximum thermal neutron flux and to elucidate the design rationale of MTR-type and single element reactors, a general discussion on reactor design is pre-pended.

Issue	Requirement	Selected controlling parameters
Neutron flux	maximize ϕ_{th} , user friendly environment, large accessible volume	core geometry; fuel-type (density, enrichment, etc.); coolant, moderator, and reflector type; power level and density
Cycle length	high, $k_{eff} \geq 1.0$ at EOL, maximize availability of facility	power level; core volume; fuel-type (density, enrichment); fuel to moderator ratio; degree of in-core moderation; reflector material; control capability
Fuel burnup and integrity	margin to failure limits, minimize fuel cycle costs	fuel-type (density, volume fraction); swelling characteristics; peak power density; oxide layer buildup
Heat transfer	maintain safety margins	surface heat flux; hydraulic instability; margin to critical heat flux (CHF); oxide layer formation; heat transfer characteristics; power density and peaking factors; fuel plate and coolant channel dimensions and tolerances
Structural stability	margin to structural limits	plate thickness and width; material strength; thermal stress; coolant pressure; flow rate
Reactor power	minimize	power density required to achieve objective neutron flux; minimum core volume
Fuel cycle costs	minimize	core lifetime (cycle length); burnup; complexity of fuel and fuel element fabrication

Table 9.1: Design constraints and trade-offs. Table adapted from [Lake et al., 1986].

²For instance, the minimum plate thickness or the minimum coolant channel width can be set at their respective original values to guarantee mechanical stability of the plate and to provide some confidence that cooling requirements and safety margins can be met. It goes without saying that the thermal-hydraulics of the modified core still have to be verified in a separate analysis.

9.1 General Aspects of Research Reactor Design

Before turning to the specific optimization approach developed and used in the framework of this thesis, general aspects of research reactor design are briefly summarized below. Basic design principles of the original MTR as well as the specific requirements of high-flux reactors operated in the so-called inverse flux-trap mode are outlined. The primary focus of the discussion is on reactor neutronics. Additional design criteria, which include a variety of thermal-hydraulical, mechanical, economical, and other considerations, are only listed briefly at the end of this section.

9.1.1 Design principles of the original MTR

The original *Material Testing Reactor* (MTR) was designed and built collaboratively by the Oak Ridge and Argonne National Laboratories (ORNL and ANL) and operated from 1952–1970 on the site of the Idaho National Engineering Laboratory (INEL). The basic design principles of this reactor were discussed in great detail by Weinberg et al. [1955] in a paper presented at the *First Atoms for Peace Conference* held in August 1955 in Geneva. The authors emphasize that the main objective of the design was to achieve as high fast *and* thermal neutron fluxes as possible, which are roughly characterized as follows.

$$P \sim \rho \sigma_f \phi_{\text{th}} V \quad \text{or} \quad \phi_{\text{th}} \sim \frac{P}{\rho V} = \frac{P}{M} \quad \text{and} \quad \phi_{\text{fast}} \sim \lambda \frac{P}{V} \quad (9.1)$$

These simple expressions illustrate that the thermal neutron flux ϕ_{th} in a nuclear system scales with P/M , where P is the power released via induced fission processes and M the total uranium-235 inventory in the system. In contrast, the fast neutron flux ϕ_{fast} directly originates from fission events and is therefore given by the number of neutrons released per unit volume, which is proportional to P/V , multiplied by the mean free path λ of fast neutrons in the medium. As a result, specific powers in both volume *and* fuel have to be maximized to achieve the original MTR design objectives. Weinberg et al. identify a set of further corollaries that result from these considerations or are related to additional premises.

- In order to maximize the P/M -ratio and the thermal neutron flux, it is necessary to provide as much heat transfer area to the uranium fuel as possible. An obvious geometry that maximizes fuel surface area to fuel volume is the plate-type design, in which the uranium fuel is embedded in thin parallel aluminum plates separated by cooling channels. This design concept increases the heat transfer area by an order of magnitude compared to previous (pin-type) reactor designs and is the

primary reason for a corresponding increase in the thermal neutron flux of MTR-type reactors.

- From early on, highly enriched fuel was available for use in research reactors built and operated in the U.S.³ Due to this particular circumstance, MTR-type fuel could be designed for low U-235 densities (less than 1 g/cc), while still accommodating sufficient uranium in the core. The dilution of the fuel in a matrix material is also consistent with the particularities of plate fabrication and guided the development of dispersion-type fuels discussed in Chapter 4.
- Combinations of light and heavy water were originally considered as potential standard coolant and moderator materials for the MTR. To a first approximation, both materials would yield the same ϕ_{th} . However, due to the longer diffusion length of neutrons in heavy water, the core volume increases in the presence of D₂O, which in turn reduces ϕ_{fast} . H₂O was therefore chosen as coolant and moderator for the original MTR design.
- The compact core size is *a priori* considered a disadvantage from the user's perspective because little in-core volume is available for experiments.⁴ Weinberg et al. emphasize however that the high multiplication factor of the MTR generates a significant neutron flux in the volume surrounding the core lattice. Experiments can therefore be carried out in the reflector volume outside the reactor core. Note that this consideration already points towards the concept of neutron beam research, which dominates scientific uses of research reactors today.

The preceding historic discussion illustrates most of the design imperatives that are still the basis for the design of research reactors today. Accordingly, modern (Western) research facilities are largely based on plate-type fuel and generally use the most compact core size that can be operated safely. In contrast, the choice and combination of coolant and moderator materials depend upon the specific design concept and primary applications of the facility. As will be discussed below, in the case of high-flux reactors optimized for neutron beam research, the use of heavy water as moderator and/or coolant is a more attractive option than previously assessed by the designers of the original MTR.

³In the last section of their contribution, Weinberg et al. [1955] briefly address the possibility of using 20%-enriched fuel instead of HEU, on which their experience and discussion is solely based. In disregarding some of the problems the RERTR program would encounter more than twenty years later, the authors conclude that there should be "little difference between the 20% enriched elements and the fully enriched elements" (p. 418). On the definition of LEU, see also Footnote 6 on Page 28.

⁴Previous research reactor designs, such as the NRX in Canada, were based on natural uranium and heavy-water-moderated. The cores of these facilities are relatively large compared to those of the MTR-type.

9.1.2 Reactors for neutron beam research

High-flux reactors are characterized by a relatively high power level, typically between 20–100 MW, and a high surface-to-volume ratio of the core, which maximizes neutron leakage into the reflector region. The maximum thermal neutron flux in facilities operated in the inverse flux-trap mode is obtained *outside* the core, where beam tubes are used to extract the neutrons and guide them to the experiments. For such a configuration, there are at least two reasons to reconsider the use of D₂O in the core:

- The fast neutron flux ϕ_{fast} is no longer the primary design objective for research facilities designed for neutron beam research, where thermal and even cold neutrons are desirable (Chapter 3). This aspect partially neutralizes the original preference of H₂O over D₂O. If fast neutrons are needed for a specific experiment, they are usually re-generated in a fission converter exposed to the thermal neutron flux in the reflector region.
- The larger diffusion length of neutrons in heavy water favors the leakage of the neutrons from the core into the reflector region. Furthermore, the maximum ϕ_{th} is reached at a greater distance from the core surface compared to H₂O and facilitates the positioning of experimental devices and beam tubes.

In concordance with these considerations, a number of high-flux reactors are indeed D₂O-moderated or even D₂O-cooled (see Table 7.1 for examples). The maximum thermal neutron flux that is obtained for such a situation, has been characterized as follows [Difilippo et al., 1986, p. 58].⁵

$$\phi_{\text{th}} \sim \frac{P}{A} \sim \frac{P}{V^{2/3}} = P^{1/3} (P/V)^{2/3} = \sqrt[3]{P \bar{\rho}^2} \quad (9.2)$$

According to this simple expression, the thermal neutron flux scales with the number of neutrons released in the fuel, i.e. with the total power level P , and is inversely proportional to the core surface area A , which these neutrons must traverse. For an idealized geometry, in which $A^3 \sim V^2$ (sphere), equation (9.2) can be rearranged to show that the average power density $\bar{\rho}$ in the core is the most important performance characteristic of a high-flux reactor and that a maximum value of $\bar{\rho}$ is even more desirable than an increased power level of the facility itself.

It should be noted, however, that the underlying assumptions in (9.2) are highly simplifying and that, in practice, the benefits of a smaller surface area A and increased power

⁵Gläser [2001] compares the performance of various research reactors using the same expression. For an in-depth discussion of the P/A -approximation, see [Difilippo, 1991, Section 9].

density $\bar{\rho}$ are much less pronounced than suggested by the preceding expression.⁶ To demonstrate this effect, MCNP calculations have been performed for various uranium spheres immersed in heavy water, each set characterized by a fixed U-235 inventory, while volume and density of the material in the sphere are varied correspondingly. Two different situations are considered: first, a set of pure uranium spheres (fast neutron spectrum) and, second, a set of U-235/H₂O-spheres with H/HM ratios that are typical for MTR-type cores.⁷

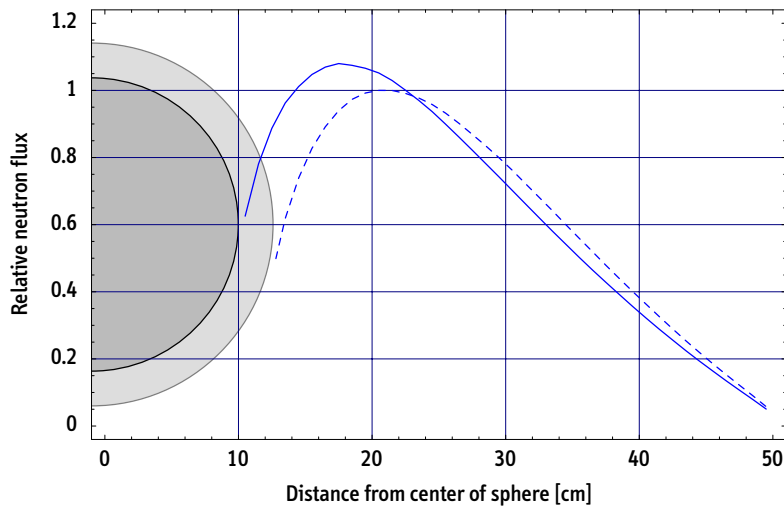


Figure 9.1: Relative neutron flux levels outside two U-235/H₂O-spheres immersed in a larger sphere of heavy water (\varnothing 100 cm). Both spheres have identical uranium inventories and are characterized by the same power level. Material densities are 1.0 g/cc uranium and 1.0 g/cc H₂O in the sphere with $R = 10.0$ cm and volume V_0 (—); respective material densities are corrected by a factor of 0.5 in the sphere with $R = 12.6$ cm and volume $2V_0$ (- -). The P/A -ratio of the smaller sphere is $\sqrt[3]{4} \approx 1.59$, but the maximum neutron flux increases by 8% only. MCNPX calculations at 300 K.

Figure 9.1 and Table 9.2 summarize the main results of these simulations. As expected, the data shows that the out-of-core thermal neutron flux does indeed increase as the P/A -ratio is raised, i.e. as the surface area is reduced and the power density increased. The effect is, however, much smaller than predicted by expression (9.2). In particular for the case of H₂O-diluted uranium, the benefit of reduced core size is moderate, with a thermal flux increase of 8% only, in contrast to the 59% suggested by the increased P/A -ratio of the smaller sphere. Even though a compact core design is therefore favorable to the performance of a research reactor, the gains are much less pronounced than generally assumed based on simple considerations.

⁶Difilippo [1991] acknowledges this fact for very small active core volumes (p. 95).

⁷Of course, the situation gets even more complex once U-238 is also included in the model.

	Pure Uranium at 10 g/cc (no H ₂ O)		Diluted uranium at 1 g/cc (1 g/cc H ₂ O)	
Radius	10.0 cm	12.6 cm	10.0 cm	12.6 cm
Density	10.0 g/cm ³	5.0 g/cm ³	1.0 g/cm ³	0.5 g/cm ³
Volume	4189 cm ³	8378 cm ³	4189 cm ³	8378 cm ³
Mass	41.9 kg	41.9 kg	4.2 kg	4.2 kg
Surface	1257 cm ²	1995 cm ²	1257 cm ²	1995 cm ²
k(eff)	1.181 ± 0.001	1.080 ± 0.001	1.147 ± 0.001	1.027 ± 0.001
⟨σ _f ⟩	1.9 b	2.5 b	18.5 b	21.7 b
ϕ _{th} ratio	1.19		1.08	
P/A ratio	1.59		1.59	

Table 9.2: Relative neutron flux and its P/A-dependency for U-235/H₂O-spheres immersed in heavy water. MCNPX calculations at 300 K. See caption of Figure 9.1 for additional details.

MCNP input decks: cc1, cc2, cc1b, and cc2b

More sophisticated analytical approaches have been suggested to describe the expected performance of modern high-flux reactors as a function of a few global parameters [Difilippo, 1991]. Due to the complexity of the problem, these discussions are typically restricted to spherically idealized problems. Approximated solutions of the radial flux profile can be obtained with significant, but manageable, effort starting from the basic integral equation for the thermal neutron flux.

$$\phi_{\text{th}}(r) = \int_0^{\infty} K(r, r') 4\pi r'^2 S(r') dr'$$

Here, $K(r, r')$ is the kernel that corresponds to a spherical shell source located at point r' and $S(r')$ is the slowing down density, which quantifies the number of neutrons moderated into thermal energies per unit volume and time. Using two-region diffusion kernels and making a variety of additional simplifying assumptions for both $K(r, r')$ and $S(r')$, Difilippo [1991] derives expressions for the maximum thermal neutron flux obtained outside the core in the moderator region. Some general findings of this analysis include:

- The performance of the neutron source can be parameterized in terms of 2×4 parameters for the core and reflector region. These are the volume, the Fermi-age of the neutrons, the thermal diffusion length, and the diffusion constant in the

respective regions. Only high-purity beryllium or D_2O are adequate materials for the reflector region, which fixes the corresponding parameters and leaves the four variables characterizing the core region.

- The performance increases monotonically with reduced core volume and with increasing neutron Fermi-age and diffusion length, which is equivalent to minimum neutron moderation and absorption in the core. Accordingly, heavy-water-cooled compact cores characterized by short cycle lengths and fueled with highly enriched uranium are preferable for optimum neutronics design of intense neutron sources based on the fission process.⁸

Exploring issues similar to the analysis performed by Difilippo, many other analysts have addressed the possibility of identifying new optimum research reactor designs, while benefitting from advanced technologies and materials developed since the 1970s, i.e. after most of today's high-flux facilities were designed and built. There is a general consensus that the current research reactor design has reached an upper limit inherent to the technology. Neutron sources with flux levels much higher than currently achievable, "will probably not come about as a simple extrapolation of the current technology. Rather, innovative use of core geometries and materials, creative cooling techniques, and perhaps revolutionary core concepts may need to be brought to bear on the problem" [Lake et al., 1986, p. 41]. Designs that have been suggested in this context include vertically split cores known as the 'double donut configuration' [Lake et al., 1986], high-flux particle bed reactors [Powell et al., 1986], or cores set-up by a series of intersecting rotating rings [Olson, 1986].⁹

Two important conclusions can be drawn from the preceding discussion:

- A compact core operated in the inverse flux-trap mode represents the optimum design concept for neutron beam research based on proven MTR-type technology using water-cooled plate-type fuel. This follows both from theoretical analyses as well as from the experience that has been accumulated in operating the fleet of high-flux reactors in existence today.
- Even though radically different reactor concepts and fuel geometries might theoretically offer improved performance of research reactors, for practical purposes,

⁸The analysis of Difilippo [1991] also includes spallation sources, which are generally found to be superior to high-flux fission reactors in terms of the neutronics efficiency. The author emphasizes, however, that other aspects, which include capital and operating costs, favor "more or less conventional fission sources" (p. 96). Similarly, the conclusion that a short core life, and in the extreme case the daily refueled reactor, represents a credible reactor design that can be operated reliably and cost-effectively, has to be interpreted with great caution.

⁹These are designs that were discussed in the context of the planning process of the U.S. Advanced Neutron Source project, which was ultimately canceled in 1995.

reactor designers involved in concrete R&D projects ultimately prefer employing and re-optimizing existing technological concepts. It is very likely that future intense-flux neutron sources will be based on the spallation process rather than on radically different and unproven fission reactor concepts.

The optimization methodology laid out in the following section therefore confines itself to the re-optimization of proven single element reactor geometries. This approach is particularly useful in the context of reactor conversion, where an initial HEU design is given and has to be replaced by an LEU design without major modifications to core and fuel geometries. Optimum LEU fuel options are then developed as perturbation to the original core parameters. This method can be considered a very powerful approach under these circumstances because all reactor design details, which are difficult or impossible to address analytically, are easily represented in the MCNP-models and may include detailed material composition as well as complex geometrical configurations of the core and the fuel.

9.2 Basic Theory of Linear Programming

Assume $\vec{x} = (x_1, \dots, x_n)$ to be a set of independent variables and a_{ij} , b_i , and c_j arbitrary real coefficients. A problem in the form stated below is then called a linear programming (LP) problem in its standard form.¹⁰

$$\text{maximize } \sum_{j=1}^n c_j x_j \quad (9.3)$$

$$\text{subject to } \sum_{j=1}^n a_{ij} x_j \leq b_i \quad (i = 1, 2, \dots, m) \quad (9.4)$$

$$x_j \geq 0 \quad (j = 1, 2, \dots, n)$$

One objective function of the independent variables x_j is maximized, while a set of additional functions of x_j has to be satisfied simultaneously (constraints). Mathematically, this type of problem is addressed with the *linear programming* (LP) technique. Typical LP problems are extremely underdetermined, i.e. there are many more independent variables than there are constraint equations ($n \gg m$). These systems can be

¹⁰Nonstandard forms of an LP problem may require minimization of the objective function and/or be characterized by more general constraint conditions. These nonstandard problems can always be transformed into standard form via redefinition of coefficients and/or variables.

solved very efficiently using the Simplex algorithm [Chvátal, 1983].¹¹ It can be shown that any LP problem belongs to one of three categories: it is either feasible with an optimal solution, is infeasible, or is unbounded, i.e. feasible without an optimum in the objective function. Due to the linearity of all expressions involved, the feasible domain described by the set of constraint conditions (9.4) is a polyhedron and the solution to the problem, if existent, will be confined to one of the edges of this domain.

Practical optimization problems are of course seldom truly linear. In this situation, one obvious approach is to linearize the fundamental equations of the problem in the vicinity of an initial feasible point \vec{x}^0 and to identify a solution in an iterative process [Reklaitis et al., 1983, Chapter 8]. Representatively for the complete set of fundamental functions defined by (9.3) and (9.4), the objective function f would be replaced by a new linear function \tilde{f} .

$$f(\vec{x}) = \underbrace{f(\vec{x}^0) + \nabla f(\vec{x}^0) (\vec{x} - \vec{x}^0)}_{\tilde{f}(\vec{x})} + O(\|\vec{x} - \vec{x}^0\|^2) \quad (9.5)$$

The literature distinguishes the *linearly constrained programming* case and the general *nonlinear programming* (NLP) case, which are briefly introduced and discussed here before turning to the practical implementation of the formalism for research reactor optimization.

For the linearly constrained problem, the objective function f is an arbitrary nonlinear function, while the constraint conditions remain linear as introduced in the original problem. In this case, the optimum solution \vec{x}^* no longer needs to be situated on the edges of the polyhedron defined by the set of constraint conditions. Rather, due to the non-linearity of f , the solution can be located anywhere inside the feasible region. The LP formalism however still remains a powerful tool because it can be used as the basis for an iterative approach. Here, the solution \tilde{x}^* for the linearized function $\tilde{f}(\vec{x})$ serves as a starting point \vec{x}^1 for a subsequent application of the Simplex algorithm, if a pre-defined convergence criterion is not yet met.¹²

Finally, in the general nonlinear programming case, both the constraint conditions *and* the objective function are nonlinear. In this case, the entire set of equations (9.3) and (9.4) has to be linearized in the vicinity of an initial feasible point \vec{x}^0 . While most of the

¹¹Even though the Simplex algorithm is of prime importance for all practical applications of the linear programming technique, it is theoretically unsatisfactory, as LP problems can be constructed for which the algorithm does not converge. In the 1970s, alternative algorithms were identified that provide the mathematical basis of linear programming, but these have not proven to be convenient or relevant in practice [Chvátal, 1983, Chapter 4].

¹²To improve the procedure further, one can also perform a line search between \vec{x}^0 and \tilde{x}^* to identify the maximum of the original $f(\vec{x})$. The coordinates that maximize $f(\vec{x})$ on this interval may be used as an even better starting point for the next iteration step.

aforementioned remains applicable, note that the solution \tilde{x}^* of the linearized problem now may be, and generally even will be, an infeasible point because of the possible non-convexity of the original feasible region. For these reasons, linearization methods have to be used with great caution, and the analyst has to carefully verify the validity of the linearized approximation. Adequate safeguards, such as step-size adjustment, may have to be taken, but even then there is no mathematical assurance that a true optimum is obtained in the process. Techniques to address these peculiarities are discussed in [Reklaitis et al., 1983, Section 8.1.2].

As may be expected for typical situations encountered in practice (sciences, economics, etc.), the simple linearization of a general nonlinear programming problem as introduced here, i.e. even without further ‘embellishments’ and safeguards, proves to be a reliable optimization method as long as all the functions involved are only mildly nonlinear in the independent variables. While the user may still have to control step-sizes between successive applications of the algorithm, the adequacy of the method is substantiated as long as improvements are made in each step of the iteration process, i.e. as long as the value of the objective function increases while a possible initial violation of the constraint conditions gradually disappears. Ultimately, the self-consistency of the approach represents a strong indicator for the applicability of the technique and justifies the simplifying assumptions made.

9.3 Implementation

The optimization of research reactor performance is obviously a nonlinear problem as both the objective function and the constraint conditions are complex functions of the reactor design variables. The linearization of these functions, as outlined in the preceding section, is therefore a prerequisite to apply the LP technique. The use of this method has been suggested and tested previously for research reactor performance optimization [Mo, 1991]. Here, a modified version will be devised that is specifically designed for single element reactor analysis. More specifically, the optimization procedure presented below is oriented towards and designed for an analysis of the FRM-II case, and takes into account its most particular design characteristics. The procedure can be applied with minor modifications to the simpler geometry of the generic single element reactor introduced in Chapter 7, or to any other single element reactor for that matter.

9.3.1 Design variables

The following standard set of independent variables $\vec{x} = (x_1, \dots, x_{11})$ is used in the following to describe the main characteristics of a single element reactor core:

x_1 : Thermal power level	x_7 : Inner core radius
x_2 : Fuel enrichment	x_8 : Outer core radius
x_3 : Effective uranium density	x_9 : Active core height
x_4 : Meat thickness	
x_5 : Cladding thickness	x_{10} : Transition radius
x_6 : Coolant channel width	x_{11} : Density ratio

Depending on the design of the reactor, not all of these variables may be needed. A subset of these design variables may be selected in advance and can therefore be excluded from the optimization process. Furthermore, most if not all design variables will be constrained, in addition to the formal operational constraints introduced later.¹³

9.3.2 Objective function

The maximum thermal neutron flux $\phi(\vec{x})$ is selected as the primary objective function to be maximized. As the functional dependency of $\phi(\vec{x})$ from the design variables is *a priori* unknown, the thermal neutron flux is linearized around an initial point \vec{x}^0 .

$$\phi(\vec{x}) = \phi(\vec{x}^0) + \sum_{i=1}^n \frac{\partial \phi}{\partial x_i} (x_i - x_i^0) \quad (9.6)$$

The partial derivatives of $\phi(\vec{x})$ are estimated in MCNP simulations for small perturbations $(x_j - x_j^0)$ of individual design variables with $\vec{x}^j = (x_1^0, x_2^0, \dots, x_j, \dots, x_n^0)$.

$$\left. \frac{\partial \phi}{\partial x_j} \right|_{\vec{x}=\vec{x}^0} \approx \frac{\phi(\vec{x}^j) - \phi(\vec{x}^0)}{x_j - x_j^0} \quad \text{with } \phi(\vec{x}^j), \phi(\vec{x}^0) \text{ from MCNP} \quad (9.7)$$

9.3.3 Constraints

The objective function $\phi(x_1, \dots, x_n)$ is maximized subject to a set of constraints, which may be formulated as follows. Note that this set of constraints (C_1, \dots, C_4) is a representative one and can be modified or extended as needed.

¹³For instance, a minimum cladding thickness will have to be provided by the analyst. Design variables may also be related otherwise. As an example, a minimum plate thickness $(x_4 + 2x_5)$ may be required to guarantee thermal-hydraulic stability. These additional conditions are added to the set of equations upon solution of the system.

$$\begin{array}{ll}
\text{Cycle length:} & C_1(x_1, \dots, x_n) \geq T_{\text{cyc}} \\
\text{Average power density:} & C_2(x_1, \dots, x_n) \leq p_{\text{ave}} \\
\text{Average heat flux:} & C_3(x_1, \dots, x_n) \leq \eta_{\text{ave}} \\
\text{Power peaking factor:} & C_4(x_1, \dots, x_n) \leq p_{\text{max}}/p_{\text{ave}}
\end{array}$$

In the above set, one power peaking factor is included but, depending upon the reactor design, additional respective constraint conditions may be required to include segments in the plate where power peaking could potentially occur. Analogous to the linearized function approximating the thermal neutron flux, the constraints are also expanded into first-order Taylor series.

$$C_j(\vec{x}) = C_j(\vec{x}^0) + \sum_{i=1}^n \frac{\partial C_j}{\partial x_i} (x_i - x_i^0) \quad (9.8)$$

The partial derivatives required to construct the linearized approximations of the constraint conditions fall into two categories: one subset can be directly derived from explicit functions of the design variables, but for a second subset, such functions are unavailable. In those cases, MCNP-based perturbation calculations are performed to acquire appropriate numerical values in the vicinity of the linearization point x^0 .

$$\left. \frac{\partial C_i}{\partial x_j} \right|_{\vec{x}=\vec{x}^0} \approx \frac{C_i(\vec{x}^j) - C_i(\vec{x}^0)}{x_j - x_j^0} \quad \text{with } C_i(\vec{x}^j), C_i(\vec{x}^0) \text{ from MCNP} \quad (9.9)$$

For the set of constraints listed above, the power peaking factor C_4 has to be determined using expression (9.9). In addition, as will be discussed below, the cycle length estimate C_1 also relies upon this method to quantify the sensitivity of the core reactivity to variations of the design variables. In contrast, the average power density in the core C_2 and the average heat flux C_3 can be directly determined, i.e. without using (9.9), from the set of core design variables. For the cylindrical geometry of single element reactors, the average power density in the core is simply given by:

$$C_2(\vec{x}) = \frac{x_1}{\pi} \frac{1}{x_9 (x_8^2 - x_7^2)} \quad (9.10)$$

In order to quantify the average heat flux, the number of fuel plates has to be known. The maximum number that can be accommodated is determined by the outer radius of the inner core tube, the thickness of the fuel plate, and the width of the coolant channel.

$$\text{Number of plates} \leq \frac{2\pi x_7}{x_4 + 2x_5 + x_6} \quad (9.11)$$

The maximum number corresponds to plates leaving the core tube perpendicularly. In practice, the largest possible integer is chosen. With the number of plates specified, the average heat flux C_3 can be approximated by the following expression, which is based upon the arc-length of an involute characterized by the specified set of design variables.

$$C_3(\vec{x}) \approx \frac{x_1}{2\pi} \frac{x_4 + 2x_5 + x_6}{x_9 (x_8^2 - x_7^2)} \quad (9.12)$$

Due to the fact that the next lower integer has to be chosen, the average heat flux will generally be slightly underestimated during the optimization process. The partial derivatives of C_2 and C_3 are immediately calculated from equations (9.10) and (9.12).

The most challenging constraint to process is the cycle length C_1 . In order to execute the LP process in a reasonable time, the objective is to estimate C_1 without actually performing burnup calculations for a given \vec{x} . Once a promising set of design variables has been finally identified, the cycle length is verified in an actual M³O burnup calculation.

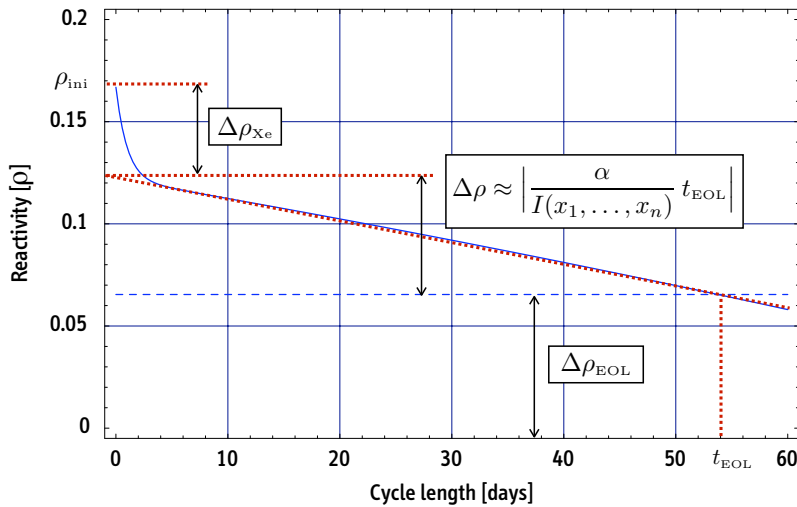


Figure 9.2: Typical reactivity loss during irradiation for a single element reactor.

As shown in Figure 9.2, the typical reactivity loss during irradiation is nearly linear once the xenon equilibrium is reached after a few days. An estimate of the average reactivity loss rate can therefore be used to obtain an approximation of the maximum cycle length, which is achieved when the reactivity drops below $\Delta\rho_{EOL}$. In the following, it is assumed that $\Delta\rho/\Delta t$ is inversely proportional to the initial uranium-235 inventory in the core.

$$\frac{\Delta\rho}{\Delta t} \approx -\frac{\alpha}{I(x_1, \dots, x_n)}, \quad \alpha > 0 \quad (9.13)$$

The characteristic constant α , which scales the reactivity loss rate, can be determined for the initial base design, and is thereupon used in the iteration process. The initial U-235 inventory can be calculated directly from the set of design variables. Introducing the unfueled radius ϵ of the plate, the total U-235 inventory in the core is given by:

$$I(\vec{x}) = \pi \frac{x_2 x_3 x_4 x_9}{x_4 + 2x_5 + x_6} \left[\left(x_{10}^2 - (x_7 + \epsilon)^2 \right) + x_{11} \left((x_8 - \epsilon)^2 - x_{10}^2 \right) \right] \quad (9.14)$$

End-of-life is reached when the core reactivity drops below a pre-defined value ρ_{EOL} . This margin is introduced to account for reactivity losses associated with experimental and other reactor devices not modeled at this stage. Figure 9.2 illustrates the corresponding reactivity balance.

$$\Delta\rho_{\text{EOL}} \stackrel{!}{=} -\frac{\alpha}{I(\vec{x})} t_{\text{EOL}} + \left[\rho_{\text{ini}}(\vec{x}) - \Delta\rho_{\text{Xe}} \right] \quad (9.15)$$

The achievable cycle length $C_1(\vec{x}) = t_{\text{EOL}}$ can therefore be approximated as:

$$C_1(\vec{x}) \approx \frac{I(\vec{x})}{\alpha} \left[\rho_{\text{ini}}(\vec{x}) - (\Delta\rho_{\text{EOL}} + \Delta\rho_{\text{Xe}}) \right] \quad (9.16)$$

In practice, fixed values are used for $\Delta\rho_{\text{EOL}}$ and $\Delta\rho_{\text{Xe}}$ in all simulations. The partial derivatives for all $C_1(x_i)$ can be calculated based on the preceding expression.

$$\left. \frac{\partial C_1(\vec{x})}{\partial x_i} \right|_{\vec{x}=\vec{x}^0} = \frac{1}{\alpha} \left[\left. \frac{\partial I(\vec{x})}{\partial x_i} \right|_{\vec{x}=\vec{x}^0} \left[\rho_{\text{ini}}(\vec{x}^0) - (\Delta\rho_{\text{EOL}} + \Delta\rho_{\text{Xe}}) \right] + I(\vec{x}^0) \left. \frac{\partial \rho_{\text{ini}}(\vec{x})}{\partial x_i} \right|_{\vec{x}=\vec{x}^0} \right] \quad (9.17)$$

The partial derivatives of $I(\vec{x})$ can be calculated directly from (9.14), while the sensitivity of the initial reactivity ρ_{ini} is determined in MCNP simulations for the perturbed problem using (9.9).

In practice, *Mathematica* generates all MCNP input decks for the perturbed models, extracts the tally data from the MCNP output, determines the required partial derivatives, and solves the linearized set of equations with an enhanced version of the Simplex algorithm [Wolfram, 2001, implementation notes, Section A.9.4].

This page intentionally blank

Chapter 10

Optimization and FRM-II

The discovery of monolithic fuel, a metallic uranium-molybdenum alloy, in early 2002 opened radically new perspectives for the conversion of the remaining HEU-fueled reactors in the world. For obvious reasons, the FRM-II would be a prime candidate to use monolithic fuels: with the start-up of the reactor in March 2004, a future conversion of the facility with important modifications to the core geometry, as discussed in Section 8.3, became significantly more difficult and therefore less likely. This is mainly due to the activation of the structural components in the moderator tank and the associated increased difficulty and costs required to replace or modify them. Crucial for the following analysis, which is entirely focused on monolithic fuels, are therefore the assumptions about fixed and variable parameters of the facility when exploring alternative fuel and core options for the existing HEU design. Optimization of the FRM-II core for use with reduced enrichment proceeds in two steps:

Preliminary conversion options (type A): These options are restricted to minor modifications of the fuel element. Specifically, the outer dimensions of the fuel element are preserved and the number of fuel plates held constant (113 plates). Minor modifications to the fuel plate geometry are allowed in order to study the impact of meat and cladding thickness variations, but only one core parameter is varied at a time. A general understanding of the sensitivity of the various design parameters is thereby established and typical parameter ranges are identified, even though the results are not optimized for maximum neutron flux at this stage.

Optimized conversion options (type B): The most comprehensive conversion options explored in this chapter foresee additional degrees of freedom, i.e. additional variable design parameters of the core geometry, in order to define an ‘upper limit’ of the conversion potential of monolithic fuel in FRM-II. Based on the linear programming technique laid out in the previous chapter, a new core geometry is

identified that optimizes the neutronics of monolithic fuel of reduced enrichment (less than 30%). Type B options are developed using selected preliminary type A options as a starting point. For the most promising candidate options, detailed neutronics calculations, including burnup calculations based on the ACS concept introduced in Section 5.2, are performed.

From a more general perspective, the broad analysis performed in this chapter also exemplifies the potential of advanced high-density fuels with reduced enrichment in a direct comparison between an HEU design and an alternative LEU design for a given reactor, while maintaining the main characteristics of the facility. Exploring and quantifying the potential and the limits of new ultra-high-density fuels is one practical objective of this study.¹

10.1 Monolithic LEU Fuel in Original Geometry

The most straightforward approach to use monolithic fuel in FRM-II would be to simply replace the U_3Si_2 dispersion-type fuel enriched to 93% with monolithic LEU fuel. The inner section of the plate, in which the uranium density currently is 3.0 g/cm^3 , would now accommodate fuel with an effective uranium density of 16 g/cm^3 . Similarly, the effective uranium density in the peripheral section of the plate would be reduced to 8 g/cm^3 at the same enrichment level.²

Detailed results of the burnup calculations are not discussed here because a simple estimate is sufficient to illustrate the inadequacy of this conversion option. The initial k_{eff} for monolithic LEU fuel in the original core reaches a value of less than 1.12 as can be read from Figure 10.1 below. Assuming a typical reactivity loss due to the xenon buildup of $\Delta k \approx -0.05$ during the first two days of operation, the k_{eff} already drops to less than 1.07, which is the pre-defined EOL reactivity limit of the core as defined in Section 8.2.3. It is therefore obvious that this conversion option is unacceptable and entirely unrealistic.³ As illustrated in Figure 10.1, an M^3O simulation confirms this unfavorable situation. If the outer radial dimensions of the core are maintained constant, enrichments beyond the LEU-limit of 20% are therefore inevitable. Obviously, FRM-II *could* be redesigned for monolithic LEU if more flexibility, such as outer fuel element dimensions, were allowed.

¹Earlier results of this analysis have been presented in [Glaser, 2004b].

²Reducing the thickness of the meat is one option, reducing the fuel enrichment would be another.

³During the FRM-II negotiations in 1999, ANL had already emphasized that LEU cannot be used in the present FRM-II geometry. Prior to the discovery of monolithic fuels, Hanan et al. [1999] concluded: "There is no possibility whatsoever that a suitable LEU fuel will ever be developed for direct substitution into the fuel plates of the HEU core. [...] Using a completely hypothetical fuel with 12.0 gU/cm^3 , the core would operate for less than 5 full power days at a power level of 20 MW."

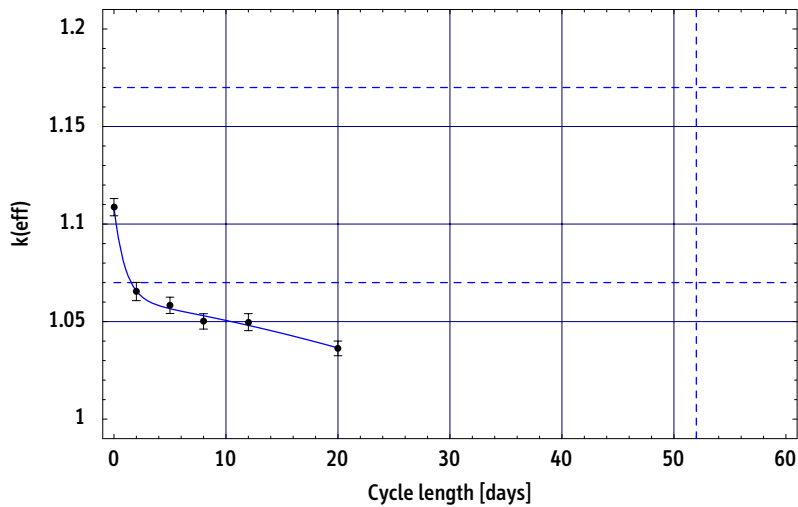


Figure 10.1: Cycle length achievable with monolithic LEU fuel in original HEU geometry.

M3O results, MCNP input deck: frm4o

10.2 Modifications to the Original Core Design

As indicated, the present objective is to define credible conversion options, which exceed the LEU-limit as little as possible, while allowing only minor changes to the core geometry, in order to facilitate a later re-licensing of the reactor. In particular, the inner and outer diameters of the core (118 mm and 243 mm, see Table 8.1) are maintained constant for all conversion options defined in this section. The following modifications are considered for the preliminary type A options below:

Height of fuel element. A moderate increase in the height of the fuel element increases the total uranium inventory as well as the initial reactivity of the core. Both effects will extend the cycle length of the reactor. Note however that an elongated fuel element is equivalent to lower average and peak power densities in the core, which ultimately reduces the absolute neutron flux in- and outside the core.

Meat thickness. For a fixed number of fuel plates, a variation the meat thickness leads to a change of both the total uranium inventory and of the H/HM (hydrogen over heavy metal) ratio. In the present case, the variations are implemented by reducing the thickness of the cladding material. As the total number of fuel plates is maintained constant, the width of a unit cell comprising plate and coolant channel is unaffected (see Figure 10.2, Mod 1).

Coolant channel width. Analogous to the previous modification, a reduced cladding thickness can be used to increase the width of the coolant channel (see Figure 10.2, Mod 2). In this case, only the H/HM ratio is affected.

Variation of the fuel plate and of the coolant channel dimensions both affect the H/HM ratio for a fixed number of 113 plates. These modifications are important, because the current core geometry (Mod 0) has been originally optimized for HEU use. Due to the substantial increase of the heavy metal inventory in the core,⁴ the average neutron spectrum in the plate can be expected to harden significantly. Consequently, both countermeasures are useful: first, overcompensating the total U-235 even more (increased meat thickness) to match a given cycle length and, second, softening the spectrum as much as possible (increased coolant channel width) in order to increase the effectiveness of U-235 in the uranium. The impact of these dimensional changes of the fuel plate, and the related variation of the H/HM ratio, are studied in some detail below.

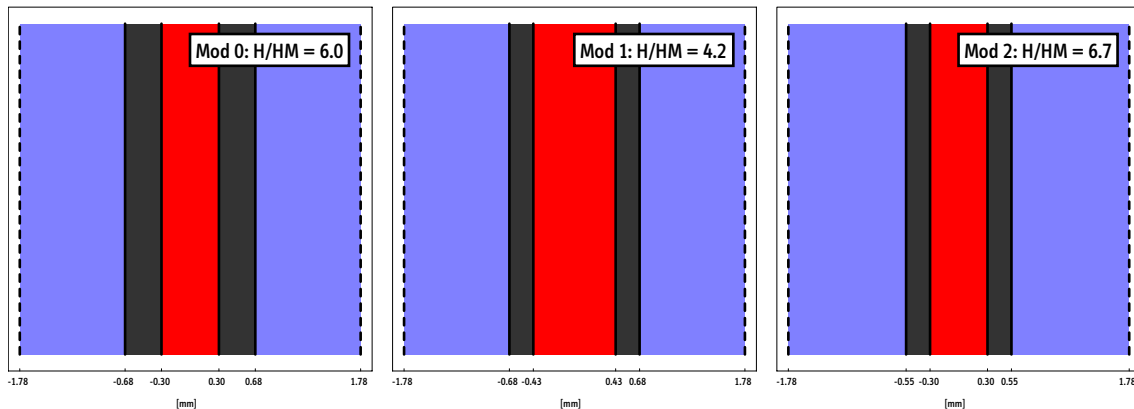


Figure 10.2: FRM-II fuel plate variations: original unit cell of the HEU design (Mod 0) for a cladding thickness of 0.38 mm and modifications with reduced cladding: increased meat thickness (Mod 1) and increased coolant channel (Mod 2). H/HM ratios are indicated for an exemplary cladding thickness of 0.25 mm.

⁴For instance, to match the original uranium-235 inventory in the core, a 4.7-fold increase of total uranium is required when replacing HEU with LEU.

10.3 Preliminary Conversion Option Candidates

Before embarking into a detailed analysis of possible conversion options based upon the types of modifications introduced above, a simple indicator is required to identify reasonable ranges of the relevant parameters. In general, the achievable cycle length is one crucial performance characteristic of a modern research reactor. For all credible conversion options considered here, the new cycle length has to reproduce or at least be close to the original one. In particular, once the outer radius of the reactor core is fixed, as it is in the present case, the cycle length becomes the leading criterion because the maximum neutron flux, the second important characteristic, can barely be influenced independently.

For a given fuel-type and core geometry, the initial reactivity of the core ρ_{ini} , or equivalently the initial k_{eff} of the core, is a useful quantity to make a first estimate of the achievable cycle length once the approximate average reactivity loss rate $\Delta k_{\text{eff}}/\Delta t$ of the fuel is known.

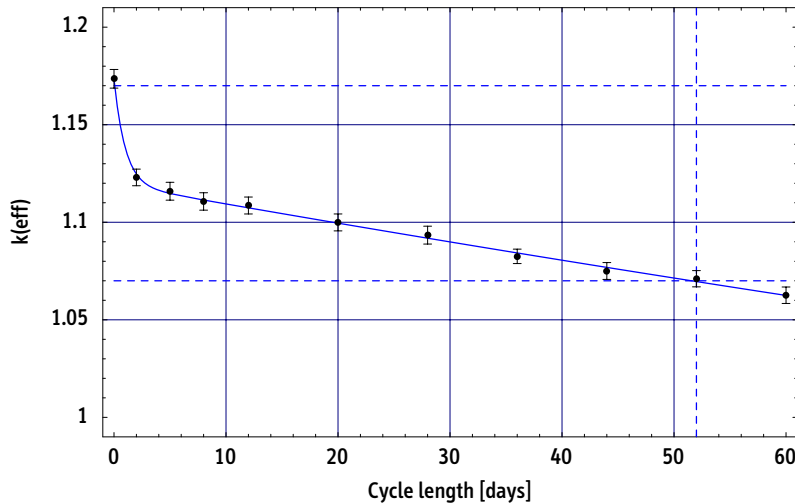


Figure 10.3: Initial reactivity, reactivity loss rate, and cycle length for monolithic fuel.

M30 results, MCNP input deck: frmvm8m (11 burnup points), conversion option A5 (Mod 2)

Figure 10.3 shows the reactivity versus cycle length evolution for monolithic fuel enriched to 27.5% and used in fuel plate modification Mod 2 (option A5, discussion below). The results demonstrate that the original cycle length of 52 days can be matched for a specified k_{eff}^* , which will be used as the reference value for all conversion options considered in this section:

$$k_{\text{eff}}^* = 1.17 \quad (10.1)$$

For obvious reasons, using the initial k_{eff} to estimate the achievable cycle length is a crude method because the total U-235 varies with enrichment and total uranium inventory. Nonetheless, U-235 consumption is generally not the limiting factor for the given high-density fuel and core geometry. In any case, once a candidate option is identified, the precise value of the cycle length has to be determined in accurate, though time-consuming, burnup calculations (as illustrated in Figure 10.3).

The impact of the fuel element variation (increased height) and the fuel plate modifications (Mod 1 and Mod 2) on initial reactivity k_{eff} have been studied in extensive MCNP Monte Carlo simulations for a broad range of enrichment levels between 19.75% and 35%. Figures 10.4, 10.5, and 10.6 display the main results of these calculations.

All preliminary conversion options discussed below (A1 through A5) are based on monolithic fuel with an effective uranium density of 16 g/cm³ in the main segment and of 8 g/cm³ in the periphery of the plate.

10.3.1 Option A1: Monolithic reference case

The most obvious and primitive strategy to use monolithic fuel in FRM-II, while satisfying the cycle length requirement, is to re-increase the enrichment of the fuel until the k_{eff}^* condition is met. No geometry changes to the core or other modifications to the fuel plate (Mod 0) are foreseen for this reference case. Based on the results shown in Figure 10.4, this situation is reached for an enrichment of about 32.5%.

10.3.2 Options A2 and A3: Elongated fuel element

Using an elongated fuel element increases the total uranium inventory, which has two simultaneous effects. First, it decreases the reactivity loss rate during irradiation. More importantly though, a fuel element of increased height raises the initial reactivity of the core for a given enrichment. Figure 10.4 illustrates this situation. To achieve the desired k_{eff}^* of 1.17 at BOL, a fuel enriched to at least 32.5% is required for the original fuel element geometry. Increasing the height from 70 cm to 80 cm reduces this minimum value to 26.0%.

The most important related consequence of increasing the height of the fuel element to 80 cm is the corresponding decrease of the power density in the core. Even though it may relax the cooling requirements of the core, this decrease also implies a reduction of the maximum thermal neutron flux observed in the moderator tank. To compensate this undesired effect of the modification, the total thermal power of the facility could be raised correspondingly. Since the total core volume increases by a factor of 1.14 (80/70), the original average power density in the core could be reproduced by a thermal power

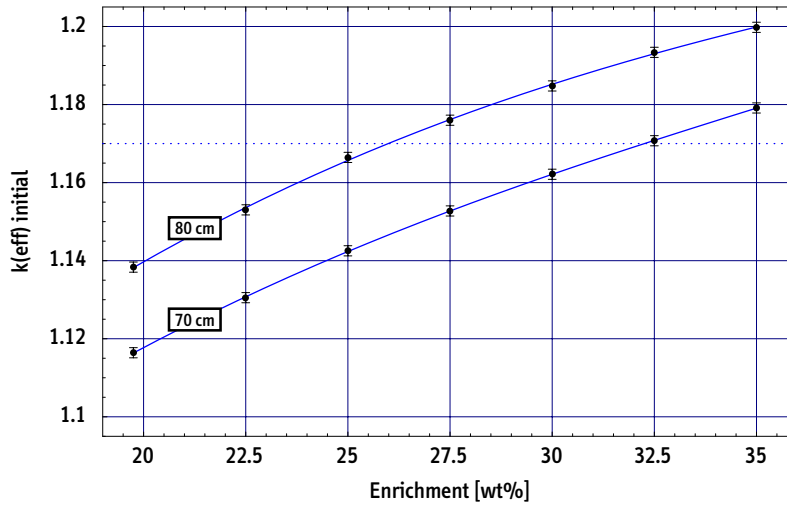


Figure 10.4: Monolithic fuel. Initial reactivity of the core as a function of enrichment. Original core height and elongated version with 80 cm. Minimum initial k_{eff} value to achieve target cycle length is approx. 1.17 for given fuel-type and core geometry.

MCNP 4B/C calculations, 4 million neutron histories each

of 22.85 MW. Even though the acceptability of such an increase may be debatable for licensing reasons, the results for a reactor uprated by 10% (22 MW) are summarized in Table 10.1 in addition to the 20 MW results (Options A2 and A3). Note that the reactivity loss rate increases slightly for an increased power level.

10.3.3 Option A4: Increased meat thickness

Figure 10.5 displays the results of MCNP calculations for a core using fuel plates with larger values of the meat thickness (fuel plate modification Mod 1). While the cladding material is reduced from 0.38 mm down to 0.30 mm and 0.25 mm, the meat can be increased from 0.60 mm up to 0.76 mm and 0.86 mm respectively, without changing the external dimensions of the plate. Figure 10.2 (Mod 1) illustrates this situation for the plate with the thinner (0.25 mm) cladding.

As expected, lower enrichments are sufficient to achieve the same initial k_{eff} if the meat thickness, and therefore the total U-235 inventory in the core, increases. The positive impact is slightly suppressed because both the neutron spectrum hardens and parasitic absorption in U-238 increase as the total loading of uranium goes up. With the thinner cladding of 0.25 mm, the reference value of k_{eff} is reached for an enrichment of 28.0%.

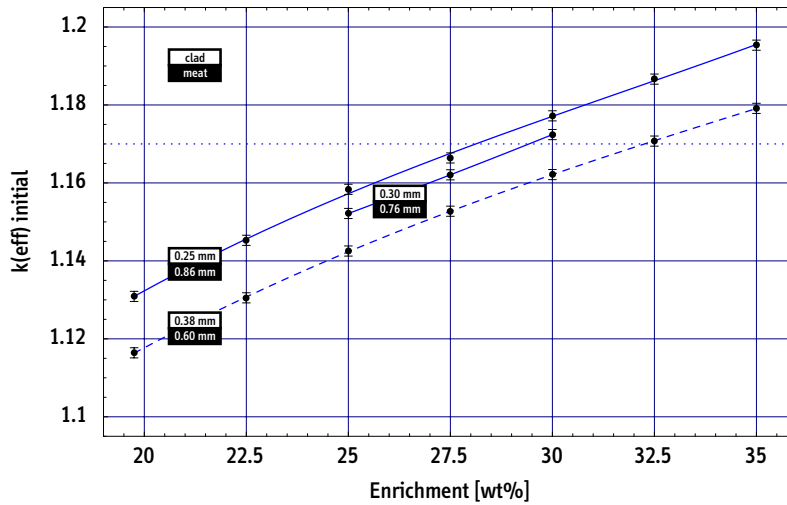


Figure 10.5: Monolithic fuel, plate modification Mod 1. Initial reactivity of the core as a function of enrichment. Original (---) and modified fuel plates with increased thickness of the fuel meat. Due to the increase of the fissile inventory, the minimum initial k_{eff} value to achieve target cycle length may be less than 1.17 for plates with increased thickness of the meat.

MCNP 4B/C calculations, 4 million neutron histories each

10.3.4 Option A5: Increased width of cooling channel

Instead of using the additional volume obtained by reducing the cladding to increase the meat thickness, the plate thickness itself can be reduced to increase the width of the cooling channel (fuel plate modification Mod 2). This measure allows for lower coolant velocities, but the vibrational stability of such a plate would have to be demonstrated for safety and licensing purposes.⁵

Results for coolant channel widths of 2.36 mm and 2.46 mm are shown in Figure 10.6. Introducing additional H₂O increases the H/HM ratio in the core: as illustrated in Figure 10.2 (Mod 2) for the thinnest cladding (0.25 mm), the H/HM value rises to 6.7 from its original value of 6.0. Neutrons are therefore more effectively thermalized, which in turn increases the relative importance of U-235 fission in the fuel. For the thinner cladding option, i.e. for a coolant channel width of 2.46 mm, the reference k_{eff} is achieved for an enrichment of about 27%. This data suggests that, for a fixed number of fuel plates, it would be slightly more efficient to use the volume that is

⁵Note that HFIR (ORNL, USA) and the High-Flux Reactor (ILL, Grenoble) both use thinner fuel plates (1.27 mm) than FRM-II (1.36 mm) for comparable coolant velocities. The minimum thickness considered here is 1.10 mm.

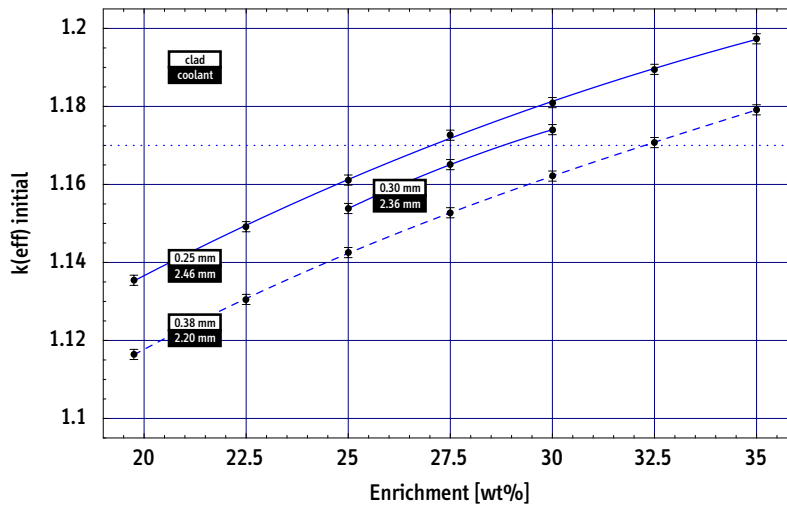


Figure 10.6: Monolithic fuel, plate modification Mod 2. Initial reactivity of the core as a function of enrichment. Original (—) and modified fuel plates with increased width of coolant channels. Minimum initial k_{eff} value to achieve target cycle length is approx. 1.17 for given fuel-type and core geometry.

MCNP 4B/C calculations, 4 million neutron histories each

made available by reducing the cladding thickness to increase the width of the coolant channels (A5) instead of increasing the fuel inventory in the core (A4).

The main results for the conversion option candidates (designated A1 through A5), i.e. for those enrichment levels that achieve the required minimum reactivity in a specified geometry, are juxtaposed in Table 10.1. The most promising candidates are briefly discussed below and a few options selected for subsequent optimization.

10.4 Comparison and Selection of Type A Options

Out of the five candidate options shown in Table 10.1, a few are selected for further consideration in the next section. The main design data as well as additional results for options A1, A3, and A5 are summarized in Table 10.2, which also lists corresponding data and results of the original HEU design. Specifically, and in addition to the cycle length and neutron flux data, Table 10.2 shows selected M³O results for the maximum power density in the core, power peaking factors, average and maximum burnup, residual uranium enrichment, plutonium buildup, as well as maximum local fission rates

	Option A1 (Mod 0) frmv4n	Option A2 frmv9o	Option A3 frmv9o	Option A4 (Mod 1)	Option A5 (Mod 2) frmv8m
Total power:	20 MW	20 MW	22 MW	20 MW	20 MW
Fueled height of core:	70 cm	80 cm	80 cm	70 cm	70 cm
Meat:	0.60 mm	0.60 mm	0.60 mm	0.86 mm	0.60 mm
Cladding:	0.38 mm	0.38 mm	0.38 mm	0.25 mm	0.25 mm
Cooling channel:	2.20 mm	2.20 mm	2.20 mm	2.20 mm	2.46 mm
Uranium inventory:	43.25 kg	49.42 kg	49.42 kg	61.99 kg	43.25 kg
Required Enrichment:	32–33%	26–27%	27–28%	27–28%	27–28%
Maximum neutron flux:	7.18E14	6.87E14	7.56E14	6.88E14	7.11E14
$\Delta\phi$ (max):	−10.7%	−14.6%	−6.0%	−14.5%	−11.5%
$\Delta\phi$ (cns):	−8.2%	−12.0%	−3.2%	−12.0%	−10.4%

Table 10.1: Preliminary conversion options candidates of type A (113 plates).

Absolute neutron flux levels in [n/cm^2s], all neutron flux losses relative to the original HEU design (93%)

and densities in the fuel.⁶

Based on the original HEU geometry, Option A1 uses monolithic fuel at an enrichment of 32.5% to reproduce the original cycle length of 52 days. The loss of thermal neutron flux is 10.7% at the maximum and 8.2% at the position of the CNS. While the performance of option A1 is comparable and even slightly better than those of A2, A4, and A5, it's the only core configuration that would require an enrichment above 30%. i.e. being further removed from the LEU-limit. In order to reduce the enrichment further, modifications of the original geometry are required to increase the initial reactivity of the core.

The most effective strategy to optimize reactor performance for monolithic fuel using the original outer diameter of the core and the original number of fuel plates (113) is to elongate the fuel element, while increasing simultaneously the thermal power of the reactor from 20 MW to 22 MW (A2 versus A3). In applying these two modifications at the same time, the average power density in the core remains nearly constant. For Option A3, the loss of maximum thermal neutron flux is 6.0% and reduces to 3.2% at the position of the CNS relative to the original HEU design. Figures 10.7 and 10.8 show reactivity vs. cycle length and thermal neutron flux in the moderator tank of

⁶Note that fission rates and densities are normalized to the volume of the fuel particles in the case of the dispersion-type fuel of the original HEU design. For monolithic fuels (options A1, A3, and A5), meat volumes and fuel volumes are equivalent.

	HEU Design frm2/frm3	Option A1 (Mod 0) frm4n	Option A3 frm9o	Option A5 (Mod 2) frm8m
Total power:	20 MW	20 MW	22 MW	20 MW
Fueled height of core:	70 cm	70 cm	80 cm	70 cm
Meat:	0.60 mm	0.60 mm	0.60 mm	0.60 mm
Cladding:	0.38 mm	0.38 mm	0.38 mm	0.25 mm
Cooling channel:	2.20 mm	2.20 mm	2.20 mm	2.46 mm
Uranium inventory:	8.1 kg	43.25 kg	49.42 kg	43.25 kg
Required Enrichment:	93.0%	32.5%	27.5%	27.5%
Cycle length:	52 days	57 days	52 days	52 days
Maximum neutron flux:	8.04E14 n/cm ² s	7.18E14 n/cm ² s	7.56E14 n/cm ² s	7.11E14 n/cm ² s
$\Delta\phi$ (max):	reference value	-10.7%	-6.0%	-11.5%
$\Delta\phi$ (cns):	reference value	-8.2%	-3.2%	-10.4%
Average power density:	6.75 kW/cc	6.75 kW/cc	6.50 kW/cc	6.75 kW/cc
Maximum power density:	12.87 kW/cc	16.69 kW/cc	15.85 kW/cc	15.76 kW/cc
Power peaking factor:	1.91	2.47	2.44	2.33
Average burnup:	17.6%	9.5%	10.6%	11.0%
Maximum burnup:	50.2%	36.7%	40.0%	40.0%
Residual uranium enrichment:	88.6%	30.3%	25.3%	25.2%
Total plutonium inventory:	9.9 g	107.1 g	129.0 g	115.8 g
Max. local av. fission rate (BOL):	26.2E14 fi/cm ³ s	4.81E14 fi/cm ³ s	4.45E14 fi/cm ³ s	4.44E14 fi/cm ³ s
Max. local fission density (EOL):	11.8E21 fi/cm ³	2.16E21 fi/cm ³	2.00E21 fi/cm ³	2.00E21 fi/cm ³

Table 10.2: Selected conversion options candidates of type A (113 plates).

M3O results, MCNP input decks as indicated in the table, fission rates are maximum local life-averaged fission rates

Option A3 as obtained at this stage with M³O simulations.

The results of the conversion options with a reduced cladding thickness (options A4 and A5) are very similar to each other as can be verified in Table 10.1. Option A5 performs slightly better than A4 and respective additional results are listed in Table 10.2. Option A5, which is based on a thinner fuel plate and a widened coolant channel (2.46 mm vs. 2.20 mm), almost reproduces the performance of Option A1 with a reduced enrichment of only 27.5%. Nevertheless, this option is not pursued further in the next section because the adequacy of the reduced cladding thickness as well as the plate's vibrational stability would have to be demonstrated separately. These aspects are beyond the scope of this analysis. If its thermal-hydraulic feasibility and safety were confirmed, option A5 would be very attractive for FRM-II conversion.

The average and maximum burnup as well as the peak EOL fission densities are very low for all conversion options, and monolithic fuel could be expected to behave well under these conditions (see Section 4.1.3).

An unfavorable, and possibly critical characteristic of all conversion options identified in Table 10.2 is the stronger spatial dependency of the power density distribution. This

is due to the substantial heavy metal inventory in the core, which increases at least 5-fold in each case relative to the original HEU core. As a result, neutron and gamma absorption in the fuel itself increases significantly. This effect is particularly pronounced in those segments of the plate that were already characterized by high fission rates and leads to further intensified power peaking. Measured in the equivalent segments of the plate, respective values increase from 1.91 for HEU to 2.33–2.47 for monolithic fuel with reduced enrichment.

Even though these values may still be acceptable, the linear programming technique introduced in the previous chapter is used to adjust and optimize the design of conversion option candidates A1 and A3 in order to satisfy all imposed constraints. The algorithm is primarily used to reduce power peaking to its original value below 2.0, while maintaining the required cycle length as well as maintaining or possibly further increasing the maximum thermal flux.

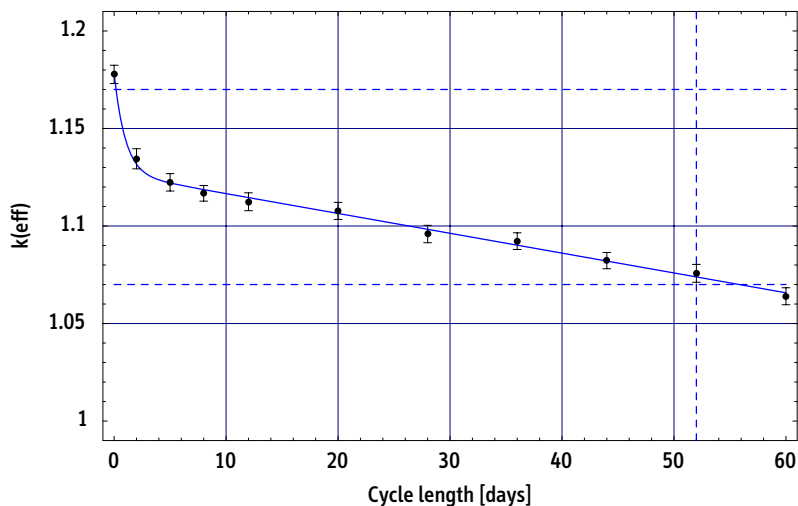


Figure 10.7: Reactivity versus burnup for the preliminary 22 MW option (A3). Elongated fuel element at 80 cm (instead of 70 cm), monolithic fuel enriched to 27.5%.

M30 results, MCNP input deck: frmv9o, 11×2 MCNP runs, 4 million neutron histories each

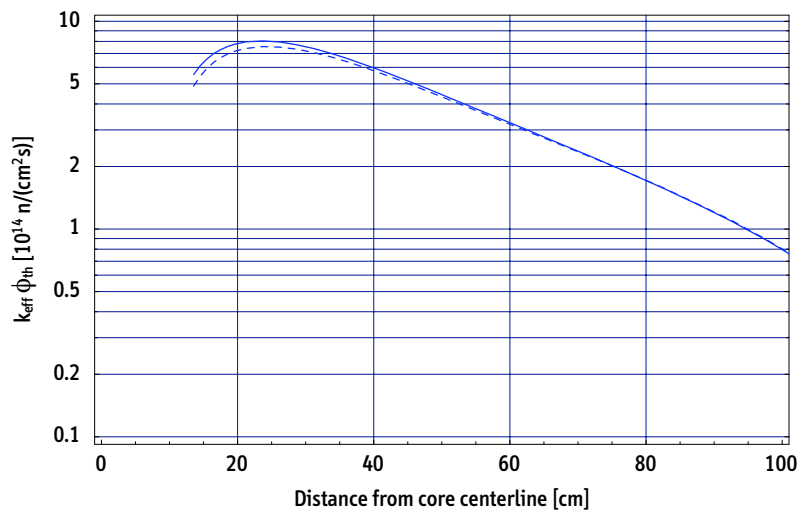


Figure 10.8: Thermal neutron flux of the original HEU design (—) and the 22 MW option (- -) of type A. Reduction in maximum: 6.0%. Thermal flux levels match at a distance of 77.5 cm from core centerline.

M3O results, MCNP input deck: frm9o, evaluated with: FRM.FluxAnalysis.PlusPlus

10.5 Optimized Options with Reduced Enrichment

Options A1 and A3 are optimized using the linear programming technique because they represent two extreme and similarly interesting alternatives. Without any changes to the original geometry, Option A1 is the most conservative approach, even though the enrichment (32.5%) is not the lowest enrichment level possible. Option A3 is studied for being the most attractive conversion option displaying a minimal performance loss relative to the HEU design and using a fuel enrichment of only 27.5%.

The linear programming technique developed in Chapter 9 is applied to address the remaining issue of excessive power peaking and to optimize the thermal neutron flux if possible. Several core design parameters are pre-defined in the optimization process: only the meat thickness (x_4), the width of the cooling channel (x_6), the transition radius (x_{10}), and the discontinuity factor (x_{11}) are allowed to vary. Table 10.3 summarizes the fixed and variable parameters of both designs as well as their respective initial values.

		x_i^0 for B1	x_i^0 for B3	Parameter range
x_1	Power level (thermal)	20 MW	22 MW	invariable
x_2	Fuel enrichment	32.5%	27.5%	invariable
x_3	Effective uranium density	16 g/cc	16 g/cc	invariable
x_4	Meat thickness	0.60 mm	0.60 mm	$0.60 \text{ mm} \leq x_4 \leq 0.80 \text{ mm}$
x_5	Cladding thickness	0.38 mm	0.38 mm	invariable
x_6	Coolant channel	2.20 mm	2.20 mm	$2.00 \text{ mm} \leq x_6 \leq 3.00 \text{ mm}$
x_7	Core radius, inner	6.50 cm	6.50 cm	invariable
x_8	Core radius, outer	11.45 cm	11.45 cm	invariable
x_9	Active core height	70.00 cm	80.00 cm	invariable
x_{10}	Transition radius	10.56 cm	10.56 cm	$9.00 \text{ cm} \leq x_{10} \leq 11.00 \text{ cm}$
x_{11}	Density ratio	0.5	0.5	$0.25 \leq x_{11} \leq 1.00$

Table 10.3: Variable core parameters and their limits.

While the cladding thickness is defined as invariable, the minimum value of the meat thickness is set at the value of 0.60 mm in order to guarantee the original minimum width of the fuel plate for stability purposes. The parameter ranges of the all variable parameters are restricted to corresponding reasonable boundaries. According to the terminology introduced in Chapter 9, the linear programming problem can be formulated using the FRM-II design data. Maximize $\phi(x_1, \dots, x_{11})$ subject to the constraints:

$$\begin{array}{ll}
\text{Cycle length:} & C_1(x_1, \dots, x_{11}) \geq 52 \text{ days} \\
\text{Average power density:} & C_2(x_1, \dots, x_{11}) \leq 1100 \text{ W/cm}^3 \\
\text{Average heat flux:} & C_3(x_1, \dots, x_{11}) \leq 200 \text{ W/cm}^2 \\
\text{Power peaking factor \#1:} & C_4(x_1, \dots, x_{11}) \leq 2.0 \\
\text{Power peaking factor \#2:} & C_5(x_1, \dots, x_{11}) \leq 2.0
\end{array}$$

Compared to the original list of constraints proposed in Section 9.3.3, an additional power peaking factor has been added at the central position of the discontinuity in the fuel plate. Using the zone designations introduced in Section 8.1.4 (Figure 8.5), C_4 is measured in a segment equivalent to zone ②, while C_5 is measured in zone ⑩.⁷

The expression to estimate the cycle length C_1 is given by:

$$C_1(\vec{x}) \approx \frac{I(\vec{x})}{\alpha} \left[\rho_{\text{ini}}(\vec{x}) - (\Delta\rho_{\text{EOL}} + \Delta\rho_{\text{Xe}}) \right]$$

In order to apply this formula, $\Delta\rho_{\text{EOL}}$ and $\Delta\rho_{\text{Xe}}$ have to be known. The EOL criterion is simply set by the analyst, while the reactivity loss due to the xenon poisoning can be estimated via the FRM-II burnup calculations performed so far.

$$\Delta\rho_{\text{EOL}} = 0.065 \quad \text{and} \quad \Delta\rho_{\text{Xe}} = 0.045 \quad (10.2)$$

Similarly, the constant α , which scales the reactivity loss rate (see Figure 9.2), is determined for each model individually using the results of the burnup calculations performed for the preliminary conversion option candidates.

$$\alpha \approx 9.3 \text{ g/day for A1} \quad \text{and} \quad \alpha \approx 10.0 \text{ g/day for A3} \quad (10.3)$$

The average power density in the core C_2 and the average heat flux C_3 are both directly determined from the set of design variables (x_1, \dots, x_{11}) . MCNP perturbation calculations are performed to calculate the partial derivatives required to approximate the maximum neutron flux ϕ (objective function), the initial core reactivity ρ_{ini} , and the power peaking factors as functions of the design variables. The *Mathematica* modules developed in the framework of this thesis (Chapter 5) are used to generate the numerous MCNP input decks required for this purpose. It should be emphasized that the number of fuel plates in the core may, and generally does, vary once the meat thickness x_4 or the width of the coolant channel x_6 is perturbed. As a consequence, the resulting

⁷In principle, a further power peaking factor could be added to control the power density at the innermost central segment of the fuel plate, i.e. close to the beryllium-follower. However, it has been found that values reached even in this part of the plate, though high and close to the maximum, are not limiting for the present geometry. If the inner radius of the element were allowed to vary, this third constraint for the power density would be mandatory.

modifications to the core model are non-obvious. In the present case, with seven design variables considered invariant (see Table 10.3), four distinct MCNP input decks and four MCNP runs are required per iteration.

Starting from the preliminary conversion option candidates A1 and A3 defined previously, the linear programming technique can now be applied to optimize these options further. As discussed, the objective of this procedure is twofold: one is to maximize the objective function, i.e. the thermal neutron flux achieved in the moderator tank. A second and even more relevant objective for options A1 and A3 is to satisfy the constraint conditions that were previously (mildly) violated, i.e. the power peaking factors, if possible without compromising the value of the objective function.

Main data and results obtained with the linear programming technique are summarized in Tables 10.4 and 10.5. The tables list the initial data of the preliminary type A options, the recommendations and predictions made by the code (LP solution), as well as results that were generated subsequently with MCNP to verify the performance of the LP algorithm. Without exception, the predicted and verified data are in excellent agreement. In particular, the estimated and verified cycle length estimates, which have been predicted without performing time-consuming burnup calculations for all perturbations, match or exceed the required minimum value of 52 days. Results of M³O simulations for the final conversion options B1 and B3 are shown in Figure 10.10 and confirm the accuracy of the initial estimates for C_1 .

For both optimized monolithic fuel options B1 and B3, the code suggests increased coolant channel widths to soften the neutron spectrum,⁸ while reducing the total number of fuel plates in the core from 113 down to 104 and 100, respectively. Most importantly, all constraints are now satisfied, particularly the power peaking conditional in the plate, and the neutron flux levels have increased slightly in both cases.

Figure 10.9 shows thermal neutron flux profile in the moderator tank for the final conversion options B1 and B3. Without any modifications to the core or the reactor (option B1), monolithic fuel could be used in FRM-II at an enrichment level of 32.5%, while the predicted loss of thermal neutron is 9.7% at its maximum and reduces to 8.2% at the position of the cold neutron source, i.e. at a distance of 40 cm from the core centerline. As expected from the discussion of type A options in the previous section, option B3 emerges as the most attractive conversion option for FRM-II. Using monolithic fuel at an enrichment of 27.5%, an elongated fuel element with an active height of 80 cm, and operated at 22 MW (instead of 20 MW), the performance loss of the facility would be marginal compared to the current design. The M³O simulations predict a maximum neutron flux of 7.6×10^{14} n/cm²s versus 8.0×10^{14} n/cm²s of the

⁸More precisely, due to the high uranium density in the fuel, thermalized neutrons re-entering the core from the moderator tank are mainly absorbed in the periphery of the plate. Wider coolant channels increase the relative importance of the central zones of the core, which is preferable for overall neutronics.

HEU design (-5.2%). At a distance of 40 cm, the loss is further reduced to -3.3% . Based on these numbers for conversion option B3, the effective performance loss of a neutron beam facility is assessed in the following chapter.

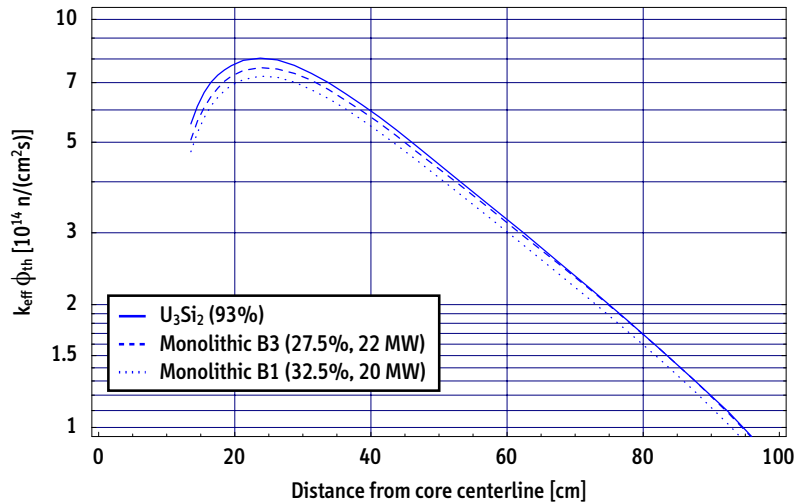


Figure 10.9: Thermal neutron flux for final FRM-II core variants with reduced enrichment.

A broad variety of additional data for options B1 and B3 are available, as has been demonstrated in the previous chapters, once the base MCNP input deck is generated and the M^3O simulation performed. In order to avoid unnecessary redundancy and since the most relevant data is already summarized in Tables 10.4 and 10.5, a full-scope discussion of these data is omitted here. Still, some exemplary results for the most attractive conversion option B3 are listed below: Figures 10.11 and 10.12 show the time-dependent inventories of the uranium and plutonium isotopes. Table 10.6 lists local and averaged burnup and residual enrichment data for the ACS zones as defined in Figure 8.5. These figures and tables can be compared to their respective counterparts in Chapter 8 for the original HEU design of FRM-II.

FRM-II Monolithic B1			
Enrichment: 32.5 wt%			
Active core height: 70 cm; Power level: 20 MW			
	Start	LP Solution	Verification
x_4	0.60 mm	0.62 mm	
x_6	2.20 mm	2.53 mm	
x_{10}	10.56 cm	10.48 cm	
x_{11}	0.50	0.45	
Plates	113	104	
$k(\text{eff})$	1.169 ± 0.001	1.173	1.172 ± 0.001
ϕ	$7.15\text{E}14 \text{ n/cm}^2\text{s}$	$7.25\text{E}14 \text{ n/cm}^2\text{s}$	$7.26\text{E}14 \text{ n/cm}^2\text{s}$
C_1	52–54 days	52 days	52–56 days
C_2	1024 W/cc	1024 W/cc	1024 W/cc
C_3	182 W/cm ²	200 W/cm ²	200 W/cm ²
C_4	1.67	1.68	1.66
C_5	2.13	2.00	1.99
$\Delta\phi$ (max)	–11.0%	–9.7%	–9.7%
$\Delta\phi$ (cns)	–8.7%	—	–8.2%

Table 10.4: Basic results for candidate option B1 with reduced enrichment using monolithic fuel. Variable core parameters recommended by linear programming algorithm (LP Solution). All neutronics calculations (Start and Verification) performed with M³O.

M3O results, MCNP input decks: cp0x0 through cp0x8 plus cp1x0; cycle length verification: FRMcpl.MCODE.11.out

FRM-II Monolithic B3			
Enrichment: 27.5 wt%			
Active core height: 80 cm; Power level: 22 MW			
	Start	LP Solution	Verification
x_4	0.60 mm	0.60 mm	
x_6	2.20 mm	2.70 mm	
x_{10}	10.56 cm	10.48 cm	
x_{11}	0.50	0.49	
Plates	113	100	
$k(\text{eff})$	1.174 ± 0.001	1.182	1.180 ± 0.001
ϕ	$7.56\text{E}14 \text{ n/cm}^2\text{s}$	$7.57\text{E}14 \text{ n/cm}^2\text{s}$	$7.62\text{E}14 \text{ n/cm}^2\text{s}$
C_1	52 days	52 days	52 days
C_2	985 W/cc	985 W/cc	985 W/cc
C_3	175 W/cm^2	200 W/cm^2	200 W/cm^2
C_4	1.73	1.67	1.66
C_5	2.08	2.00	1.99
$\Delta\phi$ (max)	-6.0%	-5.8%	-5.2%
$\Delta\phi$ (cns)	-3.1%	—	-3.3%

Table 10.5: Basic results for candidate option B3 with reduced enrichment using monolithic fuel. Variable core parameters recommended by linear programming algorithm (LP Solution). All neutronics calculations (Start and Verification) performed with M^3O .

M3O results, MCNP input decks: cq0x0 through cq0x8 plus cq1x0; cycle length verification: FRMq1.MCODE.11.out

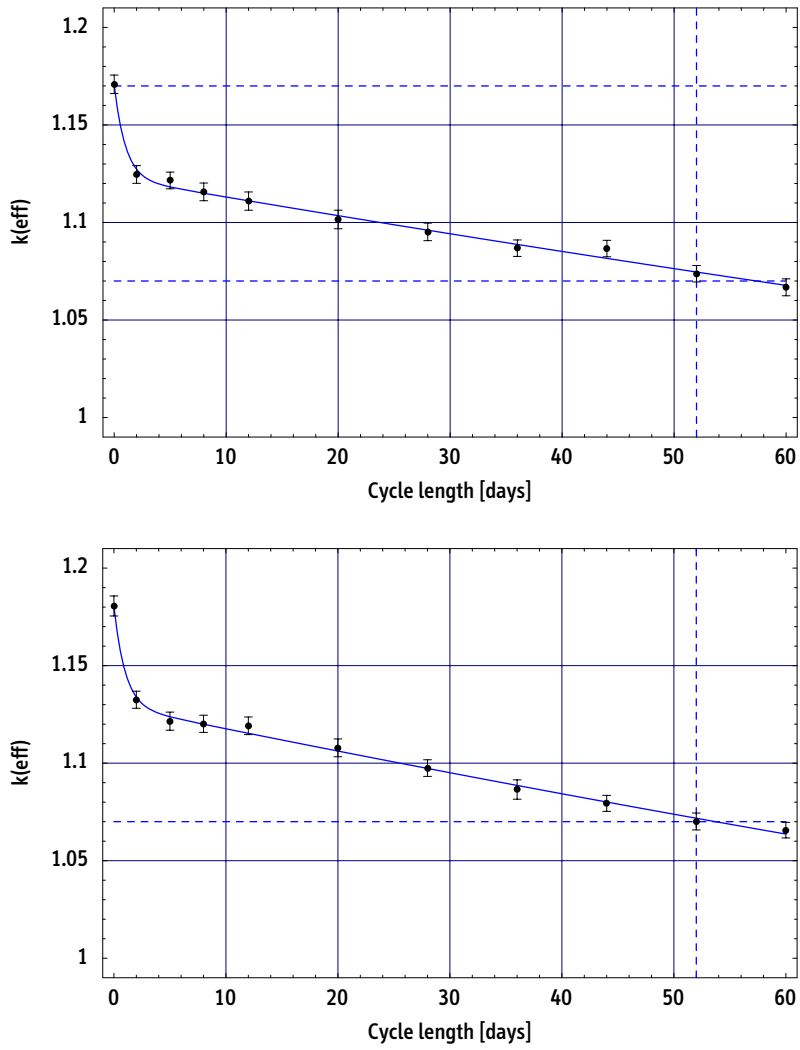


Figure 10.10: Cycle length verification for options B1 and B3.

M30 results, MCNP input decks: FRMcp1.MCODE.11.out and FRMcq1.MCODE.11.out (11 burnup points each)

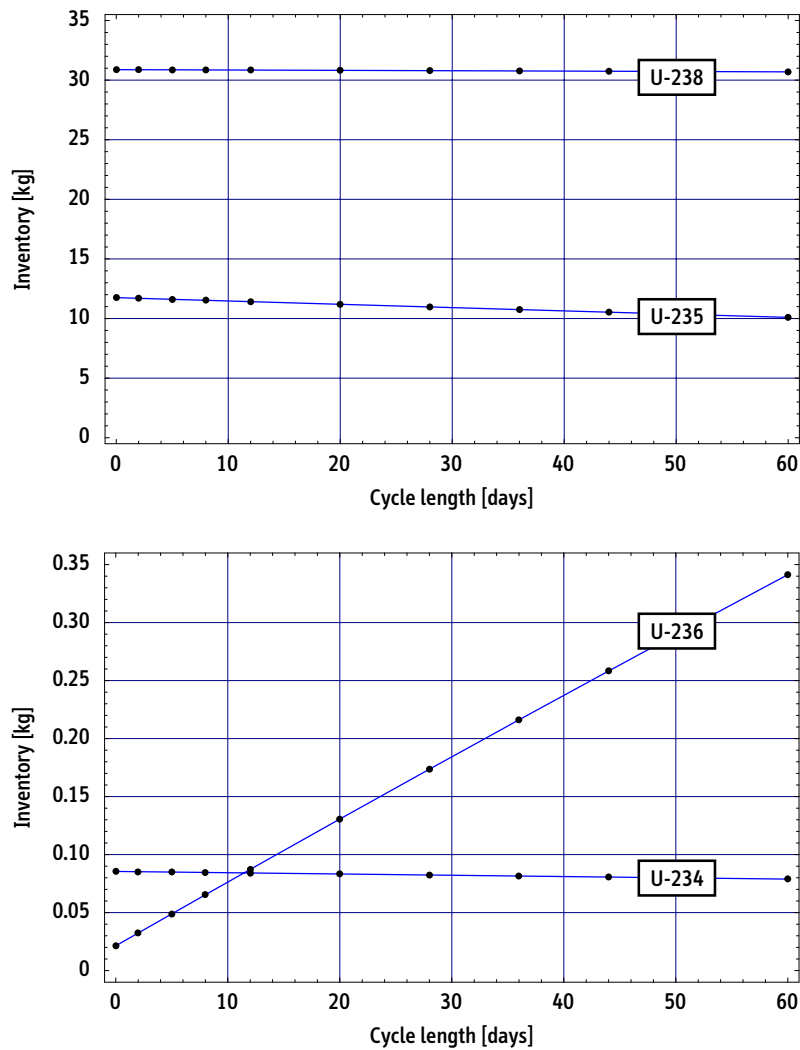


Figure 10.11: FRM-II Monolithic B3. Uranium inventory in fuel.

M3O results, MCNP input deck FRMcq1.MCODE.11.out evaluated with FRM.MCODEout.Table4
 Calculated inventories at EOL (52 days): 80 g of U-234, 10314 g of U-235, 300 g of U-236, and 30719 g of U-238

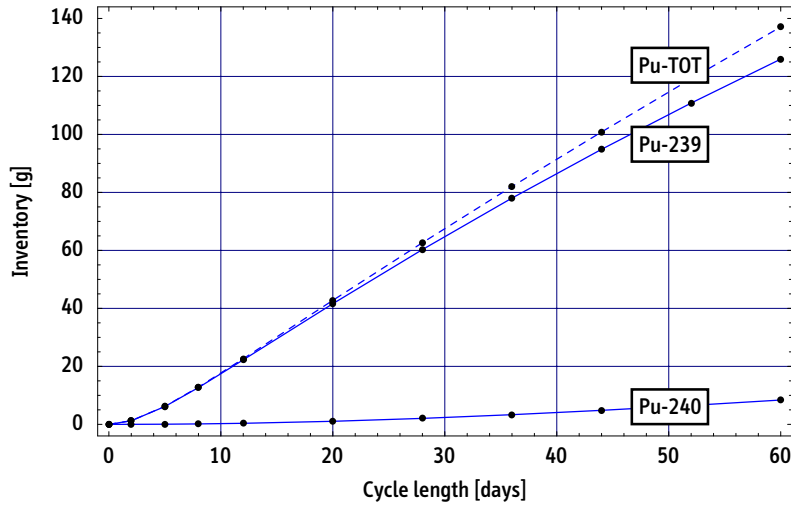


Figure 10.12: FRM-II Monolithic B3. Plutonium buildup in fuel.

M3O results, MCNP input deck FRMq1.MCODE.11.out evaluated with FRM_MCODEout.Table4
 Calculated inventories at EOL (52 days): 119 g of total plutonium, 111 g of Pu-239 and 7 g of Pu-240

#	Burnup	Residual Enrichment	#	Burnup	Residual Enrichment	#	Burnup	Residual Enrichment
1	7.3%	26.0%	8	26.6%	21.6%	15	18.6%	23.5%
2	15.4%	24.2%	9	13.3%	24.7%	16	19.6%	23.3%
3	9.5%	25.5%	10	12.9%	24.8%	17	10.1%	25.4%
4	20.2%	23.1%	11	33.8%	19.9%	18	9.7%	25.5%
5	10.1%	25.4%	12	15.9%	24.1%	19	5.6%	26.3%
6	13.3%	24.6%	13	16.7%	23.9%	20	42.3%	17.7%
7	12.9%	24.7%	14	39.7%	18.4%	21	19.8%	23.2%
Inventory weighted average							12.2%	24.9%

Table 10.6: FRM-II Monolithic B3. Local U-235 burnup and residual enrichment in FRM-II fuel plate at EOL, 1144 MWd(th), 52 effective full power days at 22 MW. See Figure 8.5 for zone assignment. Initial enrichment of the fuel is 27.5%.

M3O results, MCNP input deck FRMq1.MCODE.11.out evaluated with FRM_MCODEout.Table4

Chapter 11

The Net-Impact of Conversion on Reactor Performance

The results obtained in the M³O simulations discussed in the previous chapters have provided a wealth of data relevant to the conversion of single element reactors. The primary focus of the analysis was on the generic single element reactor (GSER) introduced in Chapter 7 to study general aspects of the computational system and, second, on the Forschungsreaktor München II (FRM-II) to evaluate the potential of advanced LEU fuels for conversion of an existing HEU-fueled facility (Chapters 8 and 10).

The results of the conversion options identified for FRM-II will be used in the following to quantify the hypothetical net-impact on the scientific usability of the facility in some more detail. As has been mentioned previously, the FRM-II can be considered the most difficult reactor to convert. Therefore, the following analysis also demonstrates the potential of monolithic fuel from a more general perspective. Nevertheless, a generic assessment of the scientific usability of a facility using relatively simple criteria, such as thermal and fast neutron flux values, inevitably remains limited in scope. For an in-depth analysis, instrument- and/or experiment-specific conditions and data would be required.

In Section 3.5, an expression has been derived to quantify the impact of variations of the signal and noise on the relative acquisition time t_2/t_1 with the requirement of constant relative error of the measurement.

$$\frac{t_2}{t_1} = \frac{1}{\alpha} \left[1 + \left(\frac{1 + \beta}{\alpha f} \right) \right] \cdot \left[1 + \left(\frac{2}{f} \right) \right]^{-1} \quad (11.1)$$

The factors α and β define the relative strength of the thermal neutron flux (signal) and of the fast neutron flux (noise) observed at the detector, respectively, and are defined

as $\phi_{th,2} = \alpha \phi_{th,1}$ and $\phi_{fast,2} = \beta \phi_{fast,1}$.¹ The factor f designates the signal-to-noise ratio at the detector, which is used to characterize the difficulty-level of a given experiment. As discussed in Section 3.5, f may be $\gg 1$ for simple experiments, but can be as low as 0.1 for the most challenging situations encountered.

In the case of FRM-II, the majority of neutron scattering experiments are carried out in the neutron guide hall supplied by neutrons from beam tube #1, which is directed on the cold neutron source in the moderator tank (see Figure 8.6 for an illustration). Being the most important experimental device, the following discussion is confined to the conditions encountered in beam tube #1.

To visualize the impact of the cold neutron source (CNS) on the neutron spectrum,² two reference simulations have been performed: one with and one without the model of the CNS present at its position in the moderator tank. Figure 11.1 shows corresponding results for the current HEU design of the reactor. The liquid deuterium, cooled down to 20 K, in the CNS reduces the average energy of the neutrons in the device towards the corresponding thermal energy. The peak wavelength of the neutrons is shifted from about 1.2 Å to a rather flat distribution peaked close to 4 Å (cold neutrons).

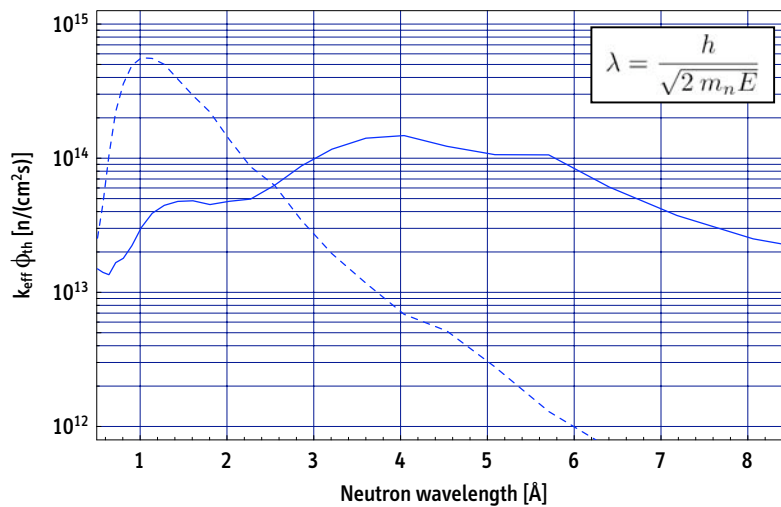


Figure 11.1: Neutron spectrum inside the cold neutron source containing liquid deuterium at 20 K (—). For reference purposes: neutron spectrum at the same position in the moderator tank, but with the CNS removed (- -).

M3O results, MCNP input deck FRMbt4e evaluated with NEWBTAnalysis2.nb

The primary objective of the analysis is to retrieve characteristic neutron spectra in

¹Here, and in the following, the original flux values carry the index 1, while the values of the test case, i.e. of the conversion option, is marked with index 2.

²A simplified models of the CNS is the basis for all calculations. See detail in Section 8.1.5.

beam tube #1 and to evaluate the data with expression (11.1). Two conversion options are compared to the original HEU design:

Monolithic fuel option B3: The conversion option identified in the previous chapter by means of the optimization process is based upon an elongated fuel element and an increased power level of 22 MW. Option B3 has been selected because it minimizes the loss in the thermal neutron flux. Due to the higher power level, however, it can be expected that the fast neutron flux increases simultaneously and may degrade the overall performance of this option.

ANL option 2a: Among the 1999 pre-criticality options, variant 2a has been analyzed in Section 8.3.2 in some more detail. All previous ANL LEU-options were based on a fuel element with an increased outer diameter. Due to this modification, an increased fast neutron flux in beam tube #1 is resulting, which is both due to the proximity of the core and due to the larger relative angle between the core surface and the beam tube (line-of-sight).

In extensive MCNP simulations, neutron spectra are determined inside the beam tube at a distance of 70 cm from the center of the cold neutron source. Figure 11.2 shows corresponding results for option B3 compared to the original HEU design. In order to apply expression (11.1), i.e. to determine α and β values, the thermal neutron flux levels are taken at their respective maxima, while the average neutron flux increase in the energy interval between 10 eV and 10 MeV is used to characterize the fast flux.

Based on the data illustrated in Figure 11.2, the thermal neutron flux of option B3, now measured in the beam tube, remains virtually constant compared to the HEU design. Indeed, it increases by approx. 1%, but due to higher uncertainty of these results (see discussion below) and in order to assess the sensitivity of the results to variations of the parameter α , three values are plotted in Figure 11.3. The average fast flux, which is used to quantify the noise-level expected at the detector, increases by approx. 6%. This value appears reasonable because the power level of the reactor relative to the original design is pushed by 10% (22 MW versus 20 MW). Everything else being equal, this 10%-value should represent an upper bound for the fast flux increase. However, due to the substantially increased heavy metal inventory in the core using monolithic fuel (more than a 6-fold increase), self-shielding of the fast-flux in the core itself can be expected to suppress this effect to some extent, which is confirmed in the simulations.

As the parameters α and β are close to unity for option B3, the calculated variations of the relative acquisition time vary mildly with the difficulty-level of the experiments. Obviously, for high signal-to-noise ratios, variations are directly related to the relative thermal neutron flux only. For typical ($f = 1$) or for difficult experiments ($f < 0.2$), the impact of the increased fast flux component is visible, but the performance variations can still be considered completely irrelevant. In the worst case ($f = 0.1$ and $\alpha = 1.0$), a 3%-increase of the measuring time is predicted by the M³O simulations. For the reference value of $\alpha = 1.01$, relative acquisition times vary between 0.99 for simple experiments and 1.01 for the most difficult ones.

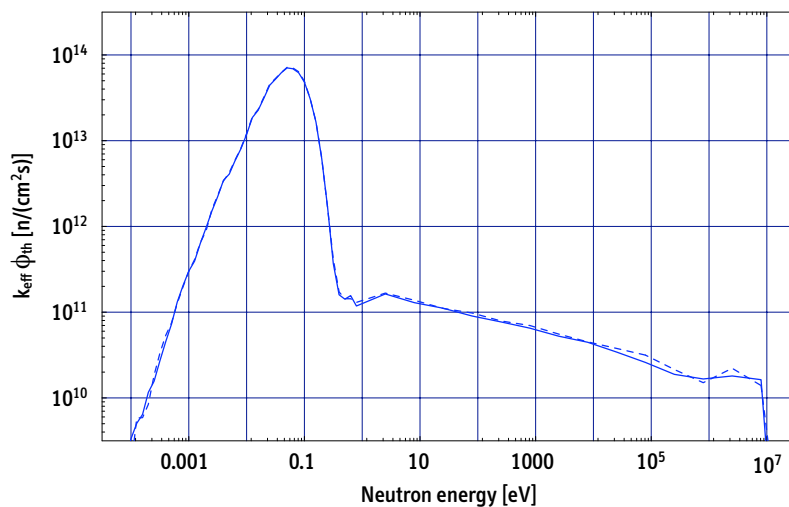


Figure 11.2: Neutron spectrum in beam tube #1 coupled to the simplified model of the cold neutron source. Standard HEU design (—) and monolithic conversion option B3 (- -).

M3O results, MCNP input decks FRMbt4e and FRMbt4e.CQ1 evaluated with NewNTAnalysis2.nb
MCNP 4B/C calculations, 40 million neutron histories for each spectrum

The situation looks much less favorable, if the results for ANL conversion option 2a are compared to those of the HEU design. A fast flux increase by a factor of $\beta = 1.17$ and a decrease of the maximum thermal neutron flux available in the beam tube by a factor of $\alpha = 0.91$ were predicted for this conversion option 2a in Section 8.3.2. Figure 11.4 shows the increase in measurement time to ensure a constant relative error predicted by (11.1). The less favorable performance parameters $\phi_{th,2}$ and $\phi_{fast,2}$ for the ANL design lead, in this case, to a significant degradation of the reactor performance for typical and difficult experimental conditions. The moderate loss of maximum thermal neutron flux of less than 10%, which may have been considered very promising, rises to a 30%-increase in measurement time for difficult experiments. Even though such an increase may still be acceptable, it is certainly more than marginal.

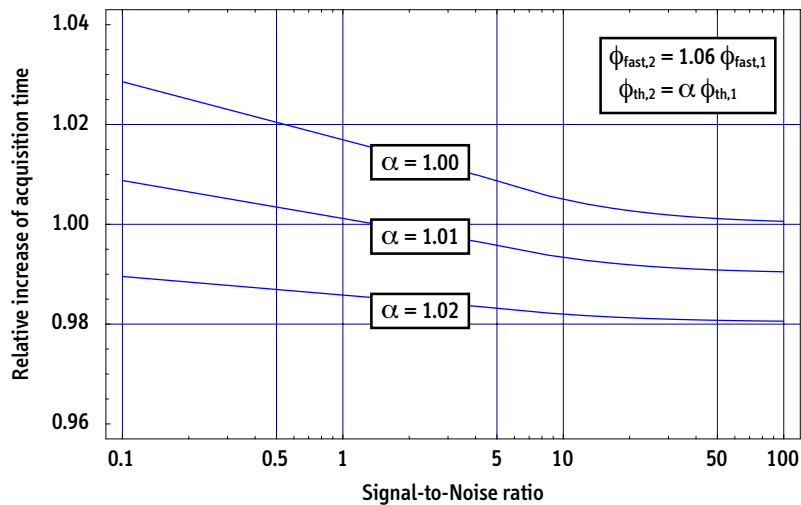


Figure 11.3: Conversion option B3. Relative increase of the acquisition time required for a constant relative error of the [desired] result as a function of the difficulty level of the experiment characterized by the signal-to-noise ratio.

The data presented in this short chapter have to be interpreted with some caution. First, complete design information on the additional components modeled, i.e. information on the cold neutron source and beam tube #1, has been unavailable and simplified models have been used instead. Results will inevitably reflect these simplifications, which may have an influence on the absolute values displayed in Figures 11.1 and 11.2. There is no indication, though, that the *relative* performance of two core options would be affected by using the slightly simplified models of the CNS and the beam tube. The assessment of acquisition time increase, which is solely based on relative results and which is of most interest here, can therefore be assumed to be in good agreement with the actual situation.

A second aspect that limits the predictive power of the results is due to computer-time restrictions and, ultimately, due to the limited scope of this analysis. The neutron spectra in the beam tube have been tallied at a net radial distance of less than 70 cm from the surface of the core. In order to generate results that reproduce the experimental conditions expected at the detector in more detail, one would have to extend the simulations further and track neutron trajectories beyond the moderator tank, beyond the light-water tank, and beyond the concrete shielding of the reactor. In the case of FRM-II, this would require a complete three-dimensional modeling of the reactor up to a radial distance of 4 meters from the core and measurement of neutron spectra in the beam tube at the same distance. Monte Carlo simulations carried out under such conditions are extremely time-intensive, even when used with variance reduction

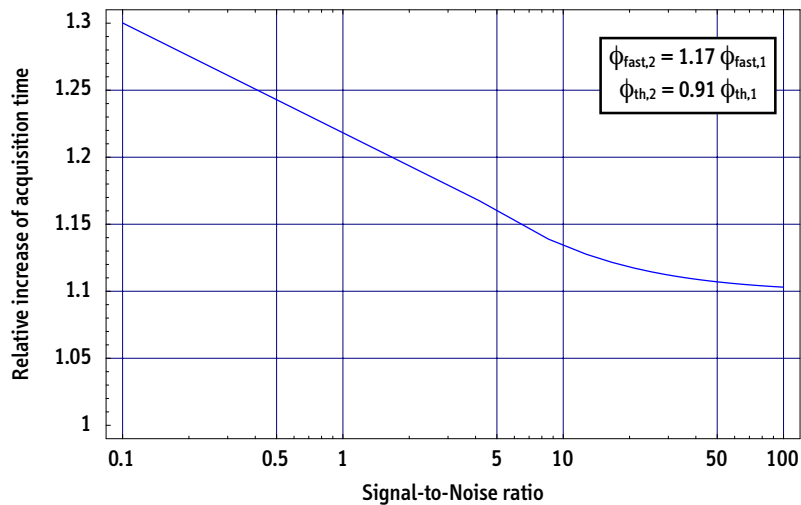


Figure 11.4: 1999 ANL option 2a. Relative increase of the acquisition time required for a constant relative error of the desired result as a function of the difficulty level of the experiment characterized by the signal-to-noise ratio.

techniques. Finally, in order to overcome some shortcomings of computer simulations in general, it would be useful and adequate to re-validate the model and the results against some experimental data (if available).

That said, and in concordance with results obtained in previous chapters, the methodology laid out above, nevertheless demonstrates that special Monte Carlo simulations, combined with criteria to characterize the data, can be used to assess the performance of various core conversion options that go beyond a relatively simple determination of neutron flux levels. In the particular case, the results demonstrate that monolithic fuel (enriched to 27.5% for option B3) could be used in FRM-II with a performance loss that is virtually nil if not even superior to the current HEU design.

Chapter 12

Conclusion and Outlook

The neutronics calculations performed in the context of this thesis confirm that monolithic fuels, which are currently under development, would offer a tremendous potential for the conversion of the remaining HEU-fueled research reactors worldwide. The calculations, however, do also show that the efficient use of low-enriched fuel in those high-flux reactors characterized by very compact cores (single element reactors) would still be a challenging undertaking that requires re-optimization of the neutronics to guarantee optimum performance of the facility.¹

In order to carry out these calculations, advanced computational systems that allow for an extremely accurate modeling of reactor cores are needed. Moreover, for practical reactor conversion analyses, the use of perturbation techniques that employ the original HEU design as a base model may be an effective strategy to re-optimize the core geometry for LEU. Both aspects are among the fundamental features of the system developed in the framework of this thesis, which has been designated M³O (*Mathematica*-MCODE-MCNP-ORIGEN2).

Among the most important advantages of the M³O environment for neutronics calculations belongs the fact that a single integrated system is used to determine all physical quantities relevant to the neutronics of the reactor under investigation. For all simulations executed during the analysis, M³O uses the very same reactor model, which is given by a full three-dimensional MCNP input deck of the core. This strategy guarantees consistent results for all data generated and facilitates comparison and assessment of various core options studied in the process.

¹If, on the other hand, future research reactors are designed for monolithic LEU fuel from the ground up, it is safe to conjecture from the available data that their performance will easily meet the performance of existing HEU-fueled facilities using traditional dispersion-type fuels. Most analysts do however predict a stronger trend towards spallation neutron sources that may inherit the role of high-flux reactors, designed and used for neutron beam research, in the future.

In M^3O , the scientific computing environment *Mathematica* has been used to set-up the core geometries of single element reactors with extremely high accuracy and immediate control of the quality of the model. Full-core burnup calculations are performed using Monte Carlo neutron transport to determine burnup-dependent cross-section and flux data for use with ORIGEN2. The specially designed adaptive cell structure (ACS) formalism provides a set of optimum burnup zones in the fuel. A sensitivity analysis, which has been performed for a generic single element reactor (GSER), demonstrates that the ACS-approach provides maximum detail and accuracy of results with a minimum computational effort, i.e. with a relatively small number of MCNP materials, by focussing the attention of the calculation on the most important segments of the fuel plate.

As indicated, re-optimization of research reactors for use with low-enriched monolithic fuel will strongly benefit from the availability of adequate optimization tools. The linear programming technique combined with MCNP-based perturbation calculations, as proposed in this thesis, is one elegant approach to address this problem. Such optimization strategies can be used both to control important operational constraints, which may be violated when moving from HEU to high-density LEU fuel, and to re-optimize reactor performance for LEU fuel. In the test-cases used to apply and verify the method, the results predicted by the algorithm for the optimized core models (cycle length, thermal neutron flux, power peaking, etc.) were verified in subsequent M^3O calculations and found to be in excellent agreement. Equally important, the use of such re-optimization tools are an essential strategy to guarantee that the lowest possible enrichment level can be identified in those rare cases, where LEU cannot be used due to geometry restrictions.

Being the reactor most difficult to convert, the FRM-II has been analyzed as one important example to explore and demonstrate the potential of monolithic fuels. Even though the primary focus of this thesis is on conceptually new approaches and methodology, not on particular numerical results, the data indicates that an enrichment level of not higher than 32.5% would be sufficient for use with monolithic fuel in FRM-II. M^3O simulations predict a loss of 8–10% in the maximum thermal neutron flux for a re-optimized monolithic fuel option with minor modifications to the core geometry, which include a reduced number of fuel plates and an increased coolant channel width. Enrichment levels of less than 28% would be feasible for FRM-II, if more significant core and reactor modifications were allowed. Here, a second conversion option has been identified, which envisions a 10% increase of thermal power (from 20 MW to 22 MW) and an increased height of the fuel element of 80 cm (instead of 70 cm). Such targeted modifications could be used to further reduce the relative loss in neutron flux, compared to the original HEU design, down to 3–5%. The M^3O neutronics analyses performed for these conversion options guarantee that the original cycle length of the reactor is matched, or even slightly exceeded, and that power peaking is not more pronounced than in the HEU-case.

Finally, in applying a simple performance index, which compares thermal and fast neutron flux levels directly in an important beam tube of the reactor, results obtained for the 22 MW option show that the original performance of FRM-II is reproduced, depending upon the difficulty level of the experiment, with $\pm 1\%$ difference compared to the HEU design. This performance variation would be entirely negligible for all practical purposes.

A much higher enrichment level of about 50% would be necessary in FRM-II to obtain a similar reactor performance with UMo-dispersion fuels, even if these fuels could be qualified for operational conditions encountered in high-flux reactors.

A complementary proliferation risk analysis performed in the framework of this thesis, with particular emphasis on research reactors, demonstrates that an enrichment level of (just less than) 20% in fact minimizes the strategic value of nuclear material associated with research reactor operation. The analysis therefore confirms the usefulness of the traditional LEU/HEU-distinction, and any deviation from this limit inevitably reduces the proliferation resistance of the fuel. In order to be potentially acceptable from a non-proliferation perspective and to be in accord with international conversion objectives, in the particular case of FRM-II, fuel options with the lowest possible enrichment level are clearly favorable and would certainly enjoy the broadest international support, if the LEU-limit cannot be met.

There are various options for further development and improvements of M³O. The system has been designed and optimized for the analysis of single element reactors, based on a very compact cylindrical reactor core. At this stage, the structure of the fuel plate is restricted to uniform meat thickness with discontinuities in the effective uranium density, which is adequate and sufficient for the analysis of the generic single element reactor, for the FRM-II, and theoretically also for the Grenoble high-flux reactor at ILL. For an analysis of the HFIR (Oak Ridge, USA), however, the capability to handle a non-uniform meat thickness is required. This design feature, which could also be a potential design modification envisioned in the conversion process for other reactors, is most relevant in radial direction and used as a measure to reduce power peaking in the fuel. The freed volume in the fuel plate can be filled with inert matrix material or a neutron poison to flatten the power density distribution further.² These extra functionalities could be implemented in a relatively straightforward manner and verified, for example, against performance data available for HFIR.

A second fundamental extension of the current computational capabilities relates to the adaptive cell structure (ACS) formalism for burnup calculations. With the current version, only static structures, which are determined at beginning-of-life, are used during the simulation of the entire irradiation cycle. If control rod movements and particular

²In addition, HFIR uses two concentrically arranged fuel elements, each with a characteristic design of the involute-shaped fuel plates. This design peculiarity would require a two-step approach to obtain a complete base MCNP model, and an adequate processing in all following M³O simulations.

arrangements of burnable poisons are included in the simulations, the profiles would cease to be axially symmetric and evolve during the cycle. Various approaches are conceivable to take into account these additional details with a dynamic ACS concept.

The linear programming technique has been applied to a test-case (FRM-II) with some core design variables held constant to account for the operational status of the facility and related constraints (power level, outer core radius, etc.). For a more general analysis of the neutronics of single element reactors, it would be valuable to use this optimization tool with the complete set of independent core design variables being allowed to vary. Again, fundamental aspects of the neutronics and reactor performance could be studied using the generic single element reactor. In addition, the FRM-II could be reconsidered for use with LEU fuel by relaxing some of the constraints that were imposed in the present analysis. Various core modifications are conceivable. From this supplementary analysis, one could determine, for instance, which modifications would be necessary to enable the use of LEU in this particular reactor.

A final, more general approach to further develop the analysis performed in the context of this thesis would be to extend the range of the M^3O simulations and to track neutrons beyond the central reactor core structures towards the experimental devices and instruments connected to the beam tubes. Calculations of that extent would certainly reach the current limits of computer simulations and validation against experimental data would be strongly indicated. One could then start to consider specific types of instruments and experiments in order to improve the quality of the theoretical predictions further.

Ultimately, having available reliable and detailed results obtained in comprehensive computer simulations will strongly encourage operators to proceed with the conversion process, which may be under consideration for a given facility. Accordingly, these simulations — and the computational tools to perform them, such as the one developed and presented in the context of this thesis — may directly contribute to the ultimate objective of phasing-out the use of highly enriched uranium in the nuclear fuel cycle at the earliest possible date.

Appendix A

Characteristics of Enriched Uranium Relevant to Its Weapon-Usability

The following discussion summarizes some important characteristics of enriched uranium (highly enriched and low-enriched) that are relevant in the context of its weapon-usability. Two main aspects are discussed: these are the critical mass and the neutron emission rate of uranium of a given composition. In conjunction with the analysis of the strategic value of enriched uranium presented in the main text (Chapter 2), these considerations clearly demonstrate the fundamental difference between highly enriched and low-enriched uranium. To conclude this appendix, highly-enriched (weapon-grade) uranium is compared to its traditional counterpart plutonium, i.e. to the second major fissile material used in nuclear weapons. In many respects, both materials have ‘complementary’ properties and no single most ‘favorable’ material from the proliferator’s perspective can be identified. Historically, both materials have played central roles in most nuclear-weapon programs. Vice versa, from a nonproliferation perspective, both materials present unique challenges regarding management, control, and disposition.

A.1 Critical Mass

The critical mass of a nuclear material is generally considered the single most important property of the material with respect to its weapon-usability and weapon-relevance. By definition, a critical mass corresponds to precisely the amount of material in a defined configuration that is required to maintain a self-sustaining neutron chain reaction. In general, the critical mass represents a reasonable estimate of the amount of material required to construct a nuclear weapon or explosive device using material of a

given composition. Figure A.1 shows the critical mass of a beryllium-reflected uranium sphere as a function of uranium-235 enrichment. The reflector thickness is 15 cm and greatly reduces the absolute values compared to the corresponding unreflected or bare critical masses shown in Chapter 2, Figure 2.1. A more comprehensive set of data is listed in Table A.1, where critical mass values of uranium for several enrichment levels and reflector thicknesses are listed. For reference purposes, data for typical plutonium compositions are also included.

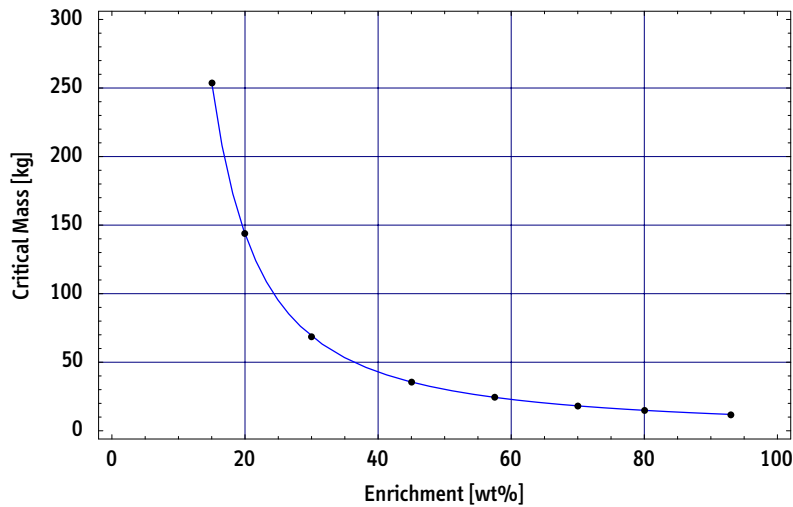


Figure A.1: Critical mass of a beryllium-reflected uranium sphere as a function of the uranium-235 enrichment. MCNP 4B/C simulations at 300 K using ENDF/B-VI cross-section libraries. Reflector thickness is 15 cm. Assumed value of uranium density is 19 g/cm³. Enrichment is given in weight percent (wt%) for a simple binary mixture of U-235 and U-238.

As pointed out in Chapter 2, the critical mass of uranium increases sharply with decreasing enrichment, which is relevant to the weapon-usability of uranium for a variety of reasons. Most importantly, a low critical mass simplifies the assembly process of the final supercritical configuration, a process that is extremely time-critical and requires extreme acceleration of the previously subcritical components.¹ A low critical mass simultaneously affects other properties that are relevant to a material's weapon-usability. One of these aspects, the total neutron emission rate, is discussed as an example below.

¹Self-evidently, a low critical mass also reduces the amount of material that has to be produced, diverted, or otherwise acquired. It also facilitates transportation, concealment, etc. of the material. See Table A.4 for a comparison of the properties of HEU and plutonium.

		Reflector Thickness			
		Bare	5 cm	10 cm	15 cm
Uranium Enrichment	10 wt%	very large	very large	1435.0 kg (\varnothing 52.4 cm)	753.0 kg (\varnothing 42.3 cm)
	15 wt%	1351.0 kg (\varnothing 51.4 cm)	758.3 kg (\varnothing 42.4 cm)	426.5 kg (\varnothing 35.0 cm)	253.8 kg (\varnothing 29.4 cm)
	19.75 wt%	782.2 kg (\varnothing 42.8 cm)	402.9 kg (\varnothing 34.3 cm)	220.7 kg (\varnothing 28.1 cm)	143.8 kg (\varnothing 24.4 cm)
	30 wt%	367.4 kg (\varnothing 33.3 cm)	171.2 kg (\varnothing 25.8 cm)	100.3 kg (\varnothing 21.6 cm)	68.7 kg (\varnothing 19.0 cm)
	45 wt%	184.7 kg (\varnothing 26.5 cm)	80.5 kg (\varnothing 20.1 cm)	49.6 kg (\varnothing 17.1 cm)	35.6 kg (\varnothing 15.3 cm)
	70 wt%	87.2 kg (\varnothing 20.6 cm)	36.5 kg (\varnothing 15.4 cm)	23.7 kg (\varnothing 13.4 cm)	18.2 kg (\varnothing 12.2 cm)
	93 wt%	53.3 kg (\varnothing 17.5 cm)	22.3 kg (\varnothing 13.1 cm)	14.9 kg (\varnothing 11.4 cm)	11.7 kg (\varnothing 10.6 cm)
Reactor-grade plutonium		14.6 kg (\varnothing 11.4 cm)	6.92 kg (\varnothing 8.86 cm)	5.29 kg (\varnothing 8.10 cm)	4.58 kg (\varnothing 7.72 cm)
Fuel-grade plutonium		13.2 kg (\varnothing 11.0 cm)	6.24 kg (\varnothing 8.56 cm)	4.76 kg (\varnothing 7.82 cm)	4.10 kg (\varnothing 7.44 cm)
Weapon-grade plutonium		11.5 kg (\varnothing 10.5 cm)	5.53 kg (\varnothing 8.22 cm)	4.26 kg (\varnothing 7.54 cm)	3.71 kg (\varnothing 7.20 cm)

Table A.1: Critical masses of uranium at various enrichment levels and thicknesses of the beryllium reflector. MCNP 4B/C calculations at 300 K using ENDF/B-VI cross-section libraries. Uranium compositions are assumed to be binary mixtures of U-235 and U-238. Values for reactor-grade, fuel-grade, and weapon-grade plutonium are included for reference purposes. For plutonium isotopics see Table A.2. Uranium and plutonium densities are 19.05 g/cc and 19.00 g/cc, respectively. Note that the plutonium may need to be stabilized in the δ -phase, which is characterized by a lower density of the metal.

	Weapon-Grade Plutonium	Fuel-Grade Plutonium	Reactor-Grade Plutonium
Pu-238	0.05%	1.20%	1.80%
Pu-239	93.60%	70.90%	59.00%
Pu-240	6.00%	15.40%	23.00%
Pu-241	0.30%	10.60%	12.20%
Pu-242	0.05%	1.90%	4.00%

Table A.2: Typical plutonium isotopic compositions [NEA/OECD, 2003, p. 34].

Composition of fuel-grade plutonium (Pu-239 content approx. 70%) based on typical values obtained in this study

A.2 Neutron Emission Rate

A second important property of a nuclear material relevant to its weapon-usability is the neutron emission rate, mainly caused by spontaneous fission events in uranium-238 or in any of the relevant plutonium isotopes. As will be briefly discussed below, there are at least two basic assembly techniques for a nuclear weapon (gun-type and implosion) and both require a characteristic assembly-time to reach the final supercritical configuration of the weapon. Assembly-times are on the order of 1 ms for gun-type and 1 μ s for implosion, respectively. A spontaneous fission event during the assembly process may lead to a premature initiation of the neutron chain reaction and ultimately cause a so-called ‘fizzle’ of the device. Table A.3 lists the reference emission rates for the main uranium and plutonium isotopes taken from [Magill, 2003].

Nuclide	Half-Life	Specific Activity	Isotopic Power	Spont. Fission Rate
U-234	2.46E+05 y	2.30E+08 Bq/g	1.79E−04 W/g	3.98E−03 1/(g s)
U-235	7.04E+08 y	8.00E+04 Bq/g	5.99E−08 W/g	5.60E−06 1/(g s)
U-236	2.34E+07 y	2.39E+06 Bq/g	1.75E−06 W/g	2.30E−03 1/(g s)
U-238	4.47E+09 y	1.24E+04 Bq/g	8.50E−09 W/g	6.78E−03 1/(g s)
Pu-238	8.78E+01 y	6.34E+11 Bq/g	5.67E−01 W/g	1.20E+03 1/(g s)
Pu-239	2.41E+04 y	2.30E+09 Bq/g	1.93E−03 W/g	7.11E−03 1/(g s)
Pu-240	6.57E+03 y	8.39E+09 Bq/g	7.06E−03 W/g	4.78E+02 1/(g s)
Pu-241	1.44E+01 y	3.82E+12 Bq/g	3.28E−03 W/g	9.18E−04 1/(g s)
Pu-242	3.74E+05 y	1.46E+08 Bq/g	1.17E−04 W/g	8.04E+02 1/(g s)

Table A.3: Properties of the most important uranium and plutonium isotopes. Data from [Magill, 2003]. Isotopic power includes contributions from α -, β -, and γ -decay.

During the development of the first nuclear weapons within the U.S. *Manhattan Project*, it became apparent that plutonium could not be used in the conceptually obvious and simple gun-type method, in which a subcritical projectile of fissile material is propelled towards a fissile target (Figure A.3). Due to the low spontaneous fission rate, only highly enriched uranium is an obvious candidate for this assembly technique, characterized by a total duration of approximately one millisecond. As can be inferred from Table A.3, pure Pu-239 requires an assembly speed that is higher by at least three orders of magnitude than is required for U-235. Assembly-times of close to 1 μ s can only be achieved using special high-explosives with an implosion-type design, in which a sphere or spherical shell of material is spherically imploded and compressed beyond its normal theoretical density.

The impact of reduced uranium enrichment levels on the weapon-usability of the material in a gun-type device is discussed in the following. For reduced uranium enrichment levels, neutron emission rates increase due to the higher fractional *and* absolute content of uranium-238 (cf. Table A.3). Eventually, a simple gun-type assembly of a uranium-device might become difficult or even impossible, assuming that the proliferator is not very experienced in the design of nuclear weapons. As the spontaneous fission process is a stochastic process, fundamental laws of probability calculus apply. The probability that k events occur in a time interval t for a process characterized by a decay constant λ is described by the Poisson distribution.

$$p(\lambda, k, t) = \left[\frac{(\lambda t)^k}{k!} \exp(-\lambda t) \right] \quad (\text{A.1})$$

In the present context, one is interested in the probability that no spontaneous fission event ($k = 0$) occurs in a given time interval Δt or, vice versa, in the failure probability p^* that at least one event occurs during this period of time.

$$p^*(\lambda, \Delta t) = 1 - \exp(-\lambda \Delta t) \quad (\text{A.2})$$

Here, the decay constant λ is given by the specific spontaneous fission rate as listed in Table A.3 multiplied by the corresponding mass of the material. The amount of material required for a simple gun-type device is on the order of one bare critical mass (see next section) and corresponding values are taken from Table A.1.

Figure A.2 shows the probability that at least one spontaneous fission event occurs in a given period of time for various binary mixtures of U-235 and U-238. These include LEU (19.75% enrichment), 45%-enriched material, and weapon-grade uranium (WGU, 93% enrichment). In addition, results are listed for HEU irradiated to a typical burnup of 50%.² The figure clearly illustrates that the chances for a neutron-free millisecond are very high (about 97.5%) if weapon-grade uranium is used in a gun-type device; but also that the chances are extremely low if low-enriched uranium is used instead (about 1.4%). Even a reduction of the assembly time down to 0.5 ms does not significantly improve the performance of the LEU, as the probability of a spontaneous fission event is still about 88% during that time-interval. Figure A.2 also demonstrates that the spontaneous fission rate in a bare critical mass of material enriched to 45% is already qualitatively different from the low-enriched material. During a time-interval of 1 ms, the probabilities of observing or not observing a spontaneous fission event are nearly identical. Clearly, using 45%-enriched material in conjunction with the gun-type design would deliver a highly unpredictable device, which would certainly be unacceptable to a nuclear-weapon state; but the material could be adequate for a low-tech proliferator

²Assumed simplified isotopics of this material are: 76.2% U-235, 13.7% U-236, and 10.1% U-238.

under certain circumstances, i.e. if no other material or design were available. Finally, the figure also illustrates that the emission rate of uranium extracted from irradiated HEU fuel with an assumed U-235 content of 76.1% is very close to the values of original WGU. The material would therefore be usable in a simple gun-type device.³

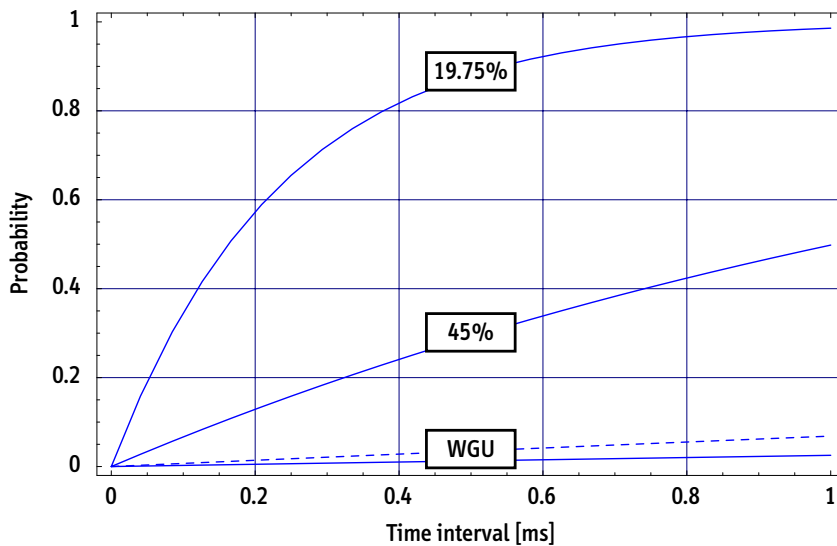


Figure A.2: Probability that at least one spontaneous fission event occurs in a given time interval Δt in one bare critical mass of uranium enriched to 93%, 45%, and 19.75%. Dashed line represents irradiated HEU research reactor fuel at 50% burnup.

0.5 ms: 1.3% (HEU), 3.5% (FGU), 29.2% (45%), and 88.1% (LEU) and 1.0 ms: 2.5% (HEU), 6.8% (FGU), 49.8% (45%), and 98.6% (LEU)

The preceding discussion highlights the fact that the critical mass alone is not a sufficient criterion to assess the weapon-usability of a nuclear material. The neutron emission rate — but also the heat rate, metallurgical properties, etc. — are additional crucial aspects in this regard, and it is plausible to assume that there are further relevant properties which are not *a priori* obvious or accessible in the open literature. This brief analysis, however, does demonstrate that there are important qualitative differences between HEU and LEU. These are particularly relevant if one is concerned about the feasibility of crude nuclear weapons or explosive devices based on the gun-type design, or even of so-called improvised nuclear devices (IND's).⁴ LEU is clearly not suitable for these scenarios.

³Note that the material used in the Hiroshima bomb was reportedly enriched to 80% on average.

⁴See for instance [Mark et al., 2002]. Alvarez [1987], a participant in the *Manhattan Project*, writes in this context: “With modern weapons-grade uranium, the background neutron rate is so low that terrorists, if they had such material, would have a good chance of setting off a high-yield explosion simply by dropping one half of the material onto the other half. Most people seem unaware that if separated U-235 is at hand it’s a trivial job to set off a nuclear explosion [...]” (p. 125).

A.3 HEU in Nuclear Weapons

The amount of HEU, or of any weapon-usable material for that matter, needed for the construction of a nuclear weapon or explosive device strongly depends upon the skills of the proliferator; no universally valid figure for this amount can be specified.

Most generally, for a simple gun-type device, more than one critical mass is needed to achieve supercriticality because no significant compression of the fissile material takes place. Assuming a reflected configuration and consistent with the data in Table A.1, a value of 50–60 kg of HEU is usually cited. The Hiroshima-bomb, a design that had never been tested before and which can be assumed to be rather conservative (Figure A.3), contained 62–64 kg of highly enriched uranium at an average enrichment of 80%. Reportedly, the South-African gun-type weapon contained a similar amount of HEU.⁵

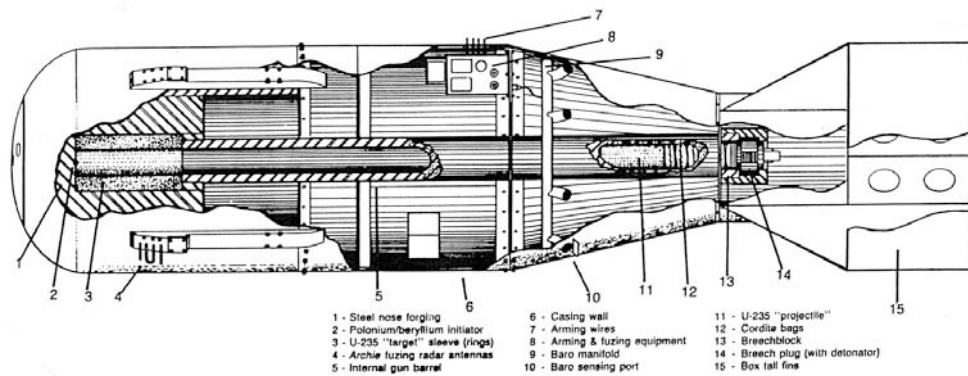


Figure A.3: Drawing of the nuclear weapon (MK-1, "Little Boy") that destroyed Hiroshima on August 6th, 1945. Figure published in [Hansen, 1988]. See [RDD-7, 2001] for a complete list of declassified U.S. nuclear-weapon-related information.

Copyright by C. Hansen, reprinted with permission, courtesy of E. Hansen (private communication, October 15, 2004)

Highly enriched uranium does not have to be used with the simple, but inefficient gun-type design. In fact, the technically more challenging implosion-type design, which was originally invented for use with plutonium, is presumably easier to apply for use with HEU. Such an approach benefits from the compression of the fissile material (by a factor of two or more beyond theoretical density) and reduces the amount of HEU

⁵Note however, that more sophisticated gun-type weapons in the U.S. nuclear weapon stockpile were extremely of low-weights, which might be an indication that fundamental design improvements are feasible. For instance, the W33 warhead, an artillery shell developed in the 1950s, had an approximate total weight of only 100 kg compared to the 4000 kg of the Hiroshima bomb. A number of early weapon-designs were based on the gun-type method and present in the active U.S. stockpile until the 1980s. See [Cochran et al., 1984] for further information.

needed in the device, while pre-ignition during the assembly process becomes a far less serious concern. Reportedly, early Chinese and current Pakistani nuclear weapons have followed such a design approach.

The International Atomic Energy Agency (IAEA) defines a value of 25 kg of HEU, i.e. of uranium enriched to at least 20% in the isotope U-235, as a so-called *significant quantity* (SQ). The concept is based on the assumption that some material is lost during the manufacturing process of the device, and may serve as an upper limit for the quantity of HEU needed to construct a first-generation implosion-type device.⁶

Various analysts, including former weapons designers, have emphasized the fact that the actual amount of HEU required to construct a nuclear weapon is *much* lower than the 25 kg limit set by the IAEA. For instance, Willrich and Taylor [1974] define numbers for ‘strategically significant’ quantities of fission explosive materials and use values of 11 kg for highly enriched uranium and of 4 kg for plutonium. Consistent with these numbers, in 1994, the U.S. Department of Energy declassified the fact that “[h]ypothetically, a mass of 4 kilograms of plutonium or uranium-233 is sufficient for one nuclear explosive device” [RDD-7, 2001, Section L, §33]. With reference to the data summarized in Table A.1, it is therefore plausible to assume that an amount of 10–15 kg of HEU is sufficient for the construction of a nuclear weapon or explosive device.⁷

The present discussion primarily focusses upon (pure) fission weapons and the potential use of fissile materials in this weapon-type. This is the primary proliferation concern for nuclear materials of any type. Note however that HEU may also play a unique role in the design of thermonuclear weapons: In the thermonuclear stage (i.e. the secondary) of an advanced nuclear weapon, significant quantities of uranium are located in the vicinity of the fusion fuel, a component usually called the pusher. When high energy neutrons emerge from the DT-fusion reactions, the uranium is fissioned and contributes significantly to the total yield of the weapon. Even though natural uranium can be used under these conditions, HEU is preferred due to its higher fission probability as shown in Table A.4. Apparently, weapon designers in the U.S. shifted from natural uranium to HEU when the latter became available in sufficient quantities in the 1980s [Alvarez and Sherman, 1985].

⁶As already referenced in Section 2.2.2, the significant quantity is defined as “the approximate amount of nuclear material for which the possibility of manufacturing a nuclear explosive device cannot be excluded. Significant quantities take into account unavoidable losses due to conversion and manufacturing processes and should not be confused with critical masses” [IAEA, 2002, §3.14].

⁷Cochran and Paine [1995] have estimated the amounts of plutonium and highly enriched uranium needed for pure fission weapons. Depending upon the technical capability of the proliferator, they conclude that an HEU mass between 4 kg (high-tech) and 14 kg (low-tech) is sufficient to construct an implosion-type nuclear weapon with a nominal yield of 10 kt(TNT).

	Total	Fission	Capture	(n,xn)	F2T-Ratio
U-235	5.865 b	2.056 b	$\sim 10^{-7}$ b	0.585 b	35.06%
U-238	5.805 b	1.136 b	$\sim 10^{-3}$ b	1.260 b	19.57%
Pu-239	5.990 b	2.338 b	$\sim 10^{-8}$ b	0.302 b	39.03%

Table A.4: Cross-sections of uranium-235, -238 and plutonium-239 for 14 MeV neutrons.

F2T (fission-to-total) ratio is used to roughly quantify 'efficiency' of material

A.4 Plutonium versus Highly Enriched Uranium

The characteristics relevant in the context of nuclear-weapon usability and proliferation risks are remarkably different for plutonium and highly enriched uranium. Table A.6 juxtaposes some proliferation-relevant general characteristics of these direct-use materials. These characteristics are primarily applicable to civilian and excess military inventories.⁸ In Table A.6, proliferation-relevant characteristics are assigned different categories, which comprise of: accessibility of the material via production or diversion/theft; observability of the acquisition process; weapon-usability of the material once it has been acquired; and aspects related to the disposition of excess material.

In order to acquire plutonium or highly enriched uranium, the material has to be either produced or acquired via diversion or theft. As discussed in Chapter 2 and in the following appendix, plutonium production requires operation of a nuclear reactor containing natural or depleted uranium in the target or fuel material. Clandestine reactor construction and operation typically are difficult to conceal and are bound to be detected sooner or later. Once the fuel is irradiated, however, plutonium extraction via reprocessing is considered a relatively simple process that has been described in detail in the open literature. Production of highly enriched uranium is considered a much more challenging undertaking, especially if based on the modern and efficient gas centrifuge process. Even then, enrichment may be preferable for a proliferator because no reactor technology is needed *and* the operation of a clandestine centrifuge facility is virtually impossible to detect with remote-sensing techniques.

Little can be said about characteristic differences regarding the acquisition of plutonium or HEU via diversion or theft. Both materials should be equally well safeguarded and protected. Nevertheless, as a result of the former and ongoing operation of HEU-fueled research reactors worldwide, the number of sites where fresh or slightly irradiated HEU

⁸For obvious reasons, the data listed in the table hardly apply to military inventories of fissile materials (located, for instance, in deployed nuclear weapons), where an 'assessment of proliferation risks' holds very little relevance.

is stored can be assumed to be still significantly higher than the number of sites with kilogram-quantities of (separated) plutonium. In addition, once a given stock of special nuclear material is known to be diverted or stolen, it is generally possible to remotely detect gamma and neutron emissions originating from plutonium (even with passive methods), while corresponding emission rates of HEU are virtually inexistent.

Once a sufficient amount of fissile material has been acquired by a proliferator, the overall utility or usability of plutonium or highly enriched uranium become relevant. Again, Table A.6 illustrates that both materials present unique challenges in that respect. HEU is relatively easy to handle and process: other than guaranteeing sub-criticality at all times, no particular precautions need to be taken; while plutonium requires remote-handling for most processing steps due to its elevated radiotoxicity. As has been discussed above, designing an HEU-based nuclear explosive device can be considered relatively straightforward, if substantial amounts of material are available (50–60 kg). Plutonium inevitably requires a more complex weapon-design, but once this technical barrier is overcome, plutonium poses particular proliferation risks for at least two reasons: almost any plutonium composition can be considered weapon-usable, and significantly less material is sufficient for a nuclear weapon or explosive device (5–10 kg).⁹

Historically, no nuclear-weapon material can be singled out as being ‘superior’ for use in nuclear (fission) weapons. Indeed, most nuclear-weapon states have procured for themselves large quantities of both materials and, reportedly, most advanced nuclear weapons contain both weapon-grade plutonium *and* uranium.¹⁰ Table A.5 lists the initial choice of fissile material for a number of nuclear-weapon states (current, former, or potential) and tentatively indicate the dominating motivation for the respective choices.

A new dimension of proliferation-relevant characteristics associated with the management of nuclear materials emerged with the nuclear disarmament process of the 1990s. As a result of these achievements, both the Former Soviet Union and the U.S. declared large amounts of weapon-grade materials (plutonium and uranium) excess to their respective military ‘needs’ and started to search for and negotiate adequate disposition strategies.

In the case of HEU, the disposition option is obvious and consists in down-blending the material to LEU. This process is both irreversible and economically attractive because the material can be subsequently sold for use in commercial power reactors.¹¹ Unfortu-

⁹For typical plutonium compositions, see Table A.2. The weapon-usability of reactor-grade plutonium is discussed in [Kankeleit et al., 1989] and [Mark, 1993].

¹⁰Reported for nuclear weapons of U.S. design, for instance, in [Cochran et al., 1984, p. 24].

¹¹Through the U.S.-Russia HEU Agreement of 1993, Russia has sold 500 MT of weapon-grade HEU (down-blended to LEU) to the U.S. Consistent with the 20-year time-frame of the agreement, about 50% of the material has been down-blended and delivered to date.

nately, and as already discussed in Section 2.3, there is also an incentive to hedge excess HEU inventories for use in naval reactors (mostly submarines) or even potentially for use in research reactors. Conversely, there is no reason to maintain larger plutonium inventories in the military sector once they become excess. Nevertheless, the plutonium disposition process is much more complicated because no obvious and optimum disposition option exists. Major studies were performed in the U.S. and elsewhere and evaluated the advantages and disadvantages of a broad spectrum of possibilities,¹² but not much progress has been made since then.

	HEU	Pu	Year	Dominating motivation for choice
United States	●	●	1942	Urgency, technological uncertainty, extensive resources
Soviet Union	●	●	1945	Urgency, extensive resources
United Kingdom		●	1945	Technological accessibility
France		●	1958	Technological accessibility
China	●	○	1960	Transfer of critical equipment from the Soviet Union
Israel		●	1960	Transfer of critical equipment from France
India		●	1964	Transfer of critical equipment from Canada and the U.S.
South Africa	●		1970	
Pakistan	●	○	1976	Technological accessibility
Iraq	○	○	1981	Technological accessibility
North Korea	○	○	2002	Technological accessibility

Table A.5: Proliferant's initial choice of fissile material. Table adapted from [Ullom, 1994]. Bullets (●) indicate successful proliferation, circles (○) represent attempts that have been stopped before assembly of an operational nuclear weapon. The year listed indicates the stage of the corresponding nuclear-weapon program when the fissile material was chosen.

¹²The most influential studies, which also first introduced the so-called *Spent Fuel Standard*, are [National Academy of Sciences, 1994, 1995]. The possibility of plutonium elimination in a dedicated plutonium-burner reactor, was studied in [Glaser, 1998]. The potential use of inert matrix fuels to burn reactor-grade or weapon-grade plutonium in commercial pressurized-water reactors is evaluated in more detail in [Pistner, 2005].

	Plutonium	Highly enriched uranium
Accessibility I (Production)	Access to (natural) uranium	Access to (natural) uranium
	Availability of a reactor	No reactor technology required
	Fuel reprocessing (simple)	Availability of enrichment technology
Observability I	Thermal signature of reactor	Some enrichment processes detectable
	Krypton-85 emissions detectable	Centrifuges impossible to detect
Accessibility II (Diversion and theft)	Large (civilian) inventories	Large (civilian) inventories
	Few owners and storage sites	Present at higher number of locations
Observability II	Radioactive signature detectable	HEU impossible to detect remotely
Utility (Material properties)	High radiotoxicity	Easy to handle and process
	Almost any composition usable	Very high enrichment favorable
	Low critical mass	2–3× more material required
	Implosion design required	Gun-type design possible
	Americium buildup	Chemically very stable
Disposition	No obvious solution	Irreversible blend-down to LEU
	No alternative military application	Use in naval propulsion reactors
	Rationality of civ. use controversial	Phase-out of civilian use possible
	High costs (delays)	Economically attractive

Table A.6: Proliferation-relevant characteristics of separated plutonium and highly enriched uranium. With the exception of material production (Accessibility I), criteria are primarily applicable to civilian and excess military inventories. Shaded entries are more problematic from a nonproliferation perspective. See text for further explanations.

This page intentionally blank

Appendix B

Plutonium Production in Research Reactors

The purpose of this Appendix is to provide the data basis required to assess the *strategic value* of nuclear material used or produced in a research reactor. In practice, a proliferator has the option to use fresh or irradiated stocks of enriched uranium fuel with the intention of fabricating an HEU-based weapon. Alternatively, the proliferator may also plan to extract plutonium from the spent fuel and may even optimize reactor operation for maximum plutonium production. Ultimately, the attractiveness of these options depends upon a variety of external factors, which are beyond the scope of this technical analysis. In particular, the availability of required infrastructure to produce and process nuclear material (enrichment or reprocessing) are important factors that determine the net strategic value of a material.

In the following, plutonium production in a typical MTR-type reactor fueled with enriched uranium is estimated in order to quantify the overall proliferation risks associated with the nuclear material required for or accumulated during operation of such a facility. At the end of this section, these results are also compared briefly to a dedicated campaign. The analysis below makes no distinction between weapon-grade versus reactor-grade plutonium because all compositions can be considered weapon-usable.¹

Before determining plutonium buildup with a more detailed approach below, a very simple estimate of the plutonium production in research reactor fuel of different enrichment levels is used to clarify the principal effects.

Assume N_0 to be the total initial uranium inventory in the core and ϵ to be the enrichment level of the fuel. If second-order production terms are neglected, a simple differential equation describes the uranium-235 consumption in the core once the

¹See for instance [Kankeleit et al., 1989] or [Mark, 1993].

spectrum-averaged one-group cross-section $\langle\sigma_5\rangle$ for neutron absorption in uranium-235 is known.

$$\dot{N}_5(t) = -\phi \langle\sigma_5\rangle N_5(t) \quad \text{and} \quad N_5(t) = \epsilon N_0 \exp(-\phi \langle\sigma_5\rangle t) \quad (\text{B.1})$$

The burnup B is defined as the fraction of the initial uranium-235 inventory consumed during irradiation of the fuel. U-235 consumption is mainly due to both fission and neutron capture in the isotope. For a specified target burnup B of the fuel, a simple relation characterizes the situation at end-of-life (EOL) of the core.

$$N_5(t_{\text{EOL}}) = \epsilon N_0 \exp(-\phi \langle\sigma_5\rangle t_{\text{EOL}}) \stackrel{!}{=} (1-B) \epsilon N_0$$

Solving this equation for (ϕt_{EOL}) yields an expression, which can be used below to substitute the *a priori* unknown fluence with the burnup specified by the user.

$$(\phi t_{\text{EOL}}) = -\frac{\log(1-B)}{\langle\sigma_5\rangle} \quad (\text{B.2})$$

In all practical situations, the fertile uranium-238 inventory $N_8 = (1-\epsilon)N_0$ will be large compared to the amount of plutonium generated in the fuel $N_9 \ll N_8$. The uranium-238 inventory can therefore be assumed constant. With this assumption, the plutonium-239 production term is also constant and a simplified differential equation, which does not explicitly consider the intervening beta decays of uranium-239 and neptunium-239, is given by:

$$\dot{N}_{\text{Pu}}(t) \approx -\phi \langle\sigma_9\rangle N_{\text{Pu}}(t) + \phi \langle\sigma_8\rangle N_8 \quad (\text{B.3})$$

Here, $\langle\sigma_9\rangle$ and $\langle\sigma_8\rangle$ are the spectrum-averaged fission cross-section of plutonium-239 and the capture cross-section of uranium-238, respectively.² A solution for this equation with the initial condition $N_9(0) = 0$ is given by:

$$N_{\text{Pu}}(t) = \frac{\langle\sigma_8\rangle}{\langle\sigma_9\rangle} (1-\epsilon)N_0 \left[1 - \exp(-\langle\sigma_9\rangle(\phi t)) \right] \quad (\text{B.4})$$

In substituting the fluence (ϕt) with the expression from (B.2), a first-order estimate of the burnup-dependent total annual plutonium production in the reactor can be given.

²The fission cross-section of Pu-239 is used instead of its total absorption cross-section in order to estimate the total plutonium buildup.

$$\text{Pu}(\text{eff}) = \frac{\langle \sigma_8 \rangle}{\langle \sigma_9 \rangle} (1 - \epsilon) N_0 \left[1 - \exp \left(\frac{\langle \sigma_9 \rangle}{\langle \sigma_5 \rangle} \log(1 - B) \right) \right] \quad (\text{B.5})$$

With representative estimates of the spectrum-averaged cross-sections for uranium-235 absorption, uranium-238 capture, and plutonium-239 fission, (B.5) can be used to estimate plutonium production rates once the total uranium demand of the reactor is specified. The required cross-sections have been obtained in MCNP simulations, but ordinary tabulated values would be almost equally satisfactory. Note that the absolute values of the cross-sections are irrelevant, since only their ratios $\langle \sigma_8 \rangle / \langle \sigma_9 \rangle$ and $\langle \sigma_9 \rangle / \langle \sigma_5 \rangle$ determine plutonium buildup and concurrent consumption in the fuel.³

Results of plutonium production estimates in a generic 30 MW MTR-type reactor are summarized in Table B.1 for four different enrichment levels (10%, 19.75%, 45%, and 93%) and three different burnup values (20%, 40%, and 60%). The total annual uranium demand has been determined based on the assumption that the reactor is operated 300 days per year, which is equivalent to a total annual exposure of the fuel of 9000 MWd(th). The uranium-235 consumption is fixed at 1.2 g/MWd(th) and includes losses due to fission and capture processes.⁴

Fuel Enrichment	10%	19.75%	45%	93%	
U-238 Capture	1.3 b	1.7 b	2.9 b	6.8 b	
U-235 Absorption	55 b	55 b	60 b	60 b	
Pu-239 Fission	100 b	100 b	100 b	100 b	
Uranium Demand	B = 20%	540 kg	273 kg	120 kg	58.1 kg
	B = 40%	270 kg	137 kg	60 kg	29.0 kg
	B = 60%	180 kg	91 kg	60 kg	19.4 kg
Plutonium Production	B = 20%	2.1 kg	1.2 kg	0.60 kg	0.09 kg
	B = 40%	1.9 kg	1.1 kg	0.55 kg	0.08 kg
	B = 60%	1.7 kg	1.0 kg	0.50 kg	0.07 kg

Table B.1: Simple estimate of the effective plutonium production for a 30 MW MTR-type research reactor. Based on expression (B.5). Spectrum-averaged cross-sections determined in MCNP simulations.

Obviously, total plutonium production increases for lower enrichment levels. In addition, net production also increases with lower average burnup because more fresh

³As shown in Table B.1, only uranium-238 capture is sensitive to the enrichment of the fuel used in the given MTR-type geometry.

⁴Typically, 1.0 g/MWd(th) is lost to fission and 0.2 g/MWd(th) to capture.

uranium fuel has to be supplied to the reactor core. As a consequence, the average plutonium concentration in the fuel is lower and its consumption via fission suppressed. As illustrated in Table B.1, annual plutonium production is below 100 g for HEU fuel and reaches 1–2 kg for LEU fuel in a 30 MW research reactor. As will be verified below, these aggregated numbers are already in close agreement with estimates obtained in actual cell burnup calculations.

The simple analysis based on (B.5) cannot be used directly to determine the residual uranium enrichment or plutonium vectors in the spent fuel. Furthermore, the evolution of the cross-section ratios during irradiation and the variation of the specific uranium-235 consumption, here fixed at 1.2 g/MWd(th), are not sensitive to burnup and enrichment. In order to get more accurate estimates of the spent fuel compositions required for the proliferation assessment made below, cell burnup calculations have been performed for a typical MTR-type reactor geometry using various initial uranium enrichments. Table B.2 summarizes the basic assumptions and input data used in the cell burnup calculations executed with M³O, i.e. with ORIGEN 2.2 and MCNP 4B/C, both linked with MCODE 1.0 (Chapter 6).

Meat thickness:	0.60 mm
Cladding thickness:	0.38 mm
Coolant channel:	2.20 mm
Average power density in core:	125 kW/l
Fixed uranium-235 density:	0.948 g/cc

Table B.2: Input data and assumptions for cell burnup calculations.

As discussed in Chapter 2, a variety of different fuel enrichments are studied, ranging from 93% down to 5%. Below that limit, operation of a standard MTR-type geometry can be considered unrealistic, especially because of the low burnup that is achievable for such fuels.⁵

The effective uranium-235 is held constant for all enrichment levels by increasing the total uranium density in the fuel matrix correspondingly. With this fixed uranium-235 density, the different fuels can be considered equivalent, although, in practice, one would have to overcompensate the effective uranium-235 density for a fixed core geometry to maintain similar performance or cycle length of the reactor. The selected value of 0.948 g(U-235)/cc corresponds to today's standard value of 4.8 g(U-tot)/cc at an enrichment of 19.75 wt%. For HEU-fuel the total density is close to 1.0 g(U-tot)/cc,

⁵For research reactors operated with slightly enriched or natural uranium, a graphite moderator or heavy water coolant would be a reasonable option. In essence, of course, such a reactor design constitutes a plutonium production reactor. See discussion below on the efficiency of dedicated plutonium production campaigns.

which represents a typical fuel density used until the late 1970s when development of higher-density LEU-fuels began.

Figure B.1 shows the specific plutonium buildup in the fuel for two selected enrichment levels. Similarly, typical fractional contents of uranium-235 and plutonium-239 are given in Figure B.2 as they decrease during irradiation. Table 2.1 in Chapter 2 summarizes the most important numerical results obtained in these calculations for U-235 target burnups of 20%, 40%, and 60%.

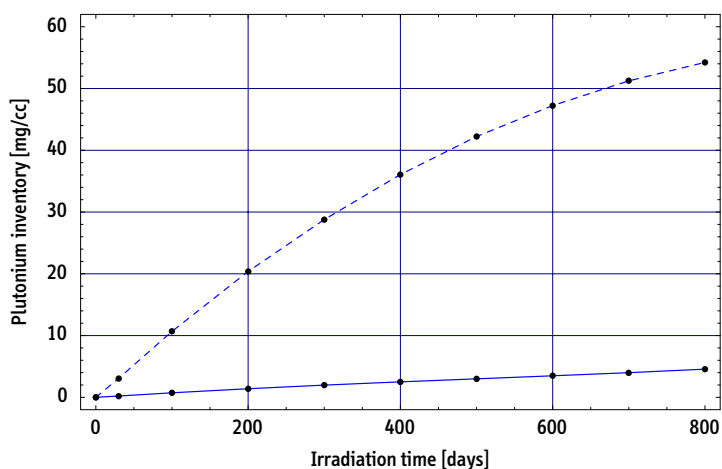


Figure B.1: Specific plutonium production in MTR-type fuel at 93% (—) and 19.75% (- -) enrichment. See Table 2.1 to correlate irradiation time with uranium-235 burnup. Cell burnup calculations with MCODE 1.0 using ORIGEN 2.2 and MCNP 4B.

M30 results, MCNP input decks: nMTR.1 and nMTR.2

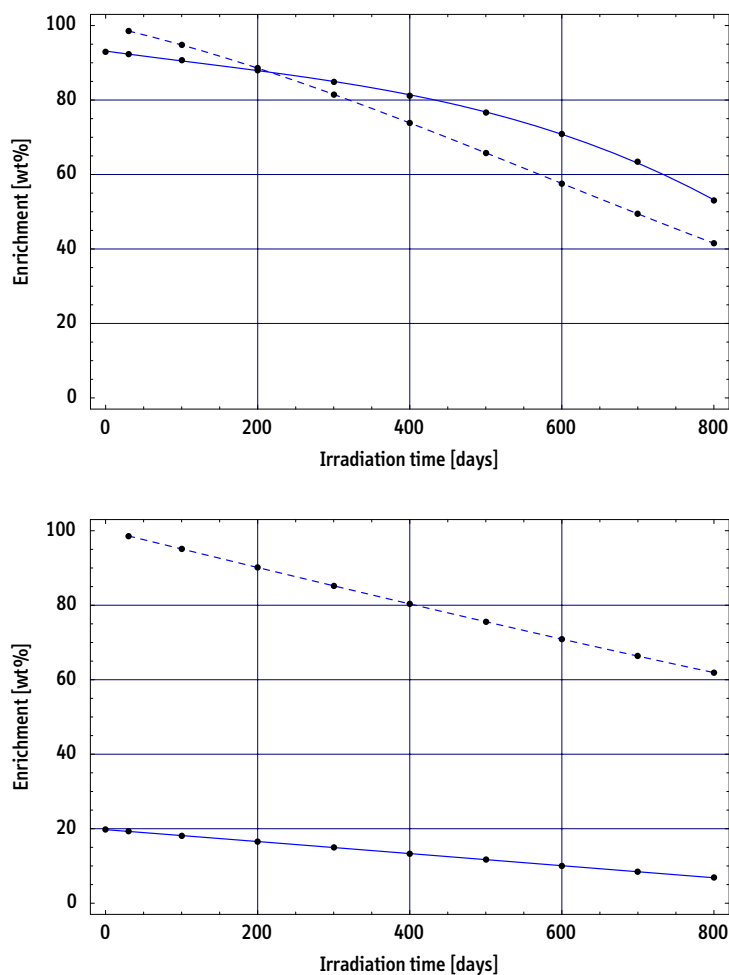


Figure B.2: Fractional isotopic content of uranium-235 (—) and plutonium-239 (- -) during irradiation of MTR-type fuel at 93% (top) and 19.75% (bottom) enrichment. See Table 2.1 to correlate irradiation time with uranium-235 burnup. Cell burnup calculations with MCODE 1.0 using ORIGEN 2.2 and MCNP 4B. Note that total plutonium buildup varies significantly in correlation to its initial fuel enrichment.

M3O results, MCNP input decks: nMTR.1 and nMTR.2

Dedicated Plutonium Production

Complementary to an assessment of the strategic value of the nuclear material associated with *regular* operation of a facility, the effectiveness of a dedicated plutonium production campaign is briefly discussed for reference purposes.

A plutonium production campaign can either take place in a specially-built military production reactor or in a research or power reactor that was not initially designed for plutonium production. In the case of the research reactor, plutonium production can be carried out covertly or overtly, i.e. an attempt can or cannot be made to conceal this mode of operation from outsiders.⁶ Plutonium production in an MTR-type reactor can be optimized if the core is loaded with so-called *driver fuel elements* to maintain the reactor critical and *target fuel elements* to generate the plutonium product. The driver fuel may be highly enriched, while the target material may contain either natural or depleted uranium.⁷

The development and analysis of detailed production scenarios is beyond the scope of this study, but a rough estimate is possible based on the neutron balance in a typical MTR-type reactor alone. The fission and neutron release rate per MW(th) can be specified using typical values for the energy and neutron release per fission event of 200 MeV and $\nu = 2.4$, respectively.

$$1 \text{ MW(th)} \text{ is equivalent to: } 3.12 \times 10^{16} \text{ fi/s} \quad \text{or} \quad 7.50 \times 10^{16} \text{ n/s}$$

Typically 25–35% of all neutrons released in an MTR-type reactor are not required to maintain criticality of the reactor and are therefore available for other purposes. Assuming that all those neutrons are absorbed in the target material and indeed lead to plutonium buildup, a theoretical upper limit of total plutonium production can be specified.

$$\xi(\text{max}) \approx 0.65\text{--}0.90 \text{ g(Pu)/MWd(th)} \tag{B.6}$$

In practice, production rates close to $\xi(\text{max})$ are not achievable. In addition to parasitic neutron absorption in structural and other materials, neutron absorption in the generated plutonium itself reduces total buildup of the material. First, neutron absorption in plutonium competes with absorption in U-238 and reduces the neutron fraction available for breeding. Second, plutonium is simultaneously consumed via fission. In

⁶The following discussion does not assess the feasibility of successfully hiding plutonium production in a safeguarded research reactor. The effectiveness of safeguards to detect covert plutonium production has been addressed, for instance, in [Miller and Eberhard, 1982], [Powers, 1983], and [Miller, 1984].

⁷Both target materials are virtually identical in terms of plutonium buildup, but energy release in natural uranium may be a significant fraction of the total thermal power of the reactor.

making the *ad-hoc* assumption that these effects decrease efficiency by an additional 30–40%, a practical plutonium production rate $\xi(\text{eff})$ can be estimated.

$$\xi(\text{eff}) \approx 0.4\text{--}0.6 \text{ g(Pu)/MWd(th)} \quad (\text{B.7})$$

Based on these values and scaled to the previously discussed generic 30 MW reactor operated 300 days per year, the maximum plutonium production rate achievable in a dedicated plutonium production campaign is 3.6–5.4 kg(Pu)/yr.

Quite consistently, more detailed analyses of production scenarios conclude that 3–6 kg of plutonium can be produced annually in a generic MTR-type reactor rated at 30 MW [Miller and Eberhard, 1982].⁸ These numbers can be compared to the regular and inevitable plutonium buildup in a 30 MW LEU-fueled reactor (19.75%), which is on the order of 1 kg(Pu)/yr (see Table 2.1). Note also that plutonium production in a fictitious MTR-type reactor fueled with slightly enriched uranium (5%) and operated at relatively low burnup of the fuel (20%) is already close to the production rate achieved in dedicated campaigns (3.46 kg with an average Pu-239 content of about 90%, see Table 2.1 in Chapter 2).

There are a variety of practical implications of dedicated plutonium production campaigns that are not further discussed here. Specifically, note that significantly less ordinary fuel elements are required to run the reactor than would be expected based on the thermal power of the facility. This is due to the significant energy release in the target material. At the same time, a very large number of target fuel elements, containing a considerable and possibly undeclared uranium inventory, has to be loaded into and discharged from the reactor. This striking discrepancy between requested fuel (low) and core management activities (high) makes covert plutonium production in an adequately safeguarded reactor rather difficult.

⁸Miller and Eberhard [1982] consider a generic MTR-type reactor rated at 50 MW and estimate an annual plutonium production of 5–10 kg.

Appendix C

Relevant Research Reactors

This appendix provides a series of tables listing the research reactors worldwide that are relevant in the context of conversion from highly enriched to low-enriched fuel. Included are only those reactors characterized by a thermal power of at least 1 MW. These reactors typically require regular refueling and therefore fuel storage as well as fuel shipments to and from the site. In contrast, reactors with power levels of less than 1 MW may not require regular refueling, or even use ‘life-time’ cores, with the important class of TRIGA reactors falling into this category. If fueled with HEU, these low-power reactors require a more case-specific analysis with respect to respective conversion priorities. Similarly, a number of critical facilities and pulsed reactors, which may contain large or very large HEU (> 1000 kg) inventories, do not show up in the tables below, even though they may pose, in some instances, serious proliferation risks compared to standard HEU-fueled research reactors. It has been suggested to extend the scope of the RERTR program, which has traditionally focused on megawatt-reactors operated in steady-state, to address these more unconventional facilities [von Hippel, 2004].¹

The data summarized in the tables is primarily based upon the research reactor database (RRDB) maintained by the International Atomic Energy Agency. Information has been retrieved from the most recent printed edition [IAEA, 2000] as well as from the corresponding online-version of the database.² As indicated in the main text, it has to be emphasized that the IAEA-database is known to be incomplete. The database is, however, the only reference with official information provided to the IAEA by its member states. There are unsafeguarded reactors in states not member to the Nonproliferation Treaty (NPT), which may or may not be included in the database.

¹Little information is available on these facilities because most of them are located in nuclear-weapon states. In this case, they are not subject to international safeguards and often not listed in the IAEA database.

²As of February 2005, available at <http://www.iaea.org/worldatom/rrdb/>

Furthermore, data from some nuclear-weapon states of the NPT, which are generally not subject to IAEA safeguards, are known to be incomplete. For these reasons, the information contained in the tables below inevitably is equally incomplete

Most data in the tables can be assumed to be reliable and accurate (criticality date, power level, etc.). However, and even though they are listed in IAEA publications, data entries on the enrichment level may be outdated in a few instances, in particular, if more than one fuel enrichment is used in the core and/or if the facility currently is in the process of conversion. Tables C.3 and C.4 also list the estimated annual HEU demand of a reactor. This data is primarily based on numbers published in [Albright et al., 1997, Appendix D] and [Matos, 1998] as well as, in some instances, on estimates by the author if no other source could be identified.³

Tables C.1 and C.2 list relevant research reactors by country. The tables includes operational HEU-fueled facilities, operational reactors in the various stages of the conversion process to low-enriched fuel, as well as shut-down facilities that had been converted while operational.⁴ To characterize the conversion status of the facilities, the following scheme is employed:

- A: Fully converted
 - B: Partially converted
 - C: Conversion planned (or awaiting fuel)
 - D: Conversion feasible
 - E: Feasibility study exists or underway
 - F: Not in program, no info available, or refuses conversion
- X: Reactor shut down

A typical conversion process for a given facility is initiated with status F and ideally runs through all stages up to status A. If available, estimated dates for a scheduled change of the conversion status are indicated. In some instances, it may have been determined that a suitable LEU fuel is currently not available (FCNA), which usually implies that a feasibility study exists (E) or that conversion is planned once the required fuel is available (B). Tables C.1 and C.2 also designate the 42 reactors that were the original focus of the RERTR program when it was created in 1977/78. These are reactors supplied by the U.S. to foreign (Western) countries and they are listed even if

³If the average burnup level of the fuel in a particular reactor is known or can be estimated, the theoretical annual HEU demand is determined once the power level and the enrichment are known. Note that some facilities are operated on a very unfrequent basis and their actual HEU demand may therefore be much lower than expected. If no consistent data for a reactor's HEU demand could be determined, or the information remained conflicting, no estimate is given, but the facility is 'ranked' at a probable position.

⁴Generally not listed are therefore shut-down HEU-fueled reactors.

some of them have been shut down since then, with or without being converted prior to that.

Tables C.3 and C.4 list operational HEU-reactors by relevance and include, as mentioned above, estimates of their annual HEU demand. Four relevance levels (categories 1–4) are used: highest relevance is assigned to HEU-fueled facilities with power levels greater 5 MW using a fuel enrichment $\geq 50\%$. Reactors are ordered by their respective HEU demand, i.e. not necessarily by their power level (Table C.3). Category 2 comprises facilities with 1–5 MW thermal power and $\geq 50\%$ enrichment. The third category should be considered a preliminary one and contains a few facilities with no reasonable estimate of the HEU demand available.⁵ The final category lists all remaining HEU-fueled facilities with a fuel enrichment of less than 50% or, in all but one case, of not more than 36%.⁶

Table C.5 lists all research reactors with power levels of at least 1 MW that were built after the start of the RERTR program and also includes facilities that are currently under construction or in the planning stages. The period between 1978 and 1980 also coincides with the United Nations *International Nuclear Fuel Cycle Evaluation* (INFCE), which recommended the conversion of HEU-fueled reactors to low-enriched fuel as an important measure to increase the proliferation resistance of the nuclear fuel cycle [IAEA, 1980a].⁷ Table C.5 illustrates that, with very few exceptions, the new design-objective of using LEU instead of HEU was largely accepted internationally. The German research reactor FRM-II has been the only research reactor designed for HEU in more than a decade. All other reactors currently planned or under construction will use LEU fuel from the very beginning. In particular, the Chinese and French projects (CARR, 60 MW, and JHR, 100 MW, respectively) stand out since they reflect the reorientation of former traditional HEU users.

⁵The Russian RBT-10/2 reactor, for instance, uses the fuel discharged from another HEU-fueled reactor located nearby. The fuel is used directly without being reprocessed and refabricated. To avoid double-counting when determining the total HEU demand, no fuel demand has been assigned to this facility. In the remaining cases, the situation is less clear.

⁶The 36%-enrichment corresponds to an intermediate enrichment level that was used for facilities exported to the countries of the Former Soviet Union. By today's internationally accepted standards, this fuel is, of course, still considered highly enriched.

⁷Respective statements can be found in Volume 9 (Summary Volume) as well as in Volume 8 (Report of INFCE Working Group 8: Advanced Fuel Cycle and Reactor Concepts, pp. 17–19, pp. 42–46, and pp. 137–172).

Country	IAEA Code	Name	Criticality	Power	Enrichment	42	Status
Argentina	AR-0002	RA-3	1968/08	5 MW	20%	•	A (1990)
Australia	AU-0001	HIFAR	1958/01	10 MW	60%	•	C, X (?)
Austria	AT-0001	ASTRA	1960/09	10 MW	20%	•	X (1999), A (1990)
Belgium	BE-0002	BR-2	1961/06	100 MW	74–93%	•	C (FCNA)
Brazil	BR-0001	IEA-R1	1957/09	5 MW	20%	•	A (1997)
Canada	CA-0001	NRX	1947/07	42 MW		•	X (1993)
Canada	CA-0002	NRU	1957/11	135 MW	20%	•	A (1993)
Canada	CA-0004	MNR	1959/04	5 MW	93%	•	B (2004)
Chile	CL-0001	RECH-1	1974/10	5 MW	20–45%	•	B (2006)
Chile	CL-0002	RECH-2	1989/09	2 MW	90%		X (?)
China	CN-0004	HFETR	1979/12	125 MW	90%		F
China	CN-0012	MJTR	1991/02	5 MW	90%		F
Czech Republic	CZ-0003	LWR-15	1957/09	10 MW	36%		E
Denmark	DK-0003	DR-3	1960/01	10 MW	20%	•	A (1990)
France	FR-0007	SILOE	1963/03	35 MW		•	X (1997)
France	FR-0014	OSIRIS	1966/09	70 MW	20%	•	A (1979)
France	FR-0017	HFR	1971/07	58.3 MW	93%	•	E (FCNA)
France	FR-0022	ORPHEE	1980/12	14 MW	93%	•	E (FCNA)
France	FR-0024	SCARABEE	1982/01	100 MW	93%	•	F
Germany	DE-0003	FRM-1	1957/10	4 MW	45–93%	•	X (2000)
Germany	DE-0004	FRG-1	1958/10	5 MW	20%	•	A (1991)
Germany	DE-0006	FRJ-2	1962/11	23 MW	80–93%	•	D, X (2006)
Germany	DE-0013	FRG-2	1963/03	15 MW		•	X (1993)
Germany	DE-0018	FMRB	1967/10	1 MW		•	X (1995)
Germany	DE-0031	BER-2	1973/12	10 MW	20%	•	A (2000)
Germany	DE-0051	FRM-II	2004/03	20 MW	93%		E
Greece	GR-0001	GRR-1	1961/07	5 MW	20–93%	•	A (2001)
Hungary	HU-0002	BRR	1959/03	10 MW	36%		E
India	IN-0001	APSARA	1956/08	1 MW	93%		B
Iran	IR-0001	TRR	1967/11	5 MW	20%	•	A (1993)
Israel	IL-0001	IRR-1	1960/06	5 MW	93%	•	D, X (2006)
Japan	JP-0001	JRR-2	1960/10	10 MW		•	X (1996)
Japan	JP-0011	KUR	1964/06	5 MW	93%	•	D, X (2006)
Japan	JP-0012	JRR-4	1965/01	3.5 MW	20%	•	A (1998)
Japan	JP-0015	JMTR	1968/03	50 MW	20%	•	A (1994)
Kazakhstan	KZ-0001	WWW-K	1967/10	6 MW	36%		E
Kazakhstan	KZ-0002	IGR	1961/01	10 MW	36%		F
Kazakhstan	KZ-0003	EWG-1	1972/01	60 MW	90%		F
Libya	LY-0001	IRT-1	1981/08	10 MW	80%		C
Mexico	MX-0001	TRIGA-3	1968/11	1 MW	20–70%	•	D

Table C.1: Part 1. Research reactors relevant in the conversion context, by country.

Listed are only facilities with at least 1 MW thermal power. See text for further explanations. Last revision: November 2004.

Country	IAEA Code	Name	Criticality	Power	Enrichment	42	Status
Netherlands	NL-0002	HOR	1963/04	2 MW	20–93%	•	A (2003)
Netherlands	NL-0004	HFR	1961/11	45 MW	20–93%	•	C (FCNA), A (2006)
North Korea	KP-0001	IRT-DPRK	1965/08	8 MW	36%		F
Pakistan	PK-0001	PARR-1	1965/12	10 MW	20%	•	A (1991)
Philippines	PH-0001	PRR-1	1963/08	1 MW		•	X (1998), A (1987)
Poland	PL-0004	MARIA	1974/12	30 MW	36–80%		B
Portugal	PT-0001	RPI	1961/04	1 MW	20–93%	•	C (2006)
Romania	RO-0002	TRIGA-2	1979/11	14 MW	20–93%	•	B (2006)
Russia	RU-0004	IR-8	1981/08	8 MW	90%		E
Russia	RU-0005	IRT-A	1967/05	2.5 MW	90%		F
Russia	RU-0008	WWR-M	1959/12	18 MW	90%		E
Russia	RU-0010	IVV-2M	1966/04	15 MW	90%		F
Russia	RU-0013	MIR-M1	1966/12	100 MW	90%		F
Russia	RU-0014	IRT-T	1967/07	6 MW	90%		F
Russia	RU-0016	PIK	—	100 MW	90%		F
Russia	RU-0019	WWR-TS	1964/10	15 MW	36%		F
Russia	RU-0020	RBT-10/2	1984/12	10 MW	63%		F
Russia	RU-0022	RBT-6	1975/10	6 MW	63%		F
Russia	RU-0024	SM	1961/10	100 MW	90%		F
South Africa	ZA-0001	SAFARI	1965/03	20 MW	87–93%	•	D (2006)
South Korea	KR-0002	TRIGA-3	1972/04	2 MW		•	X (1995)
Sweden	SE-0001	R2	1960/05	50 MW	20%	•	A (1993)
Sweden	SE-0002	R2-0	1960/06	1 MW	20%	•	A (2000)
Switzerland	CH-0001	SAPHIR	1957/04	10 MW		•	X (1994), A (?)
Taiwan	TW-0001	THOR	1961/04	1 MW	20%	•	A (1987)
Turkey	TR-0002	TR-2	1981/12	5 MW	20–95%	•	B (2006), X (1995)
Ukraine	UA-0001	WWR-M	1960/12	10 MW	36%		C (2007)
USA	US-0030	BMRR	1959/03	3 MW	42–93%		X (2000), D
USA	US-0054	GTRR	1964/12	5 MW	20%		X (1997), A (1997)
USA	US-0070	ATR	1967/07	250 MW	93%		E (FCNA)
USA	US-0120	MITR-2	1958/07	4.9 MW	93%		E (FCNA)
USA	US-0126	NBSR	1967/12	20 MW	93%		E (FCNA)
USA	US-0137	HFIR	1965/08	85 MW	93%		E (FCNA)
USA	US-0147	OSTR	1967/03	1.1 MW	70%		C (2006)
USA	US-0155	RINSC	1964/07	2 MW	20%		A (1993)
USA	US-0167	ACRR	1967/06	4 MW	35%		D
USA	US-0185	NSCR	1962/01	1 MW	70%		C (2008)
USA	US-0201	UMLR	1975/01	1 MW	93%		A (2000)
USA	US-0203	FNR	1957/09	2 MW	20%		A (1984)
USA	US-0204	MURR	1966/10	10 MW	93%		E (FCNA)
USA	US-0213	UVAR	1960/06	2 MW	20%		X (1998), A (1994)
USA	US-0215	UWNR	1961/03	1 MW	20–70%		C (2009)
USA	US-0218	WSUR	1961/03	1 MW	20–70%		C (2010)
Uzbekistan	UZ-0001	WWR-CM	1959/09	10 MW	36%		C (2007)

Table C.2: Part 2. Research reactors relevant in the conversion context, by country.

Listed are only facilities with at least 1 MW thermal power. See text for further explanations. Last revision: November 2004.

C A T E G O R Y 1						
Country	IAEA Code	Name	Criticality	Power	Enrichment	HEU Demand
USA	US-0070	ATR	1967/07	250 MW	93%	120–175 kg/yr
USA	US-0137	HFIR	1965/08	85–100 MW	93%	91–150 kg/yr
Russia	RU-0024	SM-2	1961/10	100 MW	90%	43–110 kg/yr
China	CN-0004	HFETR	1979/12	125 MW	90%	75 kg/yr
Russia	RU-0013	MIR-M1	1966/12	100 MW	90%	62.2 kg/yr
Kazakhstan	KZ-0003	EWG-1	1972/01	60 MW	90%	?
France	FR-0017	HFR	1971/07	58.3 MW	93%	54.8 kg/yr
Germany	DE-0051	FRM-II	2004/03	20 MW	93%	40.5 kg/yr
Netherlands	NL-0004	HFR	1961/11	45 MW	93%	38.3 kg/yr
Belgium	BE-0002	BR-2	1961/06	80–100 MW	74–93%	29 kg/yr
USA	US-0204	MURR	1966/10	10 MW	93%	23.5 kg/yr
Germany	DE-0006	FRJ-2	1962/11	23 MW	80–93%	19.2 kg/yr
Poland	PL-0004	MARIA	1974/12	17–30 MW	36–80%	?
France	FR-0022	ORPHEE	1980/12	14 MW	93%	15.8 kg/yr
Russia	RU-0008	WWR-M	1959/12	18 MW	90%	3.7–14.4 kg/yr
USA	US-0126	NBSR	1967/12	20 MW	93%	13 kg/yr
South Africa	ZA-0001	SAFARI	1965/03	20 MW	87–93%	12.6 kg/yr
USA	US-0120	MITR-2	1958/07	4.9–10 MW	93%	1.6–12 kg/yr
Romania	RO-0002	TRIGA-2	1979/11	14 MW	20–93%	11.8 kg/yr
Russia	RU-0010	IVV-2M	1966/04	15 MW	90%	3.5–9 kg/yr
Kazakhstan	KZ-0002	IGR	1961/01	10 MW	36–90%	?
Australia	AU-0001	HIFAR	1958/01	10 MW	60%	8.1 kg/yr
Russia	RU-0014	IRT-T	1967/07	6 MW	90%	5.6 kg/yr

Table C.3: Research reactors currently using HEU fuel, by relevance.

Listed are only facilities with at least 1 MW thermal power. See text for further explanations. Last revision: Summer 2004.

C A T E G O R Y 2						
Country	IAEA Code	Name	Criticality	Power	Enrichment	HEU Demand
Japan	JP-0011	KUR	1964/06	5 MW	93%	2.3 kg/yr
Russia	RU-0004	IR-8	1981/08	8 MW	90%	2.2 kg/yr
China	CN-0012	MJTR	1991/02	5 MW	90%	?
Turkey	TR-0002	TR-2	1981/12	5 MW		1.6 kg/yr
Russia	RU-0005	IRT-A	1967/05	2.5 MW	90%	1.1 kg/yr
Mexico	MX-0001	TRIGA-3	1968/11	1 MW	20–70%	1 kg/yr
Portugal	PT-0001	RPI	1961/04	1 MW	20–93%	1 kg/yr
USA	US-0147	OSTR	1967/03	1.1 MW	70%	0.2 kg/yr
USA	US-0185	NSCR	1962/01	1 MW	70%	0.2 kg/yr
USA	US-0215	UWNR	1961/03	1 MW	20–70%	0.2 kg/yr
USA	US-0218	WSUR	1961/03	1 MW	20–70%	0.2 kg/yr
India	IN-0001	APSARA	1956/08	0.4–1 MW	93%	?

C A T E G O R Y 3						
Country	IAEA Code	Name	Criticality	Power	Enrichment	HEU Demand
France	FR-0024	SCARABEE	1982/01	100 MW	93%	0 kg/yr
Russia	RU-0020	RBT-10/2	1984/12	10 MW	63%	0 kg/yr
Libya	LY-0001	IRT-1	1981/08	10 MW	80%	0 kg/yr
Russia	RU-0022	RBT-6	1975/10	6 MW	63%	0 kg/yr
Israel	IL-0001	IRR-1	1960/06	5 MW	93%	0 kg/yr

C A T E G O R Y 4						
Country	IAEA Code	Name	Criticality	Power	Enrichment	HEU Demand
Russia	RU-0019	WWR-TS	1964/10	15 MW	36%	20.8 kg/yr
Uzbekistan	UZ-0001	WWR-CM	1959/09	8–10 MW	36%	15.6 kg/yr
Czech Republic	CZ-0003	LWR-15	1957/09	10 MW	36%	13.9 kg/yr
Ukraine	UA-0001	WWR-M	1960/12	10 MW	36%	13.9 kg/yr
North Korea	KP-0001	IRT-DPR	1965/08	8 MW	36%	?
Kazakhstan	KZ-0001	WWW-K	1967/10	6 MW	36%	11.7 kg/yr
Hungary	HU-0002	BRR	1959/03	10 MW	36%	11.1 kg/yr
Chile	CL-0001	RECH-1	1974/10	5 MW	20–45%	1.1 kg/yr
USA	US-0167	ACRR	1967/06	4 MW	35%	?

Table C.4: Research reactors currently using HEU fuel, by relevance.

Listed are only facilities with at least 1 MW thermal power. See text for further explanations. Last revision: Summer 2004.

IN OPERATION						
Country	Code	Name	Construction start	Power	Enrichment of fuel	Status
Algeria	DZ-0001	NUR	1987	1 MW	20%	
Algeria	DZ-0002	ES-SALAM	1988	15 MW	3%	
Bangladesh	BD-0001	TRIGA II	1981	3 MW	20%	
Canada		Maple 1	1990	10 MW	20%	
Canada		Maple 2	1998	10 MW	20%	
China	CN-0007	PPR	1986	1 MW	20%	
China	CN-0010	NHR-5	1986	5 MW	3%	
China	CN-0012	MJTR	1986	5 MW	90%	*
Egypt	EG-0002	ETRR-2	1992	22 MW	20%	
Germany	DE-0051	FRM-II	1996	20 MW	93%	*
Indonesia	ID-0003	GA SIB.	1983	30 MW	20%	
Japan	JP-0008	JRR-3M	1985	20 MW	20%	
South Korea	KR-0004	HANARO	1987	30 MW	20%	
Libya	LY-0001	IRT-1	1980	10 MW	80%	*
Malaysia	MY-0001	TRIGA II	1981	1 MW	20%	
Peru	PE-0002	RP-10	1980	10 MW	20%	
Russia	RU-0020	RBT-10/2	1983	10 MW	63%	(*)
USA	US-0238	TRIGA II	1987	1 MW	20%	
USA	US-0240	TRIGA II	1986	1 MW	20%	

UNDER CONSTRUCTION OR PLANNED						
Country	Code	Name	Construction start	Power	Enrichment of fuel	Status
Australia		ANSTO RR	2002	20 MW	20%	
Canada		CNF	?	40 MW	20%	
China		CARR	?	60 MW	20%	
France		JHR	2010	100 MW	20%	
Morocco	MA-0001	MA-R1	2004	2 MW	20%	
Thailand	TH-0002	MPR-10	2004	10 MW	20%	

Table C.5: Research reactors in operation with construction start not earlier than 1980 (top) and research reactors under construction or planned (bottom) with a thermal power of at least 1 MW. Enrichment is given in weight percent, HEU-fueled reactors are starred.

Listed are only facilities with at least 1 MW thermal power. See text for further explanations. Last revision: Summer 2004.

Appendix D

MCNP Sample Input Deck

For reference purposes, a complete MCNP input deck is reproduced in this appendix. Only repeating cell, surface, and data cards, whose structure and content can be clearly inferred from preceding and following cards, are omitted to avoid unnecessary redundancy of the listing. The input deck printed below generates the full three-dimensional model of the generic single element reactor introduced and discussed in Chapter 7. For details on the MCNP syntax, the reader may consult the MCNP manuals [Briesmeister, ed., 1993, 1997, 2000]. Line numbers are added for convenience; they are not part of the original MCNP input deck.

All cell and surface data has been generated with the *Mathematica* modules introduced in Chapter 5. The file is prepared for ACS burnup calculations and therefore contains additional MCNP cells and materials to define the complex burnup zone structure used for the analysis of the reactor (93 cells in the fueled volume containing 12 burnable materials). As this sample deck is not used for neutron flux analysis in the moderator tank, corresponding cells and tallies that would be required to obtain this data are not present.

```

001 Generic Single Element Reactor 2
002 C
003 C
004 C      CELL CARDS *****
005 C
006 C      -----
007 C
008 C      CELL 001:
009 C      ACTIVE ZONE OF FUEL PLATE (IN UNIVERSE 1)
010 C      NOT LIMITED IN Z-DIRECTION
011 C      FILLED WITH UNIVERSE 2 (CLADDING AND FUEL MEAT)
012 C
013 C      1  0  -11 -13  ( 12: 14)  19  u=1  fill=2  imp:n=1
014 C
015 C      -----
016 C
017 C      CELLS 002 TO PMAX:
018 C      (PMAX - 1) ROTATIONS OF CELL 001 DEFINING ALL ACTIVE ZONES
019 C
020 C      2  like 1  but  *trcl=(0 0 0  1.946  91.946  90  88.054  1.946  90  90  90  0)
021 C      3  like 1  but  *trcl=(0 0 0  3.892  93.892  90  86.108  3.892  90  90  90  0)
022 C      4  like 1  but  *trcl=(0 0 0  5.838  95.838  90  84.162  5.838  90  90  90  0)
023 C
024 C      ...
025 C
026 C      183  like 1  but  *trcl=(0 0 0  354.162  444.162  90  -264.162  354.162  90  90  90  0)
027 C      184  like 1  but  *trcl=(0 0 0  356.108  446.108  90  -266.108  356.108  90  90  90  0)
028 C      185  like 1  but  *trcl=(0 0 0  358.054  448.054  90  -268.054  358.054  90  90  90  0)
029 C
030 C      201  3  -0.998  (    11:    13)  15  -16  -2012  -2014  2019  u=1  imp:n=1
031 C      202  3  -0.998  (   2011:   2013)  15  -16  -3012  -3014  3019  u=1  imp:n=1
032 C      203  3  -0.998  (   3011:   3013)  15  -16  -4012  -4014  4019  u=1  imp:n=1
033 C
034 C      ...
035 C
036 C      383  3  -0.998  ( 183011: 183013)  15  -16  -184012  -184014  184019  u=1  imp:n=1
037 C      384  3  -0.998  ( 184011: 184013)  15  -16  -185012  -185014  185019  u=1  imp:n=1
038 C      385  3  -0.998  ( 185011: 185013)  15  -16    -12    -14    19  u=1  imp:n=1
039 C
040 C      -----
041 C
042 C      FUEL PLATE UNIVERSE
043 C
044 C      CELLS 1501 TO 1507:
045 C      DEFINITION OF THE TWO FUEL MEAT ZONES AND THE CLADDING
046 C      FILLING ACTIVE ZONE OF FUEL PLATE
047 C
048 C      CELL 1501 REPLACED BY ACS MATERIALS IN CELLS 2001 THROUGH 2012
049 C

```

```

050 1502 4 -2.7000 41: 43 u=2 imp:n=1 $ CLA
051 1503 4 -2.7000 -42 -44 u=2 imp:n=1 $ CLA
052 1504 4 -2.7000 -41 -43 ( 42: 44) -201 u=2 imp:n=1 $ BOT
053 1505 4 -2.7000 -41 -43 ( 42: 44) 271 u=2 imp:n=1 $ TOP
054 1506 4 -2.7000 -41 -43 ( 42: 44) 201 -271 101 u=2 imp:n=1 $ PIN
055 1507 4 -2.7000 -41 -43 ( 42: 44) 201 -271 -131 u=2 imp:n=1 $ PIN
056 C
057 C -----
058 C
059 C CELL 1508:
060 C FILLING REGION BETWEEN THE TWO CORE TUBES WITH
061 C THE FUEL AND MODERATOR UNIVERSE
062 C
063 1508 0 22 -23 17 -18 fill=1 imp:n=1.0
064 C
065 C -----
066 C
067 C CELLS 1509 TO 1510:
068 C SIMPLE CORE TUBES WITHOUT BORON RING (LENGTH OF FUEL ELEMENT)
069 C FUEL ELEMENT IS "FLOATING" IN THIS SIMPLIFIED MODEL
070 C
071 1509 4 -2.700 -22 24 17 -18 imp:n=1.0 $ TUB
072 1510 4 -2.700 -25 23 17 -18 imp:n=1.0 $ TUB
073 C
074 C -----
075 C
076 C CELLS 1511 TO 1512:
077 C CENTRAL CORE TUBE (ZKR) HAVING THE MAXIMUM HEIGHT (INCLUDING H2O GAP)
078 C
079 1511 3 -0.998 25 -54 -503 500 imp:n=1.0 $ GAP
080 1512 4 -2.700 54 -55 -503 500 imp:n=1.0 $ ZKR (AG3)
081 C
082 C -----
083 C
084 C CELLS 1521 TO 1524:
085 C SIMPLIFIED CONTROL ROD (WITH WATER ABOVE AND BELOW)
086 C
087 1521 5 -1.848 -52 507 -509 imp:n=1.0 $ BER
088 1522 3 -0.998 -24 52 507 -509 imp:n=1.0 $ GAP
089 1523 3 -0.998 -24 509 -503 imp:n=0.3 $ TOP
090 1524 3 -0.998 -24 -507 500 imp:n=0.3 $ BOT
091 C
092 C -----
093 C
094 C CELLS 1531 TO 1534:
095 C CELLS ABOVE AND BELOW FUEL ELEMENT
096 C FILLED WITH LIGHT WATER (H2O)
097 C
098 1531 3 -0.998 -25 24 -17 501 imp:n=1.0
099 1532 3 -0.998 -25 24 18 -502 imp:n=1.0

```

```

100 1533 3 -0.998 -25 24 -501 500 imp:n=0.1
101 1534 3 -0.998 -25 24 502 -503 imp:n=0.1
102 C
103 C -----
104 C
105 C CELLS 1541 TO 1544:
106 C CELLS FILLED WITH HEAVY WATER (D20)
107 C
108 C
109 1541 2 -1.1000 55 -150 501 -502 imp:n=1.0
110 1542 2 -1.1000 150 -160 501 -502 imp:n=0.1
111 1543 2 -1.1000 55 -160 -501 500 imp:n=0.1
112 1544 2 -1.1000 55 -160 502 -503 imp:n=0.1
113 C
114 C -----
115 C M C O D E S P E C I A L
116 C -----
117 C
118 2001 11 0.0552600274 -41 -43 ( 42: 44) &
119 C
120 (( 202 -215 -108 119 ) : &
121 ( 202 -208 -104 108 ) : &
122 ( 208 -210 -106 108 ) : &
123 ( 257 -270 -108 119 ) : &
124 ( 264 -270 -104 108 ) : &
125 ( 262 -264 -106 108 ) : &
126 ( 215 -217 -110 118 ) : &
127 ( 255 -257 -110 118 ) : &
128 ( 202 -213 -119 122 ) : &
129 ( 259 -270 -119 122 ) : &
130 ( 202 -208 -122 125 ) : &
131 ( 264 -270 -122 125 )) vol=1001.383 u=2 imp:n=1.05
132 C
133 C -----
134 C
135 2002 12 0.0552600274 -41 -43 ( 42: 44) &
136 C
137 (( 201 -202 -104 124 ) : &
138 ( 270 -271 -104 124 )) vol= 84.150 u=2 imp:n=1.75
139 C
140 C -----
141 C
142 2003 13 0.0552600274 -41 -43 ( 42: 44) &
143 C
144 (( 217 -255 -106 123 )) vol=1359.019 u=2 imp:n=1.00
145 C
146 C -----
147 C
148 2004 14 0.0552600274 -41 -43 ( 42: 44) &
149 C

```



```
150      (( 217 -226 -103 105 ) : &
151      ( 210 -214 -101 103 ) : &
152      ( 206 -210 -101 102 ) : &
153      ( 214 -218 -102 103 ) : &
154      ( 221 -226 -105 106 ) : &
155      ( 201 -203 -101 102 ) : &
156      ( 246 -255 -103 105 ) : &
157      ( 258 -262 -101 103 ) : &
158      ( 262 -266 -101 102 ) : &
159      ( 254 -258 -102 103 ) : &
160      ( 246 -251 -105 106 ) : &
161      ( 269 -271 -101 102 ) : &
162      ( 226 -246 -104 106 )) vol= 256.657 u=2 imp:n=1.35
163 C
164 C -----
165 C
166 2005 15 0.0552600274 -41 -43 ( 42: 44) &
167 C
168      (( 217 -223 -124 127 ) : &
169      ( 202 -209 -128 130 ) : &
170      ( 223 -232 -123 126 ) : &
171      ( 212 -217 -126 128 ) : &
172      ( 220 -223 -123 124 ) : &
173      ( 209 -213 -128 129 ) : &
174      ( 208 -212 -127 128 ) : &
175      ( 249 -255 -124 127 ) : &
176      ( 263 -270 -128 130 ) : &
177      ( 240 -249 -123 126 ) : &
178      ( 255 -260 -126 128 ) : &
179      ( 249 -252 -123 124 ) : &
180      ( 259 -263 -128 129 ) : &
181      ( 260 -264 -127 128 ) : &
182      ( 223 -226 -126 127 ) : &
183      ( 246 -249 -126 127 ) : &
184      ( 201 -202 -124 130 ) : &
185      ( 270 -271 -124 130 ) : &
186      ( 232 -240 -123 125 )) vol= 408.127 u=2 imp:n=1.23
187 C
188 C -----
189 C
190 2006 16 0.0552600274 -41 -43 ( 42: 44) &
191 C
192      (( 209 -218 -129 130 ) : &
193      ( 201 -211 -130 131 ) : &
194      ( 213 -217 -128 129 ) : &
195      ( 254 -263 -129 130 ) : &
196      ( 261 -271 -130 131 ) : &
197      ( 255 -259 -128 129 ) : &
198      ( 226 -246 -126 128 ) : &
199      ( 232 -240 -125 126 ) : &
```

```
200          ( 217 -226 -127 129 ) : &
201          ( 246 -255 -127 129 )) vol= 273.487 u=2 imp:n=1.33
202 C
203 C -----
204 C
205 2007 17 0.0552600274 -41 -43 ( 42: 44) &
206 C
207          (( 214 -222 -101 102 ) : &
208          ( 250 -258 -101 102 ) : &
209          ( 218 -254 -102 103 ) : &
210          ( 226 -246 -103 104 )) vol= 151.470 u=2 imp:n=1.51
211 C
212 C -----
213 C
214 2008 18 0.0552600274 -41 -43 ( 42: 44) &
215 C
216          (( 218 -233 -129 130 ) : &
217          ( 211 -219 -130 131 ) : &
218          ( 239 -254 -129 130 ) : &
219          ( 253 -261 -130 131 ) : &
220          ( 226 -246 -128 129 )) vol= 138.847 u=2 imp:n=1.54
221 C
222 C -----
223 C
224 2009 19 0.0552600274 -41 -43 ( 42: 44) &
225 C
226          (( 222 -250 -101 102 )) vol= 58.905 u=2 imp:n=1.94
227 C
228 C -----
229 C
230 2010 20 0.0552600274 -41 -43 ( 42: 44) &
231 C
232          (( 219 -253 -130 131 ) : &
233          ( 233 -239 -129 130 )) vol= 84.150 u=2 imp:n=1.75
234 C
235 C -----
236 C
237 2011 21 0.0552600274 -41 -43 ( 42: 44) &
238 C
239          (( 210 -217 -103 108 ) : &
240          ( 215 -217 -108 110 ) : &
241          ( 217 -221 -105 106 ) : &
242          ( 203 -206 -101 102 ) : &
243          ( 208 -210 -104 106 ) : &
244          ( 255 -262 -103 108 ) : &
245          ( 255 -257 -108 110 ) : &
246          ( 251 -255 -105 106 ) : &
247          ( 266 -269 -101 102 ) : &
248          ( 262 -264 -104 106 ) : &
249          ( 201 -210 -102 104 ) : &
```

```

250          ( 262 -271 -102 104 )) vol= 286.109 u=2 imp:n=1.32
251 C
252 C -----
253 C
254 2012 22 0.0552600274 -41 -43 ( 42: 44) &
255 C
256          (( 208 -217 -122 126 ) : &
257          ( 202 -208 -125 128 ) : &
258          ( 213 -217 -119 122 ) : &
259          ( 217 -220 -123 124 ) : &
260          ( 208 -212 -126 127 ) : &
261          ( 255 -264 -122 126 ) : &
262          ( 264 -270 -125 128 ) : &
263          ( 255 -259 -119 122 ) : &
264          ( 252 -255 -123 124 ) : &
265          ( 260 -264 -126 127 ) : &
266          ( 215 -217 -118 119 ) : &
267          ( 255 -257 -118 119 )) vol= 315.562 u=2 imp:n=1.29
268 C
269 C -----
270 C
271 C CELL 9999:
272 C OUTSIDE WORLD
273 C
274 9999 0 160: -500: 503 imp:n=0.0
275
276 C BLANK LINE DELIMITER -----
277 C
278 C
279 C SURFACE CARDS *****
280 C
281 11 SQ 0.16282 0 0 0 -0.50000 0 -0.11815 9.40834 0 0
282 12 SQ 0.16591 0 0 0 -0.50000 0 0.01249 9.37920 0 0
283 C
284 13 C/Z 5.28358 8.36401 10.03419
285 14 C/Z 5.28358 8.36401 9.89819
286 C
287 15 CZ 9.99000 $ SLIGHTLY LESS THAN SURFACE 22
288 16 CZ 15.01000 $ SLIGHTLY MORE THAN SURFACE 23
289 C
290 17 PZ -36.00000
291 18 PZ 36.00000
292 C
293 19 PX 9.50000
294 C
295 C 20 P -3.59880 -1.00000 0.00000 -36.95208
296 C 21 P -0.50162 -1.00000 0.00000 -11.06797
297 C
298 22 CZ 10.00000
299 23 CZ 15.00000

```

```

300 C
301 24 CZ 9.25000
302 25 CZ 15.75000
303 C
304 41 SQ 0.16366 0 0 0 -0.50000 0 -0.08185 9.40028 0 0
305 42 SQ 0.16503 0 0 0 -0.50000 0 -0.02376 9.38732 0 0
306 C
307 43 C/Z 5.28358 8.36401 9.99643
308 44 C/Z 5.28358 8.36401 9.93595
309 C
310 52 CZ 9.10000
311 C
312 54 CZ 15.90000
313 55 CZ 16.65000
314 C
315 C 67 PZ -35.00000
316 C 68 PZ 35.00000
317 C
318 C -----
319 C
320 101 P -3.59880 -1.00000 0.00000 -36.95208
321 102 P -2.87881 -1.00000 0.00000 -30.14960
322 103 P -2.45077 -1.00000 0.00000 -26.18637
323 104 P -2.15732 -1.00000 0.00000 -23.52393
324 105 P -1.93901 -1.00000 0.00000 -21.58358
325 106 P -1.76773 -1.00000 0.00000 -20.09262
326 C 107 P -1.62822 -1.00000 0.00000 -18.90355
327 108 P -1.51138 -1.00000 0.00000 -17.92874
328 C 109 P -1.41138 -1.00000 0.00000 -17.11245
329 110 P -1.32433 -1.00000 0.00000 -16.41728
330 C 111 P -1.24747 -1.00000 0.00000 -15.81712
331 C 112 P -1.17882 -1.00000 0.00000 -15.29311
332 C 113 P -1.11690 -1.00000 0.00000 -14.83124
333 C 114 P -1.06057 -1.00000 0.00000 -14.42085
334 C 115 P -1.00895 -1.00000 0.00000 -14.05369
335 C 116 P -0.96135 -1.00000 0.00000 -13.72324
336 C 117 P -0.91721 -1.00000 0.00000 -13.42428
337 118 P -0.87607 -1.00000 0.00000 -13.15258
338 119 P -0.83755 -1.00000 0.00000 -12.90466
339 C 120 P -0.80135 -1.00000 0.00000 -12.67765
340 C 121 P -0.76719 -1.00000 0.00000 -12.46912
341 122 P -0.73486 -1.00000 0.00000 -12.27705
342 123 P -0.70416 -1.00000 0.00000 -12.09969
343 124 P -0.67494 -1.00000 0.00000 -11.93557
344 125 P -0.64704 -1.00000 0.00000 -11.78340
345 126 P -0.62035 -1.00000 0.00000 -11.64208
346 127 P -0.59476 -1.00000 0.00000 -11.51062
347 128 P -0.57017 -1.00000 0.00000 -11.38819
348 129 P -0.54650 -1.00000 0.00000 -11.27403
349 130 P -0.52367 -1.00000 0.00000 -11.16749

```

```
350 131 P -0.50162 -1.00000 0.00000 -11.06797
351 C
352 C NEW LIMITS FOR TANK
353 C
354 150 CZ 30 $ NEW DESIGNATION !!!
355 160 CZ 100 $ NEW DESIGNATION !!!
356 C
357 C
358 201 PZ -35.0000
359 202 PZ -34.0000
360 203 PZ -33.0000
361 C 204 PZ -32.0000
362 C 205 PZ -31.0000
363 206 PZ -30.0000
364 C 207 PZ -29.0000
365 208 PZ -28.0000
366 209 PZ -27.0000
367 210 PZ -26.0000
368 211 PZ -25.0000
369 212 PZ -24.0000
370 213 PZ -23.0000
371 214 PZ -22.0000
372 215 PZ -21.0000
373 C 216 PZ -20.0000
374 217 PZ -19.0000
375 218 PZ -18.0000
376 219 PZ -17.0000
377 220 PZ -16.0000
378 221 PZ -15.0000
379 222 PZ -14.0000
380 223 PZ -13.0000
381 C 224 PZ -12.0000
382 C 225 PZ -11.0000
383 226 PZ -10.0000
384 C 227 PZ -9.0000
385 C 228 PZ -8.0000
386 C 229 PZ -7.0000
387 C 230 PZ -6.0000
388 C 231 PZ -5.0000
389 232 PZ -4.0000
390 233 PZ -3.0000
391 C 234 PZ -2.0000
392 C 235 PZ -1.0000
393 C 236 PZ 0.0000
394 C 237 PZ 1.0000
395 C 238 PZ 2.0000
396 239 PZ 3.0000
397 240 PZ 4.0000
398 C 241 PZ 5.0000
399 C 242 PZ 6.0000
```

```
400 C 243 PZ 7.0000
401 C 244 PZ 8.0000
402 C 245 PZ 9.0000
403 246 PZ 10.0000
404 C 247 PZ 11.0000
405 C 248 PZ 12.0000
406 249 PZ 13.0000
407 250 PZ 14.0000
408 251 PZ 15.0000
409 252 PZ 16.0000
410 253 PZ 17.0000
411 254 PZ 18.0000
412 255 PZ 19.0000
413 C 256 PZ 20.0000
414 257 PZ 21.0000
415 258 PZ 22.0000
416 259 PZ 23.0000
417 260 PZ 24.0000
418 261 PZ 25.0000
419 262 PZ 26.0000
420 263 PZ 27.0000
421 264 PZ 28.0000
422 C 265 PZ 29.0000
423 266 PZ 30.0000
424 C 267 PZ 31.0000
425 C 268 PZ 32.0000
426 269 PZ 33.0000
427 270 PZ 34.0000
428 271 PZ 35.0000
429 C
430 C
431 500 PZ -150.0
432 501 PZ -45.0
433 502 PZ 45.0
434 503 PZ 150.0
435 C
436 C -----
437 C
438 C POSITION OF CENTRAL CONTROL ROD
439 C
440 507 PZ -41.0
441 C 508 PZ 0.0 $ UNUSED !!!
442 509 PZ 41.0
443 C
444 C -----
445 C
446 C 510 PZ -2.5 $ Reduced Height! Was: -5.0 UNUSED !!!
447 C 511 PZ 2.5 $ Reduced Height! Was: 5.0 UNUSED !!!
448
449 C BLANK LINE DELIMITER -----
```

```

450 C
451 C
452 AWTAB  34079  78.240500  38089  88.143700  38090  89.135400
453        44105 104.007000  46107 105.987000
454        47111 109.953000  48115 113.919000  50123 121.850000
455        50125 123.835000  50126 124.826000  51124 122.842000
456        51125 123.832000  51126 124.826000  52127 125.815000
457        52129 127.800000  53130 128.791000  53131 129.781998
458        54133 131.764008  58141 139.697998
459        58144 142.677000  59142 140.691000
460        59143 141.682999  61151 149.625000
461        62153 151.608002  63156 154.585007  63157 155.577000
462        96249 246.936000  97250 247.930000
463 C
464 C
465 C      DATA CARDS *****
466 C
467 C
468 M2     1002.60c  1.9960080  $  IMPURITIES IN HEAVY WATER MODERATOR:
469        1001.60c  0.0039920  $  H/D = 0.2 %
470        8016.60c  1
471 MT2     HWTR.01T
472        LWTR.01T
473 C
474 M3     1001.60c  2
475        8016.60c  1
476 MT3     LWTR.01T
477 C
478 C      -----
479 C
480 C      SIMPLIFIED MATERIAL FOR CLADDING (WAS AlFeNi)
481 C
482 M4     13027.60c  1
483 C
484 C      -----
485 C
486 M5     4009.60c  1
487 MT5     BE.01T
488 C
489 C M6     40000.60c  1  $  UNUSED MATERIAL
490 C M7     72000.60c  1  $  UNUSED MATERIAL
491 C
492 C      -----
493 C
494 C      SIMPLIFIED MATERIAL FOR VESSELS (WAS AG-3)
495 C      REPLACED WITH M4
496 C
497 C M9     13027.60c  1
498 C
499 C      -----

```

```
500 C
501 C      HEU AT 1.5 g/cc w/ U-234 AND U-236 CONTENT
502 C
503 M11    13027.60c 0.0514085820
504 C
505      36083.60c 1.0e-24      $ begin_mcode_FP
506      40093.60c 1.0e-24
507      43099.60c 1.0e-24
508      42092.60c 1.0e-24
509      42094.60c 1.0e-24
510      42095.60c 1.0e-24
511      42096.60c 1.0e-24
512      42097.60c 1.0e-24
513      42098.60c 1.0e-24
514      42099.60c 1.0e-24
515      42100.60c 1.0e-24
516      44101.60c 1.0e-24
517      44103.60c 1.0e-24
518      45103.60c 1.0e-24
519      45105.60c 1.0e-24
520      46105.60c 1.0e-24
521      47109.60c 1.0e-24
522      48113.60c 1.0e-24
523      53129.60c 1.0e-24
524      54131.60c 1.0e-24
525      54133.60c 1.0e-24
526      54135.60c 1.0e-24
527      55133.60c 1.0e-24
528      55134.60c 1.0e-24
529      55135.60c 1.0e-24
530      57139.60c 1.0e-24
531      58141.60c 1.0e-24
532      59141.60c 1.0e-24
533      59143.60c 1.0e-24
534      60143.60c 1.0e-24
535      60145.60c 1.0e-24
536      60147.60c 1.0e-24
537      60148.60c 1.0e-24
538      61147.60c 1.0e-24
539      61148.60c 1.0e-24
540      61148.50c 1.0e-24      $ ORIGEN_ID 611481
541      61149.60c 1.0e-24
542      61151.60c 1.0e-24
543      62149.60c 1.0e-24
544      62150.60c 1.0e-24
545      62151.60c 1.0e-24
546      62152.60c 1.0e-24
547      62153.60c 1.0e-24
548      63153.60c 1.0e-24
549      63154.60c 1.0e-24
```



```
550      63155.60c 1.0e-24
551      63156.60c 1.0e-24
552      64157.60c 1.0e-24      $ end_mcode_FP
553 C
554      92234.60c 0.0000348368 $ begin_mcode_ACT
555      92235.60c 0.0035844378
556      92236.60c 0.0000038379
557      92237.60c 1.0e-24
558      92238.60c 0.0002283330
559      93237.60c 1.0e-24
560      93239.60c 1.0e-24
561      94238.60c 1.0e-24
562      94239.60c 1.0e-24
563      94240.60c 1.0e-24
564      94241.60c 1.0e-24
565      94242.60c 1.0e-24
566      95241.60c 1.0e-24
567      95242.50c 1.0e-24      $ ORIGEN_ID 952421
568      95243.60c 1.0e-24
569      96244.60c 1.0e-24
570      96245.60c 1.0e-24      $ end_mcode_ACT
571 C
572 C      -----
573
574      ...
575
576 C      -----
577 C
578 C      HEU AT 1.5 g/cc w/ U-234 AND U-236 CONTENT
579 C
580 M22 13027.60c 0.0514085820
581 C
582      36083.60c 1.0e-24      $ begin_mcode_FP
583      40093.60c 1.0e-24
584      43099.60c 1.0e-24
585      42092.60c 1.0e-24
586      42094.60c 1.0e-24
587      42095.60c 1.0e-24
588      42096.60c 1.0e-24
589      42097.60c 1.0e-24
590      42098.60c 1.0e-24
591      42099.60c 1.0e-24
592      42100.60c 1.0e-24
593      44101.60c 1.0e-24
594      44103.60c 1.0e-24
595      45103.60c 1.0e-24
596      45105.60c 1.0e-24
597      46105.60c 1.0e-24
598      47109.60c 1.0e-24
599      48113.60c 1.0e-24
```

```
600      53129.60c 1.0e-24
601      54131.60c 1.0e-24
602      54133.60c 1.0e-24
603      54135.60c 1.0e-24
604      55133.60c 1.0e-24
605      55134.60c 1.0e-24
606      55135.60c 1.0e-24
607      57139.60c 1.0e-24
608      58141.60c 1.0e-24
609      59141.60c 1.0e-24
610      59143.60c 1.0e-24
611      60143.60c 1.0e-24
612      60145.60c 1.0e-24
613      60147.60c 1.0e-24
614      60148.60c 1.0e-24
615      61147.60c 1.0e-24
616      61148.60c 1.0e-24
617      61148.50c 1.0e-24      $ ORIGEN_ID 611481
618      61149.60c 1.0e-24
619      61151.60c 1.0e-24
620      62149.60c 1.0e-24
621      62150.60c 1.0e-24
622      62151.60c 1.0e-24
623      62152.60c 1.0e-24
624      62153.60c 1.0e-24
625      63153.60c 1.0e-24
626      63154.60c 1.0e-24
627      63155.60c 1.0e-24
628      63156.60c 1.0e-24
629      64157.60c 1.0e-24      $ end_mcode_FP
630 C
631      92234.60c 0.0000348368 $ begin_mcode_ACT
632      92235.60c 0.0035844378
633      92236.60c 0.0000038379
634      92237.60c 1.0e-24
635      92238.60c 0.0002283330
636      93237.60c 1.0e-24
637      93239.60c 1.0e-24
638      94238.60c 1.0e-24
639      94239.60c 1.0e-24
640      94240.60c 1.0e-24
641      94241.60c 1.0e-24
642      94242.60c 1.0e-24
643      95241.60c 1.0e-24
644      95242.50c 1.0e-24      $ ORIGEN_ID 952421
645      95243.60c 1.0e-24
646      96244.60c 1.0e-24
647      96245.60c 1.0e-24      $ end_mcode_ACT
648 C
649 C -----
```

```
650 C
651 C VOID
652 C
653 KCODE 15000 1.1 10 260
654 C
655 C KSRC 10.4670 0.1348 -30.5000 10.6980 0.2268 -25.5000 &
656 C 10.9600 0.3524 -20.5000 11.2520 0.5163 -15.5000 &
657 C 11.5680 0.7227 -10.5000 11.9050 0.9756 -5.5000 &
658 C 12.2570 1.2783 5.5000 12.6190 1.6340 10.5000 &
659 C 12.9860 2.0452 15.5000 13.3510 2.5138 20.5000 &
660 C 13.7090 3.0414 25.5000 14.0540 3.6288 30.5000
661 C
662 C -----
663 C
664 C PRINT
665 PRDMP 0 200 -1 4 0
666
667 C BLANK LINE TERMINATOR -----
```

This page intentionally blank

Appendix E

MCODE Sample Input Deck

```
1 $ TITLE line
2 TTL GSER2 HEU Design (12 Materials)
3 $ CTRL command initial-inp
4 MCD 1 /opt/mcnp4b/bin/mcnp-optimized-g77-bigmdas GSER2_4a mysrc
5 $ ORIGEN-COMMAND ORIGEN-LIBRARY-PATH decay-lib gamma-lib
6 ORG /opt/ORIGEN22/CODE/origen22 /opt/ORIGEN22/LIBS ATRDECAY.LIB GXU02BRM.LIB
7 $ total# CELL-ID TYPE IHM(g) VOL(cm3) ORG-XS-LIB
8 CEL 12 2001 1 1502.074 1001.383 ATRXS.LIB
9 2002 1 126.225 84.150 ATRXS.LIB
10 2003 1 2038.529 1359.019 ATRXS.LIB
11 2004 1 384.985 256.657 ATRXS.LIB
12 2005 1 612.190 408.127 ATRXS.LIB
13 2006 1 410.230 273.487 ATRXS.LIB
14 2007 1 227.204 151.470 ATRXS.LIB
15 2008 1 208.271 138.847 ATRXS.LIB
16 2009 1 88.357 58.905 ATRXS.LIB
17 2010 1 126.225 84.150 ATRXS.LIB
18 2011 1 429.164 286.109 ATRXS.LIB
19 2012 1 473.343 315.562 ATRXS.LIB
20 $ TOTAL VOLUME (cm3)
21 VOL 27488.940
22 $ power density, opt: WGU=W/gIHM, KWL=kW/(liter core)
23 PDE 1091.348 KWL
24 $ NORMALIZATION option, 1=FLUX, 2=POWER
25 NOR 2
26 $ Predictor-Corrector option, 1=ON, 0=OFF
27 COR 1
28 $ opt E=MWd/kg, D=EFPD
29 $ points 0 1 2 3 4 5 6 7 8 9 10 11 12 13 14
30 DEP D 0 0.2 2 6 10 15 20 25 30 35 40 45 50 55 60
31 NMD 18 36 36 36 36 36 36 36 36 36 36 36 36 36
32 STA 0 $ starting point
33 END 14 $ ending point
```

This page intentionally blank

Bibliography

- Ackermann, H., W. Buckel, F. Fujara, and W. Liebert. Zur Problematik der HEU-Nutzung im FRM-II. *Physikalische Blätter*, 55(2):16–20, 1999.
- Albright, D., F. Berkhout, and W. Walker. *Plutonium and Highly Enriched Uranium 1996. World Inventories, Capabilities and Policies*. Stockholm International Peace Research Institute (SIPRI), Oxford University Press, 1997.
- Albright, D. and K. Kramer. Stockpiles Still Growing. *Bulletin of the Atomic Scientists*, pages 14–16, November/December 2004.
- Alvarez, L. *Adventures of a Physicist*. Basic Books, 1987.
- Alvarez, R. and D. Sherman. U.S. to Resume Uranium Production for Weapons. *The Bulletin of the Atomic Scientists*, 41(4):28–30, April 1985.
- Audi, G. and A. H. Wapstra. The 1995 Update To The Atomic Mass Evaluation. *Nuclear Physics A*, 595:409–480, 1995.
- Axmann, A., K. Böning, and W. Petry. *FRM-II: Konsequenzen einer Änderung nach dem Argonne Konzept (20 MW LEU-Kern)*. Technical University of Munich, OPA 00231, April 1999a.
- Axmann, A., K. Böning, and W. Petry. *FRM-II: Konsequenzen einer Änderung nach dem Argonne Konzept (32 MW LEU-Kern)*. Technical University of Munich, OPA 00230, April 1999b.
- Bari, R. A., H. Ludewig, and J. Weeks. *Advanced Neutron Source Enrichment Study, Volume 1: Main Report*. Department of Advanced Technology, Brookhaven National Laboratory, Upton, New York, December 1994.
- BMBF. *Bericht der von der Bundesregierung eingesetzten Expertenkommission zur Prüfung der Umrüstbarkeit des Forschungsreaktors München II von HEU auf LEU*. Federal Ministry of Education and Research, Bonn, Germany, June 1999.
- BMBF. *Vereinbarung über FRM II vorgestellt*. Federal Ministry of Education and Research, Press release No. 169/2001, October 25, 2001.

- Böning, K., A. Axmann, and W. Petry. *Der FRM-II: eine umfassend optimierte Neutronenquelle für die Forschung*. Technical University of Munich, OPA 00229, April 1999.
- Böning, K., W. Gläser, J. Meier, G. Rau, A. Röhrmoser, and L. Zhang. Design of a Novel Compact Core with Reduced Enrichment for Upgrading the Research Reactor Munich FRM. In *Proceedings of the 6th International Meeting on Reduced Enrichment for Research and Test Reactors (RERTR)*, pages 321–330, Tokai, Japan, October 24–27, 1983.
- Böning, K., W. Gläser, J. Meier, G. Rau, A. Röhrmoser, and L. Zhang. Progress Report on the Design of the Compact Core for Upgrading the Munich Research Reactor. In *Proceedings of the 8th International Meeting on Reduced Enrichment for Research and Test Reactors (RERTR)*, pages 103–111, Petten, The Netherlands, October 14–16, 1985.
- Bretscher, M. M. and J. E. Matos. *Neutronic Performance of High-Density LEU Fuels in Water-Moderated and Water-Reflected Research Reactors*. Argonne National Laboratory, July 1996.
- Bretscher, M. M., J. E. Matos, and J. L. Snelgrove. Relative Neutronic Performance of Proposed High-Density Dispersion Fuels in Water-Moderated and D₂O-Reflected Research Reactors. In *Proceedings of the 20th International Meeting on Reduced Enrichment for Research and Test Reactors (RERTR)*, Seoul, Korea, October 7–19, 1996.
- Briesmeister, J. F., ed. *MCNP — A General Monte Carlo N-Particle Transport Code, Version 4A*. LA-12625-M, Los Alamos National Laboratory, November 1993.
- Briesmeister, J. F., ed. *MCNP — A General Monte Carlo N-Particle Transport Code, Version 4B*. LA-12625-M, Los Alamos National Laboratory, March 1997.
- Briesmeister, J. F., ed. *MCNP — A General Monte Carlo N-Particle Transport Code, Version 4C*. LA-13709-M, Los Alamos National Laboratory, December 2000.
- Bronstein, I. N. and K. A. Semendjajew. *Taschenbuch der Mathematik*. Verlag Harry Deutsch, Frankfurt am Main, 1989.
- Brückel, T., G. Heger, D. Richter, and R. Zorn (eds.). *Neutron Scattering — Lectures of the 5th Laboratory Course held at the Forschungszentrum Jülich from 18 to 28 September 2001*. Matter and Materials Series, Volume 9. Forschungszentrum Jülich, Germany, 2001.
- Bunn, G., C. Braun, A. Glaser, E. Lyman, and F. Steinhausler. Research Reactor Vulnerability to Sabotage by Terrorists. *Science and Global Security*, 11:85–107, 2003.

- Bunn, M., J. P. Holdren, and A. Wier. *Securing Nuclear Weapons and Materials: Seven Steps for Immediate Action*. John F. Kennedy School of Government, Harvard University, Project on Managing the Atom, Belfer Center for Science and International Affairs, May 2002.
- Canberra Commission. *Report of the Canberra Commission on the Elimination of Nuclear Weapons*. Canberra, Australia, August 1996.
- Cashwell, E. D. and C. J. Everett. *A Practical Manual on the Monte Carlo Method for Random Walk Problems*. Pergamon Press, London, 1959.
- Cetnar, J., W. Gudowski, and J. Wallenius. *User Manual for Monte-Carlo Continuous Energy Burnup (MCB) Code — Version 1C*. Department of Nuclear and Reactor Physics, Royal Institute of Technology, Stockholm, Sweden, 2002.
- Cheverton, R. D. and T. M. Sims. *HFIR Core Nuclear Design*. ORNL-4621, UC-80 — Reactor Technology, Oak Ridge National Laboratory, July 1971.
- Chunyan, Ma and F. von Hippel. Ending the Production of Highly-Enriched Uranium for Naval Reactors. *The Nonproliferation Review*, 8:86–101, 2001.
- Chvátal, V. *Linear Programming*. W. H. Freeman and Company, New York, 1983.
- Clark, C. R., G. C. Knighton, M. K. Meyer, and G. L. Hofman. Monolithic Fuel Plate Development at Argonne National Laboratory. In *Proceedings of the 25th International Meeting on Reduced Enrichment for Research and Test Reactors (RERTR)*, Chicago, Illinois, October 5–10, 2003.
- Clark, C. R., S. L. Hayes, M. K. Meyer, G. L. Hofman, and J. L. Snelgrove. Update on U-Mo Monolithic and Dispersion Fuel Development. In *Transactions of the 8th International Topical Meeting on Research Reactor Fuel Management (RRFM)*, pages 41–45, Munich, March 21–24, 2004a.
- Clark, C. R., T. C. Wiencek, M. R. Finlay, R. L. Briggs, D. M. Wachs, S. L. Hayes, G. L. Hofman, and C. J. Mothershead. Update on Fuel Fabrication Development and Testing at Argonne National Laboratory. In *Proceedings of the 26th International Meeting on Reduced Enrichment for Research and Test Reactors (RERTR)*, Vienna International Centre, Vienna, Austria, November 7–12, 2004b.
- Cochran, T. B., W. M. Arkin, and M. M. Hoenig. *Nuclear Weapons Databook. Volume I, U.S. Nuclear Forces and Capabilities*. Natural Resources Defense Council. Ballinger Publishing Company, Cambridge, MA, 1984.
- Cochran, T. B. and C. E. Paine. *The Amount of Plutonium and Highly-Enriched Uranium Needed for Pure Fission Nuclear Weapons*. Nuclear Weapons Databook. Natural Resources Defense Council (NRDC), Washington, D.C., April 1995.

- Croff, A. G. *A User's Manual for the ORIGEN2 Computer Code*. ORNL/TM7175, Oak Ridge National Laboratory, July 1980.
- Croff, A. G. ORIGEN2: A Versatile Computer Code for Calculating the Nuclide Compositions and Characteristics of Nuclear Materials. *Nuclear Technology*, 62:335–352, September 1983.
- CSEWGW. *ENDF-102 Data Formats and Procedures for the Evaluated Nuclear Data File ENDF-6*. Cross Section Evaluation Working Group, National Nuclear Data Center, BNL-NCS-44945-01/04-REV, Brookhaven National Laboratory, 2001.
- Cullen, D. E., C. J. Clouse, R. Procassini, and R. C. Little. *Static and Dynamic Criticality: Are They Different?* UCRL-TR-201506, Lawrence Livermore National Laboratory, November 2003.
- Difilippo, F. C. Physics of the Conceptual Design of Intense Steady Neutron Sources. *Nuclear Science and Engineering*, 107:82–98, 1991.
- Difilippo, F. C., W. R. Gambill, R. M. Moon, R. T. Primm, and C. D. West. A Preliminary Reactor Design for the Center for Neutron Research. *Nuclear Instruments & Methods in Physics Research*, A249(1):58–65, 1986.
- Dodd, B., T. J. Dolan, M. Laraia, and I. Ritchie. Perspectives on research reactor utilization. *Physica B*, 311:50–55, 2002.
- Dubbers, D. Particles Physics with Neutrons. *Physica B*, 234–236:1–7, 1997.
- Fender, B. Neutron Scattering. *Nuclear Instruments & Methods in Physics Research*, A249(1):1–11, 1986.
- Frost, B. R. T. *Nuclear Fuel Elements*. Pergamon Press, Oxford, 1982.
- Gambill, W. R. Thermal-Hydraulic Constraints on Water-Cooled Research Reactors. *Nuclear Instruments & Methods in Physics Research*, A249:53–57, 1986.
- Gil, C. S. *Generation of the Continuous Energy Cross Section Data for the MCNP Code*. Nuclear Data Evaluation Laboratory, Korea Atomic Energy Research Institute, Yusong-gu, Daejeon, Korea, 2001.
- Glaser, A. *Abbrandrechnungen für ein System zur Eliminierung von Waffenplutonium*. Diploma Thesis, Institute of Nuclear Physics, Darmstadt University of Technology, February 1998.
- Glaser, A. Bavaria Bucks Ban. *Bulletin of the Atomic Scientists*, pages 20–22, March/April 2002a.

- Glaser, A. The Conversion of Research Reactors and the Case of FRM-II. *Science and Global Security*, 10(1):61–79, 2002b.
- Glaser, A. Putting the Genie Back in the Bottle — Uranium and Nuclear Weapons Proliferation. *INESAP Information Bulletin*, No. 21, pages 34–38, April 2003.
- Glaser, A. Beyond A.Q. Khan — The Gas Centrifuge, Nuclear Weapon Proliferation, and the NPT Regime. *INESAP Information Bulletin*, No. 23, pages 50–54, April 2004a.
- Glaser, A. Monolithic Fuel and High-Flux Reactor Conversion. In *Proceedings of the 26th International Meeting on Reduced Enrichment for Research and Test Reactors (RERTR)*, Vienna International Centre, Vienna, Austria, November 7–12, 2004b.
- Glaser, A., F. Fujara, W. Liebert, and C. Pistner. Mathematica as a Versatile Tool to Set-up and Analyze Neutronic Calculations for Research Reactors. In *Proceedings of the 25th International Meeting on Reduced Enrichment for Research and Test Reactors (RERTR)*, Chicago, Illinois, October 5–10, 2003.
- Glaser, A. and F. von Hippel. On the Importance of Ending the Use of HEU in the Nuclear Fuel Cycle: An Updated Assessment. In *Proceedings of the 24th International Meeting on Reduced Enrichment for Research and Test Reactors (RERTR)*, pages 335–350, San Carlos de Bariloche, Argentina, November 3–8, 2002.
- Gläser, W. The Future Role of Research Reactors. In *IGORR 8 Meeting*, Munich, Germany, April 17–20, 2001.
- Glasstone, S. and A. Sesonske. *Nuclear Reactor Engineering. Volume 1: Reactor Design Basics*. Fourth Edition. Chapman & Hall, New York, 1994.
- Gobrecht, K. Progress on the Cold Neutron Source of the Garching Neutron Research Facility FRM-II. In *Proceedings of the 6th Meeting of the International Group on Research Reactors*, pages 377–390, Taejeon, Korea, April 29–May 1, 1998.
- Gobrecht, K., E. Gutmiedl, and A. Scheuer. Status Report on the Cold Neutron Source of the Garching Neutron Research Facility FRM-II. *Physica B*, 311(1–2): 148–151, 2002.
- Gutmiedl, E. and K. Gobrecht. Status Report on the Cold Neutron Source of the Garching Neutron Research Facility FRM-II. In *IGORR 8 Meeting*, Munich, Germany, April 17–20, 2001.
- Hamy, J. M., P. Lemoine, F. Huet, B. Guigon, C. Jarousse, and J. L. Emin. Status as of March 2004 of the French UMo Group Development Program. In *Transactions of the 8th International Topical Meeting on Research Reactor Fuel Management (RRFM)*, pages 46–51, Munich, March 21–24, 2004.

- Hanan, N. A., J. R. Deen, J. E. Matos, J. A. Hendriks, P. J. M. Thijssen, and F. J. Wijtsma. Neutronic Feasibility Studies for LEU Conversion of the HFR Petten Reactor. In *Proceedings of the 23rd International Meeting on Reduced Enrichment for Research and Test Reactors (RERTR)*, pages 393–403, Las Vegas, Nevada, October 1–6, 2000.
- Hanan, N. A., S. C. Mo, R. S. Smith, and J. E. Matos. An Alternative LEU Design for the FRM-II. In *Proceedings of the 19th International Meeting on Reduced Enrichment for Research and Test Reactors (RERTR)*, Seoul, Korea, October 7–10, 1996.
- Hanan, N. A., R. S. Smith, and J. E. Matos. Alternative LEU Designs for the FRM-II With Power Levels of 20–22 MW. In *Proceedings of the 22nd International Meeting on Reduced Enrichment for Research and Test Reactors (RERTR)*, Budapest, Hungary, October 3–8, 1999.
- Hansen, C. *U.S. Nuclear Weapons. The Secret History*. Orion Books, New York, 1988.
- Heger, G. Diffractometer. In T. Brückel et al., eds., *op. cit.*, pages 7.1–7.13. 2001.
- Hofman, G. L. *A Short Note on High Density Dispersion Fuel*. Argonne National Laboratory, June 1996.
- Hofman, G. L., Y. S. Kim, M. R. Finlay, J. L. Snelgrove, S. L. Hayes, M. K. Meyer, C. R. Clark, and F. Huet. Recent Observations at the Postirradiation Examination of Low-Enriched U-Mo Miniplates Irradiated to High Burnup. In *Transactions of the 8th International Topical Meeting on Research Reactor Fuel Management (RRFM)*, pages 53–58. Munich, Germany, March 21–24, 2004.
- Hofman, G. L. and M. K. Meyer. Progress in Irradiation Performance of Experimental Uranium-Molybdenum Dispersion Fuel. In *Proceedings of the 24th International Meeting on Reduced Enrichment for Research and Test Reactors (RERTR)*, pages 237–249, San Carlos de Bariloche, Argentina, November 3–8, 2002.
- Hofman, G. L. and J. L. Snelgrove. *Dispersion Fuels*. Chapter 2 of Volume 10 A (Nuclear Materials, Part 1, edited by B. R. T. Frost) in R. W. Cahn, P. Haasen, and E. J. Kramer (eds.): *Materials Science and Technology*. VCH Verlagsgesellschaft mbH, Weinheim, Germany, 1994.
- IAEA. *International Nuclear Fuel Cycle Evaluation (INFCE), Volumes 1–9*. International Atomic Energy Agency, Vienna, 1980a.
- IAEA. *Research Reactor Core Conversion From the Use of Highly Enriched Uranium to the Use of Low Enriched Uranium Fuels Guidebook*. IAEA-TECDOC-233, International Atomic Energy Agency, Vienna, 1980b.

- IAEA. *Research Reactor Core Conversion Guidebook. Volumes 1–5*. IAEA-TECDOC-643, International Atomic Energy Agency, April 1992.
- IAEA. *Nuclear Research Reactors in the World. Reference Data Series No. 3, September 2000 Edition*. International Atomic Energy Agency, Vienna, 2000.
- IAEA. *The Applications of Research Reactors*. IAEA-TECDOC-1234, International Atomic Energy Agency, August 2001.
- IAEA. *Safeguards Glossary. 2001 Edition. International Nuclear Verification Series, No. 3*. International Atomic Energy Agency, Vienna, 2002.
- Ippolito Jr., T. D. Effects of Variation of Uranium Enrichment on Nuclear Submarine Design. Master's thesis, Massachusetts Institute of Technology, May 1990.
- Kankeleit, E., C. Küppers, and U. Imkeller. *Report in the Usability of Reactor-Plutonium in Weapons*. Translation of the German original: Bericht zur Waffentauglichkeit von Reaktorplutonium, IANUS Working Paper 1/1989, Darmstadt University of Technology. UCRL-TT-112792 (1993), Berkeley Scientific Translation Service, Lawrence Livermore National Laboratory, 1989.
- Knief, R. A. *Nuclear Engineering. Theory and Technology of Commercial Nuclear Power*. Taylor & Francis, Washington, D.C., second edition, 1992.
- Krass, A. S., P. Boskma, B. Elzen, and W. A. Smit. *Uranium Enrichment and Nuclear Weapon Proliferation*. Stockholm International Peace Research Institute (SIPRI). Taylor & Francis Ltd, London and New York, 1983.
- Lake, J. A., D. K. Parsons, J. L. Liebenthal, J. M. Ryskamp, and G. N. Fillmore. Ultrahigh Flux Reactor Design Probing the Limits of Plate Fuel Technology. *Nuclear Instruments & Methods in Physics Research*, A249(1):41–52, 1986.
- Leenaers, A., S. van den Berghe, E. Koonen, L. Saannen, M. Verwerft, C. Jarousse, F. Huet, M. Trotabas, M. Boyard, and S. Guillot. Post-Irradiation Examination of Uranium-7wt% Molybdenum Atomized Dispersion Fuel. In *Transactions of the 8th International Topical Meeting on Research Reactor Fuel Management (RRFM)*, pages 59–63, Munich, March 21–24, 2004.
- Lemoine, P., J. L. Snelgrove, N. Arkhangelsky, and L. Alvarez. UMo Dispersion Fuel Results and Status of Qualification Programs. In *Transactions of the 8th International Topical Meeting on Research Reactor Fuel Management (RRFM)*, pages 31–40. Munich, Germany, March 21–24, 2004.
- Liebert, W. Open Letter Concerning the Planned Research Reactor FRM-II Using Highly Enriched Uranium. *INESAP Information Bulletin*, No. 2, pages 16–18, July 1994.

- Liu, J. S. *Monte Carlo Strategies in Scientific Computing*. Springer, 2001.
- Ludwig, S. *Revision to ORIGEN2 — Version 2.2*. Transmittal Memo, May 23, 2002.
- MacFarlane, R. E. and D. W. Muir. *The NJOY Nuclear Data Processing System, Version 91*. LA-12470-M, Los Alamos National Laboratory, 1994.
- Magill, J. *Nuclides.net — An Integrated Environment for Computations on Radionuclides and their Radiation*. Springer-Verlag, Berlin, 2003.
- Mark, C., T. Taylor, E. Eyster, W. Maraman, and J. Wechsler. *Can Terrorists Build Nuclear Weapons?* In P. Leventhal, S. Tanzer, and S. Dolley (eds.): *Nuclear Power and the Spread of Nuclear Weapons*. Brassey's, Inc., Washington, D.C., 2002.
- Mark, J. C. Explosive Properties of Reactor-Grade Plutonium. *Science and Global Security*, 41:111–128, 1993.
- Matos, J. E. Relationship between the RERTR Program and the U.S. Spent Fuel Acceptance Policy. In *Proceedings WM'98*, Tuscon, Arizona, March 1–5, 1998.
- Matos, J. E. and J. L. Snelgrove. Selected Thermal Properties and Uranium Density Relations for Alloy, Aluminide, Oxide, and Silicide Fuels. In *Research Reactor Core Conversion Guidebook. Volume 4: Fuels (Appendices I–K)*, IAEA-TECDOC-643, pages 13–29. International Atomic Energy Agency, April 1992.
- Metropolis, N. The Beginning of the Monte Carlo Method. *Los Alamos Science, Special Issue*, pages 125–130, 1987.
- Mezei, F. *Instrumentation Concepts: Advances by Innovation and Building on Experience*. Chapter 3 in: *New Science and Technology for the 21st Century. The ESS Project, Volume II*, May 2002.
- Miller, M. M. *The Potential for Upgrading Safeguards at Research Reactors Fueled with Highly Enriched Uranium: Part II*. Massachusetts Institute of Technology, prepared for The United States Arms Control and Disarmament Agency (ACDA), July 1984.
- Miller, M. M. and C. A. Eberhard. *The Potential for Upgrading Safeguards at Research Reactors Fueled with Highly Enriched Uranium*. Massachusetts Institute of Technology, prepared for The United States Arms Control and Disarmament Agency (ACDA), November 1982.
- Mo, S. C. Application of the Successive Linear Programming Technique to the Optimum Design of a High Flux Reactor Using LEU Fuel. In *Proceedings of the 14th International Meeting on Reduced Enrichment for Research and Test Reactors (RERTR)*, pages 273–284, Jakarta, Indonesia, November 4–7, 1991.

- Mo, S. C., N. A. Hanan, and J. E. Matos. Comparison of the FRM-II HEU Design With an Alternative LEU Design. In *Proceedings of the 18th International Meeting on Reduced Enrichment for Research and Test Reactors (RERTR)*, Paris, France, September 18–21, 1995.
- Monkenbusch, M. Neutronenspektroskopie. In *Femtosekunden und Nano-eV: Dynamik in kondensierter Materie*, Matter and Materials Series, Volume 3, pages B5.1–B5.37. Forschungszentrum Jülich, Germany, 2000.
- Monkenbusch, M. Time-of-Flight Spectrometers. In T. Brückel et al., eds., *op. cit.*, pages 10.1–10.22. 2001.
- Monkenbusch, M. and R. Zorn. Neutron Spin-Echo Spectrometer, NSE. In T. Brückel et al., eds., *op. cit.*, pages 11.1–11.18. 2001.
- Moore, R. L., B. G. Schnitzler, C. A. Wemple, R. S. Babcock, and D. E. Wessol. *MOCUP: MCNP-ORIGEN2 Coupled Utility Program*. INEL-95/0523, Idaho National Engineering and Environmental Laboratory, September 1995.
- National Academy of Sciences. *Management and Disposition of Excess Weapons Plutonium*. National Academy Press, Washington, D.C., 1994.
- National Academy of Sciences. *Management and Disposition of Excess Weapons Plutonium. Reactor-Related Options*. National Academy Press, Washington, D.C., 1995.
- NEA/OECD. *Burn-up Credit Criticality Benchmark. Phase IV-A: Reactivity Prediction Calculations for Infinite Arrays of PWR MOX Fuel Pin Cells*. NEA-NSC-DOC(2003)3, Nuclear Energy Agency, Organisation for Economic Co-Operation and Development, 2003.
- Olander, D. R. *Fundamental Aspects of Nuclear Reactor Fuel Elements*. Technical Information Center, Energy Research and Development Administration. TID-26711-P1. U.S. Department of Energy, 1976.
- Olson, A. P. Very-High-Flux Research Reactor Concepts. *Nucl. Inst. Meth.*, A249: 77–90, 1986.
- ONNP. *Report on the Use of Low Enriched Uranium in Naval Nuclear Propulsion*. The Director of the Office of Naval Nuclear Propulsion, Report to the U.S. Congress, 1995.
- ORNL. *RSICC Data Library Collection, MCNPDATA*. DLC-200, Oak Ridge National Laboratory, 2001.
- Pfennig, G, H. Klewe-Nebenius, and W. Seelmann-Eggebert. *Karlsruher Nuklidkarte*. 6th Edition 1995, Revised Reprint, December 1998.

- Pistner, C. *Entwicklung und Validierung eines Programmsystems für Zellabbrandrechnungen plutoniumhaltiger Brennstoffe*. Diploma Thesis, Institute of Nuclear Physics, Darmstadt University of Technology, May 1998.
- Pistner, C. *Neutronenphysikalische Untersuchungen zu uranfreien Brennstoffen*. PhD thesis, Darmstadt University of Technology, 2005.
- Pond, R. B. and J. E. Matos. *Nuclear Mass Inventory, Photon Dose Rate and Thermal Decay Heat of Spent Research Reactor Fuel Assemblies (Rev. 2)*. Argonne National Laboratory, 1995.
- Poston, D. L. and H. R. Trelue. *User's Manual, Version 2.0 for MONTEBURNS Version 1.0*. LA-UR-99-4999, Los Alamos National Laboratory, September 1999.
- Powell, J. R., H. Takahashi, and F. L. Horn. High Flux Research Reactors Based on Particulate Fuel. *Nuclear Instruments & Methods in Physics Research*, A249(1): 66–76, 1986.
- Powers, J. A. *Safeguarding Research Reactors*. STR-118 (Draft), International Atomic Energy Agency, March 1983.
- Press, W. H., S. A. Teukolsky, W. T. Vetterling, and B. P. Flannery. *Numerical Recipes in C. The Art of Scientific Computing*. Cambridge University Press, second edition, 1995.
- RDD-7. *Restricted Data Declassification Decisions 1946 to the Present*. U.S. Department of Energy, Office of Declassification, January 1, 2001.
- Redmond II, E. L. Monte Carlo Methods, Models, and Applications for the Advanced Neutron Source. Master's thesis, Massachusetts Institute of Technology, June 1990.
- Reklaitis, G. V., A. Ravindran, and K. M. Ragsdell. *Engineering Optimization — Methods and Applications*. John Wiley & Sons, Inc., New York, 1983.
- Richter, D. and T. Springer. *A Twenty Years Forward Look at Neutron Scattering Facilities in the OECD Countries and Russia*. European Science Foundation, Organisation for Economic Co-operation and Development (OECD), Megascience Forum, November 1998.
- Ritchie, I. G. Growing Dimensions — Spent Fuel Management at Research Reactors. *IAEA Bulletin*, 40(1), 1998.
- Röhrmoser, A. *Neutronenphysikalische Optimierung und Auslegung eines Forschungsreaktors mittlerer Leistung mit Zielrichtung auf einen hohen Fluss für Strahlrohrexperimente*. PhD thesis, Technical University of Munich, Department of Physics, July 1991.

- Röhrmoser, A., W. Petry, K. Böning, and N. Wieschalla. Reduced Enrichment Program for the FRM-II, Status 2004. In *Proceedings of the 26th International Meeting on Reduced Enrichment for Research and Test Reactors (RERTR)*, Vienna International Centre, Vienna, Austria, November 7–12, 2004.
- Sangren, W. C. *Digital Computers and Nuclear Reactor Calculations*. John Wiley & Sons, Inc., New York, 1960.
- Schwahn, D. Small-Angle Scattering and Reflectometry. In T. Brückel et al., eds., *op. cit.*, pages 8.1–8.16. 2001.
- Schwartz, J. P. *Uranium Dioxide Caramel Fuel — An Alternative Fuel Cycle for Research and Test Reactors*. Communication presented at the International Conference on Nuclear Non-Proliferation and Safeguards. Atomic Industrial Forum, New York, October 22–25, 1978.
- Sesonske, A. and J. G. Yevick. Description of Fast Reactors. In J. G. Yevick and A. Amorosi, editors, *Fast Reactor Technology: Plant Design*, pages 677–746. The M.I.T. Press, Cambridge, MA, 1966.
- Taylor, J. R. *An Introduction to Error Analysis: The Study of Uncertainties in Physical Measurements*. Oxford University Press, 1982.
- Travelli, A. The U.S. Reduced Enrichment Research and Test Reactor (RERTR) Program. In *Proceedings of the 1978 International Meeting on Reduced Enrichment for Research and Test Reactors (RERTR)*, pages 3–15, Argonne National Laboratory, Argonne, Illinois, November 9–10, 1978.
- Ullom, J. Enriched Uranium versus Plutonium: Proliferant Preferences in the Choice of Fissile Material. *The Nonproliferation Review*, 2(1), Fall 1994.
- United Nations. *A More Secure World: Our Shared Responsibility*. Report of the Secretary-General's High-Level Panel on Threats, Challenges and Change, New York, December 2004.
- von Hippel, F. A Comprehensive Approach to Elimination of Highly-Enriched Uranium From All Nuclear-Reactor Fuel Cycles. *Science and Global Security*, 2004.
- Waters, L. *MCNPX User's Manual, Version 2.4.0*. LA-CP-02-408, Los Alamos National Laboratory, September 2002.
- Weinberg, A. M., T. E. Cole, and M. M. Mann. The Material Testing Reactor and Related Research Reactors. In *Proceedings of the International Conference on the Peaceful Uses of Atomic Energy, Volume 2: Physics; Research Reactors*, pages 402–419, Geneva, Switzerland, August 8–20, 1955. United Nations, New York (1956).

- Willrich, M. and T. B. Taylor. *Nuclear Theft: Risks and Safeguards*. Ballinger Publishing Company, Cambridge, MA, 1974.
- Wilson, R. A Nuclear Physics Program and Experimental Needs. *Nuclear Instruments & Methods in Physics Research*, A249(1):34–40, 1986.
- Wolfram, S. *The Mathematica Book, Fourth Edition*. Cambridge University Press, 1999, Version 4.1.5, 2001.
- Xu, Z. *Design Strategies for Optimizing High Burnup Fuel in Pressurized Water Reactors*. PhD thesis, Massachusetts Institute of Technology, January 2003.
- Xu, Z., P. Hejzlar, M.J. Driscoll, and M.S. Kazimi. An Improved MCNP-ORIGEN Depletion Program (MCODE) and its Verification for High Burnup Applications. In *PHYSOR*, Seoul (Korea), October 7–10, 2002.
- Yeldon, W. B., G. J. Ehrhardt, and R. M. Brugger. Use of Radioisotopes (1–92) Made at a Steady State Neutron Facility. *Nuclear Instruments & Methods in Physics Research*, A249(1):20–25, 1986.
- Zhang, L. *Neutronenphysikalische Konzeption und Optimierung eines neuartigen Kompaktkerns für Hochfluss-Forschungsreaktoren*. PhD thesis, Technical University of Munich, Department of Physics, July 1986.

LEBENS LAUF

Bildungsweg

- 2000–2005 Promotionsstudium an der Technischen Universität Darmstadt in Zusammenarbeit mit der Interdisziplinären Arbeitsgruppe Naturwissenschaft, Technik und Sicherheit (IANUS)
- 09.2001–08.2003 Stipendiat am *Massachusetts Institute of Technology* und wissenschaftlicher Mitarbeiter des *MIT Security Studies Programs*
- 1996–1998 Diplomarbeit: “Abbrandrechnungen für ein System zur Eliminierung von Waffenplutonium” am Institut für Kernphysik (IKP) der TU-Darmstadt in Kooperation mit der IANUS Gruppe
- Mai 1998 Physikdiplom
- 1990–1998 Studium der Physik an der Technischen Universität Darmstadt sowie an der *Université Pierre & Marie Curie* (Paris VI, Frankreich)
- Juni 1988 Abitur
- 1985–1988 Gymnasiale Oberstufe, Babenhausen (Hessen)
- 1980–1985 Integrierte Gesamtschule, Babenhausen (Hessen)
- 1975–1980 Grundschule, Babenhausen (Hessen)

Persönliche Daten

- Geburtsdatum: 26. März 1969
Geburtsort: Groß-Umstadt (Hessen)
Eltern: Werner Glaser und Christine Zenkert geb. Wörz
Familienstand: verheiratet

Hiermit erkläre ich an Eides Statt, dass ich die vorliegende Dissertation selbstständig und nur mit den genannten Hilfsmitteln erstellt habe. Ein früherer Promotionsversuch wurde nicht unternommen.

A handwritten signature in black ink, appearing to read 'Alex Glaser'. The 'A' is large and stylized, and the 'G' is a large circle.

Alexander Glaser
Darmstadt, den 9. Februar 2005

Documents, programs, and data
associated with this thesis are available at
www.atoms4peace.org

Typeset in $\text{T}_{\text{E}}\text{X}$
using the primary typefaces
Computer Modern Roman by D. E. Knuth and
Info Display Medium by E. Spiekermann

